LOCAL AND REGIONAL SCALE LANDSLIDE HAZARD ANALYSES OF GUWAHATI CITY, INDIA

Submitted in the Partial Fulfilment of the Requirements for the Degree of
Doctor of Philosophy

By

Chiranjib Prasad Sarma
(ROLL NO: 126104035)

Under the Guidance of

Dr. A. Murali Krishna
and
Dr. Arindam Dey

DEPARTMENT OF CIVIL ENGINEERING
INDIAN INSTITUTE OF TECHNOLOGY GUWAHATI
GUWAHATI – 781039
July 2019

CERTIFICATE

This is to certify that the thesis entitled **"Local and Regional Scale Landslide Hazard Analyses of Guwahati City, India",** submitted by Chiranjib Prasad Sarma, to the Indian Institute of Technology Guwahati, for the award of the degree of Doctor of Philosophy (PhD) in Civil Engineering, is a record of bonafide research work carried out by him under our supervision and guidance. The thesis work, in our opinion, has reached the requisite standard fulfilling the requirement for the degree of Doctor of Philosophy.

The results contained in this thesis have not been submitted in part or full to any other University or Institute for award of any degree or diploma.

IIT Guwahati
Date:

Dr. Arindam Dey
Associate Professor
Department of Civil Engineering
Indian Institute of Technology Guwahati
Guwahati- 781039
India

Dr. A. Murali Krishna
Associate Professor
Department of Civil Engineering
Indian Institute of Technology Guwahati
Guwahati- 781039
India

STATEMENT

I do hereby declare that the matter embodied in this thesis is the result of investigations carried out by me in the department of Civil Engineering, Indian Institute of Technology Guwahati (IITG), Guwahati, Assam, India.

In keeping with the general practice of reporting scientific observations, due acknowledgements have been made wherever the work described is based on the findings of other investigators.

IIT Guwahati
Date:

Chiranjib Prasad Sarma
Roll No: 126104035
Department of Civil Engineering
Indian Institute of Technology Guwahati
Guwahati- 781039
India

ACKNOWLEDGEMENTS

I would like to express my sincere thanks and gratitude to my supervisors, Dr. A. Murali Krishna and Dr. Arindam Dey. This research work was made possible because of the continuous guidance and support of my supervisors.

I am also grateful to my doctoral committee members Prof. Arup Sarma, Prof. Chandan Mahanta and Prof. Sreedeep S. for their valuable suggestions and encouragement at every stage of this research work.

I take this opportunity to thank all the faculty members, staff members of Civil engineering department, IIT Guwahati. I am also thankful to the staff members of the Geotechnical Laboratory, Civil engineering department, IIT Guwahati with special mention of Mr. Hariram Upadhaya for the help giving to me while doing the laboratory tests.

I am thankful to IITG for providing research facility that helped in the study.

I would like to acknowledge the love, friendship and support of all my colleagues in Indian Institute of Technology Guwahati, with special mention of Dr. Shiv Shankar Kumar, Dr. Dooradarshi Chatterjee and Dr. Pradeep Dammala.

I am very grateful to my family members, my father, Late Dr. Jwala Prasad Sarma, my mother, Mrs. Uma Rani Sarma, my brother, Jyothishman Sarma and my aunt Ms. Pratibha Devi, for their support and encouragement during my PhD tenure.

I also acknowledge the help in the form of grants and project funding from the NRDMS Division, Department of Science & Technology, Government of India provide for the research work under the Networking Programme for NE Region.

I thank the divine mother for her blessings on me.

Chiranjib Prasad Sarma

ABSTRACT

Rainfall-induced landslides constitute a major geo-hydrological hazard and form a significant component of the natural disasters that affect most of the hill slopes of Guwahati region, Assam, India. Although such rainfall-triggered landslides are mostly of shallow slips involving relatively lesser volumes of soil, they exhibit a recurrent temporal and spatial frequency of occurrence. The catastrophic nature of such landslides in the urbanized areas cause significant damage to infrastructure and loss of life. Hence, it is immensely necessary to conduct a well-focused research to address this phenomenon for the assessment of the landslide-induced hazard. Hill slopes within the city of Guwahati primarily comprise unsaturated residual soils. As a result, the conventional saturated soil mechanics approach falls inadequate in assessing the stability of these slopes in this region. In order to address this critical issue, the potential susceptibility to rainfall-induced landslide is assessed for the region through an effective modelling of water content and matric suction variation, upon subjected to different rainfall infiltration scenarios. This study highlights the applicability of physically based models, namely TRIGRS (Transient Rainfall Infiltration and Grid-Based Regional Slope-Stability Model), for assessing the landslide susceptibility and hazard assessment for the Guwahati region. This model is capable of computing the transient changes and progressive degradation of the hillslope stability due to rainfall infiltration, while considering the in-situ conditions and mechanical properties of the involved soils. TRIGRS offers a geotechnical perspective to the rainfall induced landslide hazard of the study area.

As an input to TRIGRS, in-situ and laboratory investigations are conducted to ascertain the hydrological and geotechnical characteristics of the hillslope soils. Actual rainfall events of varying patterns and duration, which are known to trigger landslides within the study area, are used as input into TRIGRS model to simulate the slope stability condition of the hill-slopes. Digital Elevation Model (DEM) is used to represent the topography of the area and is subsequently used to derive all other topographic parameters that are required as input to TRIGRS model. The influence of various DEMs on the prediction of the rainfall-induced landslides is also assessed. The rainfall intensity-duration-frequency (I-D-F) curves are evaluated and subsequently used to compute the rainfall intensities corresponding to a specific return period and duration of rainfall. These events are further considered as input into TRIGRS simulation to generate the Factor of Safety (FoS) maps of the region. The outcomes from various such maps are then combined to develop the landslide hazard map of

the study area. Further, to assess the efficacy of the simulations, the Receiver Operating Characteristic (ROC) and LR_{class} of the FoS maps is evaluated by overlaying the landslide locations in the form of GPS (Latitude-Longitude) points. To address the uncertainties related to input values of the soil shear strength parameters considered for the analysis, a probabilistic methodology is developed in which the TRIGRS simulation is aided by Monte-Carlo simulation while considering the soil parameters as random variables. The outcome of the analysis is provided in the form of a Probability of Failure (PoF) map.

The overall study shows that TRIGRS can be efficiently applied to assess the landslide susceptibility and hazard of the region. It is also observed that the choice of DEM makes a significant impact on the simulation results. The soils present in the hill slopes of Guwahati have moderate-to-low permeability (ranging from 10^{-5} to 10^{-7} ms^{-1}). The outcomes indicate that the longer duration rainfall events are more influential in triggering the landslide events. Further, the antecedent rainfall condition plays a significantly potent role in the gradual degradation of slope stability. The most critical landslide events are observed when the antecedent rainfall is followed by a landslide-triggering rainfall. Finally, the probabilistic analysis elucidated that hillslopes of Guwahati region belong to moderately stable or marginally stable state with the Probability of failure ranging from 20.0 – 37.63 %. Hence, it can be stated that across the major areas of the hillslopes, a minor-to-moderate destabilizing scenario will possibly lead to significant instability.

.

TABLE OF CONTENTS

LIST OF FIGURES

LIST OF TABLES

Chapter 1. INTRODUCTION

1.1. GENERAL

Landslides constitute a major hydro-geological hazard and form a significant component of the natural disasters that affect most of the hilly regions round the globe. Apart from causing deaths and injuries, landslide also adds to the woes of the suffered communities by causing destruction of land and property. Huge economic losses are incurred due to destruction of infrastructure. Obstructions caused particularly to the road transport add to these losses, as sometimes they are the only means of transport in mountainous regions. Such obstruction not only cause economic loss to the country, but also bring severe difficulties to the communities depended on that lifeline.

Large parts of India, especially the Himalayas, the Northeastern hill ranges, the Western Ghats, the Nilgiris, the Eastern Ghats and the Vindhyas, are severely affected by frequent landslide occurrence. Such landslides are a result of unique combinations of active tectonic setting, diverse geological formation, high rates of weathering, and profuse precipitation. These causatives are furthers aggravated by human interference in the form of rapid urbanization and unplanned development of infrastructure, thereby adversely affecting the fragile ecosystem of this mountainous terrain. Nearly 15% of India's landmass (approximately 0.49 million sq. km area) is prone to landslide hazard, of which 20% falls in the North Eastern Region (GSI, 2013a). Northeast India is a seismically active zone with a subtropical climatic condition, which are the most favorable conditions for causing and triggering of landslides. As per the Global Landslide Susceptibility Map (Froude and Petley, 2018), this region falls in the medium-to-high and high severity category of landslides. Example of landslides from the northeastern region can fit into every description and poses to be a problem of perplexing assortment. Numerous examples can be cited for both earthquake-induced and rainfall induced landslides in the North Eastern Region (Kalita, 2001; Kumar, 2013).

Assam experienced several landslides in the hilly areas, the prime causes of which attributed to both natural causes (e.g. intense rainfall) as well as human induced causes (unplanned urbanization), that have led to marked structural and hydrological changes in the region. Between 5th and 8th October 2004, owing to 750 mm of rainfall over three days, many landslides occurred around Guwahati urban areas, resulting in the death of 17 persons and

damaging properties worth millions of rupees. About 100 landslides of varying dimensions occurred within a distance of 80 km along NH 44, i.e. the Guwahati-Shillong road (GSI, 2013b). Similar circumstances and occurrences were experienced in the month of June 2012. Seven different landslide occurrences led to the death of four persons (Goswami, 2013). Steep hill slopes and their encroachment could be identified as the most significant causal factors, while heavy concentrated rainfall was considered as the triggering factor for these landslide occurrences. Several such examples of discrete landslide occurrences can be cited from North East Indian context. Landslides triggered by precipitation in the district of Kamrup Metropolitan have caused severe economic losses and fatalities over the years (ASDMA, 2011). Thus, formulation of an efficient disaster risk-management system is required to tackle this problem.

1.2. RAINFALL-INDUCED SLOPE INSTABILITY

The impact of rainwater infiltration in causing landslides is widely recognized. Rainfall infiltration results in the increment of water content and decrement of the matric suction, thereby raising the unit weight and reducing the shear strength of soil in the colluvium of the landslide. The rise of groundwater level or the development of perched water table is the most potent factor in triggering of landslides. The in-situ hill slope residual soils are mostly in unsaturated condition, and therefore the conventional saturated soil mechanics approach falls inadequate to assess the stability of such slopes. To assess the potential susceptibility to rainfall-induced landslide, an effective modeling is essential to address the evolution of water content and matric suction in response to rainfall infiltration. Several studies can be found in literature presenting the rainfall-induced slope stability analysis considering different rainfall-intensity-duration scenarios (Kim *et. al*., 2004; Huat *et al*., 2006) and antecedent conditions (Gasmo *et al*., 2000; Tsaparas *et al*., 2002; Tofani *et al*., 2006; Rahardjo *et al*., 2007). The available researches highlighted the importance of unsaturated soil characteristics to explain the phenomenon of rainfall induced slope stability/instability. Researchers have studied the combined effect of rainfall characteristics and unsaturated soil characteristics on the rainwater infiltration and landslide triggering mechanisms (Bear, 1979; Anderson and Richards, 1987; Ng *et al*., 2001, Zhan *et al*., 2007; Rahimi *et al*., 2010; Wesley, 2010; Fredlund *et al*., 2012; Lu and Godt, 2013; Zhang *et al*., 2015). In these studies, the intensity and duration of precipitation, as well as the ‘soil water characteristic curve (SWCC)’ and the ‘unsaturated hydraulic conductivity curve (UHCC)’ were considered.

1.3. VARIABILITY OF SOIL PROPETIES

Soil is a naturally occurring material and the resulting variability in geotechnical properties is a well-established fact. Such variability primarily arises out of depositional and post-depositional nature of the geological and geomorphological formation processes (Lee *et al*., 1983; Lacasse and Nadim, 1996; Baecher and Christian, 2003). A factor of safety (FoS), which is mostly based on experience and engineering judgment, is assumed to address the different forms of uncertainty. (Elkateb *et al*., 2002). However, it is debated that factor of safety is not a reliable measure of risk (Li and Lumb, 1987). Rather, in order to address the variability and uncertainty, probabilistic treatment can readily be applied to the conventional slope stability analysis methods and due attention towards this approach is highlighted in the literature (Alonso, 1976; Wu and Siddle, 1995; Liang *et al*., 1999; Auvinet, 2000; Low, 2005; Cho, 2007). Researchers have elucidated the efficacy of random finite element methods (RFEMs) for addressing the variability in soil properties while determining the probability of failure of a slope (Vanmarcke, 1977a&b; Fenton and Griffiths, 2008).

1.4. GIS APPLICATION IN LANDSLIDE RESEARCH

The widespread availability of Geographical Information Systems (GIS) provides the necessary platform for effectively implementing the analytical models for the forecasting of potential triggering of landslides. Thus, GIS-based landslide susceptibility and hazard mapping can contribute to greater knowledge and understanding of the occurrence of landslides at a particular location. Several contributions can be found in literature which can be grouped in two broad categories, namely qualitative and quantitative (Soeters and Van Westen, 1996; Glade and Crozier, 2005). Statistical methods have also been applied for long to address the susceptibility analysis of rainfall-induced shallow landslides (Carrara *et al*., 1992; Bai *et al*., 2009; Cervi *et al*., 2010; Li *et al*., 2012; Reichenbach *et al*., 2018).

The GIS-based analytical models, which consider the in-situ conditions and mechanical properties of the involved soils, have presented a geotechnical perspective to the subject. Several physically based models have been developed, namely SHALSTAB (Shallow Landslide Stability Model) (Montgomery and Dietrich, 1994), SINMAP (Stability Index Mapping) (Pack *et al*., 1998), PROBSTAB (Probability of Stability PC Raster GIS package) (Van Beek and Van Asch, 2004), TRIGRS (Transient Rainfall Infiltration and Grid based Regional Slope-stability) (Baum *et al*., 2002; Savage *et al*., 2004), and SLIP (Montrasio and Valentino, 2008; Montrasio *et al*., 2012). TRIGRS is widely used due to its

ability to compute transient pore-pressure changes as a response to any complex rainfall event and provides the changes in the factor of safety (Baum et al., 2002; Savage et al., 2004, Salciarini *et al*., 2006; Salciarini *et al*., 2008; Sorbino *et al*., 2010; Kim *et al*., 2010; Park *et al*., 2013; Saadatkhah *et al*., 2014; Schilirò *et al*., 2015).

1.5. MOTIVATION OF THE STUDY

A significant amount of studies related to landslide hazard assessment of hillslopes around the world can be found in the literature. Statistical methods have long been applied for the susceptibility analysis of rainfall-induced shallow landslides (Carrara *et al*., 1991; Bai *et al*., 2009; Cervi *et al*., 2010; Li *et al*., 2012; Reichenbach *et al*., 2018). Similarly, Geographical Information Systems (GIS)-based analytical models have been developed to consider the in-situ geo-hydrology for assessment landslide susceptibility and hazard (Montgomery and Dietrich, 1994; Pack *et al*., 1998; Van Beek and Van Asch, 2004; Baum *et al*., 2002; Savage *et al*., 2004; Montrasio and Valentino, 2008).

In India, sufficient attention has been focused to assess and identify the landslide hazard in the Northern and Northwestern Himalayan region. However, not much emphasis has been given to study the landslide hazard in the state of Assam, and specifically Guwahati urban area, even though the area succumbs to immense damage due to annually occurring rainfall-induced landslides. Based on two factors, vis. the slope of the site and its land use, Phukon *et al*. (2012) identified the potential landslide risk zones around the city of Guwahati using GIS application. Five probable causal factors that triggered the past landslides were considered for the study. Bhusan *et al.* (2014) presented a hazard zonation of Guwahati city using Analytical Hierarchical Process (AHP) based on the available thematic data vis. landslide inventory, Cartosat–1 stereo data, lithology, fault/lineament, drainage, geomorphology, soil depth, soil texture, land use / land cover, rainfall and earthquake incidences. The undertaken studies and the derived conclusions/recommendations were based on statistical or semi–heuristic methods, thereby relying on qualitative assumption and judgment of the event. Goswami (2013) conducted 'Rapid Visual Screening (RVS) for potential landslide areas of Guwahati'. Based on engineering judgment, 366 sites that are vulnerable to landslides were identified. A questionnaire was prepared and a reconnaissance survey was conducted. The questions were answered based on the visual observation and judgment, and qualitative conclusions were drawn based on the gathered response. Goswami (2013) proposed that a detailed geotechnical investigation should be done to understand the

mechanism of rainfall induced landslides. The report provided a feedback of the in-situ conditions, although failed to provide a detailed analysis of the problem that could be possibly used to predict the probability of future occurrences. The approach did not consider the effect of soil suction in stabilizing the hill slopes composed of unsaturated residual soils and thus failed to clarify the phenomenon of rainfall-induced instability.

As can observed from previous reports, there have been recurrent widespread fatalities and loss of property due to frequent landslides across the Guwahati city. An understanding of the landslide hazard of the region might be instrumental in planning of early-warning and mitigation of the future events, which provides an avenue to the social responsibility involving the noble deed of saving lives through prevention. Hence, the amalgamation of the geotechnical perspectives with the GIS-based analytical models is ardently needed to address the issues of rainfall-induced landslides in the Guwahati city, which provides the motivation to conduct the present dissertation work. This dissertation work is to investigate the rainfall-induced slope instability annually occurring in the region of Guwahati city, India, and develop a comprehensive rainfall induced landslide hazard zonation map of the region. The objective will be addressed through the application of physically based models, while considering the geotechnical and geo-hydrological aspects of landslide in the region. The variability of soil properties will be incorporated through a probabilistic analysis probability of failure maps will be developed for the region.

1.6. ORGANISATION OF THE REPORT

This dissertation comprises nine chapters, the briefs of which are listed as follows:

Chapter 1 provides a general perspective of the rainfall-induced landslides and their damaging effects in the study area. A brief of the existing studies are highlighted to elucidate the motivation of the dissertation work.

Chapter 2 presents the critical review of the literature pertaining to the study. The reviews are reported in three parts: rainfall-induced slope stability studies, studies on probabilistic slope stability analysis, and landslide susceptibility and hazard analysis. The summary of the literature with key objectives and scope of the present research is presented. A brief note is also provided about the novelty of the present dissertation work.

Chapter 3 gives a description of the study area, its geographical location, geomorphology, hill slope soils and geology, as well as information about the prevalent rainfall and climate of the study region.

Chapter 4 describes the laboratory and in-situ tests conducted for basic characterization of the soils, as well as to determine their shear strength and hydraulic conductivity properties. The summary of the test results highlighting the range of various soil properties is provided.

Chapter 5 presents the analysis of a homogeneous slope simulated with soil parameters relevant to the study area and subjected to infiltration scenarios. The effects of rainfall intensity and duration on the stability of slope are discussed. The chapter also presents the probabilistic slope stability analysis in a local scale. The procedure for simulation of random distribution and effect of the spatial variability of the soil parameters on the slope stability is illustrated.

Chapter 6 discusses the TRIGRS model in detail and describes the calibration of the input parameters for an efficient simulation of the landslide scenario of the hillslopes of Guwahati region.

Chapter 7 presents the regional scale landslide susceptibility and hazard assessment of Guwahati using TRIGRS model. Few particular rainfall events that are known to have triggered landslides in the past are used as input for the model. The rainfall intensity-duration-frequency curves were developed and used for simulation for landslide recurrence. The effect of the Digital Elevation model (DEM) on the simulation results are presented. The results are validated with the locations of the landslide events triggered by rainfall event of June 2012. The effect of rainfall pattern on the landslide triggering is also discussed.

Chapter 8 presents the regional-scale probabilistic analysis of Guwahati city using TRIGRS model, while considering randomly distributed soil properties for generating the probability of failure map of the study area.

Chapter 9 presents a summary of the thesis and the conclusions derived from the research, along with the limitations of the study and possible future scope.

Chapter 2. LITERATURE REVIEW

2.1. INTRODUCTION

Broadly, the review of literature is classified into two categories, local scale approach of slope stability analysis and regional scale approach for landslide susceptibility and hazard analysis. The local scale approach is again subdivided into two sections, vis., rainfall induced slope instability analysis and probabilistic methods of slope stability analysis. The section on regional scale approach consists of studies related to assessment of landslide susceptibility and hazard within the framework of geographic information system aimed at prediction of the landslide occurrence and mapping of potential triggering areas. The literature also presents the definition and usage of various terms related to landslide studies.

2.2. DEFINITION

Bates and Jackson (1987) defined a landslide as the transport of soil and rock material down slope under gravitational influence, the displaced material moving over relatively confined zone or surface of shear.

Cruden (1991), as well as Cruden and Varnes (1996), defined landslide as “the movement of rock, debris, or earth down a slope”, where landslides can range in size from a single boulder in a rock fall to a very large avalanche of debris with huge quantities of rock and soil that can be spread across many kilometers.

Crozier (1999) demarcates landslides as a subset of a broader group of slope processes that is referred to as mass movement. The definition of mass movement includes all those processes that involve the outward or downward movement of slope forming material under the influence of gravity. Landslides are those mass movements that are capable of moving at relatively high velocity and have clearly identifiable boundaries, often in the form of shear surfaces.

2.3. CLASSIFICATION

The most common classification for landslides is based on the type of material involved and the mode of movement. A variety of movements associated with landslides are flowing, sliding, toppling or falling movements. Many landslides exhibit a combination of two or more types of movements. The classification of landslides by the British Geological

Survey follows the scheme based on Cruden and Varnes (1996) and Varnes (1978). The United States Geological Survey gave a similar classification based on Varnes (1978) and Hutchinson (1988). Instead of the main types of distinct movement processes, one complex class might exist comprising two or more different movement processes acting together along with down slope movement of the landslide mass. Table 2.1 summarizes the classification criteria. A second widely acknowledged classification of landslides is based on movement velocity, as proposed by Cruden and Varnes (1996), which ranges from 'extremely fast' to 'extremely slow' (Table 2.2). The landslide classification followed by British Geological Survey (BGS) is presented in Figure 2.1 .

Table 2.1 Landslide classification based on published research (Varnes, 1978; Hutchinson, 1988; Cruden and Varnes, 1996)

Type of movement		**Type of Material**		
		Rock	**Debris**	**Earth**
Topple		Rock topple	Debris topple	Earth topple
Fall		Rock fall	Debris fall	Earth fall
Slide	Translational	Rock slide	Debris slide	Earth slide
	Rotational			
Flow		-	Debris flow	Earth flow
Spread		-	-	Earth spread

Table 2.2 Classification based on velocity scale proposed by Cruden and Varnes (1996)

Velocity Class	Description	Velocity	Probable Destructive Significance
7	Extremely rapid	5 m/ sec	Major catastrophe; buildings destroyed by impact of displaced material; escape unlikely
6	Very rapid	3 m/min	Velocity too great to permit total evacuation
5	Rapid	1.8 m/hour	Escape, evacuation possible
4	Moderate	13 m/month	
3	Slow	1.6 m/year	Structures can be maintained with frequent maintenance
2	Very slow	15 mm/year	
	Extremely slow		Imperceptible without instruments; construction possible with precautions

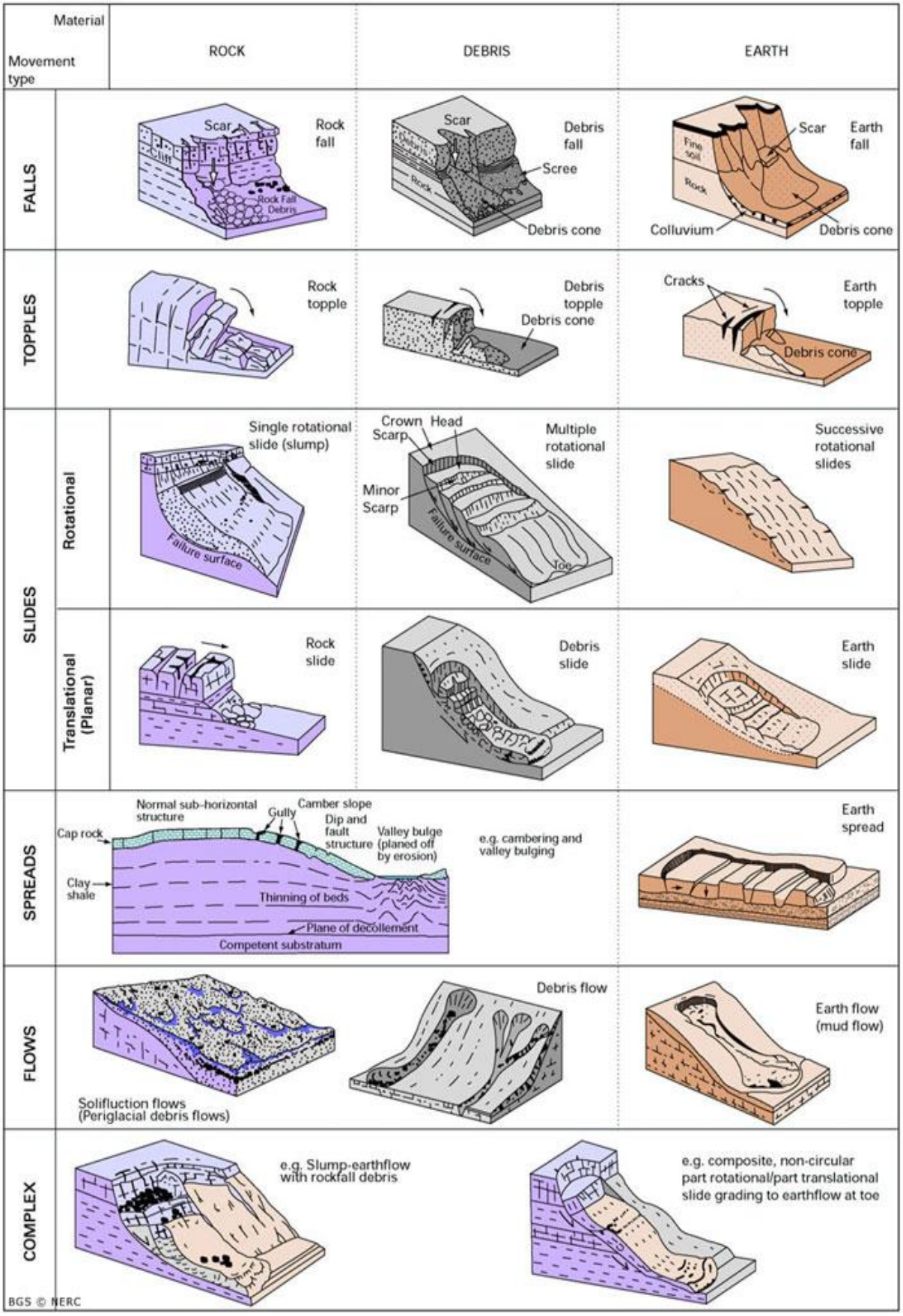

Figure 2.1 Classification of landslides by the (BGS, 2014)

2.4. CAUSAL FACTORS

Glade and Crozier (2005 a, b) visualize slope stability as a dynamic phenomenon of which, on one end, there is a stable slope which is subject to preparatory factors which convert the slope to a marginally stable state. Leroueil (2004) distinguishes stages of landslide movement, namely (a) a pre-failure stage including deformation process leading to failure, (b) the onset of failure characterized by the formation of a continuous shear surface through the entire soil mass, (c) a post failure stage starting from failure until the mass stops, and (d) in some cases, a reactivation phase when sliding occurs on a pre-existing shear surface. Various causal factors that can be considered significant for landslide occurrence are summarized in Table 2.3.

Table 2.3 Causal factors for landslide occurrence (after Selby, 1993);

Natural Causes	Geological Causes	➢ Weathering	▪ Chemical ▪ Physical ▪ Biological
		➢ Structure	▪ Stratification ▪ Orientation
	Morphological Causes	➢ Topography	
		➢ Surface Cover	
		➢ Slope inclination	
		➢ Erosion	▪ Toe erosion ▪ Gully erosion ▪ Subterranean • Solution • Piping
		➢ Deposition	▪ On slope face ▪ On crest
		➢ Tectonic activities	▪ Uplift
	Hydrological Causes	➢ Rainfall	
		➢ Infiltration	
		➢ Seepage of Pore Water	
		➢ Rise in Ground Water Level	
Anthropogenic Causes		➢ Encroachment	
		➢ Deforestation	
		➢ Unscientific cutting of hill slopes	
		➢ Unplanned Infrastructure Development	

2.5. TRIGGERING FACTORS

The triggers associated with occurrence of landslide are mostly of geological origin, such as seismic shaking due to earthquakes, or hydrological origin such as intense rainfall, rapid snowmelt (Glade and Croizer, 2005 a, b). At this point, triggering factors exceeding certain thresholds can alter the state of the slope to actively unstable that leads to continuous or intermittent movement. In the majority of cases, the main trigger of landslides is heavy or prolonged rainfall. For rainfall occurring over a short time interval, it is usually necessary to have very high rainfall intensities. For a long duration rainfall event, the intensity of rainfall may only be moderate (Glade and Croizer, 2005 a, b).

2.6. LANDSLIDE STUDY APPROACH

Landslide studies can be qualitative or quantitative; qualitative approaches focus on descriptive analysis and prediction based on the opinion of experts, while quantitative applications are based on mathematical description or numerical simulations of the landslide phenomenon (Carrara *et al*., 1991). Again, landslide study approaches can broadly be separated into two streams (Crozier and Glade 2005), local models (focusing on single landslide processes) and regional models (focusing on landslide phenomena across greater spatial extent).

Landslide analysis from a geotechnical engineering standpoint have been confined mostly to local approach within the long tradition of slope stability practice. Models for the analysis of single slope failures have frequently been applied in geotechnical engineering application to assess the stability of human-made or natural slopes, and the design of slopes, such as embankments, road cuts, open-pit mines etc. The biggest advantage of such an approach is that it allows detailed investigation of failure processes, effects of triggering events, and assessment of the effectiveness of remedial / stabilization measures..

Guzzetti et al. (1999) identified two methods, one based on the statistical analysis of geo-environmental factors related to the occurrence of landslides; and the other one being the deterministic modelling based on simple mechanical laws that control slope instability, for regional scale landside studies. Statistical models provide a quantitative and objective way of ascertaining the spatial pattern of landslides but do not explicitly incorporate the temporal aspects of movement, and such methods are heavily dependent of the historical records of landslide occurrences (Ardizzone *et al*., 2002). Physically-based models are capable of taking into consideration the various geotechnical and geo-hydrological factors and provide rational

description and forecasting of the spatial and temporal occurrence of landslide (Guzzetti, 2002).

2.7. SLOPE–STABILITY ANALYSIS

Many researchers have performed stability analysis of slopes by using different methods with different assumptions satisfying a variety of conditions. The simplest and most used method is the limit equilibrium method, which considers force and moment equilibrium of a mass of soil above a potential failure surface. Duncan (1996) provided a review of the limit equilibrium method and finite element method used in stability analyses of slopes. The different advantages and disadvantages of the two methods were also discussed in the study. Cheng et al. (2007) compared the limit equilibrium method and finite element method for different soil slopes and concluded that the results from the two methods were comparable for homogeneous slopes.

2.7.1. Rainfall – Induced Slope Instability

Wesley (2010) gave an elaborate description of behaviour of residual soils particularly pertaining to slope stability. Wesley (2010) noted that slopes composed of residual soil can occasionally stand stable at steep angles and at height greater than 10 m. Slope failures in residual soils, even when steep slopes are involved are more likely to be shallow with slightly curved or planar surfaces. The cementation within the soil particles play an important role in the behaviour of residual soils but, the shear strength arising from the zone of negative pore pressure above the water table contributes as a major factor in the stability of slopes. Landslides in residual soils are generally triggered by rainfall, because of temporary increase of pore water pressure in the topmost layers of the slope. This phenomenon highlights the importance of antecedent pore-water condition generated from seasonal effects.

Several studies concerning rainfall, infiltration and landslide mechanism can be found in literature. Numerical models were developed to study the variation of infiltration in a slope with respect to rainfall intensity and its effect on the slope stability.

Gasmo *et al*. (2000) developed numerical models to study how infiltration into a slope varied with respect to rainfall intensity and how this infiltration affected the stability of the slope. The transient seepage analysis was done using SEEP/W (GeoSlope, 2007) and the results were imported to SLOPE/W (GeoSlope, 2007) to calculate the Factor of Safety.

Figure 2.2(a) shows the soil water characteristic curve (SWCC) while Figure 2.2(b) shows the unsaturated hydraulic conductivity curve (UHCC) or the Permeability function of the soil used for the numerical study. The study revealed that the amount of infiltration was highest at the crest of a slope and that infiltration rates are affected by the intensity of rainfall and antecedent moisture condition. Comparison with field data revealed that it was difficult to quantify the amount of infiltration occurring in a slope with the numerical model, but was able to illustrate the effect of infiltration on slope stability through the combined use of seepage and slope stability analyses. Figure 2.3(a) shows the idealized slope used for the case study and Figure 2.3(b) shows the comparison of pore pressure profiles obtained from field and numerical analysis. The study revealed that reduction in the factor of safety was of the order of 15% to 30%. Figure 2.4 shows the factor of safety for the case study slope from 21 July 1996 to 10 August 1996. The study also revealed that antecedent moisture condition has a significant effect on stability condition, high antecedent moisture condition allowed a rainfall of lower intensity and duration to initiate a failure. Rate of infiltration is affected by the ratio between saturated coefficient of permeability and the intensity of rainfall, inclination of slope surface, surface cover and antecedent moisture condition.

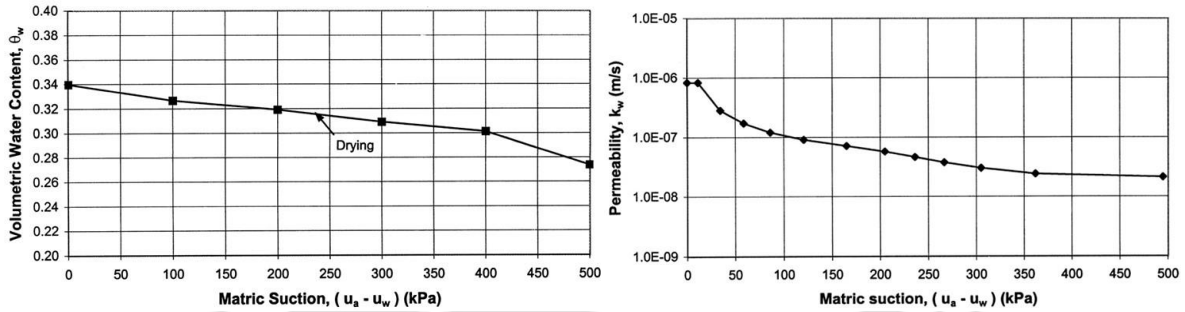

Figure 2.2 (a) Soil water characteristic curve (SWCC) (b) Unsaturated hydraulic conductivity curve (UHCC) (Permeability function) of the soil used for the numerical study (Gasmo *et al*., 2000)

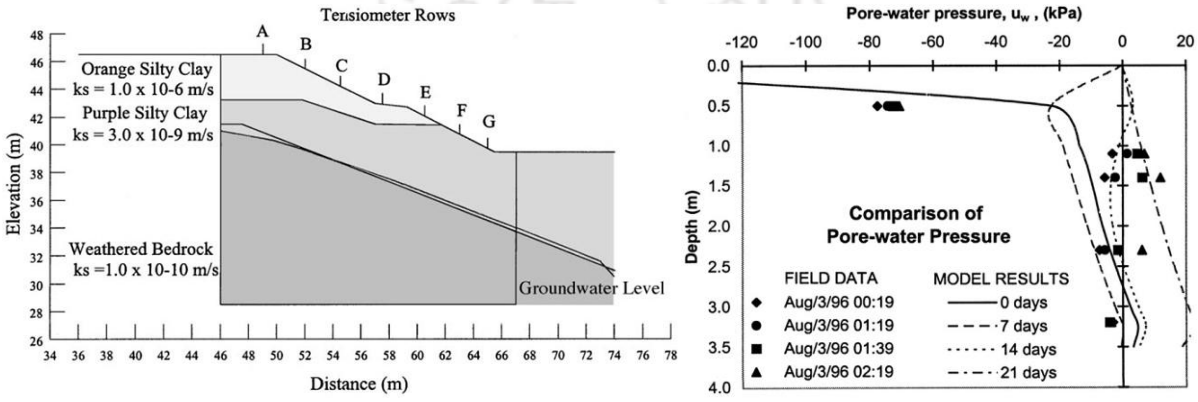

Figure 2.3 (a) Idealized profile of case study slope (b) Comparison of field and model pore water pressure profiles for Row A from 00:19 to 02:19 on 3 August 1996, as a result of infiltration (Gasmo *et al*., 2000)

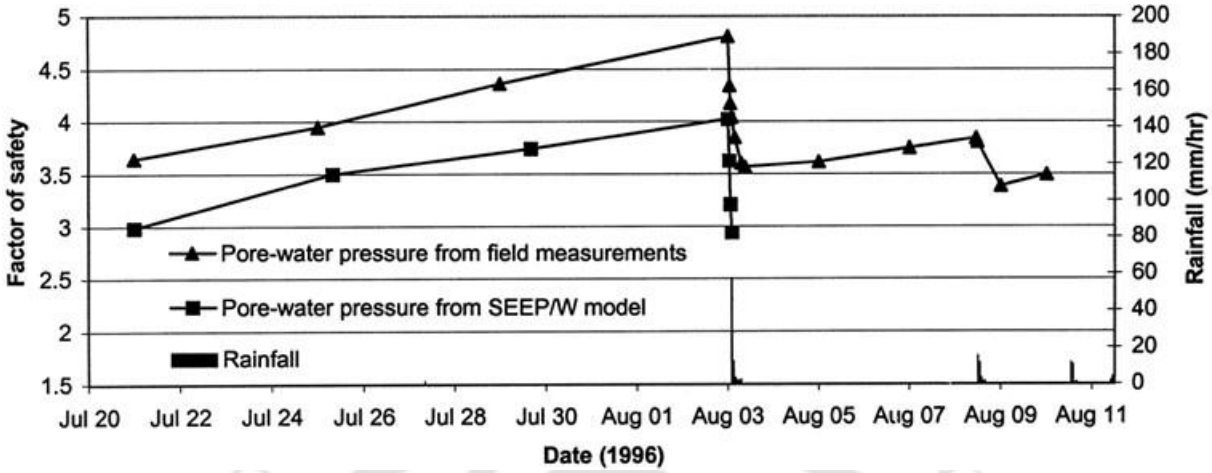

Figure 2.4 Factor of safety for the case study slope from 21 July 1996 to 10 August 1996 (Gasmo *et al*., 2000)

Tsaparas *et al*. (2002) identified the influence of some of the controlling parameters on the stability of an unsaturated soil slope during rainfall. Figure 2.5 (a) shows the soil water characteristic curve (SWCC) while Figure 2.5(b) shows the unsaturated hydraulic conductivity curve (UHCC) corresponding to varying saturated permeability of the soil used in the numerical study. Figure 2.6(a) shows the homogenous slope model. The results of the analysis show that the ratio between the saturated coefficient of permeability and the rainfall patterns can significantly influence the seepage pattern within an unsaturated soil slope. The study revealed that rate of infiltration is dependent on both the permeability of the soil and the intensity of rainfall. If the ratio between rainfall intensity and saturated permeability is low, then more water will infiltrate the ground and less amount of the rainfall will be lost as runoff; whereas, if the ratio is too small, negative pore–water pressures may not even be affected by the infiltration. Figure 2.6(b) shows the lowest factor of safety (*FoS*) for all the different distributions of the 240 mm of rainfall and for all the saturated coefficients of permeability with respect to duration of the rainfall. The initial *FoS* for all the cases is 1.32. In the analysis, for the distribution of 240 mm of rainfall over 2 h, the lowest *FoS* that was predicted is 1.28 at the end of the rainfall for $k_{sat}=10^{-5}$ m/s. This means that if the total rainfall of 240 mm is distributed over 2 h, then the decrease of the *FoS* at the end of the rainfall is very small. If the rainfall is distributed over 4 h (60 mm/h intensity), then the FoS drops to 1.14 at the end of the rainfall. For $k_{sat}=10^{-5}$ m/s the *FoS* of the slope at the end of the 16-h long rainfall with an intensity of 15 mm/h is as low as 0.88. The study revealed that for

moderate and low permeable soils antecedent rainfall has significant impact in reducing the factor of safety and is more potent factor then the major rainfall event triggering landslides, and can severely affect the seepage conditions even if its amount is very small in comparison to the major rainfall. For moderate and low permeable soils, in comparison to the high-intensity rainfalls, antecedent rainfall has significant impact in reducing the factor of safety and is more potent factor than the major rainfall event triggering landslides, and can severely affect the seepage conditions

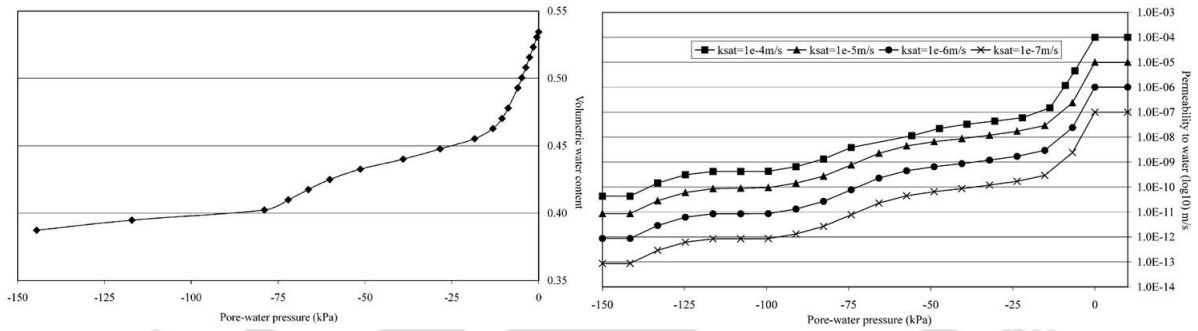

Figure 2.5 (a) Volumetric soil–water characteristic curve (b) Permeability function for different saturated coefficients of permeability (Tsaparas *et al*., 2002)

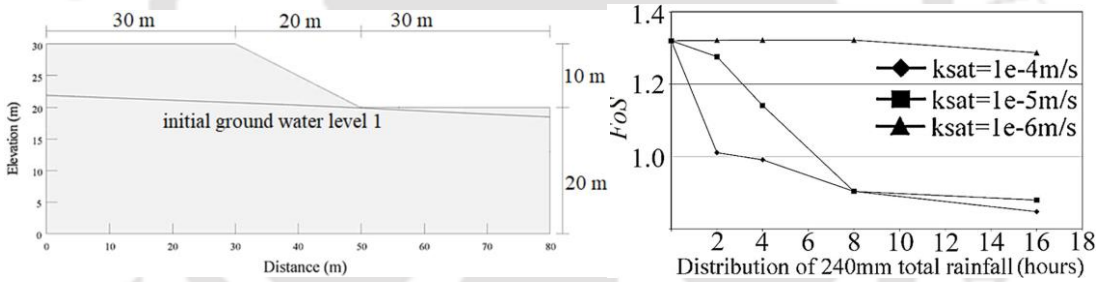

Figure 2.6 (a) Geometry of the homogenous slope used for the numerical analysis; (b) lowest values of the factors of safety for all saturated coefficients of permeability with respect to distributions of 240 mm total rainfall (redrawn after Tsaparas *et al*., 2002)

Tofani *et al*. (2006) investigated one of the documented landslides due to the storm of 20–21 November, 2000, with a return period of 100 years (Figure 2.8a) which triggered over 50 landslides within the province of Pistoia in Tuscany (Italy). Pore-water pressure variations and the effects of these variations on slope stability during the rainfall event were studied by modeling the ground water infiltration process. Figure 2.7 shows the slope geometry, soil water characteristic curve (SWCC) and unsaturated hydraulic conductivity curve (UHCC) for the numerical model representing the Collodi site. For the investigated site, the trend of the factor of safety indicates that the critical time for failure occurs about 18 h after the storm commences (Figure 2.9), and highlights the key role played by the soil permeability and thickness of the wetting band in controlling the response in terms of slope instability. The

study revealed that response of the material involved is largely dependent on its permeability. In high-permeability soils, the build-up and dissipation of positive pore pressures during intense precipitation events could be very rapid, in these cases slope failures are caused by high intensity rainfall and antecedent rainfall has little influence on landslide occurrence. On the contrary, in low-permeability soils slope failures are caused by long duration-moderate intensity rainfall events and the reduction in soil suction and the increase in pore water pressures due to antecedent rainfall is considered a significant and necessary condition for landslide occurrence. It was observed that higher soil permeability coupled with a shallower depth of the impermeable boundary leads to a very rapid response to the storm, causing the formation of a perched water table only 8 h after the rainfall initiation and the subsequent trigger of the slope failure. Figure 2.8(b) shows pore water pressure values at four-time steps along the B^{i}–B^{ii} positioned in the middle of the failure. The groundwater table continues to rise as a consequence of the prolonged contribution of rainfall water from the slope surface, reaching its maximum elevation at step 21, during this step the soil is completely saturated.

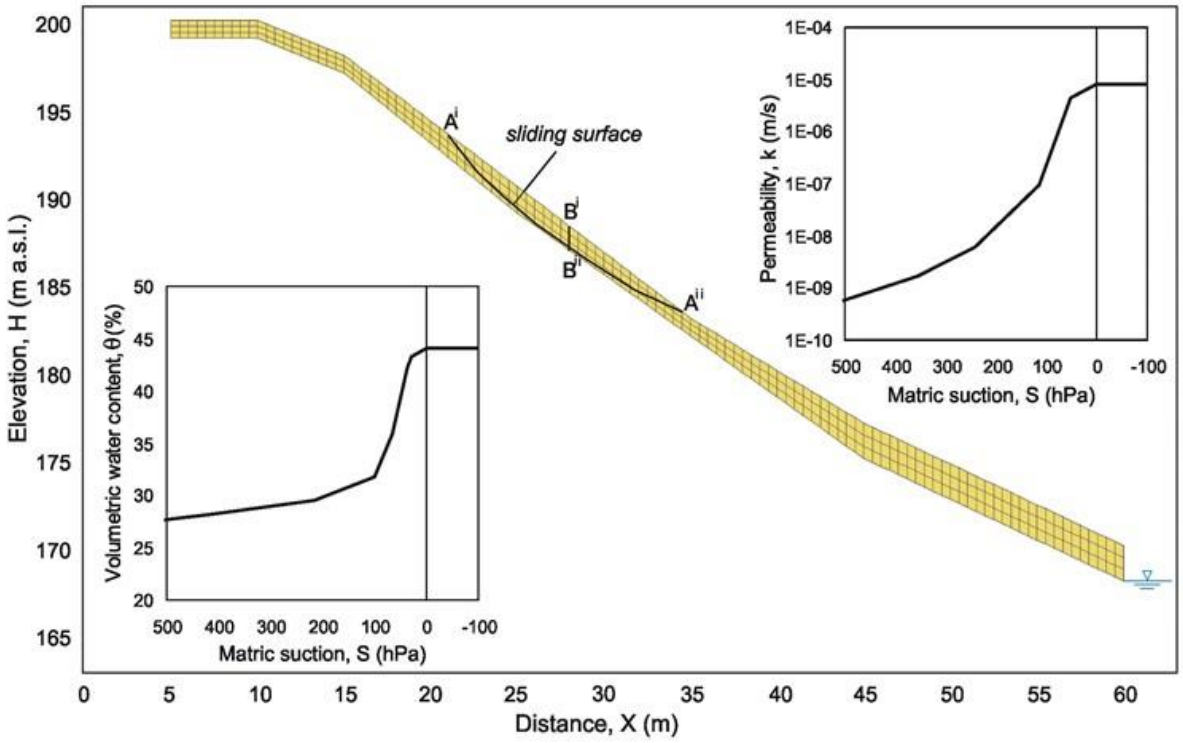

Figure 2.7 Finite element description of slope geometry, SWCC and UHCC for Collodi site (Tofani *et al*., 2006)

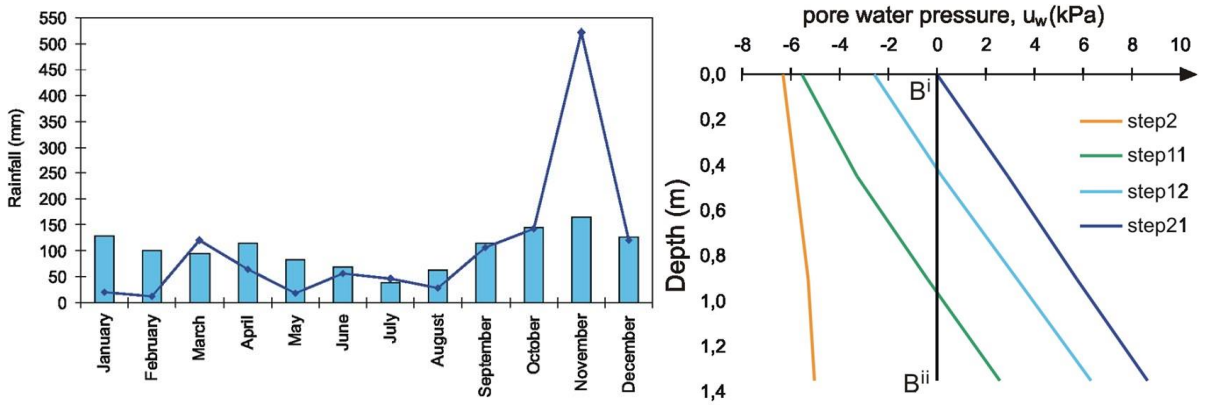

Figure 2.8 (a) Precipitation recorded in Pescia rain gauge station, with bars the mean monthly precipitation from 1970 to 2000, with the line the monthly precipitation in 2000; (b) pore water pressure profile at location B^i–B^{ii} during four time steps (Tofani *et al*., 2006)

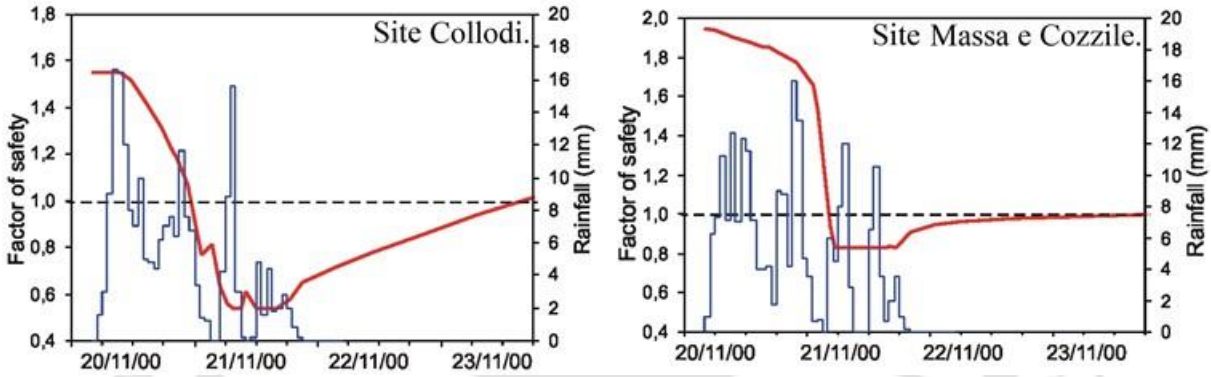

Figure 2.9 Trend of factor of safety and rainfall during November 2000 event (Tofani *et al*., 2006)

Rahardjo *et al*., (2007) conducted parametric studies on a homogeneous slope under various rainfall intensities to investigate the effects of soil parameters, rainfall intensity, initial ground water table location and slope angle and height. Figure 2.10 shows the soil properties considered in the study. Figure 2.11(a) shows the slope geometry. Figure 2.11(b) shows the plots of variation in factor of safety versus elapsed time for a homogeneous soil slope under different rainfall intensities where rainfall intensity was varied as a function of saturated permeability (k_s) of respective soil. They concluded that rainfall intensity and soil properties were the most important factors responsible for slope failures under infiltration conditions. Homogeneous soil slopes with a low saturated coefficient of permeability ($k_s \leq 10^{-6}$ m/s) are safe from short-duration rainfalls ($T_r \leq 24$ h) regardless of the rainfall intensity applied to the slopes. However, the effect of antecedent rainfalls is significant in assessing the instability of homogeneous soil slopes with low k_s ($k_s \leq 10^{-6}$ m/s). For a given rainfall duration, there is a threshold rainfall intensity, beyond which there is not much decrease in the factor of safety. The value of threshold rainfall intensity is proportional to saturated

coefficient of permeability. The effect of slope geometry and initial water table location are secondary in the rainfall-induced slope failures, and only determine the initial factor of safety. The actual failure conditions are mostly controlled by the rainfall applied to the slope and the properties of the soil in the slope. Hence, when dealing with rainfall-induced slope failures, emphasis should be on the rainfall intensity and soil properties, particularly the saturated coefficient of permeability.

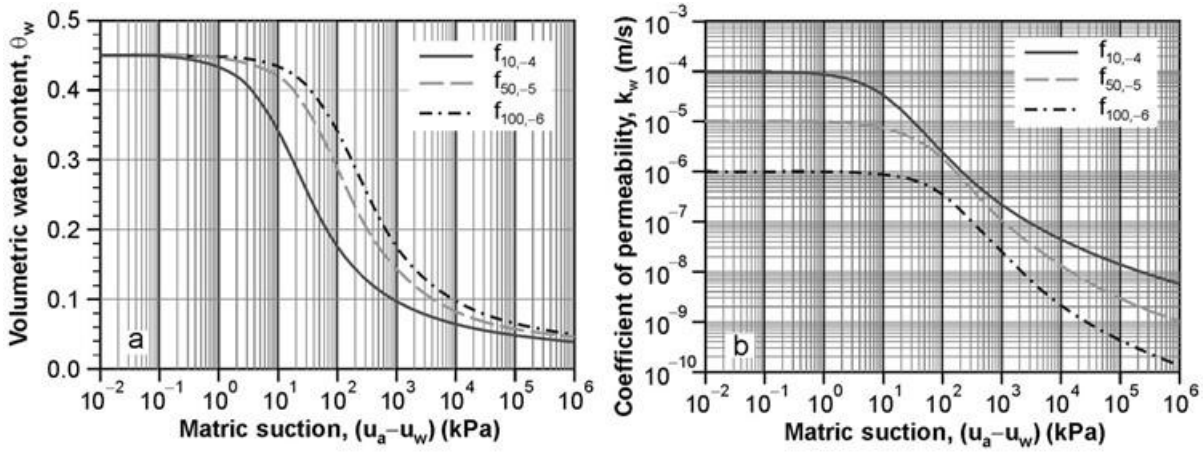

Figure 2.10 Soil-water characteristic curves (a) and permeability functions (b) for three types of soils used in study (Rahardjo *et al*., 2007)

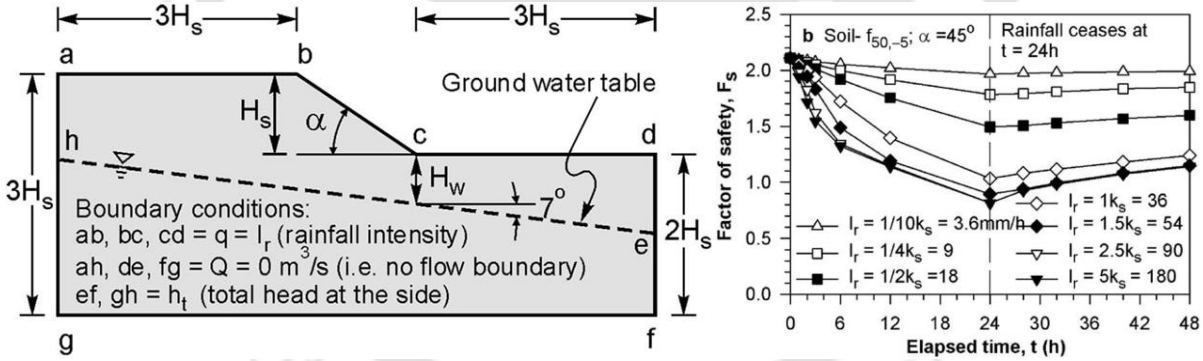

Figure 2.11 (a) Slope geometry and boundary conditions for homogeneous soil slope used in parametric study (b) Effect of rainfall intensity on variation of factor of safety with time for homogeneous soil slope of constant H_s (10 m), H_w (5 m), and α (45°) subjected to rainfall for 24 h with soil $f_{50,-5}$ (Rahardjo *et al*., 2007)

Rahimi *et al*. (2011) performed parametric studies on homogeneous slopes (Figure 2.12) to investigate the influence of rainfall pattern and distribution of antecedent rainfall on slope failures. To study the effect of antecedent rainfall patterns on stability of slopes, two types of soil were considered, vis., high-conductivity (HC) soil and low-conductivity (LC) soil. Figure 2.13 shows the soil water characteristic curve (SWCC) and unsaturated permeability function, of HC and LC soils. The maximum cumulative 5-day rainfall was

found to be 450 mm from the available rainfall data, and then distributed based on the idealized rainfall patterns as shown in Figure 2.14. Figure 2.15 shows the factor of safety of HC and LC slopes under delayed, normal, and advanced rainfall patterns. It was concluded that the soil properties like saturated coefficient of permeability and unsaturated permeability function affected the stability of low permeable soils more than high permeable soils. The decrease in factor of safety with time was controlled by the pattern of antecedent rainfall. Antecedent rainfalls affected the stability of LC soil slope more significantly than HC soil slope. Antecedent rainfalls could cause up to 45% reduction in the factor of safety of LC soil slope and up to 13% reduction in the factor of safety of HC soil slope before the occurrence of major rainfall.

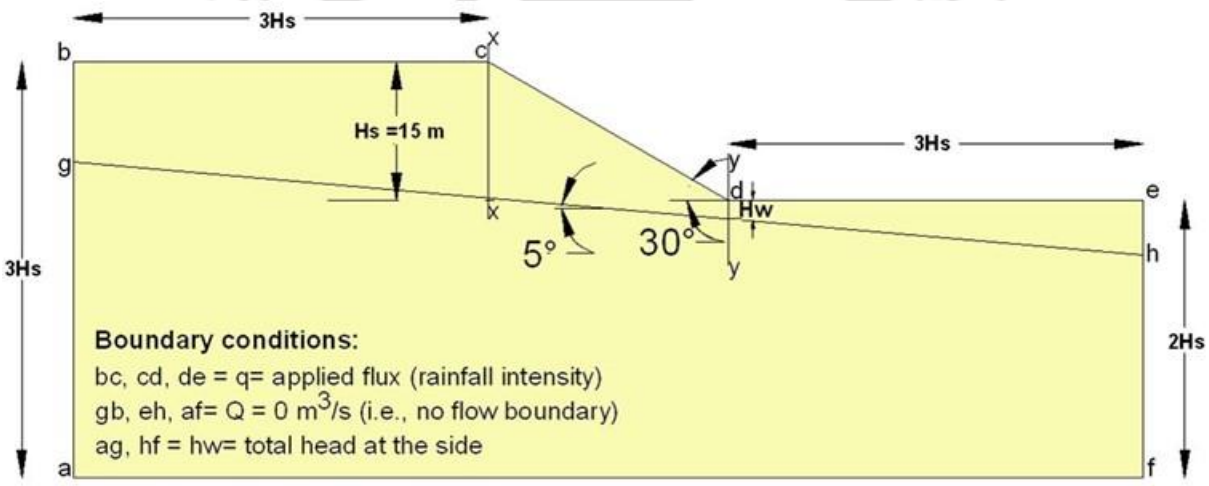

Figure 2.12 Slope geometry and boundary conditions for a homogeneous soil slope (Rahimi *et al.*, 2011)

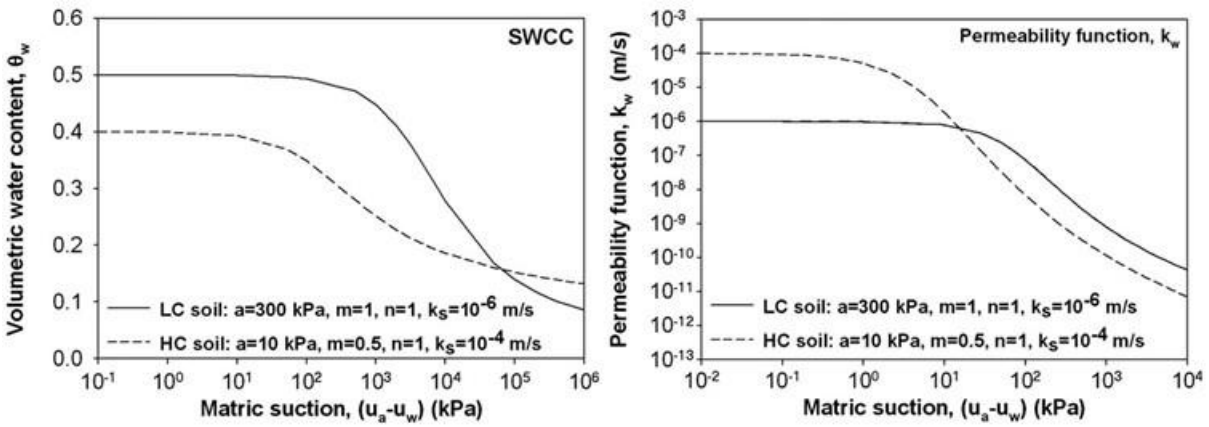

Figure 2.13 SWCC and UHCC of the High Conductivity (HC) and Low Conductivity (LC) soil (Rahimi *et al.*, 2011)

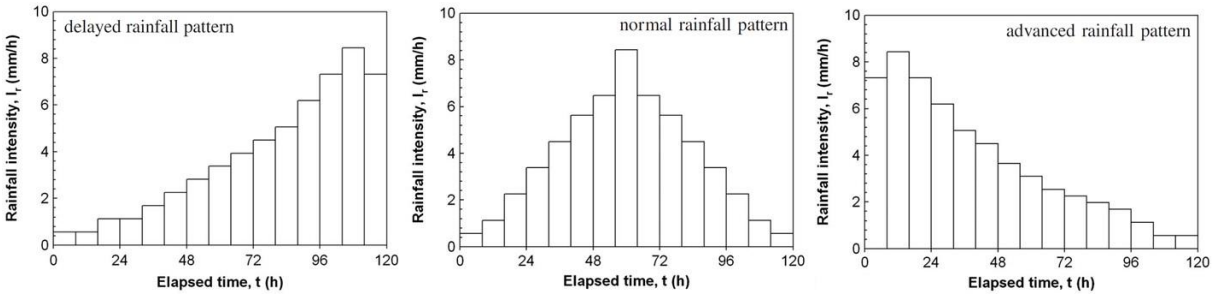

Figure 2.14 Designed rainfall patterns: (a) delayed rainfall pattern; (b) normal rainfall pattern; (c) advanced rainfall pattern (Rahimi *et al*., 2011)

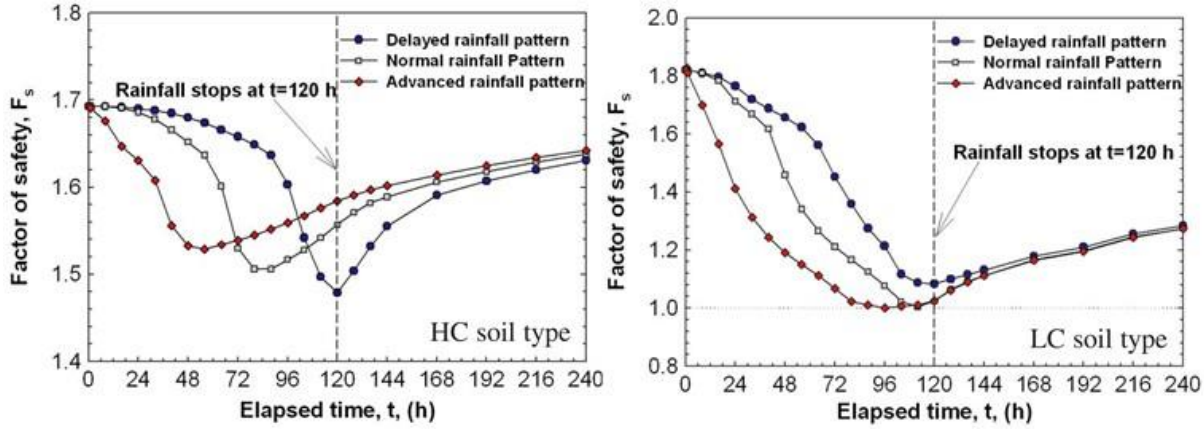

Figure 2.15 Normalized factor of safety, F_{sn}, versus time, t, for various rainfall patterns: (a) HC soil type; (b) LC soil type (Rahimi *et al*., 2011)

Yubonchit *et al*. (2016) conducted parametric studies utilizing the finite element method to investigate the effects of antecedent rainfall, saturated permeability of soil and slope angle on a shallow slope. The model of the slope is depicted in Figure 2.16. Figure 2.17 shows the SWCC, permeability functions and the strength envelopes. The cohesion and friction angle of the soils range from 0.0 to 17.60 kN/m^2 and from 32° to 38.6°, respectively. Figure 2.18(a) presents the pore-water pressure profiles along the depth of a vertical section located at the middle of the slope the pore-water pressure increases and becomes positive due to the rising water table. The researchers concluded that the shallow slope failures occur due to either rise of ground water table or rainfall infiltrating the soil slope. The rising water table after the end of the infiltration stage results in an increase of positive pore-water pressure and hence the loss of shear strength specifically at the interfacial zone of the soil and the bedrock. Figure 2.18(b) presents variations of *FoS* against the simulated rainfall duration to failure. The *FoS* decreases drastically, indicating the slope failure might take place immediately after the rainfall period reaches a critical threshold without any sign of physical response.

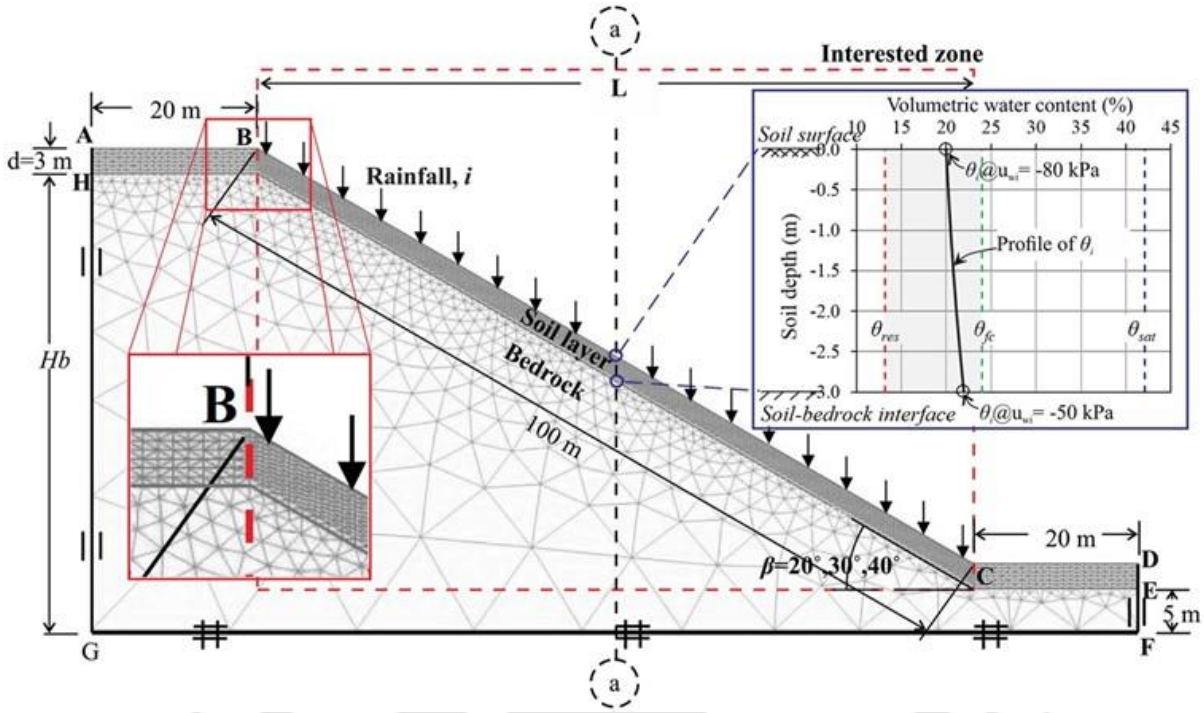

Figure 2.16 Slope geometry and boundary conditions (Yubonchit *et al*., 2016)

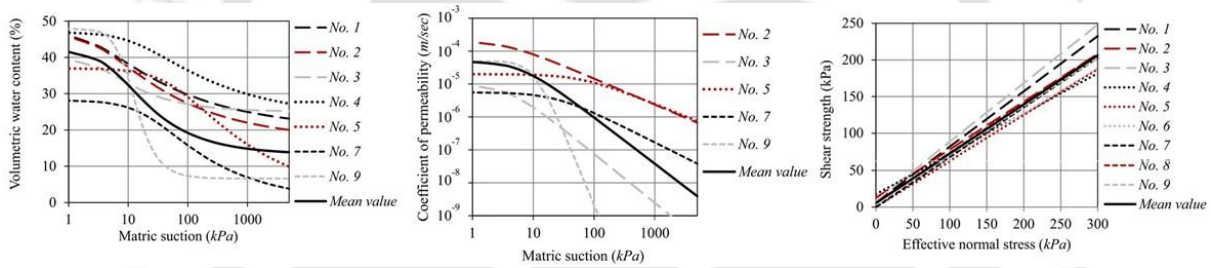

Figure 2.17 Soil properties: (a) SWC curves; (b) permeability functions; (c) shear strength envelopes (Yubonchit *et al*., 2016)

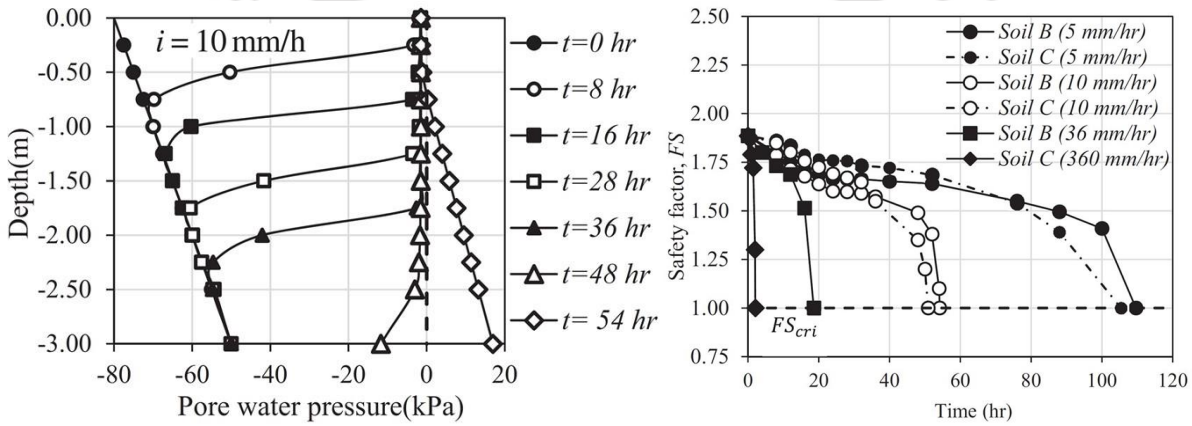

Figure 2.18 (a) Development of pore-water pressure profile in Soil B for rainfall intensity of 10mm/h; (b) Relationship between safety factor and simulated rainfall duration under four constant rainfall intensities and two types of soil with medium (Soil B) and high (Soil C) permeability (Yubonchit *et al*., 2016)

2.7.2. Probabilistic Methods

Li and Lumb (1987) and Elkateb *et al*. (2002) noted that variability depends on multiple causes, including (i) the natural variability in the geotechnical and hydrological properties of the soils, (ii) the inability of determining accurate values for the geotechnical and hydrological parameters, and (iii) the fact that the models are simplified and are incapable of representing the natural (physical) conditions in the study area.

Uncertainty issues are always associated with landslide susceptibility analysis. The parameters required for stability analysis of a landslide are slope geometry, unit weight and shear strength parameters of materials involved, magnitude of pore-water pressures. The basic tool for assessing the stability of a landslide narrows down to slope stability analysis that was mostly developed to assess the stability of constructed earth embankment where, the influencing parameters can be controlled to a much higher degree than a landslide in a natural hill slope (Stark *et. al.*, 2005). Uncertainty issues can arise from many different factors. Soil in a heterogeneous complex deposit and therefore the first factor of uncertainty arises from the determined soil properties. Spatial variation of the soil properties, the randomness of boundary conditions, and the irregularity of topography are some issues that can only be addressed by statistical estimation along with quantified measurements. The second factor of uncertainty arises from the mathematical modeling itself, due to limitations in the ability to model the real world. Mathematical models are constructed based on simplified assumptions about the real process. The uncertainty results due to simplification and factors that may not be contained in the models for their unknown effects. The concept of probability is thereby applied to address such issues (Shen, 2012).

In a deterministic analysis, the *FoS* is defined as the ratio of resisting to driving forces on a potential sliding surface. The slope is considered safe only if the calculated safety factor clearly exceeds one. Whereas, in a probabilistic framework the *FoS* is expressed in terms of its mean value as well as its variance. Reliability analysis is therefore used to assess uncertainties in engineering variables such as the *FoS* of slope stability. Such uncertainty is usually assessed by applying different approaches such as the First-order second-moment (FOSM) method, Point Estimate method, and Monte Carlo simulation method. Several researchers applied a probabilistic approach in analyzing slope stability using the first-order second-moment method (Alonso, 1976; Vanmarcke, 1977 a, b; Christian *et al.*, 1994, Cho, 2007). Recently, a number of applications of probabilistic slope stability studies using other

numerical approaches, such as Monte Carlo simulation have been reported in the literature (Griffiths *et al.*, 2007; Fenton and Griffiths, 2008)

Griffiths *et al*. (2009) presented the analysis of the probability of failure of slopes using both traditional and more advanced probabilistic analysis tools. The advanced method, called the random finite-element method (RFEM), uses elastoplasticity in a finite-element model combined with random field theory in a Monte-Carlo framework. RFEM enables the failure mechanism to seek out the weakest path through the heterogeneous soil mass that can lead to higher probabilities of failure than would be predicted by ignoring spatial variation. Figure 2.19 shows typical failure mechanisms corresponding to different spatial correlation lengths of Θ_{Cu} = 0.2, and a relatively high spatial correlation length of Θ_{Cu} = 2. The dark regions depict higher c_u values meaning higher shear strength while the light depict "weak" soils or lower c_u. Figure 2.20(a) shows the random finite element simulation results giving probability of failure (p_f) of a 1:1 drained slope with *FoS*=1.47 (corresponding to the mean value) and cross correlation (ρ) of 0.5. Figure 2.20(b) shows the critical coefficient of variation υ_{crit} against the spatial correlation length in dimensionless form Θ for different *FoS* values (corresponding to the mean value) for a 2:1 drained slope ρ=0.5. The traditional method, called the first-order reliability method, computes a reliability index that is the shortest distance (in units of directional equivalent standard deviations) from the equivalent mean-value point to the limit state surface and estimates the probability of failure from the reliability index. The study showed that simplified probabilistic analyses in which spatial variability of soil properties is not properly accounted for, could lead to unconservative estimates of the probability of failure if the coefficient of variation of the shear strength parameters exceeds a critical value (υ_{crit}).

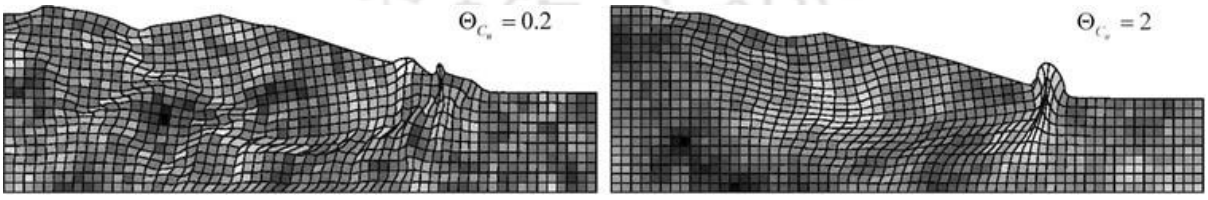

Figure 2.19 Influence of the spatial correlation length in RFEM analysis (Griffiths *et al*., 2009)

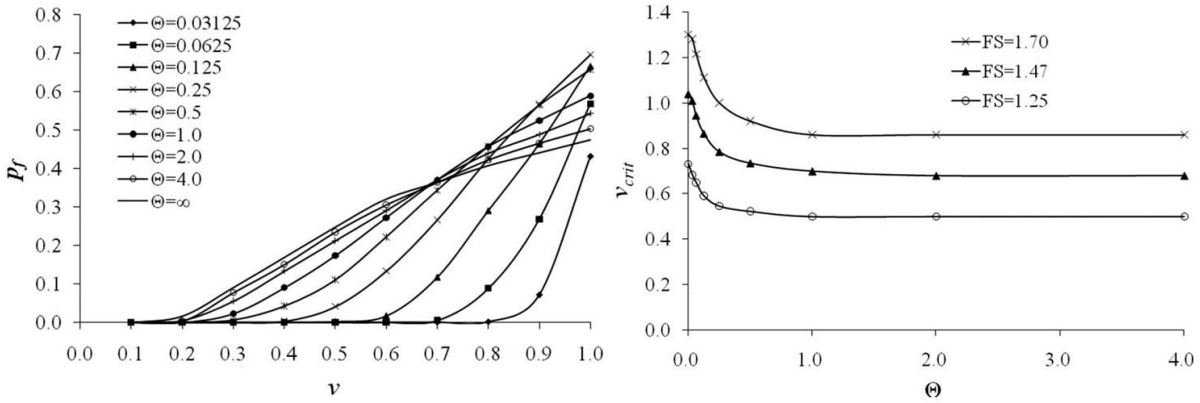

Figure 2.20 (a) RFEM results giving p_f of a 1:1 drained slope with *FoS*=1.47 (based on the means) ρ=0.5 (b) υ_{crit} vs Θ for different *FoS* values (based on the means) for a 2:1 drained slope ρ=0.5 (Griffiths *et al.*, 2009)

Suchomel and Masin (2010) compared three probabilistic methods for calculation of slope stability using a well-documented case study of the slope failure in the Lodalen, Norway. A finite element method considering spatial random fields of uncorrelated parameters *c* (cohesion) and φ (friction angle) is compared with (FOSM) methods. Figure 2.21 shows a typical random field distribution for the case θ = 10 m. Figure 2.22(a) shows the evaluation of the probability of failure for θ = 10 m based on results of 250 Monte-Carlo realizations. The researchers showed that the density function could be fitted to Gaussian distribution. Figure 2.22(b) plots the probability of failure as a function of correlation lengths θ. The study showed that the FOSM method leads to different values of probability of failure as compared to the RFEM method. Several limitations of the FOSM method for calculating probability of a slope failure are identified. The researchers concluded that this is caused by the fact that the equivalent statistical distributions of soil properties, which effectively control the stability of a slope, are significantly different as compared to the original statistical distributions, which are used as an input into the basic FOSM simulations.

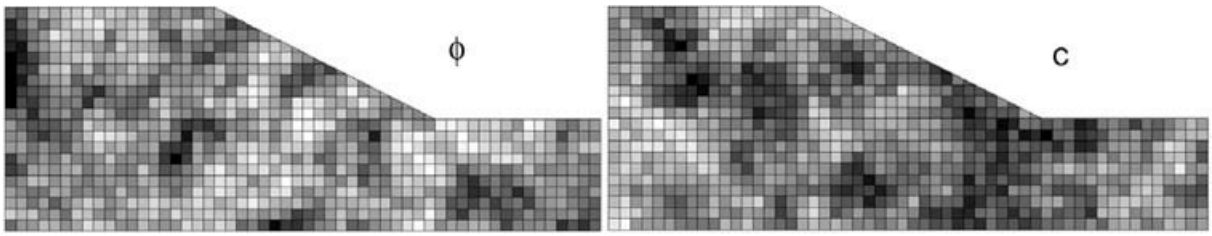

Figure 2.21 Typical realization of random fields of uncorrelated variables φ and *c* for θ = 10m (Suchomel and Masin, 2010)

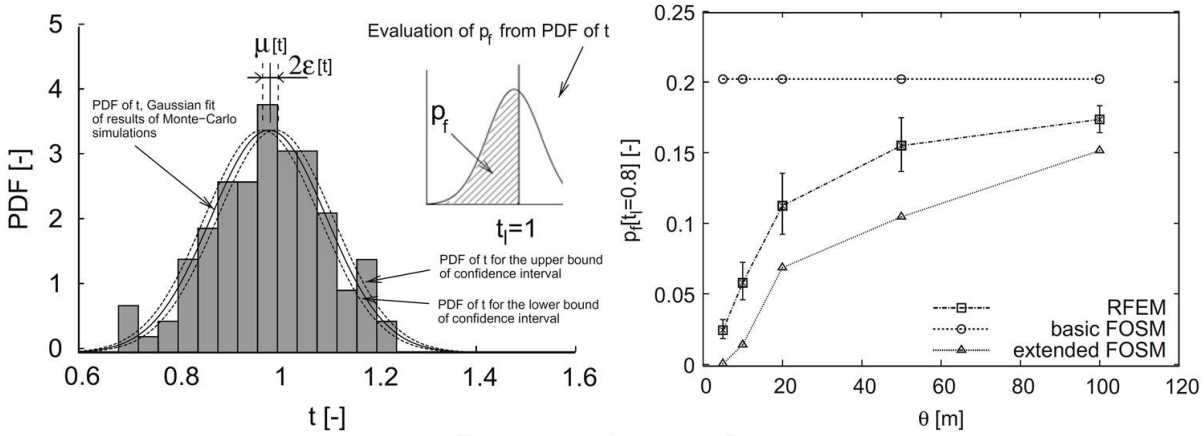

Figure 2.22 (a) Evaluation of the probability of failure for θ = 10 m based on results of 250 Monte-Carlo realizations; (b) Probability of failure as a function of correlation lengths θ (Suchomel and Masin, 2010)

Srivastava *et al.* (2010) modelled the spatial variability of soil permeability parameters using random field theory. The parameter is considered spatially correlated log-normally distributed random variable and its influence on the steady state seepage flow and on the slope stability analysis are studied. The study investigated the influence of coefficient of spatial variation of permeability parameter for different soil slopes as well as effect of change in the mean value of permeability properties and its variations on the stability of the given slope. Figure 2.23(a) shows the permeability parameter modelled as a random field and the values distributed across the slope. Figure 2.23(b) shows the results of the stability analysis of the given soil slope (1 V: 1.5 H, height = 5.0 m) for spatially varying permeability parameters [correlation distance = 0.5 m]. The figure shows the influence of coefficients of variation (CoV %) and change in the mean value of permeability property on the stability of the given slope. The mean factor of safety increases with a decrease in the mean value of permeability parameter for a particular value of CoV.

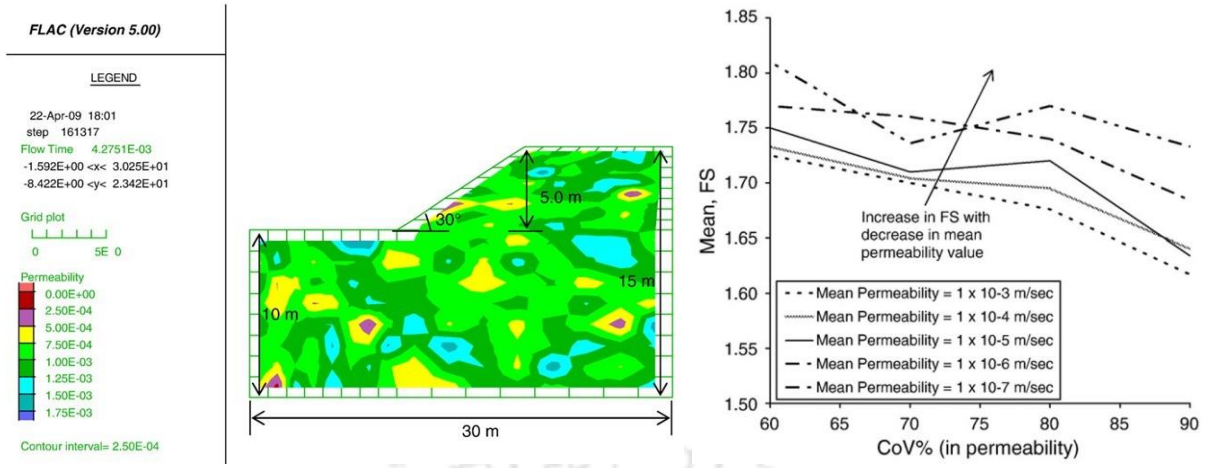

Figure 2.23 (a) Numerical modelling of spatially variable permeability (m/s) parameter; (b) Influence of variation in mean value of spatially variable permeability on the stability of the given slope (1 V: 1.5 H) under steady state seepage conditions (Srivastava *et al*., 2010)

Griffiths *et al*. (2011) described a methodology in which parameters such as the soil strength, slope geometry and pore pressures, are generated using random field theory. Figure 2.24(a) shows a typical infinite slope as a column split into 100 equal slices parallel to slope surface and a 1-d random field of the required property is assigned to each slice. Figure 2.25 shows the computed probability density plots of *FoS* values for two different cases of coefficients of variation given by υ_{cu} = 0.1 and υ_{cu} = 0.5. Also included in the figures are the analytical normal and lognormal fits to the *FoS* distributions based on the computed mean and standard deviation values. Figure 2.24(b) shows the results of the random field analyses compared with FORM for a range of correlation lengths. The study showed that analytical methods (e.g. FOSM and FORM) applied to the infinite slope problem gave very similar results to each other, but inevitably underestimated the probability of failure compared with the random field analyses, because the failure plane in those cases is always assumed constant at a particular depth. Probabilistic slope stability methods that predefine the potential failure surface using deterministic methods are liable to overestimate the factor of safety or underestimate the probability of failure. The researchers concluded that the random field results converged on the first order values as the spatial correlation length was increased, because as the spatial correlation length increases, the greater homogeneity of the soil column means that the probability of the critical mechanism occurring above the base is reduced.

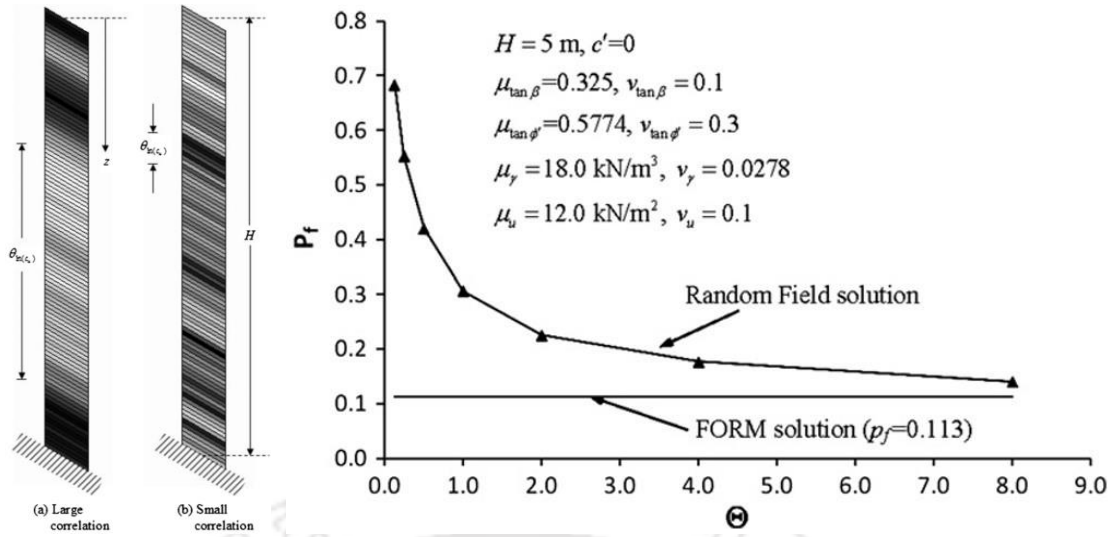

Figure 2.24 (a) Typical random fields of c_u with large and small spatial correlation (b) Comparison of FORM and Random Field results showing the influence of the spatial correlation length Θ (log normally distributed tan φ') (Griffiths *et al*., 2011)

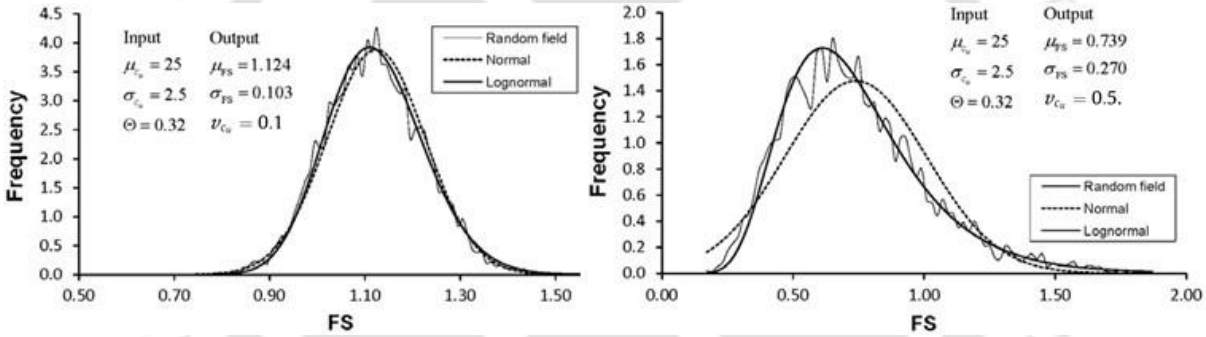

Figure 2.25 Histogram of *FoS* frequency distribution for normal and lognormal fits based on the computed mean and standard deviation (Griffiths *et al*., 2011)

Cho (2014) conducted a series of seepage and stability analyses of an infinite slope based on one-dimensional random fields to study the effects of uncertainty due to the spatial heterogeneity of hydraulic conductivity on the failure of unsaturated slopes due to rainfall infiltration. Figure 2.27(a) shows the infinite slope model with shallow impermeable layer. Figure 2.26 shows the soil–water characteristic curve and the hydraulic conductivity function of a typical weathered granite soil, sampled in Seochang, used for in the study. Probabilistic stability analyses were conducted for a weathered residual soil slope with shallow impermeable bedrock to study the failure mechanism of rainfall-related landslides. Figure 2.28(a) shows the pore pressure and the, (b) variance of the factor of safety with propagation of the wetting front. Figure 2.27(b) shows the influence of the autocorrelation length of lnk_s in the vertical direction (*lv*) and the coefficient of variation (COV$_{ks}$) on the estimated

probability of failure for slope stability after 24 hours. The study showed that a probabilistic framework could be used to consider efficiently various failure patterns caused by spatial variability of hydraulic conductivity in rainfall infiltration assessment for a shallow infinite slope. It was observed from the study, if the duration of rainfall is sufficient, majority of the failure surfaces forms at the interface of the impermeable bedrock, irrespective of the random distribution of soil properties.

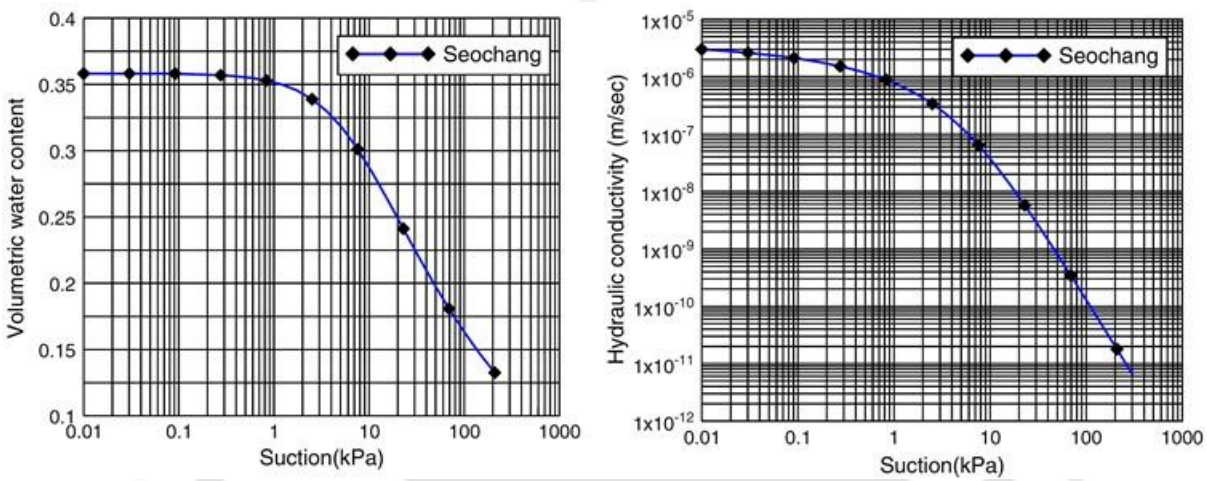

Figure 2.26 Hydraulic properties for analysis: (a) Soil–water characteristic curve; (b) Hydraulic conductivity function (Cho, 2014)

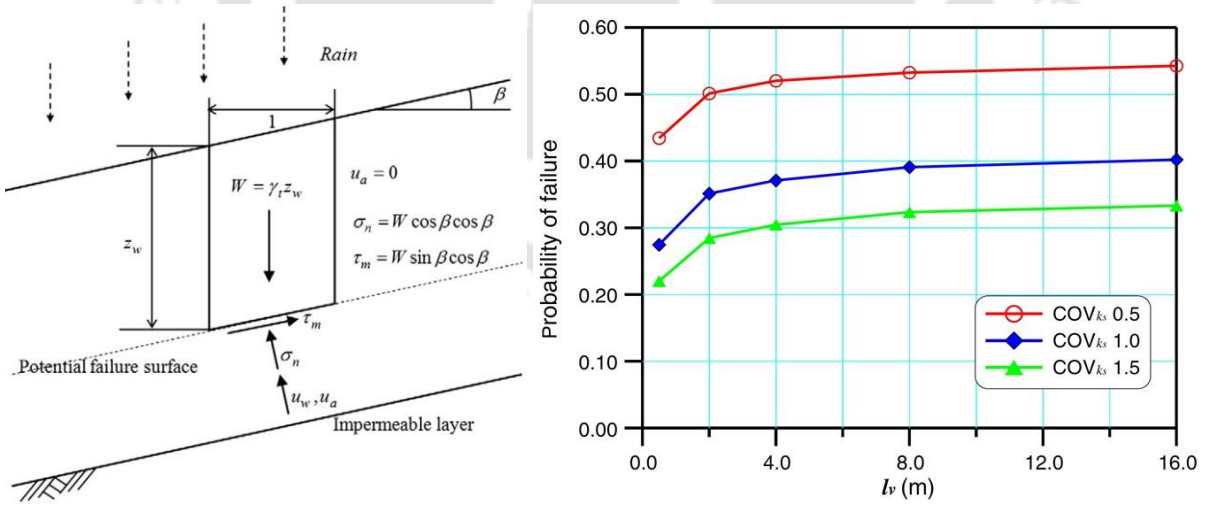

Figure 2.27 (a) Stability analysis of an infinite slope with shallow impermeable layer; (b) Influence of the *lv* and COV$_{ks}$ on the estimated probability of failure for slope stability after 24 h (Cho, 2014)

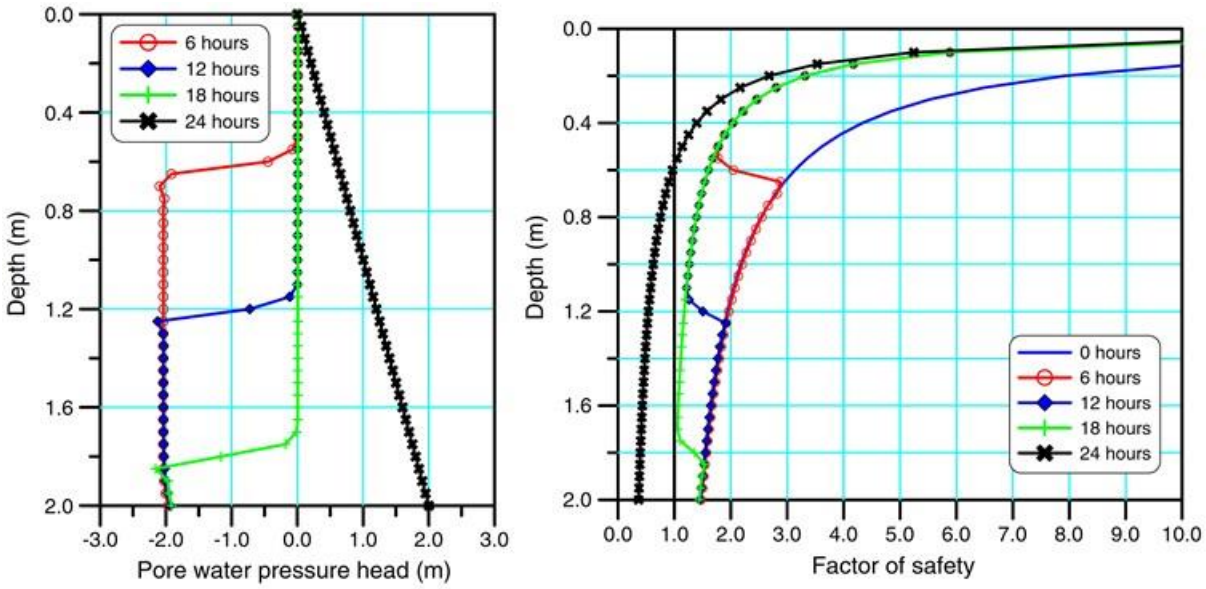

Figure 2.28 (a) Pore pressure head profiles (b) Variance of the factor of safety with propagation of the wetting front (Cho, 2014)

Ering and Babu (2016) presented a methodology to back-analyze the Malin landslide occurrence to identify the mechanisms responsible for landslide initiation. Bayesian analysis is employed for the back analysis. The input parameters are considered as random variables in the analysis and are described by their probability distributions. The input parameters were updated based on the simulated slope behavior. Figure 2.29(a) shows the rainfall data recorded from different rain gauge stations located around Malin from 22 July to 30 July 2014. Figure 2.29(b) shows the soil water characteristic curve used in the analysis. Figure 2.30(a) shows the changes in *FoS* due to rainfall infiltration since the initial state of the slope where time t = 0 corresponds to 1st June and t = 60 corresponds to 30th July. Figure 2.30(b) shows the state of slope after the rainfall event. The researchers concluded that antecedent rainfall contributed in decreasing the factor of safety of the slope, but the low intensity and long duration rainfall infiltration was not sufficient to cause slope instability, it was high intensity and short duration rainfall infiltration at the end that triggered the slope failure. It is important to consider the uncertainties of soil parameters, pore pressures, field observations and that of method of analysis.

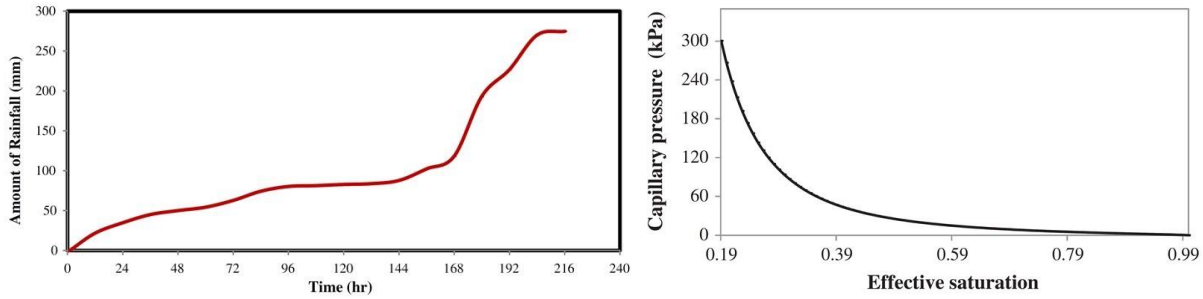

Figure 2.29 (a) Rainfall data; (b) Capillary pressure versus effective saturation (Ering and Sivakumar Babu, 2016)

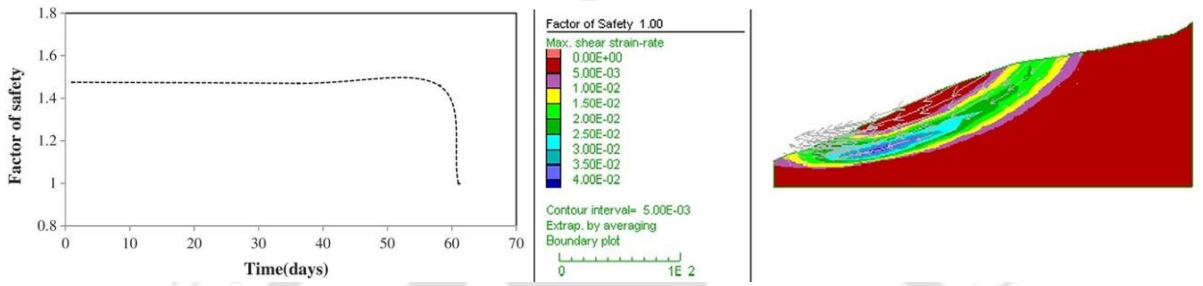

Figure 2.30 (a) Factor of safety with time (b) Slope after triggering rainfall infiltration (Ering and Sivakumar Babu, 2016)

2.8. REGIONAL SCALE LANDSLIDE ANALYSIS

The basis for landslide hazard zonation is the fact that the conditions and processes that promote instabilities can be identified. The relative contribution of some significant factors can then often be rated and weighed in qualitative or semi-quantitative manner. This makes it possible to estimate their effects in a given area and thus be mapped and correlated with each other and with past failures for the prediction of future landslide occurrence (Varnes, 1984).

Several approaches for Landslide Susceptibility Zonation (LSZ) mapping have been proposed that can be grouped into two broad categories, namely qualitative and quantitative respectively (Soeters and Van Westen, 1996; Glade and Crozier, 2005). Soeters and Van Westen (1996) distinguished between four distinct approaches for regional landslide analysis, i.e. inventory-based, heuristic, statistic and deterministic approaches. Landslide inventory allow for detailed analyses of landslide distribution and form the basis for regional modelling of landslide susceptibility, hazard and risk. Heuristic methods integrate the knowledge and experience of geomorphological and geotechnical experts to derive a regional map of landslide susceptibility and hazard.

Statistical methods are the most frequently applied method to model regional landslide susceptibility and hazard, and to predict future slope failures where, a statistical relationship between possible landslide causative factors and the presence of existing landslides is established, and used for prediction of future landslide by spatial interpolation. Statistical methods have long been applied for susceptibility analysis of rainfall-induced shallow landslides (Carrara *et al*., 1991; Bai *et al*., 2009; Cervi *et al*., 2010; Li *et al*., 2012). Reichenbach *et al*. (2018) provided a list of statistical methods, of which the most frequently applied are bivariate regression, multiple regression, discriminant analyses, logistic regression and neural networks, along with an extensive critical review of statistical methods for landslide susceptibility modelling and associated terrain zonation. The most common statistical classification methods for susceptibility assessment were observed to be, logistic regression, neural network analysis, data-overlay, index-based and weight of evidence analyses, with a preference towards machine learning methods in recent years. The researchers concluded that no particular method could be singled out over the other.

Regional deterministic models apply physically-based simulations to assess landslide susceptibility expressed as *FoS*, and quantitatively represent the landslide processes (Carrara *et al*., 1992). Physically based models (or geotechnical slope models) consider the in-situ conditions and mechanical properties of the soils, thus providing a hydrogeological and geotechnical perspective to the subject within a GIS framework, and are capable of providing detailed description of potential instability under changing environmental and climatic conditions. Cascini (2008) concluded that physically based models are most appropriate for areas ranging from 10 to 1000 sq. km. Zoning methodology employing physically based models is likely to yield better results for large scale (1:25,000 to 1:5000) application.

2.8.1. Landslide Susceptibility

Dai *et al*. (2002) defined that the term ‘susceptibility’ is applied to maps that present a quantitative or qualitative assessment of landslide classification, velocity, volume and area, and spatial distribution of landslides which exist or potentially may occur in an area including a description of the intensity of the existing or potential landsliding.

Fell *et al*. (2008) noted landslide susceptibility zoning involves the spatial distribution of existing and potential landslides that could occur within the study area. It may also include the classification and description of the magnitude (area or volume), travel distance, velocity and intensity of the existing or potential landslide. Landslide susceptibility zoning usually

involves developing an inventory of landslides that have occurred in the past together with an assessment of the areas with a potential to experience landslides in the future, but with no assessment of the temporal probability of the occurrence of landslides.

2.8.2. Landslide Hazard

Varnes (1984) defined hazard as the probability of occurrence of a potentially damaging phenomenon within a specified period of time and within a given area.

Fell *et al*. (2008) distinguished landslide hazard from landslide susceptibility and defined that landslide hazard indicates those areas that are, or could be, affected by landslides, assessing the probability of such landslides occurring within a specific period of time, with the potential for causing an undesirable consequence.

Landslide hazard zoning applies the conclusions of landslide susceptibility mapping and assigns a temporal probability measure to the potential landslide activity. Landslide hazard therefore refers to the probability of a landslide of a given size occurring within a specified period of time within a particular area.

2.8.3. GIS for Landslide Analysis

The Geographic Information System (GIS) provides strong functionality in both geostatistical analysis and database processing. In addition, the extension of the methodology to include analysis of a slope failure can be performed easily and effectively using physically based models within a GIS framework. Deterministic Models provide detailed description of potential instability under changing environmental and climatic conditions. Several authors have developed GIS models by coupling a dynamic hydrological model that simulates the pore pressure over time with a slope stability model that quantifies the susceptibility at the critical pore pressure threshold.

2.8.4. Physically–based Models for Landslide Analysis

Several physically based models have been developed such as, Shallow Landslide Stability Model (SHALSTAB) (Montgomery and Dietrich, 1994), Stability Index Mapping (SINMAP) (Pack *et al*., 1998), Probability of Stability PC Raster GIS package (PROBSTAB) (Van Beek and Van Asch, 2004), Transient Rainfall Infiltration and Grid based Regional Slope-stability (TRIGRS) (Baum *et al*., 2002; Savage *et al*., 2004), SLIP (Montrasio and Valentino, 2008; Montrasio *et al*., 2012).

TRIGRS (Transient Rainfall Infiltration and Grid based Regional Slope-stability) is widely used due to its ability of computing transient pore-pressure changes and changes in the factor of safety as response to complex rainfall event (Baum et al., 2002; Savage et al., 2004, Salciarini *et al*., 2006; Salciarini *et al*., 2008; Sorbino *et al*., 2010; Kim *et al*., 2010; Park *et al*., 2013; Saadatkhah *et al*., 2014; Schilirò *et al*., 2015)

Salciarini *et al*. (2006) modelled the rainfall-induced initiation of shallow landslides over an area in the eastern Umbria Region of central Italy with the application of TRIGRS. Input data for the TRIGRS model include time-varying rainfall, topographic slope, colluvium thickness, initial water table depth, and material strength and hydraulic properties. A DEM of the study area was created for this application using the available regional topography of 1:5,000 scale with 5-m contour intervals. The Topogrid function in Arc Info GIS was used to create grids with 5-m cells and to quantify slope gradient, aspect, upslope contributing area, and elevation for each cell of the DEM. No corrective measures were applied to remove the sources of error in the DEM. Figure 2.32(a) shows the shaded relief maps of the study area along with the location of shallow landslides from the Italian Council for National Research (CNR) inventory as blue dots; Figure 2.31(a) shows the Slope map of the study area. The depth of basal boundary is considered as an exponential relation of the slope angle α (Figure 2.31(b)). Because of a paucity of input data, parametric analyses were done to calibrate and test the model and show the effect of variation in material properties and initial water table conditions on the distribution of simulated instability in the study area in response to realistic rainfall. Figure 2.32(b) shows the TRIGRS results with one set of soil property over the region. Areas shown in red are simulated to be unstable (FS≤1.0) after 16 h of rainfall. Despite the paucity of input data more than 80%, agreement between predicted shallow landslide susceptibility and the inventory was observed. From the simulation outcome, the researchers concluded that the minimum data set should comprise a high-resolution digital elevation model. Second, a previous rainfall history for a known landslide event is required. Third, TRIGRS requires a known spatial distribution of the depth of the lower impervious boundary and of the initial water table. The analysis demonstrated that reasonable approximations or estimates of soil thicknesses and initial water table heights, based on a limited number of measurements in the study area, could produce satisfactory results.

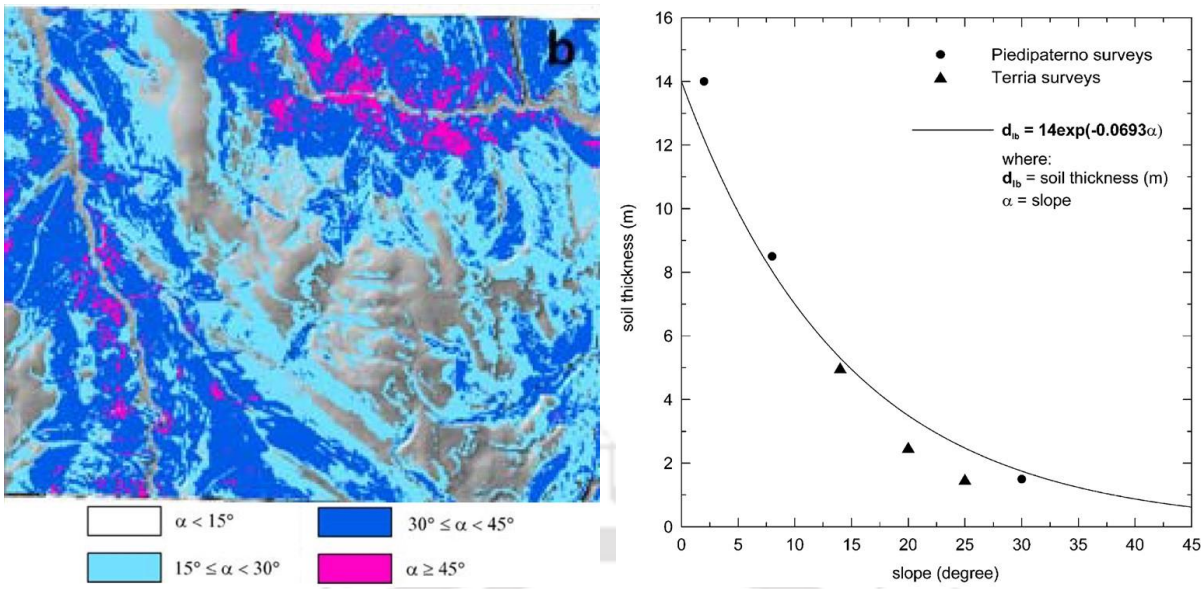

Figure 2.31 (a) Slope map of the study area; (b) Exponential soil thickness model (Salciarini *et al*., 2006)

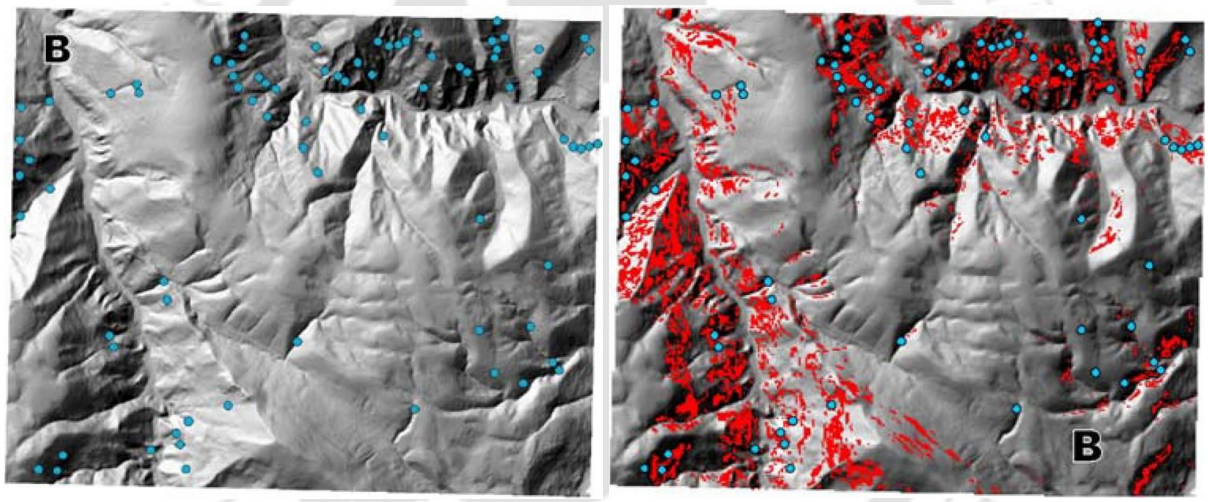

Figure 2.32 (a) Shaded relief maps of the study area. Blue dots indicate the location of shallow landslides from the CNR inventory (b) TRIGRS results with one set of soil property. Areas shown in red are simulated to be unstable (FS≤1.0) after 16 h of rainfall (Salciarini *et al*., 2006)

Godt *et al*. (2008) presented the application of TRIGRS over a study area north of Seattle, Washington. Rainfall information were adopted from previously defined empirical rainfall intensity–duration threshold and material strength and hydraulic properties were measured both in the field and laboratory. Topographic information was derived from high-resolution (1.8 m) LiDAR data. Pore-pressures and factors of safety are computed on a cell-by-cell basis. Figure 2.33 compares the results from the TRIGRS model that accounts for the transient effects of rainfall infiltration on pressure head with results from a static infinite-

slope analysis assuming two water-table conditions, keeping other factors constant between the three analyses. TRIGRS analysis results were presented corresponding to the rainfall intensity and duration known to trigger shallow landslides in the study area. Results were validated by comparison with a shallow landslide inventory, using the Receiver Operating Characteristics (ROC). Receiver Operating Characteristics (ROC) is a technique to assess the performance of models, by way of comparisons, for which results can be assigned to two classes or states. For slope stability models, the states or classes can be stable (i.e., FoS ≥ 1.0) or unstable (i.e., FoS < 1.0). Comparing the results of grid-based slope stability predictions models with that of a landslide inventory, four outcomes are possible for each grid cell. If the grid cell is modelled to be unstable and is coincident with a mapped landslide in the inventory, it is counted as a true positive; if it falls outside a mapped landslide, it is counted as a false positive. If the grid cell is modelled to be stable and it falls outside a mapped slide, it is counted as a true negative; if it falls within a mapped slide, it is counted as a false negative. The comparison counts can be entered in a 2×2 contingency table that is the confusion matrix. Figure 2.34(a) shows the confusion matrix for calculation of ROC. The true positive rate is the ratio of the number of true positives to the total number of positives (landslide cells). The false positive rate is ratio of the number of false positives to the total number of negatives (non-landslide cells). Figure 2.34(b) plot the ROC comparing the results from each of the three models. The study showed that with simple assumptions of slope dependent boundary and initial conditions and material strength and hydraulic properties for hillside materials measured in the field and laboratory, yielded an improved spatial prediction of shallow landslide occurrence. The simulation outcome showed that the spatial and temporal accuracy of the shallow landslide susceptibility model could be further improved with accurate characterization of the initial and boundary conditions and spatial distribution of material properties. Incorporation of the effects of the unsaturated zone on infiltration and slope stability will further the accuracy of the analysis.

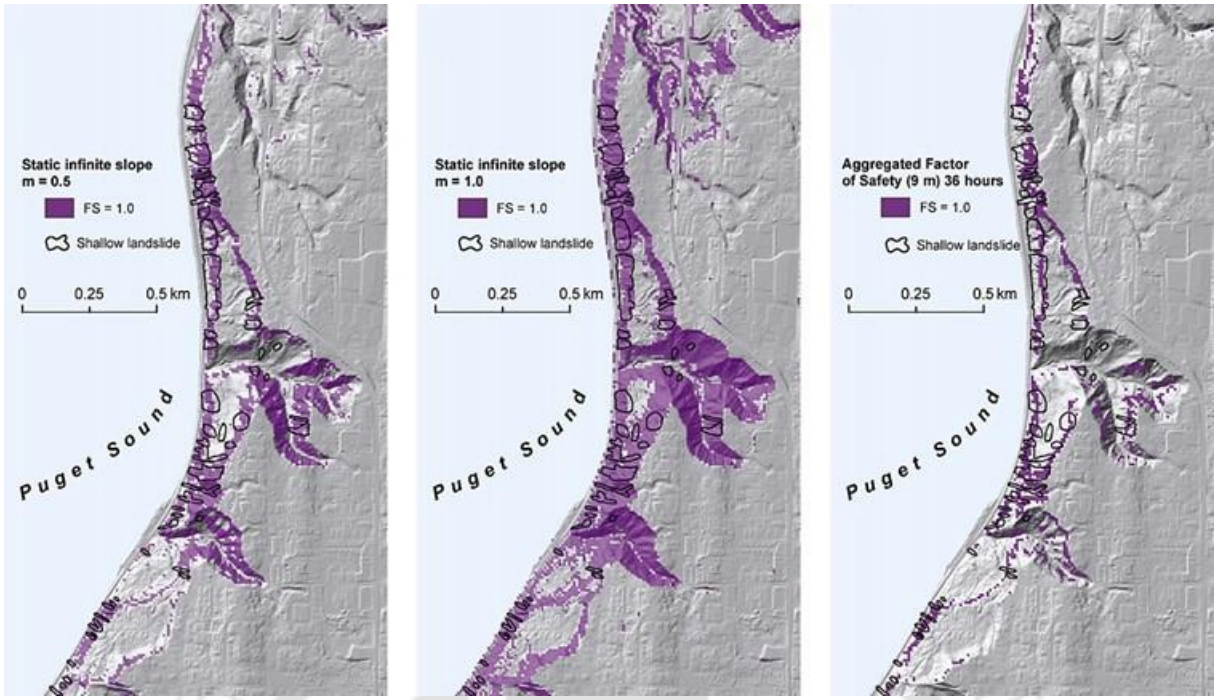

Figure 2.33 Extent of unstable area for static infinite-slope stability calculation assuming the water-table depth is half the depth to the lower boundary (A) (m=0.5), at the ground surface (m=1.0) (B), and for the transient solution in the TRIGRS model after 36 h of rainfall (Godt *et al*., 2008)

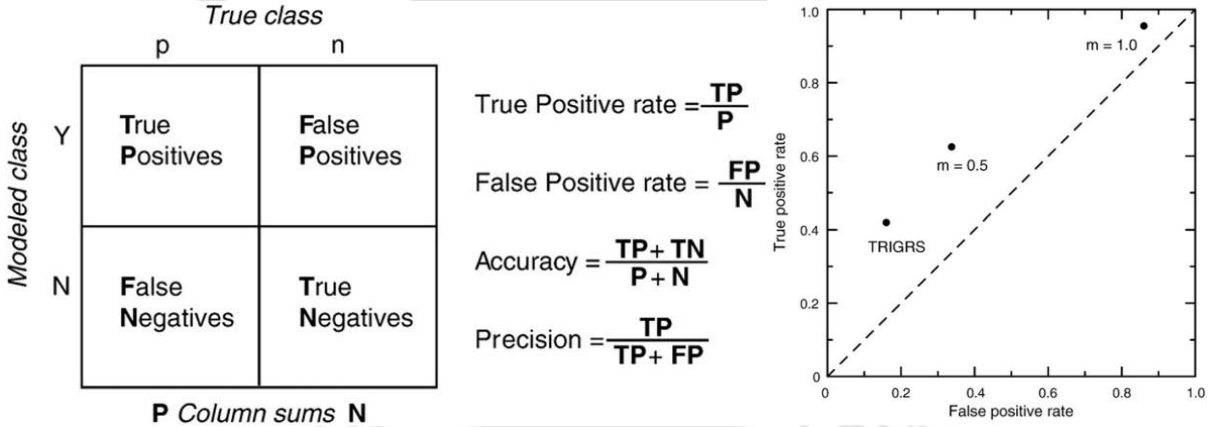

Figure 2.34 (a) Confusion matrix for calculation of ROC (b) ROC graph comparing the results from each of the three models. Grid cells with slopes ≤15° were excluded from the analysis (Godt *et al*., 2008)

Salciarini *et al*. (2008) presented results to demonstrate how a transient infiltration model coupled with an infinite slope stability calculation may be used to assess shallow landslide frequency in the City of Seattle, Washington, USA. For estimating deterministic rainfall threshold, TRIGRS analysis is combined with a statistical treatment of rainfall using a GEV (General Extreme Value) probabilistic distribution to produce maps showing the shallow landslide recurrence induced, on a spatially distributed basis, as a function of rainfall

intensity-duration and hillslope characteristics. Figure 2.35(a) shows the intensity-duration-frequency curves for the Seattle–Tacoma rain gauge. The rainfall events obtained using a GEV probability distribution were applied into the model and the results analysed to give shallow landslide occurrence as a function of rainfall recurrence time. Figure 2.36 shows the results obtained from TRIGRS for a rainfall duration of 24 h, a typical duration of triggering rainfall in Seattle. The cells classified as unstable from the model are subdivided into different categories, based on the estimated recurrence intervals. The cells with the most prolonged recurrence period, RI=100 years are shown in blue; the areas with higher frequency of destabilization are shown in green, yellow and red zones. Figure 2.35(a) shows the effect of increasing recurrence interval on the extent of potential instability. The study showed that the model is feasible for cases where failures occur after prolonged rainfall. The researchers' notes that thresholds that predict the occurrence of landslides from storms that have short return periods are exceeded by many storms that do not produce landslides. In other words, thresholds for short-return-period storms over predict, or, exceedance of such thresholds corresponds to a low probability of landslide occurrence. Thresholds for long-return-period storms are exceeded by fewer storms and a larger percentage of those storms produce landslides.

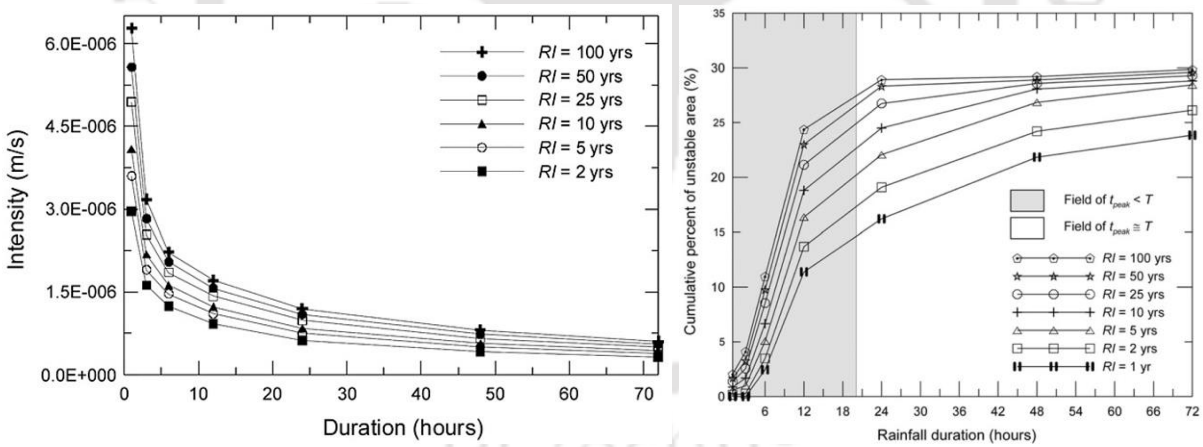

Figure 2.35 (a) Intensity duration frequency curves for the Seattle–Tacoma rain gauge (b) Variation of the cumulative percentage of unstable cells in the study area with rainfall durations for differing recurrence intervals (Salciarini *et al*., 2008)

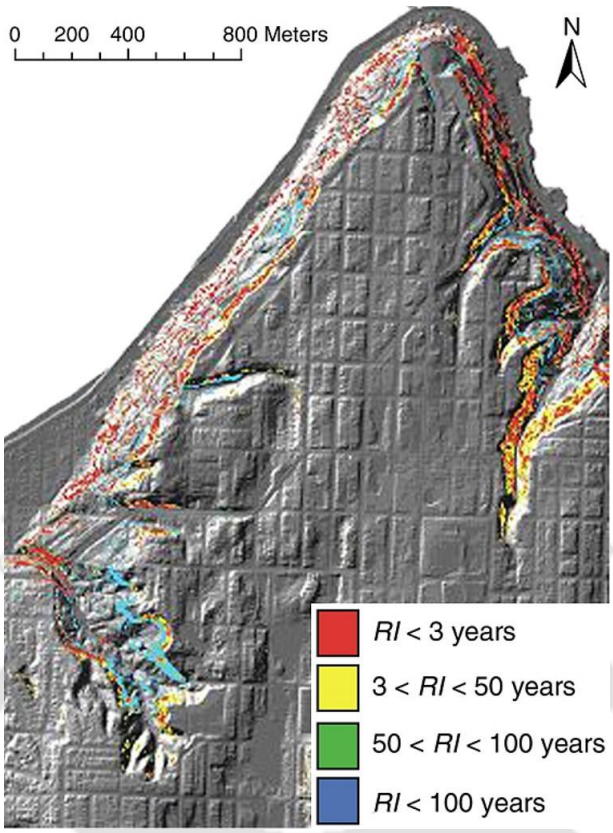

Figure 2.36 Maps showing shallow landslides predicted by TRIGRS for Critical Rainfall Frequency (Salciarini *et al*., 2008)

Sorbino *et al*. (2010) presented the analysis of the rainfall-induced shallow landslide phenomena involving volcanoclastic soils, which occurred in May 1998 inside an area of about 60 km^2 in the Campania Region in southern Italy. Physically based models, SHALSTAB and TRIGRS, that are able to analyse stability conditions using information about in situ conditions and mechanical properties of the involved soils are used for the analysis. The application is based on an extensive data set of topographical, geomorphological and hydrogeological features of the affected area, as well as on both stratigraphic settings and mechanical properties of the involved soils. The input parameters of the models were chosen through the available dataset and indirect analyses. Figure 2.37(a) shows the mapped shallow landslides and debris flow that occurred on 5–6 May 1998 around the Pizzo d'Alvano massif. Figure 2.37(b) shows the daily rainfall recorded from 1 January to 1 June 1998, the arrow indicating the triggering rainfall, along with a typical example of the occurred landslide phenomena (c) and the damage caused (d). Figure 2.38 shows the geotechnical properties of the soil types. The selection of the values of the input parameters for TRIGRS simulation was based on an indirect procedure. Slope models representative of the in-situ stratigraphic conditions was analysed using the finite element code SEEP/W (Geo-

Slope 2005), considering the geotechnical properties derived from the results of the laboratory tests. Similar models were analysed using TRIGRS for saturated and unsaturated infiltration conditions with different values of the hydraulic properties varying in the range adopted for the finite element analyses. Figure 2.39 shows the pore-water pressure profiles obtained with the SEEP/W, TRIGRS codes. Table 2.4 shows the value of the input parameters used for TRIGRS modelling. Figure 2.40 shows the map of the instability scenarios obtained with TRIGRS with unsaturated infiltration condition. The results obtained from the three models are compared with mapped landslide occurrences. The TRIGRS application with unsaturated soil parameters is shown to be more suitable than TRIGRS application with conventional soil parameters neglecting the unsaturated characteristics, due to its capability to model transient infiltration process in unsaturated conditions characterising the analysed shallow landslides events.

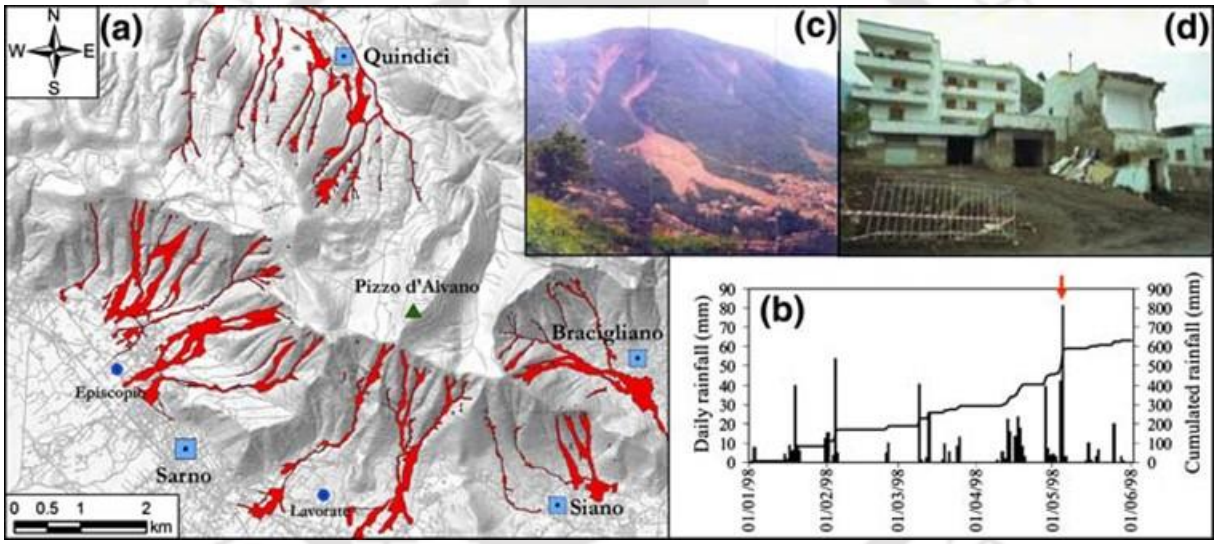

Figure 2.37 (a) Overview of the Pizzo d'Alvano massif with the main May 1998 shallow landslides of flow-type events; (b) daily rainfall recorded from 1 January to 1 June 1998 (the arrow indicates the landslides occurrence); (c) an example of the occurred phenomena and (d) of the produced damage (Sorbino *et al*., 2010)

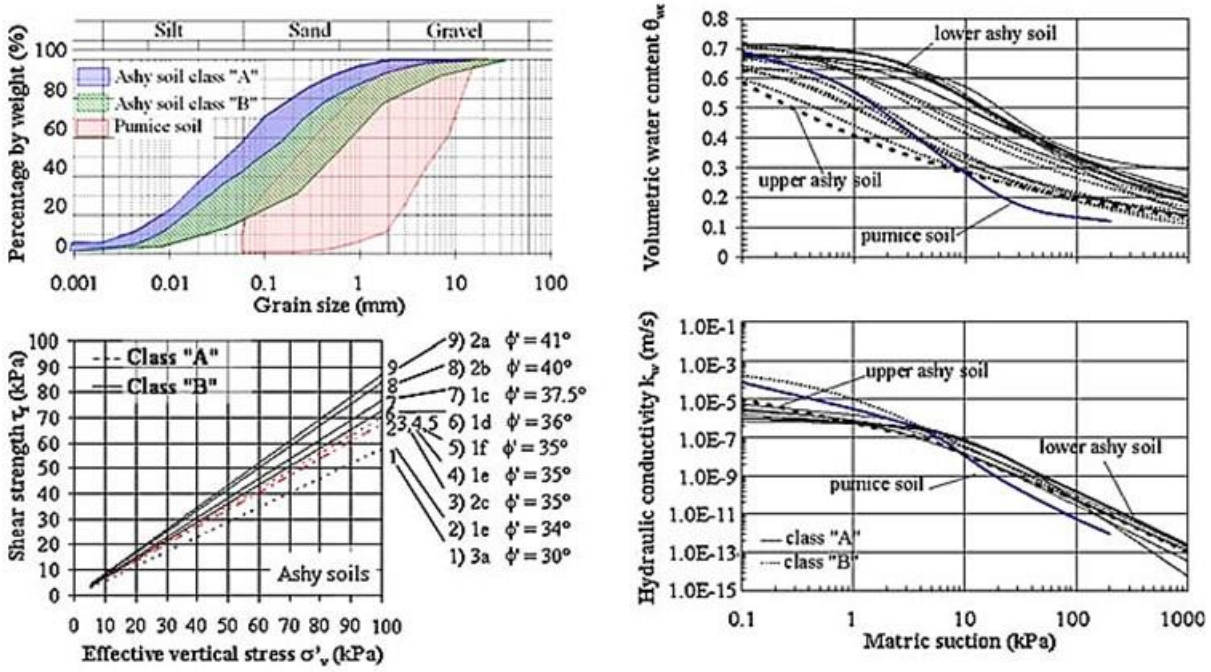

Figure 2.38 Physical and mechanical properties of volcanoclastic soils: (a) grain size distribution; (b) soil water characteristic curves; (c) unsaturated hydraulic conductivity functions; and (d) shear strength of the main ashy soil classes (Sorbino *et al*., 2010)

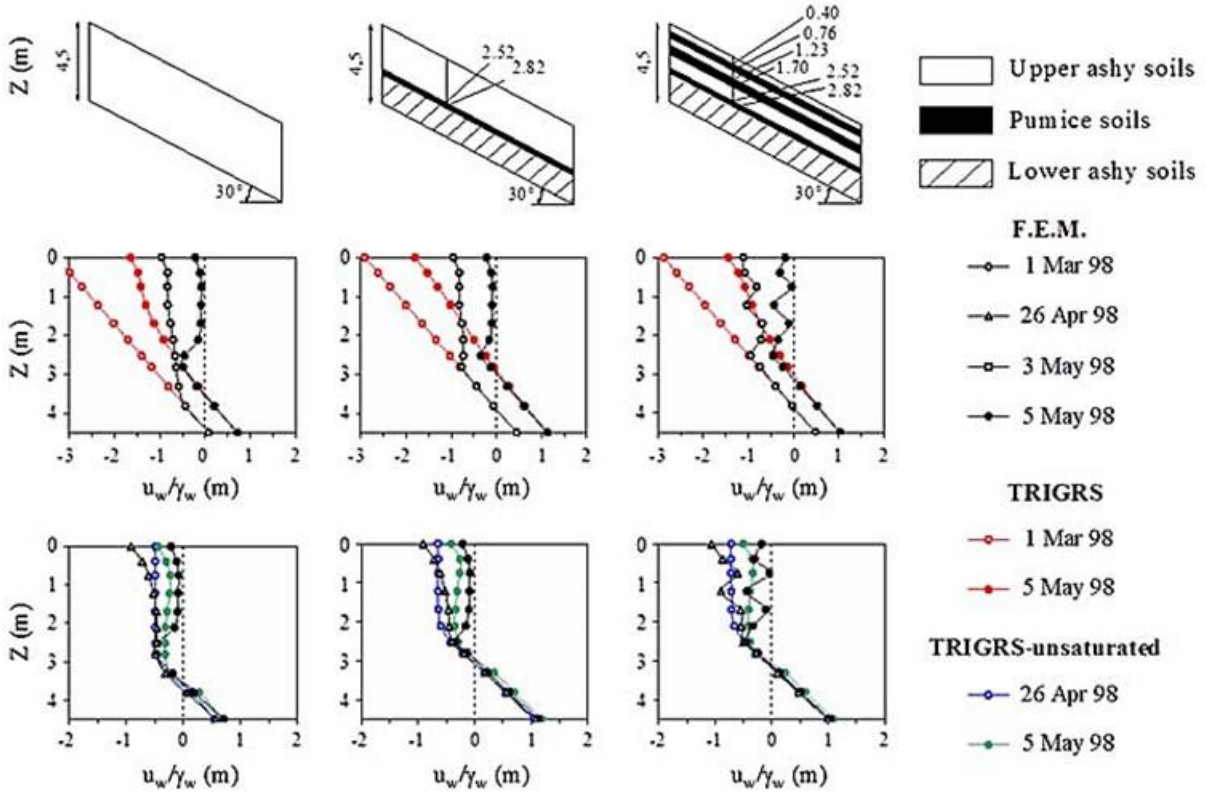

Figure 2.39 Pore-water pressure profiles obtained with the SEEP/W, TRIGRS and TRIGR-unsaturated codes: (from the top to the bottom) the analysed schemes, F.E.M. versus TRIGRS, and F.E.M. versus TRIGRS unsaturated (Sorbino *et al*., 2010)

Table 2.4 Parameters used for TRIGRS modelling (Sorbino *et al*., 2010)

Sector	Hydraulic conductivity k (m/s)	Soil depth $h_{SHALSTAB}$ (m)	Diffusivity D_{TRIGRS} (m^2/s)	Parameters of Gardner's curves *TRIGRS-unsaturated*		
				α (m^{-1})	Residual Water Content θr	Saturated Water Content θs
Sarno	1.0×10^{-5}	2.65	5.9×10^{-5}	6.3	0.20	0.66
Siano	8.0×10^{-6}	2.80	5.6×10^{-5}	7	0.20	0.60
Bracigliano	6.0×10^{-6}	2.00	4.5×10^{-5}	8	0.25	0.53
Quindici	6.0×10^{-6}	2.25	4.5×10^{-5}	8	0.25	0.53

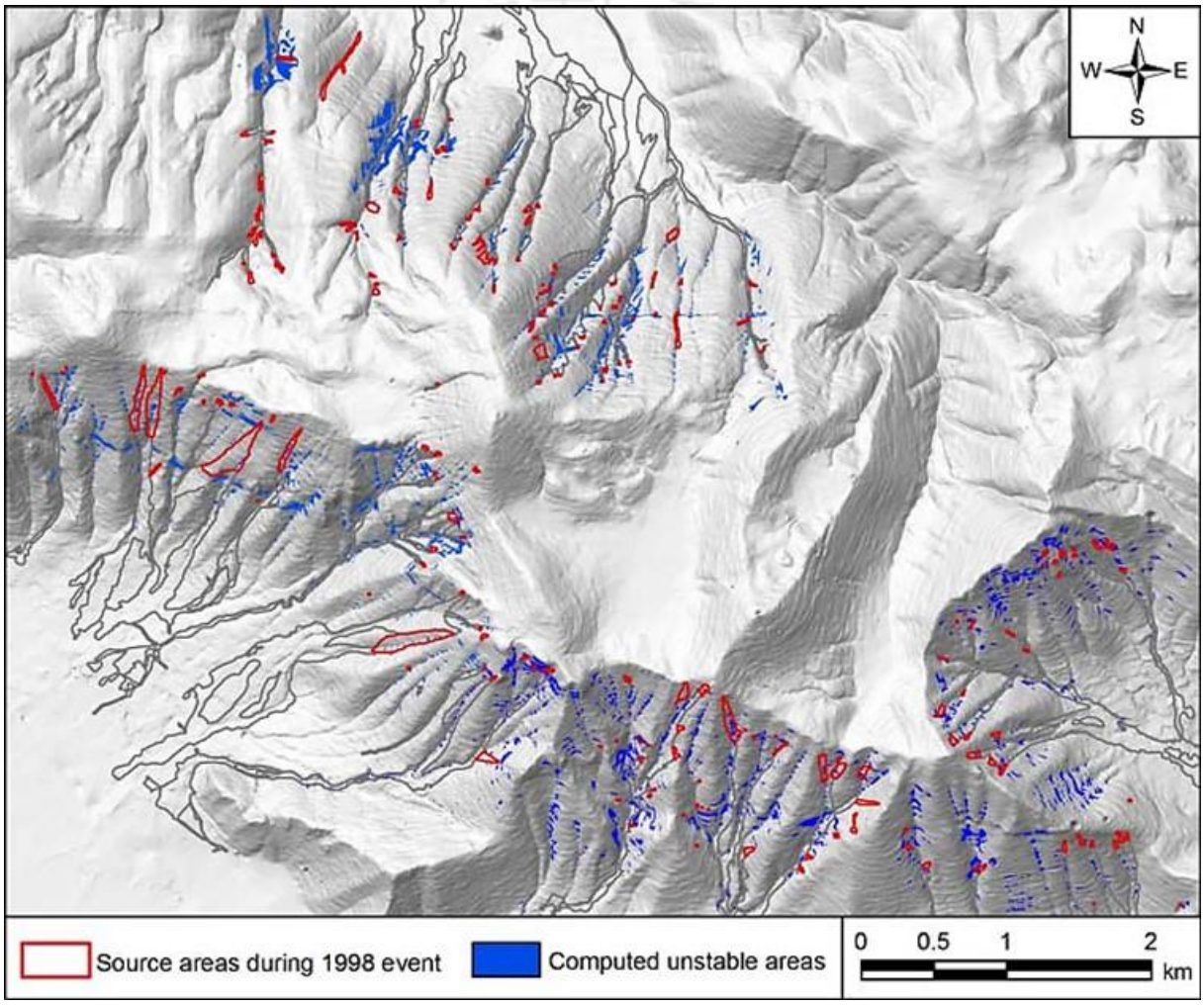

Figure 2.40 Instability scenarios obtained with TRIGRS-unsaturated (Sorbino *et al*., 2010)

Park *et al*. (2013) presented the results from the application of TRIGRS for landslide occurrence within the region of Woomyeon Mountain, Seoul, South Korea. The study compared the observed landslide and debris flow events with those predicted by the TRIGRS model. The results predicted by the TRIGRS model are presented as *FoS* maps corresponding to transient rainfall events. 147 catastrophic landslides occurred, triggered from the rainfall

event of 26–27 July 2011 (470 mm in two days). Figure 2.41(a) shows the hourly rainfall history from 25 July to 27 July in 2011. Figure 2.41(b) shows the Soil water characteristic curve fitted to van-Genuchten model. Topographic analyses for slope angle and aspect were calculated from elevation grids with 10m cells created from 1:5000 maps. Figure 2.42 shows the topographic information relevant to landslide triggering. The analysis showed that most of the landslides were triggered on terrain around the mid-altitude ranges and on steeper slopes (>25º–30º), and landslides were predominantly triggered in the spots of concave relief. Figure 2.43 shows the factor of safety (*FoS*) at different times in the study area overlaid with the landslide locations and depict the temporal and spatial dynamics of FoS values induced by heavy rainfall during the 48-h duration. Initially at 0 h, the area was stable characterized by high FoS. With the application of rainfall infiltration, TRIGRS modelled the initiation or triggering of landslides in the form of decreasing FoS. The areas having FoS<1.0 progressively expanded when the rainfall became more intense, implying large numbers of the landslides being triggered by the intense rainfall. The study showed that the model is applicable for susceptibility analysis of debris flow in catchments with limited data availability. TRIGRS output is dependent on the resolution and accuracy of DEM and precision of the geotechnical parameters used, but more investigation and data the TRIGRS model output can be significantly improved.

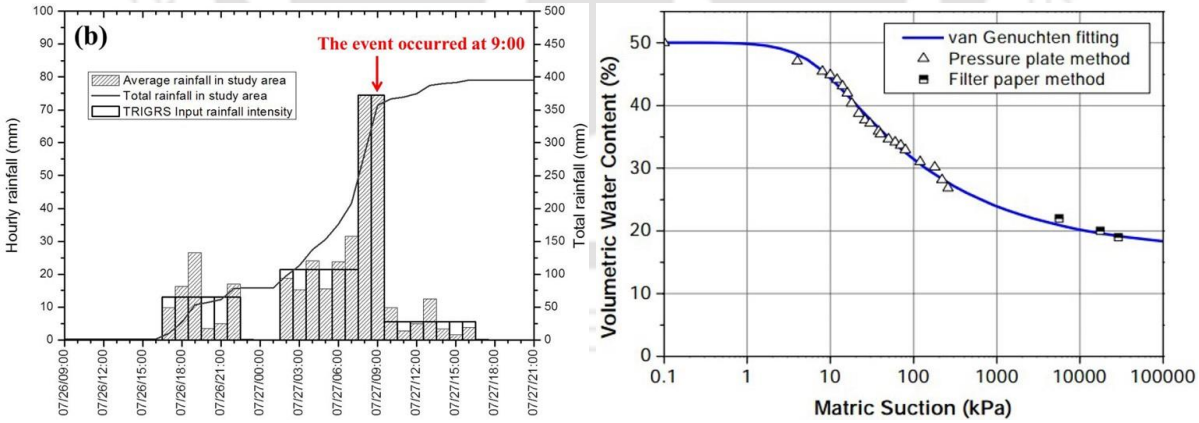

Figure 2.41 (a) TRIGRS input rainfall intensity distribution of the event on 25–27 July 2011; (b) Soil water characteristic curve in study area (Park *et al*., 2013)

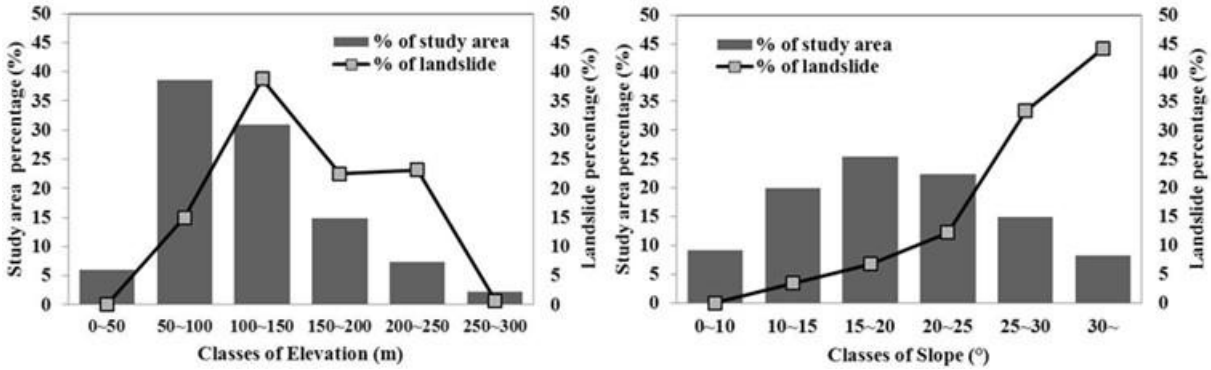

Figure 2.42 Landslide triggering against classes of topographic parameters (elevation and slope angle) in the study area (Park *et al*., 2013)

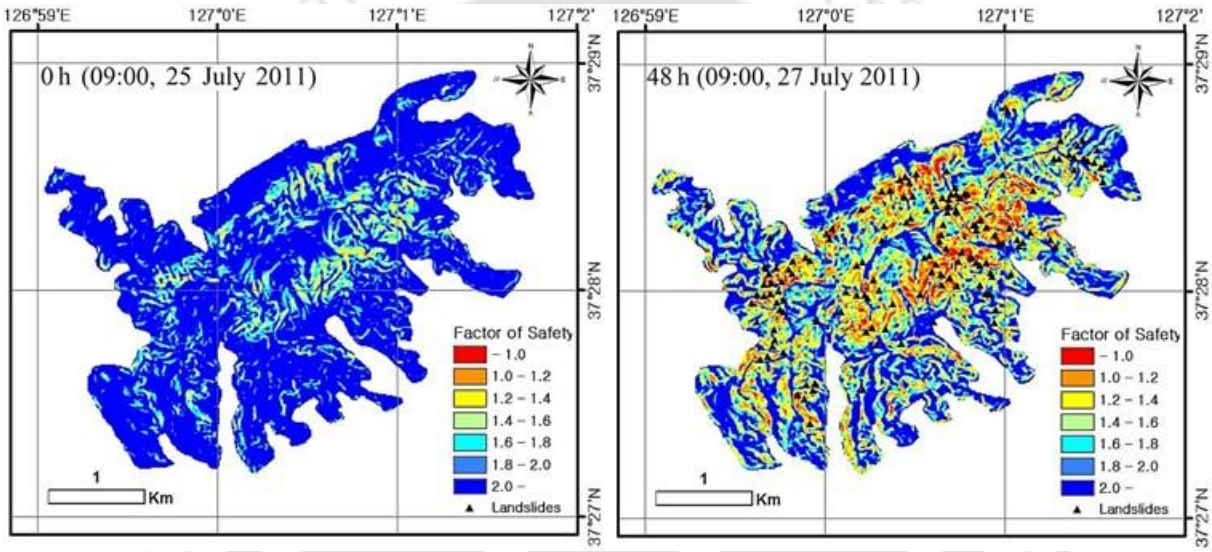

Figure 2.43 Factor of safety (*FoS*) at different times in the study area overlaid with the landslide locations (Park *et al*., 2013)

Raia *et al*. (2014) proposed a modified version of the original TRIGRS code, TRIGRS-P considering a probabilistic Monte Carlo approach to the distributed modelling of rainfall-induced shallow landslides. TRIGRS-P copes with the natural variability inherent to the mechanical and hydrological properties of the slope materials by allowing values of the TRIGRS model input parameters to be sampled randomly from a given probability distribution. The range of variation and the mean value of the parameters can be determined by the usual methods used for preparing the TRIGRS input parameters. The probabilistic approach allowed the investigation of the combined effects of the natural variability inherent in the model parameters, and of the uncertainty associated with their definition over large areas. Figure 2.44(a) shows the minimum, the maximum, and the standard deviation of the computed *FoS* values. The researchers note the map of the standard deviation, in particular,

provides quantitative and spatially distributed evidence of the uncertainty associated with the distributed modelling of landslide instability. Figure 2.44(b) shows histograms for the distribution of the values of the *FoS* in selected grid cells, obtained for a single lithological type. TRIGRS-P has only two options of probability density functions (pdf) for generating the random modelling parameters, vis., the normal distribution function or the uniform distribution function. The geotechnical and hydrological properties were treated explicitly as independent i.e., uncorrelated variables and that there is no spatial correlation of the individual variables. The researchers noted that it is a simplified assumption and that in reality some dependence (correlation) as well as spatial correlation exists between the different geo-hydrological properties. The researchers concluded that the probabilistic approach results in a number of model outputs, each representing the geographical distribution of the *FoS* values and availability of multiple results allows for the analysis of the sensitivity of the model to variations in the input parameters controlling the stability conditions. However, the approach cannot separate the causes for the variability and is not concerned regarding the validation of the physics in the model better than the deterministic approach.

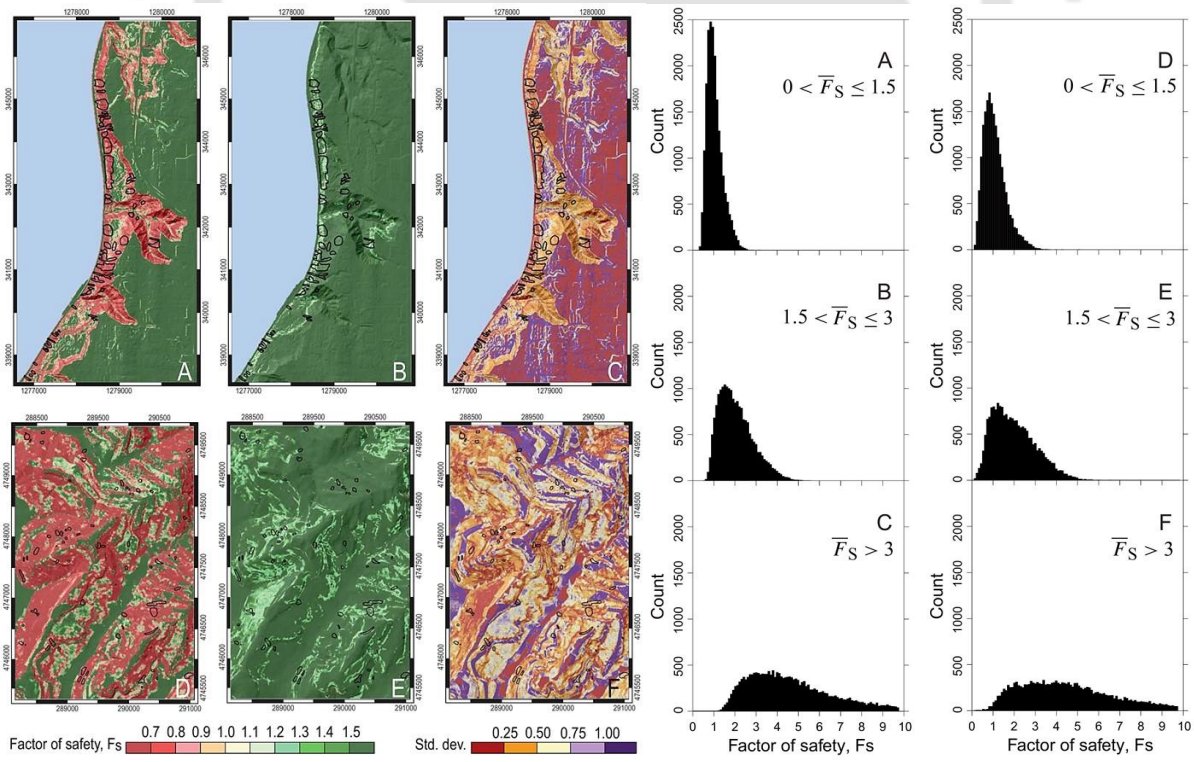

Figure 2.44 (a) Maps showing the minimum (A,D), maximum (B,E), and standard deviation (C,F) of the factor of safety for the Mukilteo (A,B,C) and the Frontignano (D,E,F) study areas. (b) Histograms showing the distribution of the *FoS* values of the for the Mukilteo (left, A, B, C) and the Frontignano (right, D, E, F) study areas (Raia *et al*., 2014)

Saadatkhah *et al*. (2014) presented the application of TRIGRS model in the Hulu Kelang area, Malaysia where rainfall-induced slope failures often occur in the residual soil profile, formed over a bedrock interface as a shallow slope failure, with slip surfaces orientated parallel to the slope surface. The topographical data for TRIGRS model were generated from 1:10,000 scale standard topographic maps. A 30×30-m cell digital elevation map (DEM) data was constructed for the terrain analysis. Figure 2.45(a) shows the DEM overlaid with the landslide locations as red dots. Three rainfall threshold conditions (vis., the intensity–duration of 3-day rainfall threshold, cumulative 30-day rainfall– number of rainy days, and cumulative –30-day antecedent precipitation followed by 3-day rainfall conditions) that is capable of producing slope instability in the study area, as predicted by TRIGRS, is compared with the empirical rainfall I–D thresholds for possible landslide occurrence in the study area. Figure 2.45(b) plots the Success Index (SI) and Error Index (EI) obtained with the TRIGRS model corresponding to the intensity–duration of 3-day rainfall threshold chart (I–$D)_3$ – ETR1; the cumulative 30-day rainfall–number of rainy day (API_{30}–N) – ETR2; and the cumulative 3-day rainfall–30-day antecedent precipitation index threshold chart (E_3–API_{30}) – ETR3. The cumulative 3-day rainfall–30-day antecedent precipitation gave the closest approximation regarding the prediction of landslides in the Hulu Kelang area, highlighting the predominant effect of the antecedent conditions. The results showed that TRIGRS is capable of reproducing the patches of terrain predicted as unstable by the model, which match the frequency size statistics of landslides in the study area.

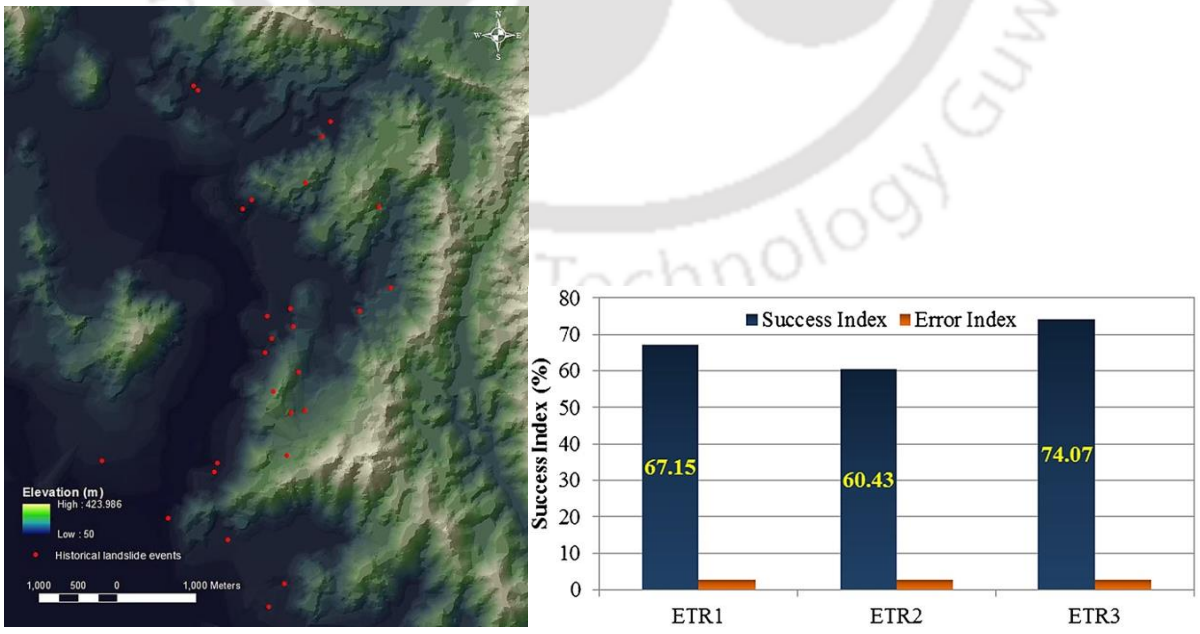

Figure 2.45 (a) DEM and Landslide inventory of Hulu Kelang area (b) “Success” and “error” indexes obtained with the TRIGRS model (Saadatkhah *et al*., 2014)

Viet *et al*. (2016) conducted study to predict shallow landslide-prone areas by using the TRIGRS model. The landslide occurrence on July 27, 2011, in Mt. Umyeon, Seoul, was modelled, and the stability results were compared with 140 observed landslide points in both time and location to evaluate the performance of TRIGRS. Figure 2.46(a) shows the Digital elevation model (DEM), along with the observed sliding locations as black dots. For evaluating the performance of TRIGRS, actual data sets of sliding points were compared with the predicted results. The *FoS* values from 140 observed sliding points were then extracted and analysed. The prediction indicated a good agreement with the landslide inventory map. Simulated outcomes from five different raster cells of 5, 10, 15, 20, and 25 m with the same background information were compared to identify the ultimate grid scale. The evaluation revealed that in location estimation, smaller grid size resulted in results that are more accurate. However, in timing assessment, the 10 and 15-m grid sizes gave better results. Figure 2.47 gives map of *FoS* during a rain event. Before the rainfall event began, the slope remained dry and the *FoS* values were significantly larger than 1.0 for the entire study area. The *FoS* values decreased with rainfall because of the rise in ground water table, leading to landslide occurrence. Figure 2.46(b) plots the series of boxplots showing the distribution and the average of *FoS* at 140 observed sliding points at each time step, together with the cumulative rainfall. The figure shows the decreasing *FoS* with the rainfall duration. The study concluded that despite some limitations of data acquisition, TRIGRS is a strong tool for shallow landslide estimation, particularly in large areas where input data for simulation is not fully available. The results predicted by TRIGRS can be improved by increasing the reliability of the initial groundwater conditions, soil depth map, topographic map and the engineering properties of geologic units.

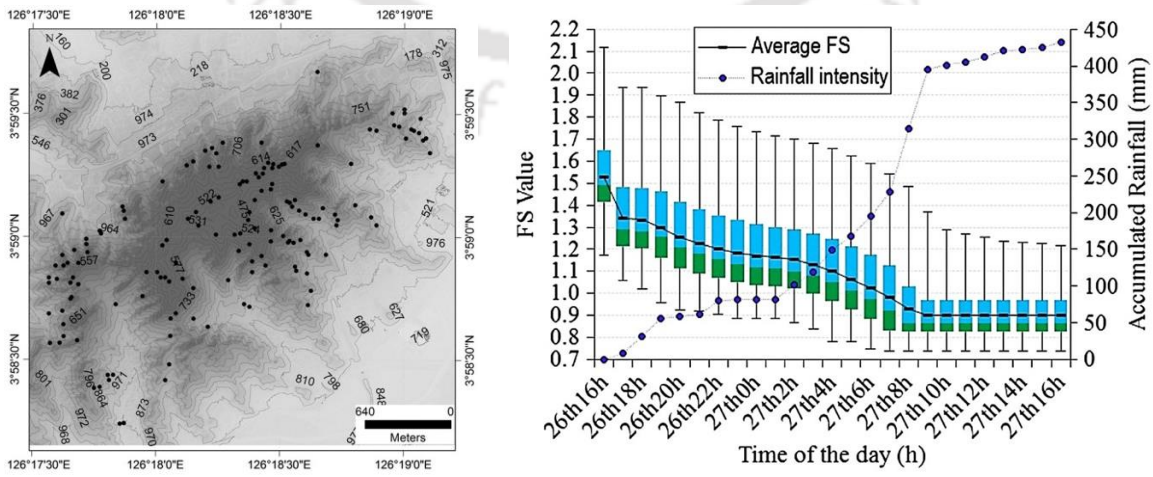

Figure 2.46 (a) Digital elevation model (DEM). The black dots show the observed sliding locations (b) Boxplots show the change of *FoS* with time (Viet *et al*., 2016)

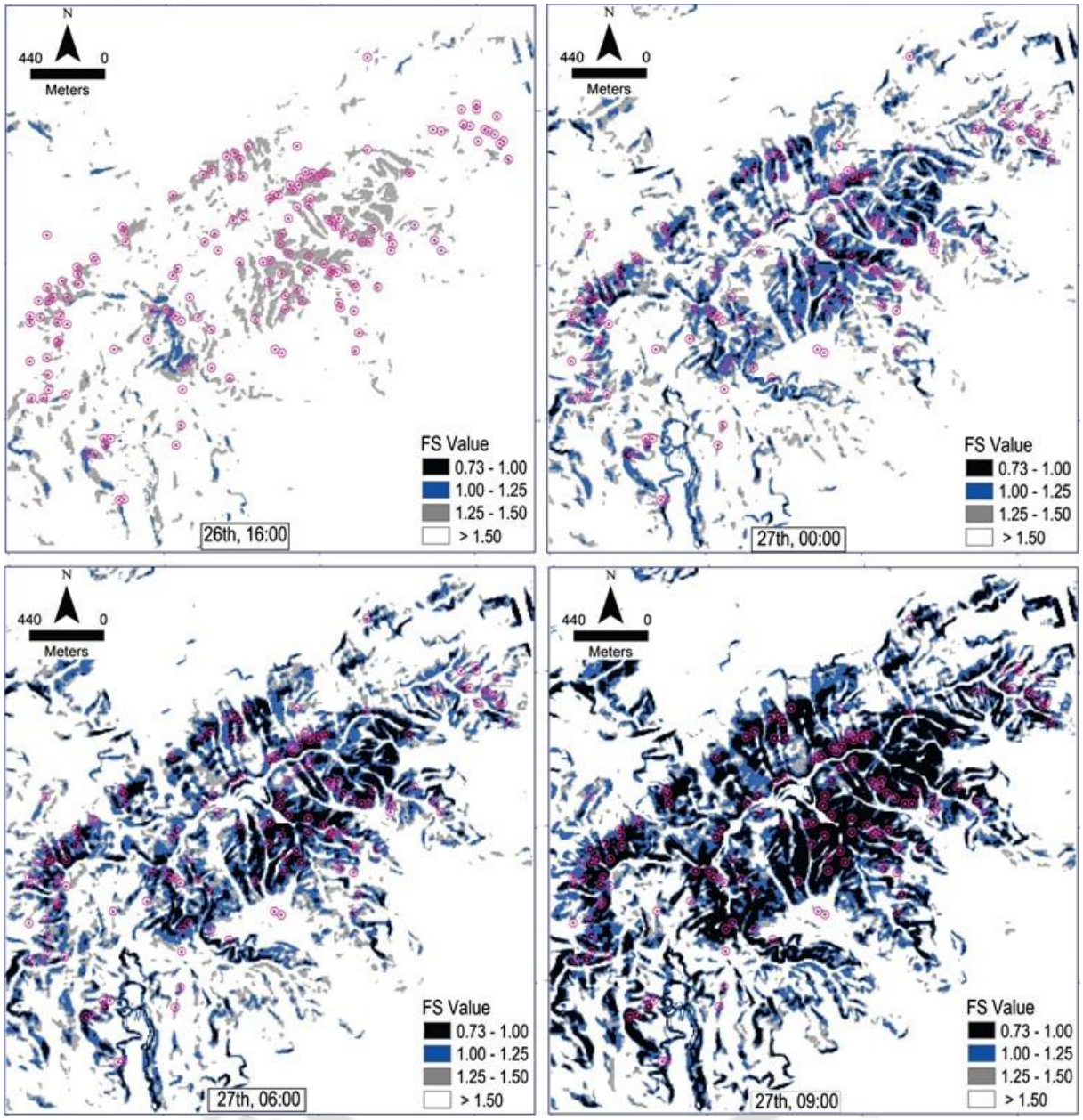

Figure 2.47 Factor of safety at different times (Viet *et al*., 2016)

2.8.5. Indian Standard Code Provisions

Bureau of Indian Standards (BIS) has given guidelines for Macro level landslide hazard zonation in the scale of 1:50,000, IS 14496, Part 2 1998 (Reaffirmed 2002) in India. BIS based Landslide Hazard Evaluation Factor (LHEF) rating scheme for landslide susceptibility zonation is a heuristic approach to landslide hazard assessment. Figure 2.48 shows the procedure for Landslide Hazard Zonation. BIS identified six landslide causative factors for hazard zonation viz. lithology, structure, slope morphometry, relative relief, land use-land cover and hydrological condition. In this method, the area under investigation is

divided into small mapping units to which numerical weights are assigned for each thematic data layer and finally TEHD (Total Estimated Hazard) is obtained by adding weights of all variables for each mapping unit and Landslide Hazard map is produced. The unit of study as recommended by BIS for Landslide Hazard Zonation is a slope facet. A slope facet is a part of hill slope showing consistent slope direction and inclination. The slope facets over a region are generally delineated from Topographical maps considering ridges, spurs, gullies and rivers. The slope facet map is considered as base map to prepare thematic data layers. Depending on the THED values the facets are grouped in to Very Low Hazard (< 3.5), Low Hazard (3.5-5.0), Moderate Hazard (5.0-6.0), High Hazard (6.0-7.5) and Very High Hazard (>7.5) classes. BIS based LHEF rating scheme is a very simple and cost-effective method of landslide hazard mapping. However, subjectivity in weight assignment procedure exists in this method, which can affect the level of accuracy of hazard zonation map.

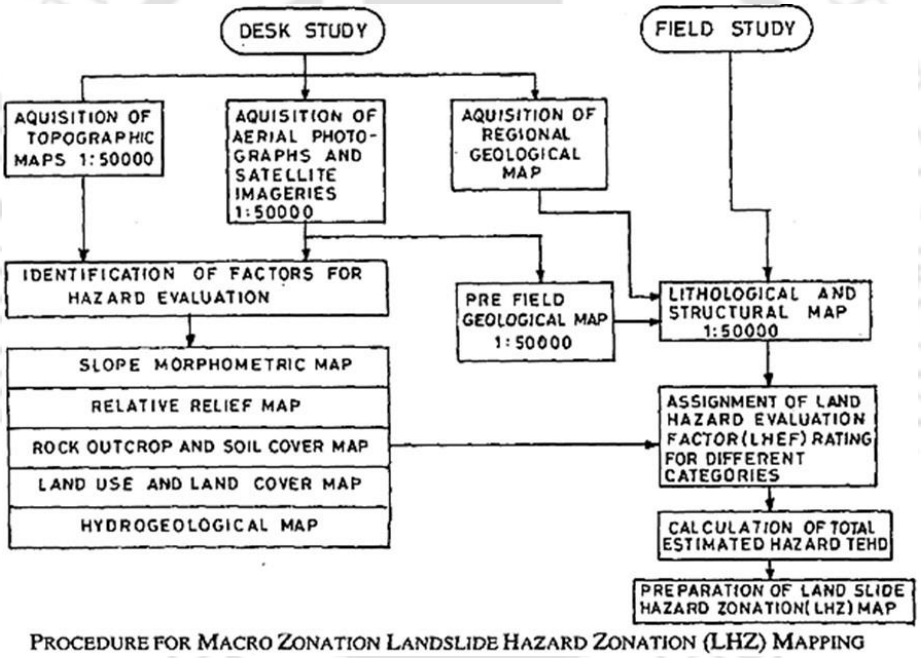

Figure 2.48 Landslide Hazard Zonation Procedure (IS 14496, Part 2 - 1998)

IS 14496 (Part 1) Mega-Regional (> 1:50,000), IS 14496 (Part 3) Micro-Regional (1:1,000 – 1:2,000) are yet to be framed and prescribed. No guidelines are available for Landslide Hazard Zonation on Meso-Scale (1:5000/10,000) and for further large scale (NDMA, 2004).

National Disaster Management Authority (NDMA) put forward an official document in the form of Management of Landslides and Snow Avalanches (2009). The document gives the definition of various terms associated with landslide studies. It defines Landslide Hazard

Zonation (LHZ) mapping is a tool to identify those areas that are, or could be, affected by landslides and assessing the probability of such landslides occurring within a specified period of time. The preparation of a LHZ map should include the study of the regional geology and geomorphic setting, slope conditions including existing and potential instability, and land use information.

The document highlights that scale is an important factor of LHZ mapping. Maps of 1:1,00,000 or 1:50,000 scales are inappropriate for regional studies since these are only indicative and do not provide adequate details. Larger scale maps on 1:10,000 or more should be taken up for detailed studies at the local level. There is also a lack of landslide inventory data, which lead to problems in validating landslide hazard maps. No organisation in our country has a sound database on landslide inventory. Taking into consideration the importance of developing a sound database on landslide inventory, the GSI has recently initiated a programme for the generation of landslide inventory maps and databases covering the landslide prone regions of our country.

The document reports that site-specific studies involving geotechnical investigations, including monitoring, have been carried out at some of the landslides. These include work on the Kaliasaur landslide along NH-58 near Srinagar, the Nainital landslide at Sher Ka Danda and 9.5 Mile, B2 and Lanta Khola landslides in Sikkim, the Powari landslide at km 367 on NH-21, Kinnaur district, Himachal Pradesh, and the Patalganga landslide on NH-58 near Pipalkoti, Uttarakhand. The DST has initiated various research projects such as the ones for NH-1A Sonapur in Meghalaya, the Tirumala Hills, eight specific sites in Uttarakhand, etc.

Standard Operating Procedure (SOP) – Landslide Investigation – put forward by the Geological Survey of India (GSI) states that at present there is no Guidelines available for LHZ on Meso Scale (1:5000/10,000). The main purpose of LHZ mapping on Meso Scale is to develop a detailed LHZ Map of a small area e.g. around a township, to assess the stability status of an existing localities incorporating more recognized important causative factors inducing slope instability, which cannot be considered in case of LHZ mapping on Macro Scale. GSI has also developed a methodology incorporating some more causative factors like slope erosion, shear strength of rock and overburden material etc. by modifying the BIS Code for LHZ on Macro Scale. GSI has proposed to develop a most acceptable Guideline both for Landslide Hazard Zonation/Landslide Risk Zonation on Macro (1:25,000/50,000) and Meso (1:5000/10,000) Scales as there are many shortcomings in the existing guidelines, however is still in preparation phase.

The SOP (GSI) states that an important aspect of landslide investigation called "Stability Analysis" is seldom carried out. However, a landslide investigation cannot be completed without stability analysis, which is a direct measure of degree of instability of a slope. Proper geotechnical investigation of a landslide should be carried out to establish the causative factors of landslide. Detailed geotechnical mapping of landslide depicting geometry of the slide, crown and toe of the slide. Locations of longitudinal and transverse cracks, slide scars, old slide scar, plunge of striation lineation., Disposition of different litho-units, structure and state of weathering of rocks, type and composition of overburden. Location of severe toe erosion by streams or rivers, scouring pattern of slope along natural drainage, locations and attitude of steep, moderate and gentle slopes around the slide zone Zones of gully erosion, seepage/spring locations, dry or wet slope, elements at risk, tentative run out. Such a study is essential for suggesting most appropriate remedial measures in a cost-effective manner to contain the slide.

Besides the above-mentioned codes and official documents, the IS 14680:1999 Landslide Control – provides some "Guidelines Landslide control methods for effective correction measures to avoid landslides in hill areas".

The BIS codes for slope stability analysis, vis., IS 7894:1975 Code of Practice for Stability Analysis of Earth Dams and IS 8237:1985 Code of Practice for Protection of Slope for Reservoir Embankment are developed for, as the name suggest, for stability analysis of earth dams and reservoir embankment.

2.9. LANDSLIDE STUDIES IN THE INDIAN CONTEXT

Several studies related to landslide susceptibility and hazard mapping can be found in the literature pertaining to study areas within India. However, almost all of the studies have based on heuristic, semi-heuristic or statistical approaches.

Anbalagan (1992) proposed a quantitative approach in the form of landslide- hazard evaluation factor (LHEF) rating scheme, and adopted the same for case study of landslide hazard zonation in the Himalaya. The researcher proposed that the areas demarcated as high hazard and very high hazard through the LHEF, detailed studies on larger scales should be conducted to evaluate the nature of the instabilities, in order to come to appropriate mitigation measures to protect the geo-environmental stability of the area.

Saha *et al*. (2005) applied the Information Value (InfoVal) and the Landslide Nominal Susceptibility Factor (LNSF) methods that are based on bivariate statistical analysis for Landslide susceptibility zonation (LSZ) mapping in a part of the Himalayas. Slope, aspect, relative relief, lithology, buffer zones along thrusts, faults and lineaments, drainage density and land cover are the factors considered in the study and have been generated using remote sensing and GIS techniques.

Pandey *et al*. (2007) carried out Landslide Hazard Zonation (LHZ) of Dikrong river basin of Arunachal Pradesh applying a weighting–rating system based on the relative importance of various causative factors, such as slope, photo-lineament buffer, thrust buffer, relative relief map, geology and land use / land cover map to calculate the Landslide Hazard Index (LHI) for each cell. The weight-rating values were re-adjusted using trial and error method.

Sarkar and Anbalagan (2008) used Landslide Hazard Evaluation Factor rating scheme for the landslide hazard zonation of an area of about 80 km^2 to the south of the Alaknanda River in between Srinagar and Rudraprayag. The mapping was done in a macro level scale of 1:50,000.

Kuriakose *et al*. (2009) applied dynamic and distributed hydrological model (STARWARS) coupled with a probabilistic slope stability model (PROBSTAB) to the upper Tikovil River basin (55·6 km^2). Figure 2.49(a) shows the general framework of the STARWARS and PROBSTAB models. STARWARS is a distributed dynamic hydrological model designed to evaluate the effects of vegetation on hillslope hydrology. Soil hydrological properties can be assigned to specific land use types. Unsaturated zone within the soil mantle over a semi-impervious basal rock contact can be modelled. PROBSTAB calculates the FoS based on the infinite slope model for the entire soil column, and if required the depth of failure, based on the daily variation of water level and volumetric moisture content, which are the outputs of STARWARS. Some modifications to the original physically based model were made to accommodate the data poor conditions in the region. Figure 2.49(b) the locations of shallow landslides plotted over predicted slope instability. The study showed that despite the poor input, the model captured the general temporal and spatial pattern of instability in the area.

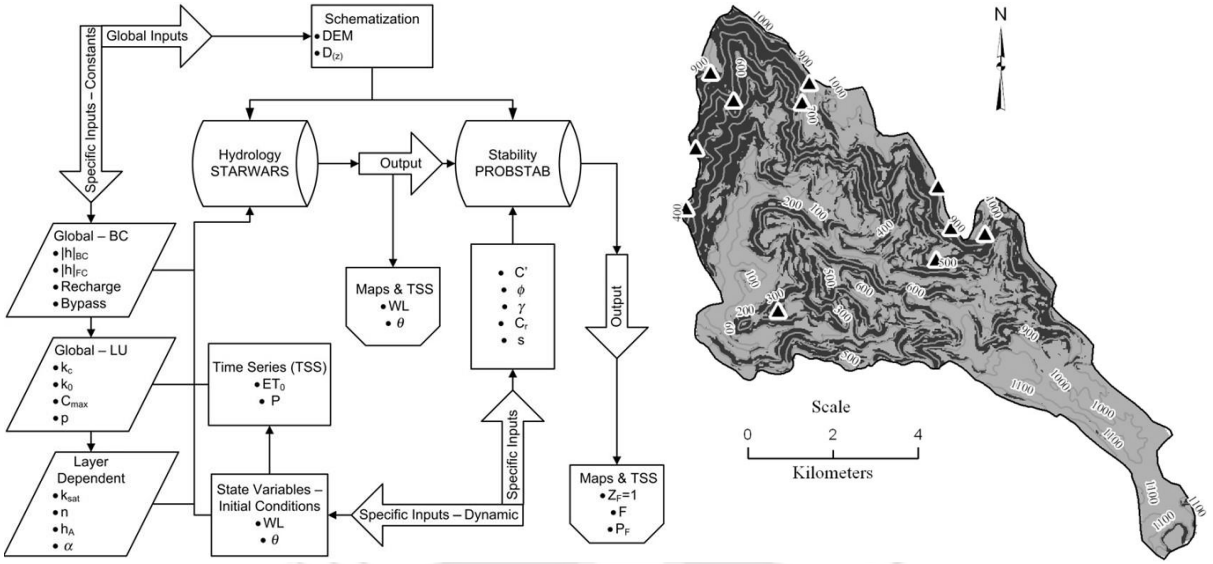

Figure 2.49 (a) General framework of the STARWARS and PROBSTAB models; (b) Actual locations of shallow landslides plotted over predicted slope instability (Kuriakose *et al*., 2009)

Mathew *et al*. (2009) applied multivariate statistical method called binary logistic regression (BLR) analysis for LSZ mapping in part of the Garhwal Lesser Himalaya, India. The predictive logistic regression model has been validated by receiver operating characteristic curve analysis.

Jaiswal *et al*. (2010) used logistic regression model to determine the spatial probability of landslides within a transportation corridor of the Nilgiri Hills in southern India, taking the source area of the existing landslides as dependent, and slope angle, aspect, regolith thickness and land use as independent variables. The temporal probability of landslides was estimated indirectly using the exceedance probability of the rainfall threshold required to trigger landslides for the first time on natural slopes. The models were validated using the rainfall and landslide events that occurred during 2008 and 2009.

Sengupta *et al*. (2010) proposed an alternative rainfall threshold that predicts sliding if normalized cumulative rainfall more than a particular value within defined duration, for Lanta Khola debris slides characterized by fine-grained, low permeability debris material, highly susceptible to landsliding. Figure 2.50(a) shows a typical cross-section through the slide along with the strength of the slide materials and the results of the stability analyses. Figure 2.50(b) shows the data of the local rainfall and landslide occurrence. The researchers suggested that rainfall threshold could not be defined by typical exponential relationships

between cumulative rainfall and rainfall duration based on the analysis of the available rainfall and landslide activity data for the area between 1998 and 2006.

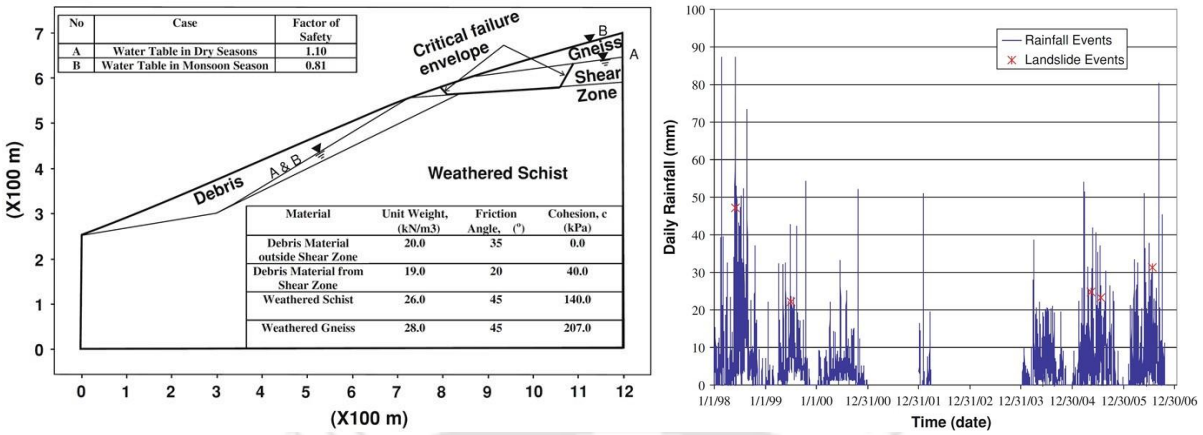

Figure 2.50 (a) Slope stability analyses for the Lanta Khola Slide; (b) Rainfall and landslide data for the Lanta Khola slide, shown from January 1998 to the end of December 2006 (Sengupta *et al*., 2010)

Mani and Saranaathan (2017) conducted a landslide hazard zonation mapping on meso-scale (1:10,000) in SH-37 Ghat section, Nadugani, Gudalur, the Nilgiris, India applying the LHEF rating scheme (IS 14496, Part 2 1998) developed for macro level landslide hazard zonation in the scale of 1:50,000.

Ramesh *et al*. (2017) conducted macro landslide hazard zonation (LHZ) mapping and slope stability analyses of selected rock slope (RS) sections along 27 km Kuppanur–Yercaud Ghat road section, Tamil Nadu, India. The macro LHZ map was prepared on 1:50,000 scale using landslide hazard evaluation factor (LHEF) rating scheme proposed by Bureau of Indian Standard IS 14496 (Part-2) 1998.

Chawla *et al*. (2018) used Particle Swarm Optimization-Support Vector Machine technique and Genetic Programming method for the generation of landslide susceptibility map of an area of 201 km^2. The study area is a part of the Darjeeling district, Eastern Himalaya. Drainage, lineament, slope, rainfall, earthquake, lithology, land use/land cover, fault, valley, soil, relief, and aspect were considered as the influencing factors. Numerical weight and rating for each factor was assigned using the overlay analysis method. The resulting landslide susceptibility zonation map demarcated the study area into four different susceptibility classes: very high, high, moderate, and low.

Dikshit *et al*. (2018) conducted in-situ study by installing tilt sensor and volumetric water content sensors for developing early warning and monitoring system with a low

probability of false alarms in Chibo Pashyor region in the state of West Bengal. The sensors were installed at shallow depths and was monitored for the tilting angle of the instrument, the variation of which corresponds to lateral displacement at slope surface. Figure 2.51(a) shows the surface tilt sensor that is equipped with a MEMS (micro-electro-mechanical systems) tilt sensor and a volumetric water content sensor. The time histories of the tilting angles of the sensors in X and Y directions are depicted in Figure 2.52. The volumetric water content and the recorded rainfall are plotted in Figure 2.51(b). The researchers concluded that antecedent rainfall of 3–10 days leads to displacement of slope that has also been observed earlier studies conducted in this region. With sufficient data from the system rainfall threshold can be validated as well as empirical equation based on site-specific conditions can be formulated.

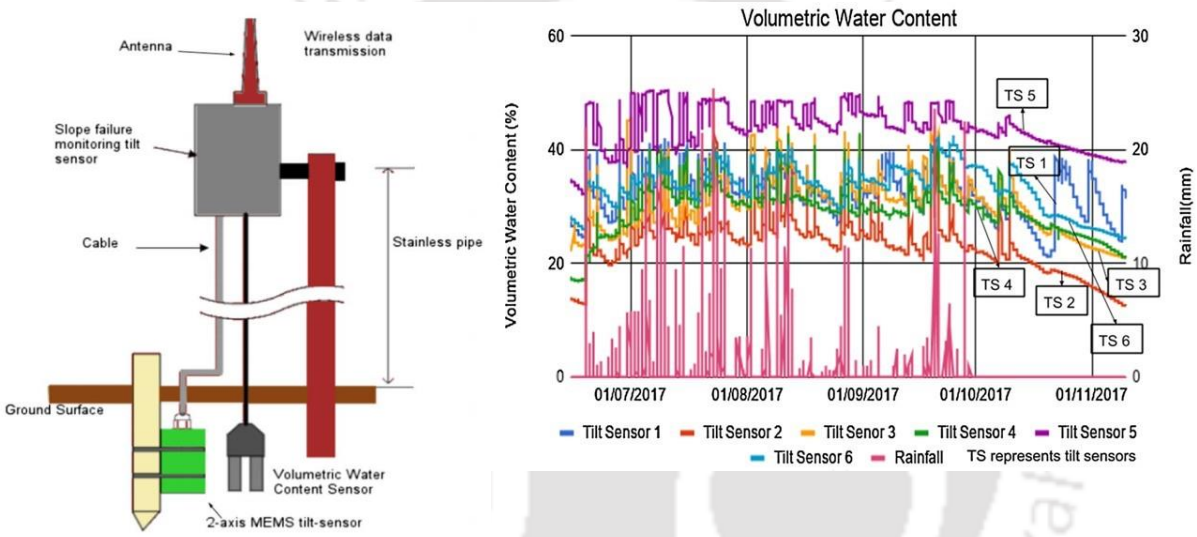

Figure 2.51 (a) MEMS sensor and volumetric water content sensor (b) Detailed time history of volumetric moisture content for the in-situ sensors (Dikshit *et al*., 2018)

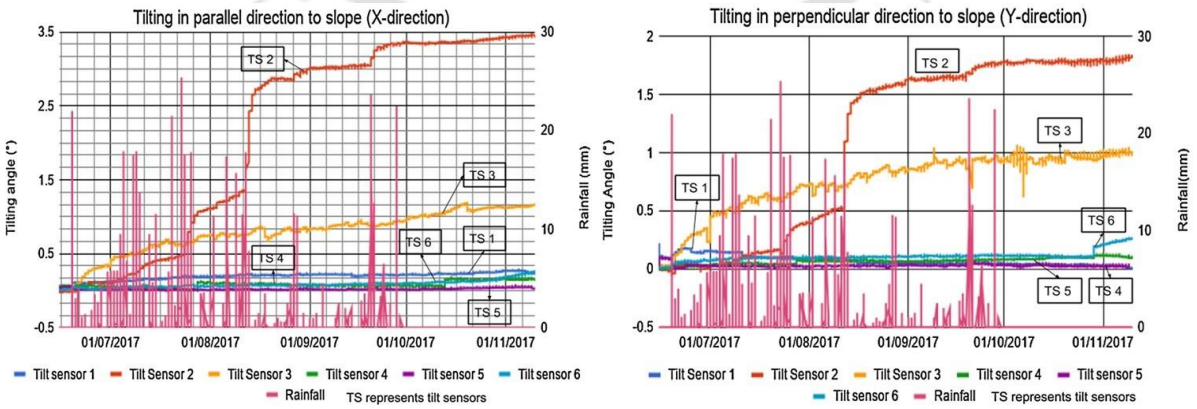

Figure 2.52 Time history of tilting angle in (a) parallel direction to slope, (b) tilting angle in perpendicular direction to slope (Dikshit *et al*., 2018)

2.10. LITERATURE PERTAINING TO STUDY AREA

Though a significant amount of studies related to landslide stability and hazard assessment can be found in the literature, not much notice has been given to the state of Assam, and specifically Guwahati, where huge amount of economic loss has been incurred, and most importantly loss of life due to occurrence of landslide.

Phukon *et al.* (2012) identified the potential landslide risk zones around the city of Guwahati and prepared a landslide susceptibility zonation map using Analytic Hierarchy Process (AHP) (Saaty, 1980) and Geographic Information System (GIS). Five probable causal factors that triggered the past landslides were considered for the study, vis. slope (Figure 2.53a), lithology (Figure 2.53b), land use (Figure 2.54a), drainage (Figure 2.54b), and lineament (Figure 2.55a). Landslide susceptibility index (LSI) was used in GIS environment to prepare a landslide susceptibility map (Figure 2.55b) of Guwahati city (Fig 2.12). The statistics shows that ~11% of the study area are in high susceptibility zone while ~6% and 83% areas are in moderate and low to very low susceptibility zones respectively, and that ~71% of the past landslides are from the high susceptibility zone and ~26% are from the moderate susceptibility zone. The high susceptibility zones were observed to be mostly concentrated around the steep slopes of the hills in and around the study area.

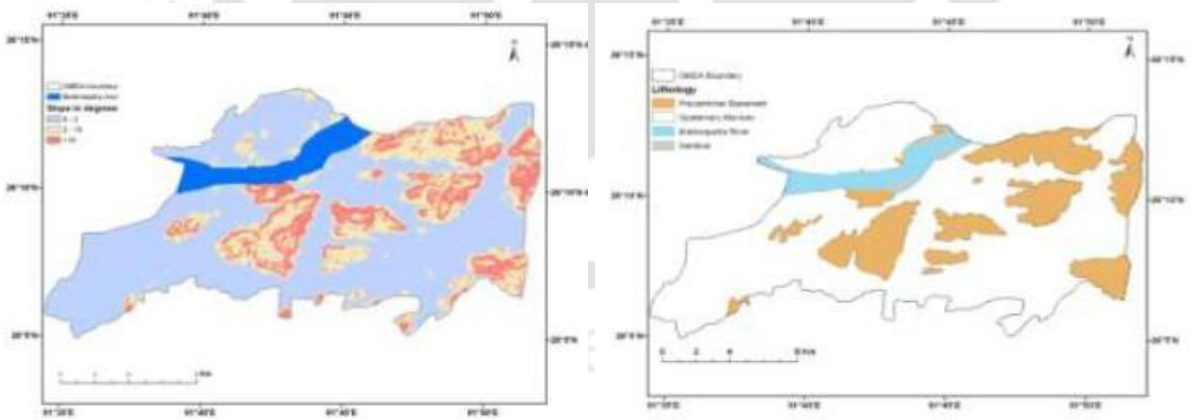

Figure 2.53 (a) Slope Map; (b) Lithology Map (Phukon *et al.*, 2012)

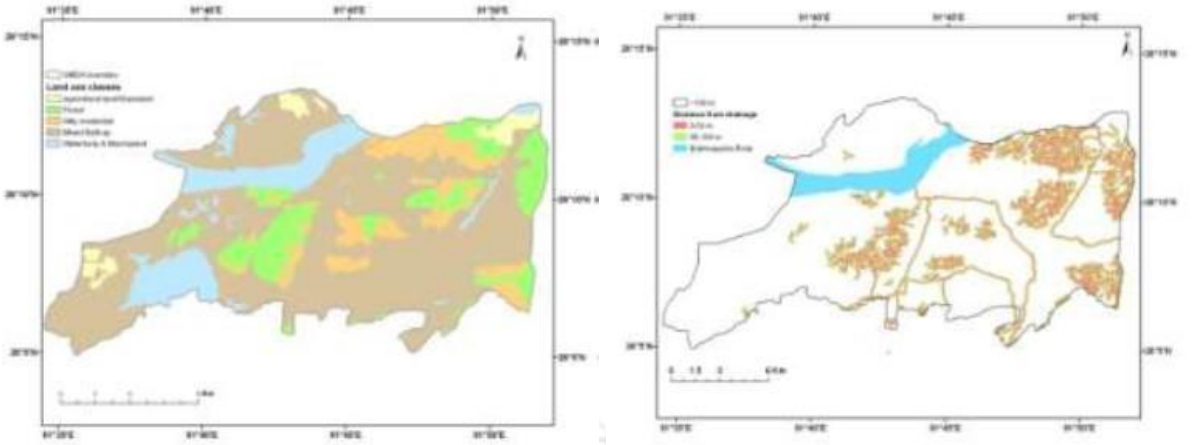

Figure 2.54 (a) Land Use Map; (b) Drainage Map (Phukon *et al.*, 2012)

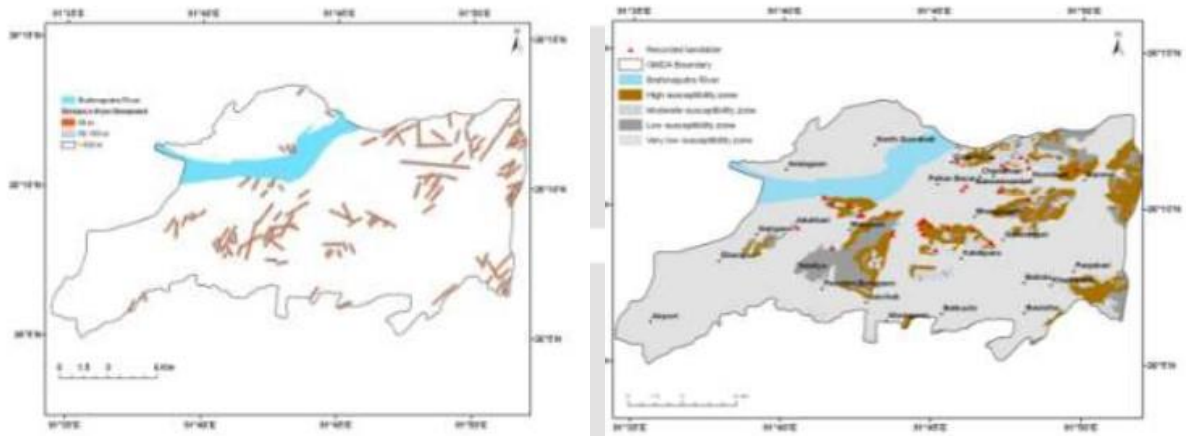

Figure 2.55 (a) Lineament Map; (b) Landslide Susceptibility Map (Phukon *et al.*, 2012)

Bhusan *et al*. (2014) presented a hazard zonation of Guwahati city (Figure 2.56) under the aegis of North Eastern Space Applications Centre (NESAC) Government of India, Department of Space Umiam, Meghalaya. The study applied Analytical Hierarchical Process (AHP) integrating various thematic data vis. landslide inventory, Cartosat–1 stereo data, lithology, fault/lineament, drainage, geomorphology, rock weathering, soil depth, soil texture, slope parameter, slope discontinuity relationship, land use/ land cover, rainfall and earthquake incidences depending on their role in causing slope instability. Thematic maps are generated using RS and GIS techniques, field surveys and from collateral data representing geo-environmental parameters of the study area. However, though it is termed as a Landslide Hazard Zonation Map it is actually a Landslide Susceptibility Zonation Map which aims to predict where failures are most likely to occur without any clear indication of when they are likely to take place hence ideally this map can be defined as landslide susceptibility maps. The landslide occurrence maps have three classes, such as active landslides as surveyed

during 2010 to 2011, old dormant landslides as reported before 2010 that can reactivate potential areas of future landslides. LHZ map is generated based on the database prepared from satellite images acquired during 2009-2011. Therefore, the hazard zonation map indicates landslide susceptibility based on the prevailing ground condition during 2011.

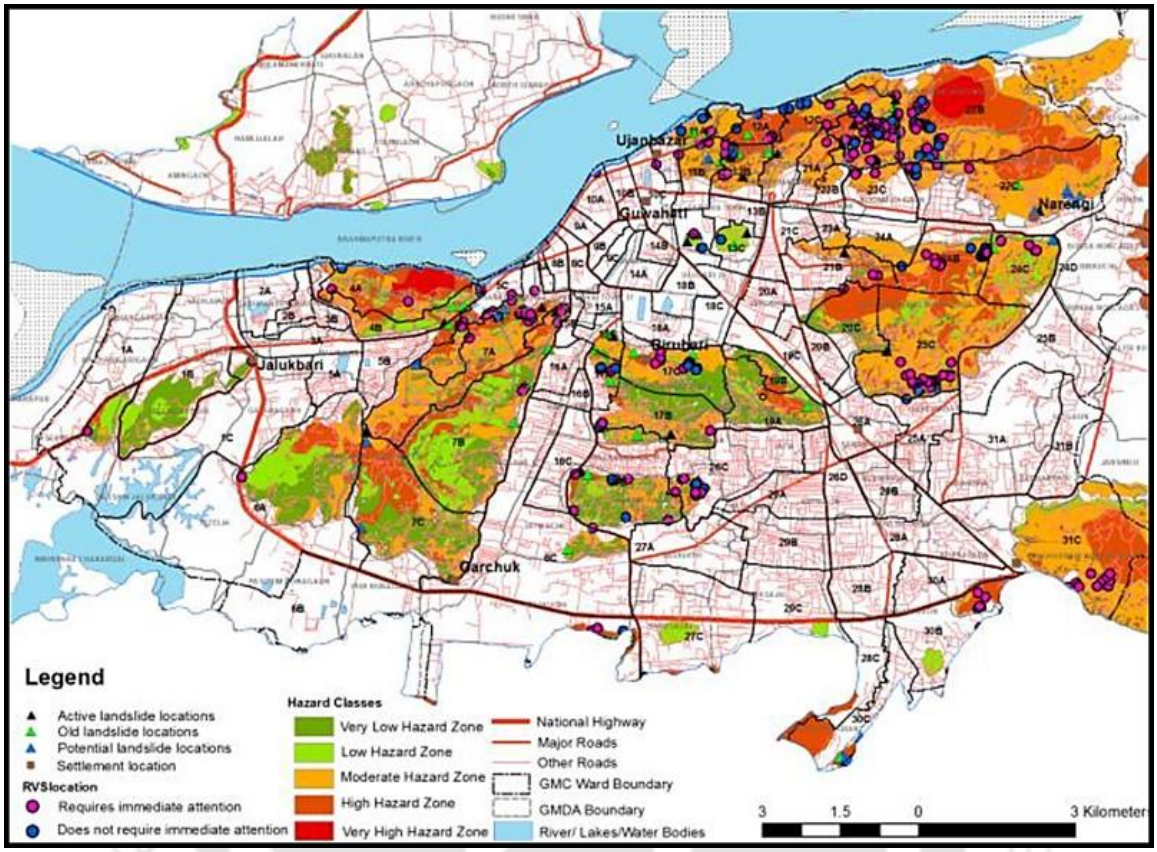

Figure 2.56 Landslide Hazard Map of Guwahati city (Bhusan *et al*., 2014)

Goswami and Singh (2008) noted that hills of Guwahati city are capped with lateritic soil, and although the slopes originally consisted of hard and strong rocks, their stability have been reduced by weathering, heavy rainfall and seepage flows. Encroachments and cuttings on the hill slopes due to unplanned urbanization have aggravated the problem. Weathering of the rocks led to a gradual transition forming natural residual saprolite soil, resulting in increase of pore spaces that facilitated more water absorption. During or after a continuous spell of rainfall, these residual soils became easily saturated with water causing an increase in driving force and a decrease in shear strength of the slope resulting in failure. These Landslides such as those in Dispur Kacharibasti, Rupnagar and Nabagraha occurred due to such reasons. Das and Saikia (2010) reported that the hilly areas of the northeastern part of India are mostly covered by residual soils. From field investigation of the hill slopes around Guwahati, Das and Saikia (2010) concluded that they are composed of mostly two types of

residual soils. A top layer of Reddish residual clay, varying in thickness from few centimeters to about tens of meters and underlain by Pale Yellowish residual soil of silty nature with low plasticity. Pore-water in the soil layers will be subjected to seasonal changes leading to shallow depth slope failures during periods of heavy rainfall.

Apart from the above-mentioned literature, several projects have been undertaken for landslide hazard assessment of Guwahati city. Saikia *et al*. (1996 and 2002) applied a modified version of the Landslide Hazard Evaluation Factor (LHEF). Rainfall intensity, Earth Cutting, Land Cover, Slope Angle – relative relief, Soil erosion – Weathering, Geological formation, Drainage density, were combined with the Geotechnical factors using Slope stability analysis of homogenous slopes with GWT (Ru) ultimately giving the Landslide susceptibility map.

It is to be noted that Landslide Studies concerning Guwahati city have been mostly based on the LHEF, which is a semi–heuristic method. The weight factors based on lithology Soil and Rock given almost similar weights Hydrogeology – surface indications Dry – Damp – Wet – Dripping – Flowing Landslide triggering mechanism not included Landslide susceptibility map

2.11. CRITICAL APPRAISAL

Cascini (2008) provided a review of the applicability of different landslide susceptibility and hazard zoning methodologies at various scales from European experience of Landslide Hazard Zonation. Table 2.5 gives the level of sophistication in relation to the models used for landslide susceptibility and hazard zonation. Table 2.6 gives the methodology that is more appropriate in relation to a particular zonation scale for landslide studies. Considering Guwahati city (approximate area of 328 sq. km), the most appropriate scale is ‘Large Scale’ (1:25,000 to 1:5000) which should be adopted for areas ranging from 10 to 1000 sq. km. Therefore, from the recommendation of Cascini (2008), physically–based (sophisticated or geotechnical slope models) zoning methodology along with advanced zoning levels is likely to yield better results.

Table 2.5 Methodology and criteria considered for Landslide Susceptibility and Hazard Zonation (Cascini, 2008)

Method	Procedure \ Input	Topography, landslide inventory, geology, geomorphology	Adding soil classification and depth, terrain units	Adding hydrogeology and geotechnics
Basic	Heuristic or empirical models	*		
Intermediate	Statistical analyses	*	*	
Sophisticated	Deterministic (physically based or geotechnical) models	*	*	*

Table 2.6 Methods, levels, and types of zoning at different scales (Cascini, 2008)
* – Applicable; (*) – May be applicable; [*] – Not recommended or not commonly used

Scale description	Indicative range of scales	Zoning methods			Zoning levels			Types of zoning		Purpose
		Basic	Intermediate	Sophisticated	Preliminary	Intermediate	Advanced	Susceptibility	Hazard	
Small	<1:100,000	*			*			*		Regional zoning - Information
Medium	1:100,000 to 1:25,000	*	(*)		*	(*)		*	(*)	Regional zoning - Information - Advisory
Large	1:25,000 to 1:5000	*	*	*	*	*	*	*	*	Local zoning - Information - Advisory - Statutory
Detailed	>1:5000	[*]	(*)	*	[*]	(*)	*	(*)	*	Site specific zoning - Information - Advisory - Statutory - Design

Generally, in an Indian context, van Westen *et al*. (2011) noted that the procedure of landslide susceptibility assessment, which is followed by Geological Survey of India (GSI), is based on a heuristic approach that uses fixed weights or ranking of geofactors, while following guidelines of the Bureau of Indian Standards (BIS). However, this method is debated for providing inaccurate results. The researcher gave an overview on how the existing methods for landslide inventory, susceptibility and hazard assessment in India could be improved. It was concluded that deterministic methods using several dynamic slope-hydrology and slope stability models could be applied to evaluate the landslide susceptibility and hazard. However, such model has limitations of applicability where the probability of transition of land use pattern outweighs the rainfall quantity in determining the spatio-temporal probability of shallow landslide occurrences.

Pardeshi *et al*. (2013) noted that there are several methods of Landslide Hazard Zonation (LHZ) viz. heuristic, semi quantitative, quantitative, probabilistic and multicriteria decision-making process. However, no particular method is accepted universally for effective

assessment of landslide hazards. Heuristic and semi quantitative techniques involve subjectivity in assigning of weights, and hence the validity of these maps cannot be assessed. Quantitative methods, on the other hand, provide objective methods for determining the weights for a given parameter based on their relationships with landslide occurrence. The advanced multivariate techniques are proved effective in spatial prediction of landslides; however, such methods are largely dependent on the availability and quality of data to be used for the analysis. Physical process-based models have been observed to perform well in LHZ mapping even in the areas with poor database of already occurred landslides.

For any landslide study to be scientific, systematic and comprehensive, it is immensely necessary to have a detailed knowledge of the causal and triggering factors, and their interconnection to landslide processes. A comprehensive LHZ is based on proper identification of the conditions and processes that promote instabilities. It is often possible to estimate the relative contribution of the causative factors and give them some qualitative or semi-quantitative measures. In a given area, most of these causative factors can be recognized with their effects rated and weighed, and thus can be mapped and correlated with each other and with the past landslide occurrences.

Landslide study approaches can broadly be separated into ‘local models’ that focus on single landslide event, and ‘regional models’ that focus on landslide phenomena across a greater spatial extent. Existing statistical or empirical methods may be found suitable for Landslide Susceptibility Zonation at scales of 1:25000 to 1:50000. However, logical explanations of the results and exact knowledge about the dependencies of the causal and triggering parameters are mostly absent in such methods.

Understanding the processes that lead to landslide is very crucial to any successful Landslide Hazard Zonation. Deterministic models can provide a very detailed perspective to the landslide process, which can be utilized to understand and obtain a quantitative relation among various causal and triggering factors. The greatest advantage of such physically-based models is that they allow detailed investigation of failure processes, assessment of the effects of triggering events, and the evaluation of the remedial measures and stabilization works.

The characteristic behavior of the soil undergoing failure should be considered for efficient landslide modelling. In case residual soils, landslides are mostly rainfall induced. The shear strength above the water table, arising from the zone of negative pore pressure, contributes as a major factor in the stability of such slopes. Slope failure occurs because of

the temporary increase of pore water pressure in the topmost layers of the slope. Several studies concerning rainfall, infiltration and landslide mechanism can be found in literature. Numerical models were developed to study the variation of infiltration in a slope with respect to rainfall intensity and its effect on the slope stability.

Deterministic Models are capable of providing detailed description of potential instability under changing environmental and climatic conditions. However, residual soils exhibit high degree of heterogeneity in soil strength, hydraulic conductivity, seepage conditions and other soil parameters. Therefore, the efficacy of deterministic analytical methods in evaluating the stability of slopes comprising residual soils is very limited. The importance of uncertainties in geotechnical engineering and engineering geology is widely understood. There are uncertainties related to the estimation of geotechnical parameters because of the limits on the extent and quality of investigation and testing. It is also necessary to consider the spatial and temporal inherent natural variability of parameters. Such uncertainty is usually assessed by applying different approaches such as the First-order second-moment (FOSM) method, Point Estimate method, and Monte Carlo simulation method. Various researchers applied a probabilistic approach in analyzing the slope stability using the first-order second-moment method. Recently, a number of applications of probabilistic slope stability studies, while considering spatial variability, using other numerical approaches, such as Monte Carlo simulation, have been reported in the literature.

A wide range of methods, from the simplest to the most sophisticated, are available for the geotechnical analysis of slopes for a variety of conditions relating to the infiltration, seepage and drainage of water. Considering regional slope stability, comprehensive databases and intricate geological models can be combined within a GIS framework to assess and use relevant information and data for the analysis of slopes. For a proper assessment of landslide hazard, a combination of such methodologies is required.

A significant amount of studies related to landslide stability and hazard assessment of various regions in India can be found in the literature. Yet, not much notice has been given to the state of Assam, and specifically Guwahati, where huge amount of economic loss and loss of lives have been incurred due to the annual occurrences of landslide. Hill slopes within the city of Guwahati consist of residual soils, often in unsaturated condition. Hence, the conventional saturated soil mechanics approach in assessing the stability of these slopes falls inadequate. To assess the potential susceptibility to rainfall-induced landslide, an effective modeling of changes in water content and matric suction in response to rainfall infiltration is

essential. Few of the projects undertaken and the corresponding derived inferences were based on statistical properties of the event, where the qualitative assumption and judgment were based on well-established procedures. However, the data used for the analysis was very limited for the results to be effectively accurate. Geotechnical, geological, and hydrological processes play a major role in influencing the landslide susceptibility of a particular site. Therefore, at the foremost preliminary stage, any engineering study should be targeted to quantify various parameters that can be identified to be the influential towards the stability of a hill-slope. This approach would be better suited to model the landslide zone with sufficient accuracy and arrive at a thoroughly worked out mitigation or protection measure.

2.12. OBJECTIVES AND SCOPE OF THE STUDY

The primary objective of this study is to develop a comprehensive rainfall induced landslide hazard zonation map of landslide prone areas of Guwahati, considering geotechnical aspects of landslide through the application of physically based model, TRIGRS. The objective is supposed to be achieved based on the following scopes of study:

a. Determine the geotechnical parameters related to strength and stability of potential landslide areas in Guwahati city.

b. Assess the infiltration capacity and hydraulic conductivity of the residual soils typically found in this region. Further, determine the unsaturated soil characteristics of local hill slope residual soils, vis., Soil Water Characteristic Curve (SWCC) and unsaturated hydraulic conductivity curve (UHCC).

c. Conduct numerical/analytical studies to ascertain the landslide susceptibility, by applying the results obtained in the previous steps. The numerical model will be used to carry out coupled transient seepage and stability analysis, assess the variation of safety factor of the slope with time, and capture the mechanism of rainfall-induced slope instability.

d. Correlate the past measured rainfall and the observed slope failures associated with corresponding rainfall event. Further, apply the developed curve to calibrate the numerical models for increasing prediction capability of the developed model.

e. Assess the rainfall recurrence and correlate it with landslide occurrence to determine the landslide hazard of the study area.

f. Develop the Landslide Hazard Zonation map of Guwahati city by presenting the obtained results from TRIGRS simulation within a GIS framework.

g. Address the uncertainty issues in landslide hazard analysis and thereby develop probability of failure maps for the region.

2.13. NOVELTY OF THE PRESENT STUDY

A significant fraction of literature addressing landslide hazard studies within India is based on the landslide hazard evaluation factor (LHEF) rating scheme that is proposed by the Bureau of Indian Standard IS 14496 (Part-2): 1998. Application of any physically based GIS model can be counted to a few. The geotechnical perspectives, considering the soil properties and the response of the in-situ soil to rainfall infiltration, have been mostly applied within a local-scale slope stability analysis. The study reports the application of a physically based model, TRIGRS, within a GIS framework to investigate the rainfall-induced regional-scale landslide hazard scenario for Guwahati city, India. The regional rainfall Intensity-Duration-Frequency (IDF) relationships are evaluated and the selected rainfall events (or varying duration and intensity) are considered as input into TRIGRS simulation to generate the Factor of Safety (FoS) maps for the region. The FoS maps corresponding to various such rainfall events are further combined to form the landslide hazard map of the study area, thereby considering the aspect of spatial and temporal landslide recurrence return-period.

Several studies have been conducted to address the effect of DEM resolution on landslide hazard analysis. Few studies can be found addressing the effect of the resolution on TRIGRS simulation results. There are few DEM datasets publicly available vis., CartoDEM, ALOS-AW3D30-DEM, SRTM-DEM, and ASTER-GDEM. Taking the aid of such sources is an economically reasonable and practicable option. Several literatures can be found addressing the accuracy of DEMs for different landslide studies, reporting a wide range of variations in the outcome from the choice of the DEMs. However, until date, no literature has highlighted the influence of the choice of DEMs and its accuracy on the outcomes from TRIGRS simulations. The DEM and its derived parameters are an important input into the simulation process. The accuracy of the DEM is bound to affect significantly the outcome from TRIGRS simulations. The effects of dissimilarity in DEMs on the TRIGRS simulation output are studied and reported in the present dissertation work. Significant differences are obtained among the outputs from the usage of various base DEMs, thereby highlighting the importance of the analysis.

Several studies can be found in literature that reports the analysis of rainfall-induced slope instability while considering the rainfall intensity duration and antecedent conditions. Thus, the importance of the unsaturated soil characteristics in rainfall induced slope failure studies is emphasized. Most of the available studies have considered a constant rainfall intensity over a particular duration, along with the changes in the initial simulation conditions to account for antecedent conditions. Very few studies have considered the effects of varying rainfall patterns on slope stability in local or regional scale. The effect of variations of the rainfall pattern on landslide triggering on a regional scale have never been addressed. In the present dissertation work, the changes in the hill-slope stability due to rainfalls having various patterns, durations, and return periods, is studied with the application of a physically-based model, TRIGRS, on a regional scale within a GIS framework. A detailed comparison was provided about the stability condition of the hillslopes as a response to actual rainfall events that triggered landslides to other rainfall events that were unable to trigger landslides. The study is successful in highlighting the complex mechanism of the antecedent rainfall and in-situ conditions, along with the intensity and duration of the triggering rainfall.

Even within an apparently homogenous soil layer, there exists noticeable variability in the geotechnical properties. Such variability arises out of depositional and post depositional, geological and geomorphological processes. In practice, uncertainty in geotechnical analysis or design arises as a very insignificant portion of the total volume of soil can be sampled. This mostly results in insufficient data that does not lead to any sufficiently conclusive inferences about the soil condition. Deterministic approaches ignore such spatial variability and relies on an analysis based on single-valued or equivalent soil parameters. A factor of safety (FoS), mostly based on experience and engineering judgment, is assumed to address different forms of uncertainty. Although this approach might be just sufficient for local scale analysis involving a particular landslide, it fails to corroborate to the actual landslide scenarios in a regional or global scale. Hence, in the present study, the conventional methodology is extended to consider the uncertainty and variability of the soil parameters to assess the probabilistic landslide hazard scenario of Guwahati city, India. A code was developed to generate random soil parameters with different probability density functions (pdf). The dependence, or correlation, among the various parameters are also incorporated in the code. An auxiliary code is developed to execute the TRIGRS simulation within a MatLab environment, aided by Monte Carlo simulation techniques to generate Probability of Failure maps for the study area.

Hence, overall, the present dissertation study is successful in blending the geotechnical and geological perspectives in a physically based model, TRIGRS, operating in a GIS platform, to portray the deterministic landslide hazard maps and probability of failure maps for the Guwahati city, India. Both local and regional scale landslide hazard analysis are successfully elucidated in the present dissertation work. As per the knowledge of the author, such detailed and intricate landslide hazard study of this region has not yet been reported.

2.14. SUMMARY

This chapter presented the literature relevant to the research topic, with emphasis on rainfall induced slope failure, and rainfall induced landslide susceptibility and hazard assessment. The review of literature illustrates the methodology adopted to analyze stability of slopes under the condition of rainfall infiltration. The literature review also illustrates how various researchers have considered the uncertainty issues and developed methodology to quantify the uncertainty through a probabilistic approach. The literature review illustrated how various researchers have applied different methodologies to assess the landside susceptibility and hazard. The application of physically based models by several researchers to quantify the landslide susceptibility and hazard of their respective study area is also elucidated. The critical appraisal of the literature review was presented in short followed by the objective and scope for further work.

Chapter 3. STUDY AREA & METHODOLOGY

3.1. INTRODUCTION

The city of Guwahati is located approximately within latitude (91°33' – 91°52'6") E and longitude (26°4'45" – 26°14') N with its cardinal points as latitude 26°10′N and longitude 92°49′E covering an area of approximately 328 sq. km, and is an important city of the state of Assam (Figure 3.1) (GMDA, 2009). Guwahati is the gateway to the entire North Eastern India. The city has a well-developed connectivity with the rest of the country and acts as a trade, socio-economic and communication center. Hence, the development of the city is not only critical to the state of Assam but also to the entire Northeast. The city has as such undergone an exponential growth. It is therefore extremely important that, the city follow a holistic and an all-round development.

The economic growth in the city has led to massive population influx in the past two decades. The hills of the Guwahati city is been put serious anthropogenic pressure. Given the socio-economic significance of the city to the entire region, it is quite evident that population of the city would continue to grow rapidly in the future. Unwise expanded development of human activities can increase the incidence of landslide disasters. Thus, the Guwahati city is been chosen as the study area bearing in mind its importance and its vulnerability in the perspective of landslide hazard.

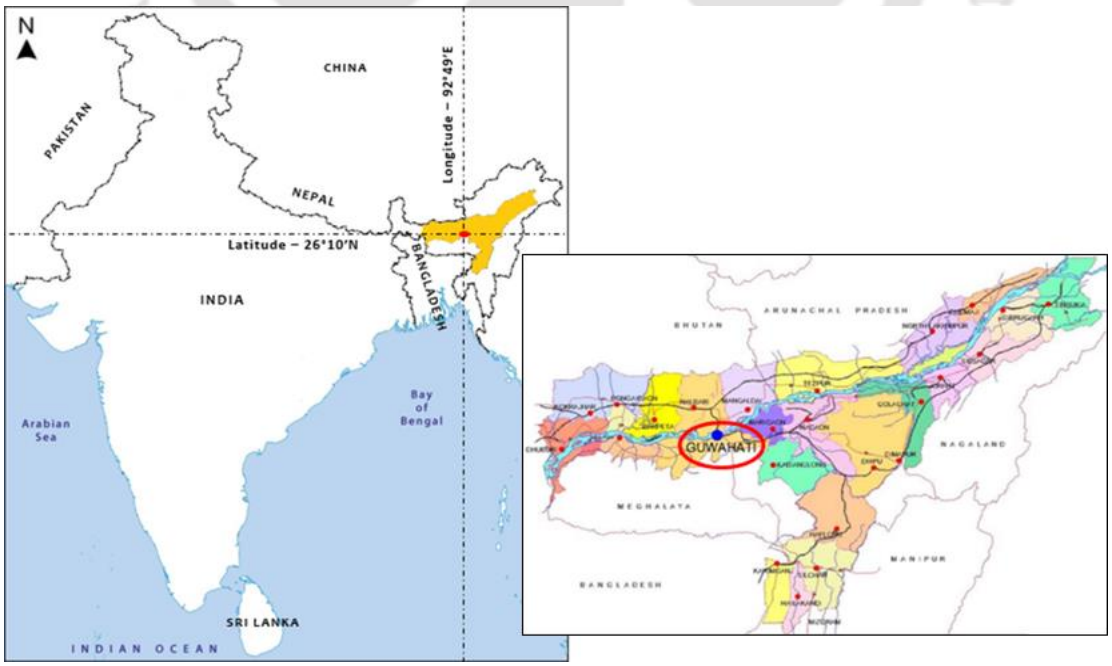

Figure 3.1 Geographic location of study area – Guwahati (GMDA, 2009)

3.2. HISTORY OF LANDSLIDE OCCURENCE

The first reported landslide occurrence on 18 September 1948 caused an estimated 500 fatalities (Petley and Bulmer, 2004). It was mentioned that that highest number of fatalities in Asia occurs from small landslides. However, the number of fatalities is usually being under-estimated due to fact that majority of the landslide events remain unreported. Table 1 lists a few of the recorded landslide occurrences in the hillslopes of Guwahati city area, as reported in several literature (Deka, 1991; Sarma and Goswami, 1991; Das 1992; Sarma and Bora, 1994; Saikia *et al*, 1996; Saikia 2002; Das, 2003; Goswami and Singh, 2008; Goswami, 2013; Bhusan *et al*., 2014).

Table 3.1 Summary of the documented landslide events in Guwahati city

Year	**Month/ Date**	**Locality**	**Hill Series**	**Brief description of the landslide as reported in literature**
1982	14th August	Birubari	Fatasil	Occurred after heavy rainfall. Destroyed the house in the path of the sliding mass killing all four members of that family.
1986	September	Chandangiri	Nabagraha-Sunsali-Noonmati	Sudden toppling failure of soil and rock mass. Open drainage of wastewater into the slope crest and face by uphill inhabitant was the prime causal and triggering factor. The landslide killed two persons. Two more slides followed in the rainy season of 1989 and 1991.
1987	5th September	Dhirenpara	Fatasil	Sudden translational failure accompanied by dislodging of corestones occurred. The debris moved to a considerable distance downhill damaging eighteen numbers of small houses. The length of the landslide was approximately 50m and width approximately 40m. Seven days prior to the landslide, an earthquake caused cracks to develop in the rocky outcrops along with a subsidence in the toe region of the landslide area. Heavy seepage developing into a stream of water was observed after the landslide.
	26th September	Nabagraha	Nabagraha-Sunsali-Noonmati	

Year	Month/ Date	Locality	Hill Series	Brief description of the landslide as reported in literature
1988	10th July	Rupnagar	Narakashur	Shallow translational failure which evolved into mud flow followed by dislodging of corestones
		Kharghuli	Nabagraha-Sunsali-Noonmati	
		Nabagraha	Nabagraha-Sunsali-Noonmati	
	27th August	Pahartali, Kalapahar	Narakashur	The landslide claimed 6 lives. Dislodging of Corestones occurred, which then rolled downslope destroying everything in its path.
1989	15th July	Nabagraha	Nabagraha-Sunsali-Noonmati	
		Kacharibasti	Narakashur	Slow translational failure. Small-dislodged corestones moved along with the sliding soil mass. Failure occurred along the basal rock interface. Seepage was observed over the exposed rock surface.
		Rajbaripath		
1989	29th July	Bishnunagar	Fatasil	Occurred after a total cumulative rainfall of 165 mm in a duration of two days.
1991	3rd August	Dakshin Sarania	Nabagraha-Sunsali-Noonmati	
	14th October	Kacharibasti	Narakashur	The landslide claimed 30 lives. Occurred after a total cumulative rainfall of 248 mm within just two days. Shearing and dislodging of Corestones occurred, which then rolled downslope destroying everything in its path.
1999	15th July	Anandanagar	Nabagraha-Sunsali-Noonmati	Sudden translational failure. The length of the landslide was approximately 25m and width approximately 20m.
2000	10th July	Luit Nagar	Nabagraha-Sunsali-Noonmati	Sudden translational failure of a steep slope following toe cutting.
	7th August	Anandanagar		Slow translational failure.

Year	Month/ Date	Locality	Hill Series	Brief description of the landslide as reported in literature
	14th August			
	19th August			Sudden translational failure.
2002	20th August	Khanapara	Khanapara	Slow translational failure. Movement continued for 2 days. The length of the landslide was approximately 100m and width approximately 50m.

Apart from the documented landslides, there are numerous occurrences of slope instability occurring over the years, which remain unreported in the literature. As can be deciphered from the collated literature, landslides in the northeastern region of India are primarily rain triggered, although the anthropogenic causal factor cannot be denied. In most cases, the initial destabilization is caused by human activities such toe cutting or change in drainage pattern, leading to the excessive runoff or drainage water accumulation into the hillslope face. Mostly, the landslides are initiated as sudden translational movement, while the rainwater infiltration leads to the triggered failure by decreasing the soil suction. The landslides can be classified as 'Earth slides' (Varnes, 1978; Hutchinson, 1988; Abramson *et al*., 1996) (complex slides involving rolling down of dislodged corestones in some cases), having 'extremely rapid' (5 m/sec) to 'very rapid' (3 m/min) velocity (Cruden and Varnes, 1996). The corestones embedded in the soil matrix may be exposed due to the slide itself or due to and washing off of the soil from slope face, resulting in aggravated debris flow adding to the catastrophe. Thus, although the landslides in this region involves relatively lesser volumes of soil (typically 100-400 m^3), their catastrophic characteristics and their proximity to urbanized areas cause significant damage to infrastructure and loss of lives.

3.3. ASDMA REPORT OF THE JUNE, 2012 EVENT – RVS POINTS

In the month of June 2012, seven landslide occurrences were reported in the Guwahati city along with the death of four persons in two separate landslide events (Figure 3.3 & Figure 3.5). Following the events, the State Government of Assam, India, ordered an official investigation into the occurrences in the month of July 2012. A visual reconnaissance of the landslide areas was conducted under Assam State Disaster Management Authority (ASDMA).

Rapid Visual Screening (RVS) for landslide in and around Guwahati was conducted to identify landslide prone and make a field observation of the anthropogenic causative factors and various geo-environmental processes that finally triggers a slope failure.

Hillocks in Guwahati were visited with a GPS instrument, digital camera and data sheet. Factors such as type of soil comprising the slope, slope inclination, height, land movement, tilting trees, crack in the slope, elevation difference across cracks, seepage of water within the slope, significant change in the water level in nearby the wells were considered for delineating landslide prone areas.

The findings were published in the form of an official report – "Rapid Visual Screening (RVS) of Potential Landslide Areas of Guwahati" (Goswami, 2013). The report presented the location of the landslide occurrences in the month of June 2012 along with other landslide prone areas in the form of GPS Latitude-Longitude coordinate point, overlaid on top of Google Earth Imagery (Figure 3.2).

Presently, it is the only document publicly available, describing the in-situ landslide scenario of the Guwahati hill slopes. The areas delineated in the report were revisited in-situ, and 347 locations were considered for this study. The locations, henceforth, will be referred as RVS-points. The RVS locations are then used for comparative assessment, evaluation and validation of the simulation outcomes.

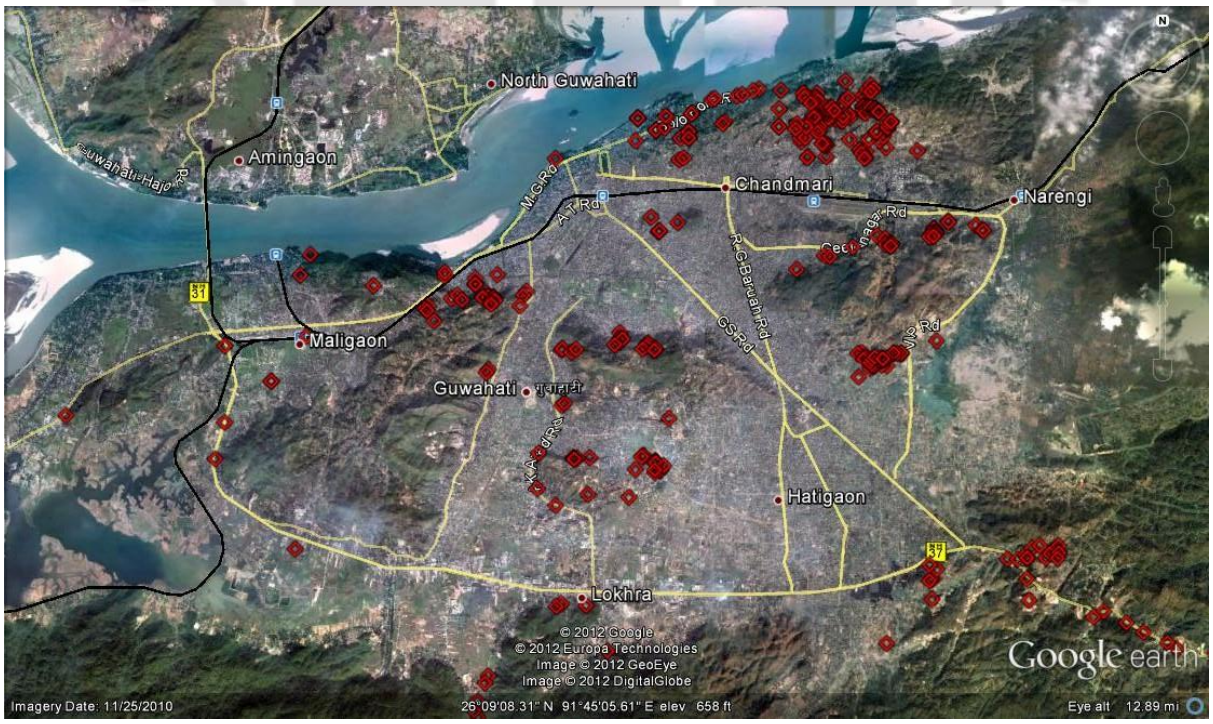

Figure 3.2 Landslide prone areas of Guwahati city shown by RVS points (Goswami, 2013)

Figure 3.3 Landslide at Dhirenpara Tila, Fatasil Hill (26º 09' 2.2" N, 91º 43' 39.7" E) (Goswami, 2013)

Figure 3.4 Landslide at Mathuranagar, Santipur, Fatasil hill (26º 09' 50.5" N, 91º 43' 41.7" E) (Goswami, 2013)

Figure 3.5 Landslide at Khanapara hill (26º 0' 10.7" N, 91º 51' 48.9" E) (Goswami, 2013)

3.4. GEOMORPHOLOGY

The area presents a tough topography, exhibiting three prominent geomorphological feature vis., the residual hills, the low–lying alluvial plains and the marshy wetlands. The hills with altitude ranging 100–300 meter are interspersed with elongated low–lying alluvial plain with varying altitudes of 49–56 meter above mean sea level (MSL). The hillslope angles vary from a gentle 10° slope to as steep as 70°. Eight major hill series can be identified within the city of Guwahati and are numbered for easy reference (Figure 3.6) as follows: (1) Noonmati and Sunsali hill series, (2) Japorigog hill, (3) Sonaighuli and Jutikuchi hill series, (4) Narakashur hill, (5) Nilachal hill, (6) Fatasil hill, (7) Jalukbari hill, (8) Khanapara hill. Agyathuri hills (9) (Figure 3.6) on the North-West of the area has also been included in this study though it does not fall within the municipal boundary of Guwahati city.

Much of the relief of the hillslopes can be directly attributed to differential weathering, drainage conditions, landslides and erosion acting most effectively in the weaker zones and

along lines of structural weakness (Selby, 1993). Zones of well drained regions with thick soil formation as well zones of moderate, imperfectly and poorly drained regions with exposed rock layers (Das and Saikia, 2010; 2011) due to mantle stripping leading to formation of etch forms and inselbergs are prominent from the geomorphology of the area. The topography of these hills is of the most tortuous nature with repeatedly undulating terrain.

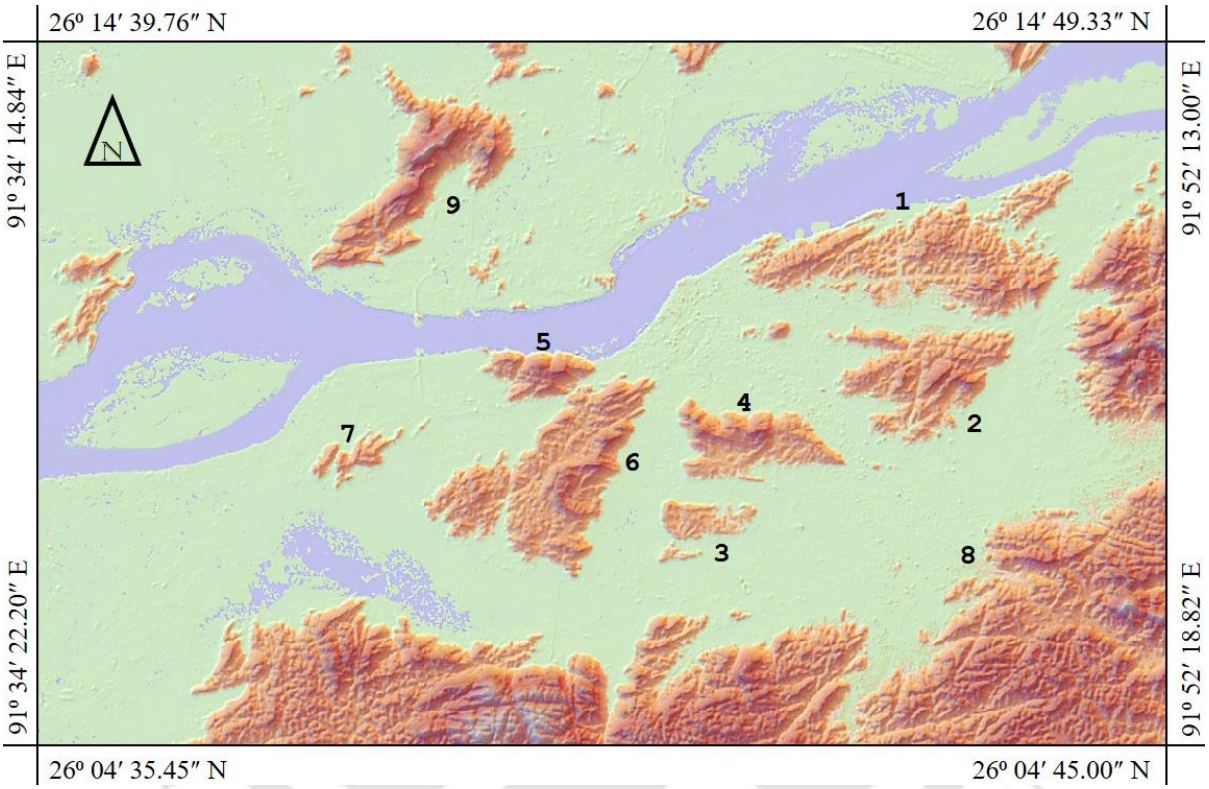

Figure 3.6 Hills within Guwahati city

3.5. CLIMATE

The region has a subtropical climate, with hot humid summers, severe monsoons, and mild winters. The study area is surrounded by the Himalayas to the north, the Meghalaya plateau to the south and the hills of Nagaland, Mizoram and Manipur to the east. Monsoon winds originating from the Bay of Bengal move northeast, the mountains force the moist winds upwards, causing them to cool releasing heavy precipitation on these slopes. Some parts of the region, surrounding the study area are regarded as the rainiest region in the world (Jain *et al*., 2013).

3.6. RAINFALL

The North Eastern Region of India experiences heavy rainfall during the monsoon season spread across the month of April to September. The wetting cycle starts from the month of April to mid of October and drying cycle starts from of November up to March, March being the hottest and driest month of the year. High evaporation rate during the drying cycle leads to the development of considerable suction within the residual soils covering the hilly areas around Guwahati. This phenomenon enables the residual soils to remain stable at much steeper and higher slopes. However, during monsoon season infiltration of rain water into the soil slopes brings about a reduction in the matric suction and ultimately may lead to slope failures. Figure 3.7 gives the mean and the standard deviation (in form of error bars) of monthly rainfall (India Water Portal, 2013) for a period of 1901 – 2002 along with the maximum and minimum recorded rainfall, in the Kamrup district region within which the Guwahati city is located. The data represent the area average rainfall for the whole district for this period. It can be observed that the extreme rainfall events can be occasionally of intensity twice as much the mean of the recorded data. The coeffeicient of variation can be of the order of 45 % for the monsoonal rainfall indicating high variability in the rainfall pattern in the study region.

Area averaged-time series TRMM (Tropical Rainfall Measuring Mission) daily (24–hour) rainfall data set (TRMM_3B42_Daily v7), for the period from 1998 to 2015 has been collected and analyzed to understand the rainfall pattern and its variation across years. The rainfall data set is distributed publicly through the Goddard Earth Sciences Data and Information Services Center (GES DISC). The area-averaged rainfall represents the average of the rainfall estimate over the entire area of the study region for each time interval of data recording. The rainfall data is area averaged over the Guwahati city. Figure 3.8 gives the maximum rainfall intensity (mm/hour) that occurred within a particular year, for the period 1998 – 2015, considering total duration of 24 hours, 36 hours, 48 hours, 60 hours and 72 hours along with the total cumulative rainfall for an entire year.

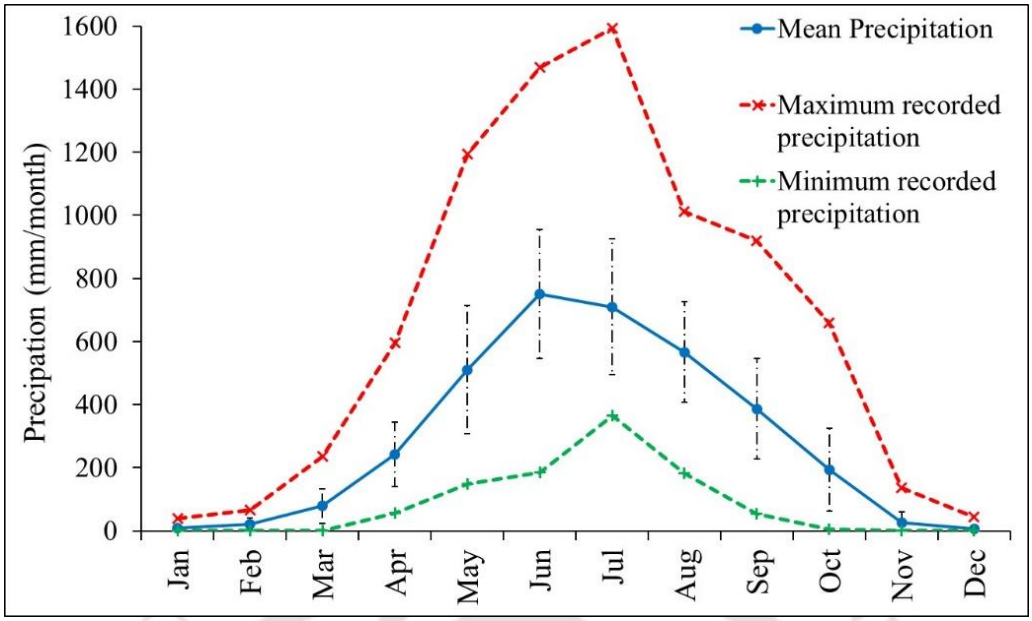

Figure 3.7 Monthly mean rainfall (for a period of 1901 – 2002) in the district of Kamrup

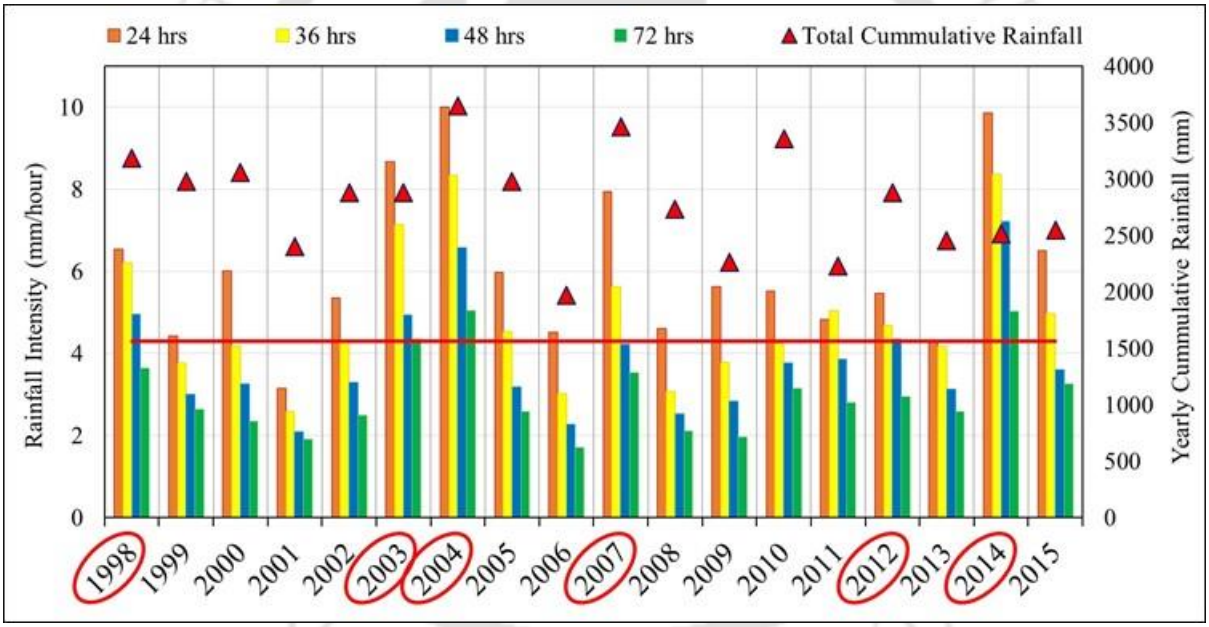

Figure 3.8 Maximum rainfall intensity and yearly cumulative rainfall for the period 1998–2015

Guwahati region experienced several landslide events in the years 1998, 2003, 2004, 2007, 2012 and 2014. The years are marked in Figure 3.8 for easy reference. An approximate landslide triggering rainfall intensity threshold of 4.3 mm/hour (100 mm/day) for a duration 48 hours can be inferred from Figure 3.8. Figure 3.9 and Figure 3.10 shows the rainfall for the year 2012 and 2014 respectively over Guwahati city.

Further to provide more information about the rainfall variation in the Guwahati city for a particular year, daily rainfall data for the years 2012 and 2014 have been presented in

Figure 3.9 and Figure 3.10. The figures show the daily variations of the cumulative rainfall for both the years. The landslide triggering rainfall event is demarcated in the figures.

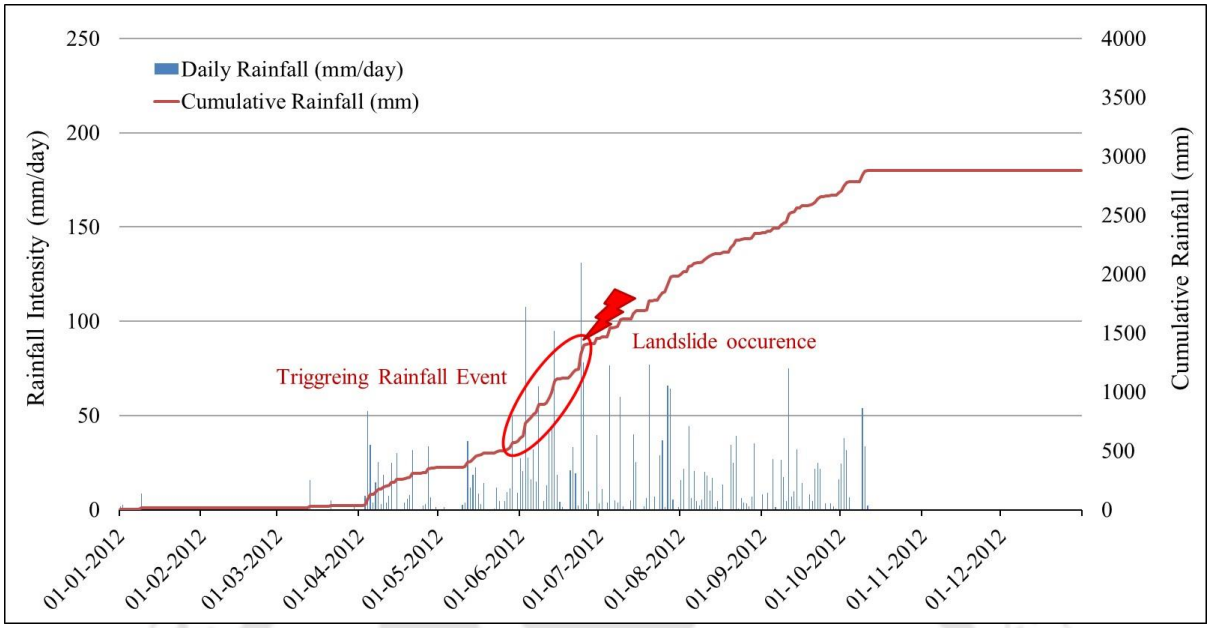

Figure 3.9 Rainfall for the year 2012 over Guwahati city (TRMM_3B42_Daily v7 data set)

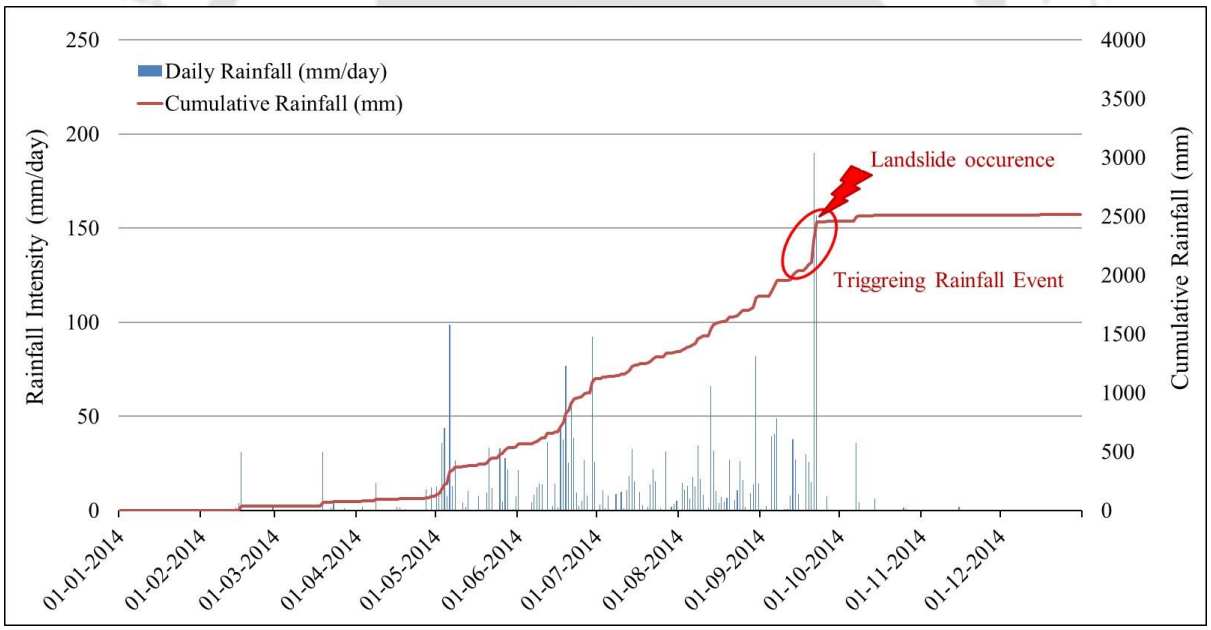

Figure 3.10 Rainfall for the year 2014 over Guwahati city (TRMM_3B42_Daily v7 data set)

3.7. GEOLOGY

The residual hills of the study area are part of bowl like basement of Precambrian Granite–gneisses complex, which is an extension of the Shillong plateau towards its north. The bowl like configuration of this base complex enables the formation of static water bodies

leading to the development of marshy wetlands in the low–lying areas. A cover of Quaternary deposit of Pleistocene–Holocene sediments composed of unconsolidated sand, silt and clay of variable thickness and thin layers of residual clays inter–wind with tracks of the typical Brahmaputra sand, forms the low–lying alluvial plains over this complex. (Phukon et al, 2012).

The hills are made up of the gneisses, granite, porphyritic granite affected by several sets of joints, intruded by quartz and quartz–feldsphetic veins, aplite and pegmatite. Quartzite, amphibolites and biotite schists, occur as thin bands or lenses parallel to the foliation (Figure 3.11 a & b) (Maswood and Goswami, 1974; Maswood, 1981, 1982; Shukla, 1989). The study area falls within a tectonically active region of high seismicity and is subjected to high tectonic shearing, due to which the rocks have developed cracks, fractures, fissures and foliation to high degree.

The stratification is typical of tropical and sub–tropical climatic conditions with very high amount of annual precipitation and excessive fluctuation of the ground water condition. Weathering generally decreases with depth; however, no well-defined boundary can be observed between soil and rock. Depending on the degree of weathering, the soil can retain much of the fabric, or structural features, of the parent rock. Figure 3.12 shows soil profile of a cut slope

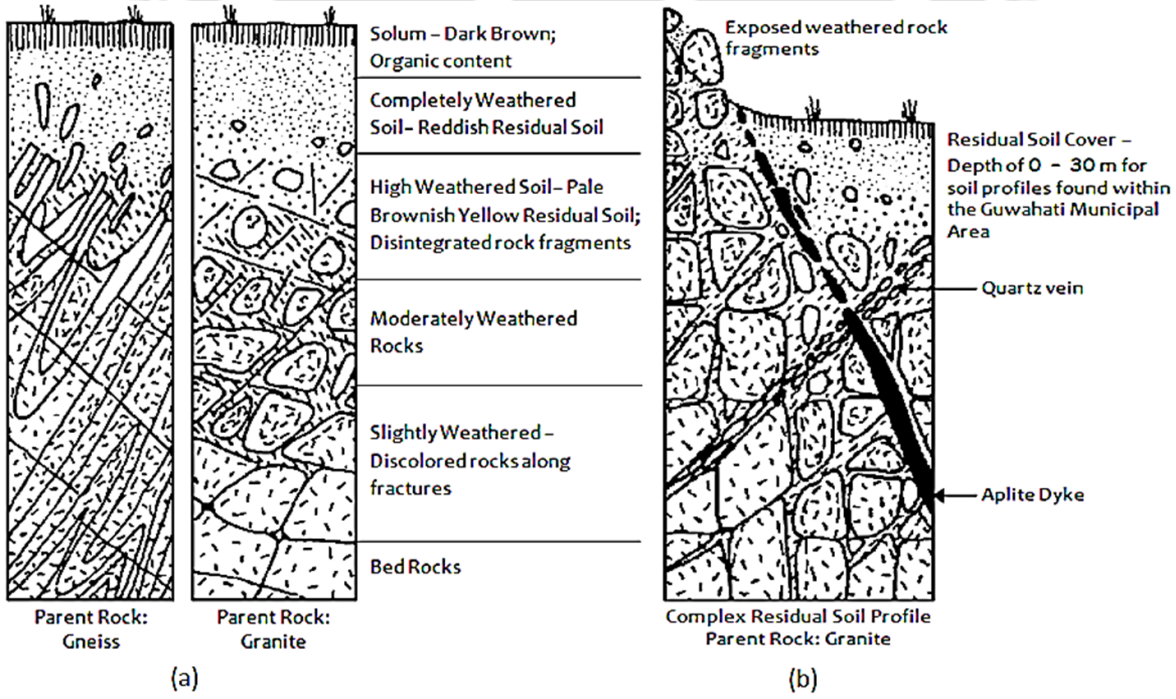

Figure 3.11 (a) Typical Residual Soil Profile and (b) Complex features found in residual soil profile of hill slopes of Guwahati (adapted from Selby, 1993)

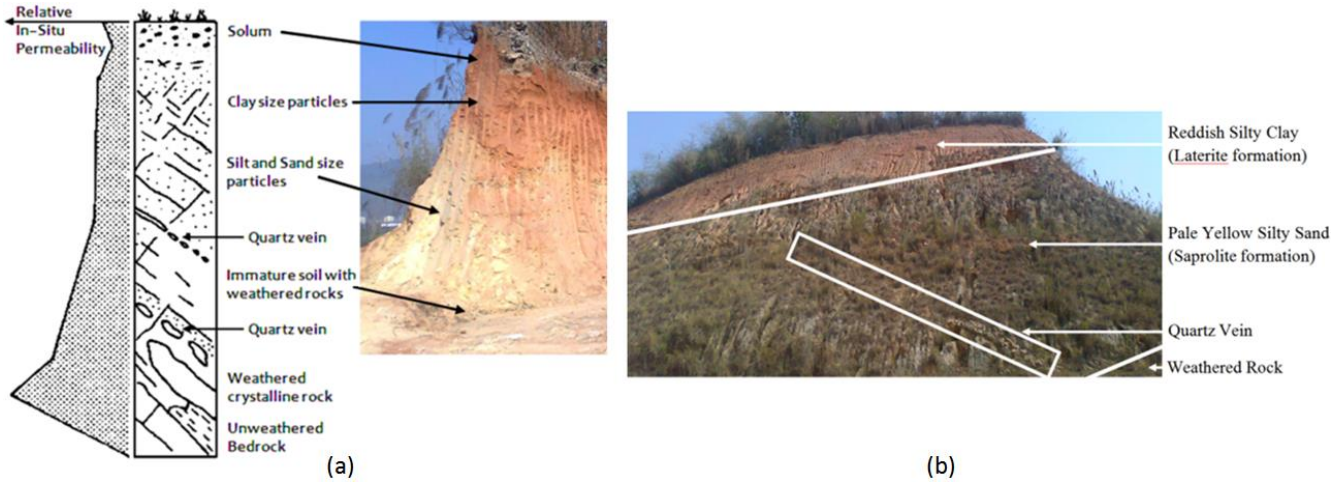

Figure 3.12 (a) Soil profile of a cut slope (from Selby, 1993) (b) soil profile of another cut slope at the IIT Guwahati Campus

From field investigation of the hill slopes around Guwahati, Das and Saikia (2010, 2011) reports two types of commonly found residual soils. Figure 3.13 gives the images of the cut slope at various location of Guwahati. The soil formation is observed to be considerably similar for different hillslopes of Guwahati. Two distinct layers of soil can be easily identified from the images. Macro-structural features such as relict joints, relict veins, secondary clay seams, relatively less weathered intact rock slabs, irregular zones of contrasting weathering, differentially weathered dykes, corestones, etc. can be observed from Figure 3.13. Hill slopes within the city of Guwahati consist of geological stratification, that characterize progressive stages of residual weathering, which can be categorized as basal rock, decomposed granitic rock and corestones, saprolitic and lateritic residual overburden.

3.8. TOPOGRAPHICAL DATA – DIGITAL ELEVATON MODELS

Digital Elevation Model (DEM) is a representation of the topography of particular area in Raster form. The DEM itself consists of a matrix of numbers. The DEM gives the height information of a particular predefined area referred to as cells. The dimension of the individual cells defines the resolution of the DEM. A DEM is often required for flood or drainage modelling, land-use studies, landslides studies, geological applications, and other applications. There are few DEM available publically for the study area, vis., Indian Space Research Organisation (ISRO) CartoSat-DEM (CartoDEM - 1/3 and 1 arc sec), Advanced Land Observing Satellite (‘DAICHI’), AW3D30-DEM (ALOS-3D), Shuttle Radar Topography Mission (SRTM-DEM), Advanced Space Borne Thermal Emission and

Reflection Radiometer- Global DEM (ASTER-GDEM). Figure 3.7 shows the AW3D30-DEM for the study area.

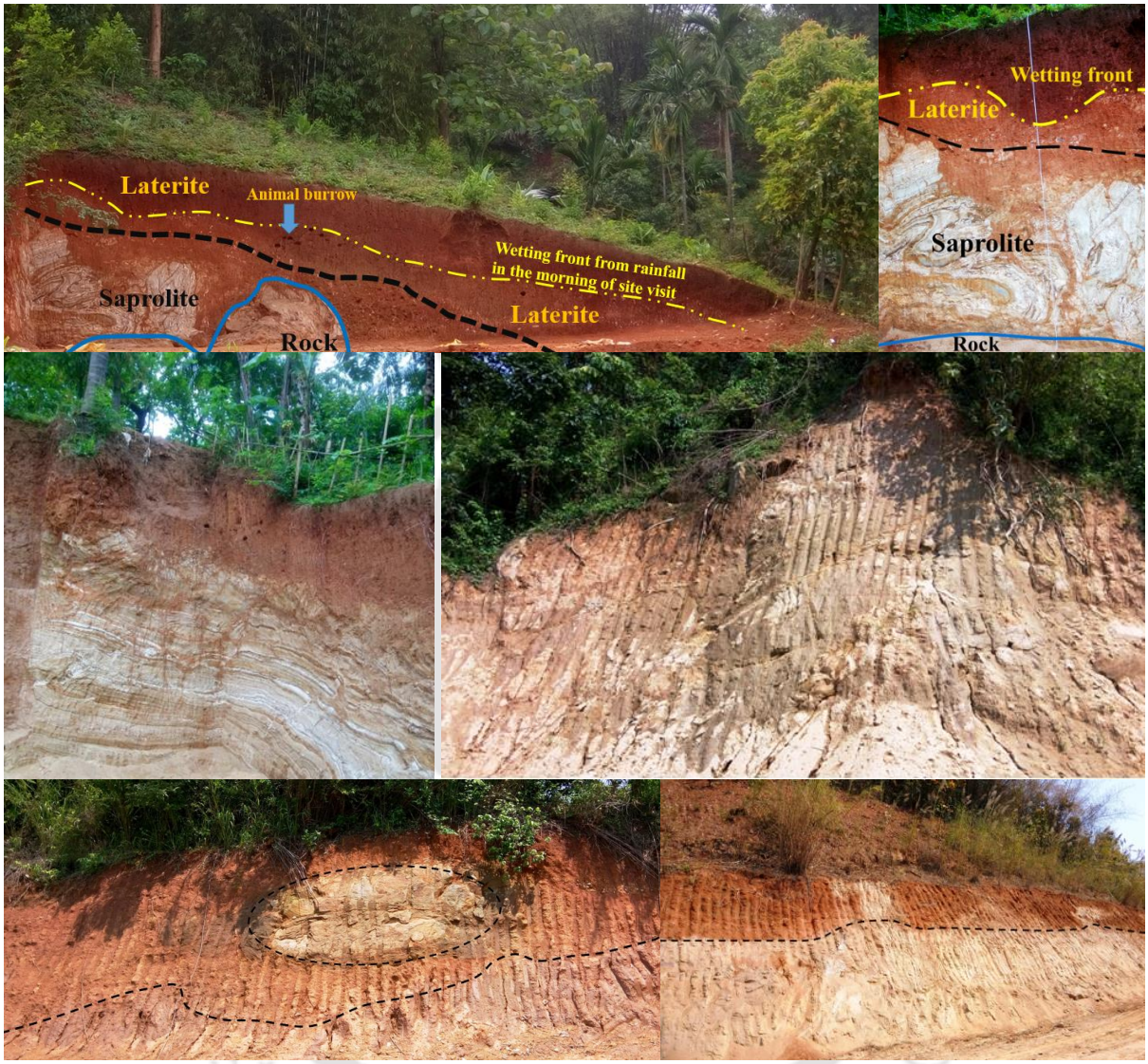

Figure 3.13 Cut-slopes at Nabagraha-Sunsali-Noonmati hill series (top) and hillock at IIT Guwahati campus near Agyathuri hills (bottom)

3.9. METHODOLOGY

The basic objective of this research is to study the landslide susceptibility and hazard of the hill region of the study area. With that purpose in mind, simulation within a GIS platform using physically based model for generating the factor of safety map is carried out. Extensive field and laboratory investigations are conducted to ascertain the hydrological and geotechnical characteristics of the hillslope soils. Numerical analysis of the failure mechanism involved in rainfall-induced landsliding is carried out using soil input parameters obtained from field and laboratory tests. Based on the numerical simulation results along with

field observation, refinement of the physically based model is done to model the timing and location of landslide occurrence with reasonable accuracy. The rainfall intensity–duration–frequency are evaluated. Landslide recurrence of the study area is determined as response to applied rainfall of intensity–duration representative of the return periods. The outcome is then combined to form the landslide hazard map of the study area. Probabilistic slope stability is carried out the physically based model to generate the probability of failure map, taking into account the variability of the soil parameters. Figure 3.14 gives a diagrammatic representation of the methodology adopted for the present study, and shows the connectivity and flow of the steps involved in the work done.

3.10. SOFTWARES AND CODES

These sections provides a brief introduction of the software and codes applied in the research work.

3.10.1. GeoStudio

GeoStudio is a geotechnical software suite within which the modules SLOPE/W and SEEP/W are present. SEEP/W is a finite element code capable of analysis steady state / transient flow of water through a saturated / unsaturated porous medium. SLOPE/W calculates the Factor of Safety (*FoS*) of finite slope using the Limit Equilibrium Method. The analysis result of SEEP/W can be incorporated into SLOPE/W to model the gradual degradation of slope stability with rainfall infiltration.

3.10.2. FLAC

FLAC (ITASCA, 2005) is the abbreviation of “Fast Lagrangian Analysis of Continua” and is developed by ITASCA. The FLAC software is based on the explicit finite difference method. Highlight of FLAC is the programing interface FISH, which presents a great deal of flexibility to the usage of the software. The finite difference zones modelled in FLAC can be assigned different values of parameters over single continua providing the required platform for simulating random field and performing probabilistic slope stability analysis.

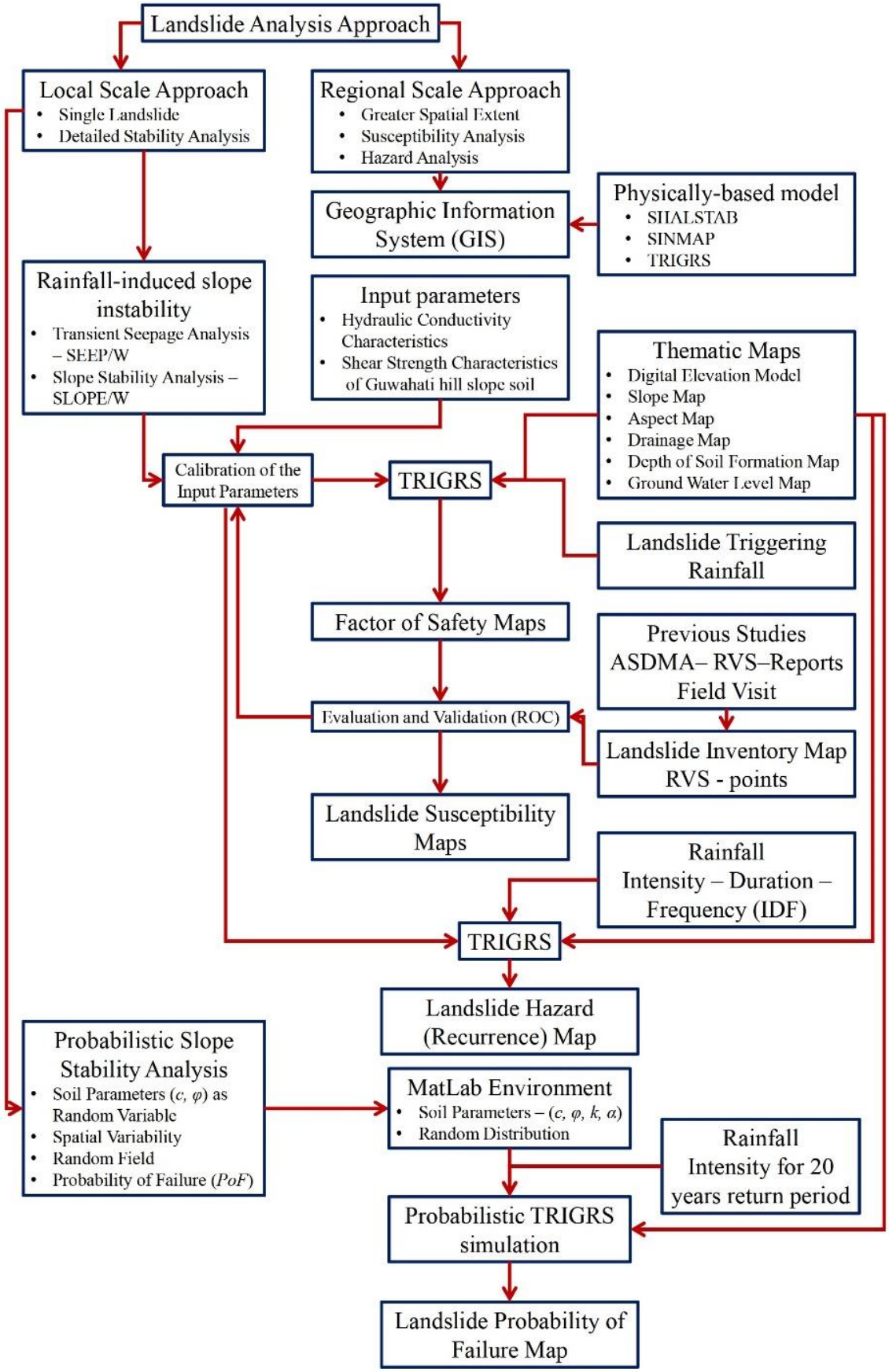

Figure 3.14 Methodology of the study

3.10.3. Geographic Information System

ILWIS

The Integrated Land and Water Information System (ILWIS) is a GIS and remote sensing software, developed by International Institute for Geo-Information Science and Earth Observation, University of Twente. ILWIS comprises a package of image processing, spatial analysis and digital mapping software. ILWIS is capable of geo-statistical analyses and advanced geo-hydrological process modelling on DEM.

QGIS

QGIS is a free and open-source cross-platform desktop geographic information system (GIS) application that supports viewing, editing, and analysis of geospatial data. QGIS can import – export geospatial data in various available formats. QGIS offers a wide range of user-friendly tools for efficient editing such snipping, extracting and merging of geospatial data.

SAGA-GIS

System for Automated Geoscientific Analyses (SAGA GIS) is a geographic information system (GIS) computer program. Developed initially by the Department of Physical Geography, University of Göttingen, Germany. SAGA-GIS has several terrain analysis tools for geomorphometric calculations such as slope, aspect, curvatures, curvature classification, analytical hill shading, sink elimination, flow path analysis – upslope catchment area and catchment delineation along with grid tools for merging, resampling, gap filling of geospatial data.

3.11. PHYSICALLY-BASED MODELS

Infinite slope stability model

The infinite slope stability model (Figure 3.15) demands a mention at the onset since the TRIGRS models that have been applied in this study is particularly based on this stability concept. This model compares the destabilizing stresses and restorative strength of the material on an infinite plane parallel to the soil surface. No slope can be considered infinite in extent; as such, infinite slope is purely conceptual. However, when the depth of the slip surface is much less compared to the areal extent of the landslide and the field condition remains nearly identical, then such a mathematical model can be applied for estimating a close approximation of the stability condition (Bromhead, 1992). The other most

advantageous feature of this model is that, it is readily applicable to the grid-based GIS framework for determination of the stability condition on a spatially distributed setting. The Factor of Safety (*FoS*) can be calculated for each cell of the grid and the results presented in the form of a FoS–map.

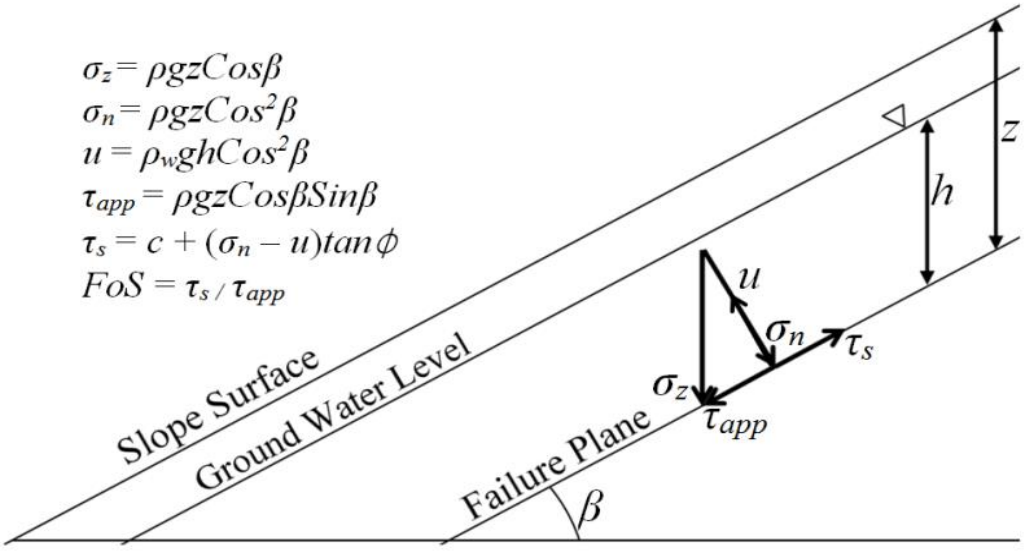

Figure 3.15 Infinite slope model

Factor of Safety based on Limit-equilibrium concept is defined as ratio of the shear strength of the material to the destabilizing stresses along an assumed failure plane, and is expressed as in Equation 1.

$$FoS = \frac{Shear\ \ Strength\ \ of\ \ concerned\ \ material}{Applied\ \ Shear\ \ stress} = \frac{\tau_s}{\tau_{app}} \tag{3.1}$$

Mohr–Coulomb failure criterion (Eq. 2) gives the shear strength of the material as a function of the soil cohesion and frictional resistance due to the effective normal stress on the failure plane

$$\tau_s = c' + (\sigma_n - u_w)\tan\varphi' \tag{3.2}$$

where, τ_s is the shear strength of the soil, c' is the effective soil cohesion, φ' is the effective angle of internal friction, and, σ_n and u_w are the total normal stress and pore water pressure on the failure plane.

The basic formulation of the *FoS* for an infinite slope can thus be expressed as:

$$FoS = \frac{c'}{\rho g z \sin\beta \cos\beta} + \left(1 - \frac{\rho_w}{\rho}\frac{h}{z}\right)\frac{\tan\phi'}{\tan\beta} \tag{3.3}$$

where ρ is the bulk density of soil, ρ_w is the bulk density of water, z is the vertical depth of failure plane from slope surface, β is the slope angle, h is the vertical depth of failure plane from ground water level, and g is the acceleration due to gravity. If the shear strength is greater than applied shear stress then $FoS > 1$, and the slope is considered stable from the viewpoint of limit equilibrium. If the applied shear stress exceeds the shear strength, or somehow the shear strength decreases due to increase in pore water pressure, then the existing applied shear stress, then the *FoS* falls below 1, and slope consequently is subjected to failure.

Selby (1993) proposed a modification of the infinite slope stability model for accommodating various in-situ factors

$$FoS = \frac{c_r + c_s}{\rho_s g z \sin\beta \cos\beta} + \left(1 - \frac{\rho_w}{\rho_s}\frac{h}{z}\right)\frac{\tan\phi}{\tan\beta} \tag{3.4}$$

where ρ_s is the saturated soil density, c_r is the root cohesion, and c_s is the soil cohesion. Saturated soil density parameter is used due to its similarity to field conditions when a landslide is triggered. It must be noted that *FoS* value does not represent absolute stability or instability. The decrease of *FoS* occurs with an increase of the water level and corresponding reduction of effective stress. During a rainfall event, the water table elevation reduces *FoS*. The probability of slope failure increases with increasing intensity and duration of the rainfall event. During dry season the water table recedes and the stability increases with an increase of *FoS* values (Selby, 1993).

Steady-state Sub-surface Hydrology

Hydrological factors have a direct influence on the slope stability–instability condition. Therefore, it is essential to apply a hydrological model for estimating the depth of ground water level. Both SHALSTAB and SINMAP is based on the hydrological concept as is described in TOPMODEL (Beven and Kirkby, 1979) and TOPOG (O'Loughlin, 1986) for modeling steady-state shallow subsurface ground water condition. The models map the spatial variation of the ground water table in the form of the Wetness Index derived from the upslope contributing catchment area, soil transmissivity and slope angle for a steady-state recharge. The final formulation of the Wetness Index is as that given in Equation 3.5.

$$W = \frac{qa}{bT\sin\beta} = \frac{h}{z} \tag{3.5}$$

$$T = K_s z \cos \beta \tag{3.6}$$

where, q is the steady state recharge, a is the upslope catchment area draining through contour length of b, T is the soil transmissivity and K_s is the saturated hydraulic conductivity, considered homogeneous along the soil depth. The area a represents the watershed elements obtained through the intersection of contours and drainage boundaries orthogonal to the contours. For the present study, the Multiple Flow Direction method, termed as $D\infty$ method developed by Tarboton (1997), is applied for flow routing for all the three models. Based on the flow routing procedure, the upslope catchment area is computed using a recursive procedure proposed by Mark (1988). Wetness Index, $W > 1$ indicates saturation of the soil layer, and W is reset to 1 and the remaining water flows as surface run-off. The basic assumption of this model is that of constant soil transmissivity, which can ultimately be interpreted as constant soil thickness considering identical value of saturated permeability over the entire depth of soil layer.

3.11.1. SHALSTAB

Numerical models of instability Expressing Equation 4 in terms of h/z for $FoS = 1$ results in the saturation amount necessary for the landslide to occur:

$$\frac{h}{z} = \frac{\rho_s}{\rho_w}\left(1 - \frac{\tan\beta}{\tan\phi}\right) + \frac{c}{\rho_w g z \cos^2\beta \tan\phi} \tag{3.7}$$

Thus, replacing the term h/z from Equation 5 into Equation 7 and rearranging, the infinite slope and steady-state hydrological models are coupled and the final formulation of SHALSTAB is presented in the form of the steady-state recharge required to initiate slope instability (Montgomery and Dietrich, 1994):

$$q = \frac{bT \sin\beta}{a}\left\{\frac{\rho_s}{\rho_w}\left(1 - \frac{\tan\beta}{\tan\phi}\right) + \frac{c}{\rho_w g z \cos^2\beta \tan\phi}\right\} \tag{3.8}$$

Therefore, SHALSTAB classifies the region based on the amount of recharge required to initiate instability. The output from this model is expressed in [L/T] of steady-state recharge, lower values indicate a greater propensity for instability and otherwise. However, the problem lies in the proper categorization of the range of recharge for dividing the region into zones of higher and lower instability. As is noted by Montgomery and Dietrich (1994), the steady-state recharge cannot be considered as a long-term average of rainfall. The output q is affected by climatological and hydrogeological factors, slope

inclination, surface vegetation cover, infiltration characteristics of the soil and soil and bed rock transmissivity. For correct interpretation of the SHALSTAB results, correlation of these various factors needs to be considered (Pack et al., 1998).

3.11.2. SINMAP

The Stability Index Mapping (SINMAP), like SHALSTAB, applies a steady-state hydrological model coupled to an infinite slope model within a probabilistic framework (Pack *et al*., 1998). The output of the SINMAP model is in the form of Stability Index (*SI*), which represents the probability that the *FoS* of a slope will be greater than 1.0, assuming uniform probability distribution of the parameters over the uncertainty range. However, unlike SHALSTAB, the maximum and minimum value of the ratio *Tb*/*qa* over the uncertainty range is to be input into the SINMAP model. The steady-state hydrological model as used in SHALSTAB, (Eq. 5) is applied to estimate the soil saturation, assuming that the maximum value is equal to 1. The *FoS* is thus expressed in the form as in Equation 9.

$$FoS = \frac{c_a + \cos\beta\left\{1 - Min\left(\frac{qa}{bT\sin\beta}, 1\right)r\right\}\tan\phi}{\sin\beta} \tag{3.9}$$

where, c_a is the non-dimensional cohesion, and r is the ratio of water and wet soil density, given by

$$c_a = \frac{c_r + c_s}{\rho_s g z \sin\beta} \tag{3.10}$$

$$r = \frac{\rho_s}{\rho_w} \tag{3.11}$$

The input parameters *Tb*/*qa*, c_a and φ are described in terms of maximum and minimum thresholds, except for ρ_s, for which its mean value is used. The uncertainty ranges of the input parameters generate a probability distribution of slope stability (in terms of evaluated *FoS*) between the threshold boundaries. If the lowest value of *FoS* obtained for any combination of the input parameters within the range of uncertainty, is greater than 1, the output is denoted symbolically by FoS_{min} [FoS_{min} = (lowest calculated value of *FoS*) > 1]. At any locations where the minimum *FoS* < 1, there is a probability of failure, and the Stability Index (*SI*) value is then expressed as in Equation 12.

$$SI = \text{Prob}\{FoS > 1\} \tag{3.12}$$

Pack *et al*. (1998) proposes six classification ranges for zonation of the region into stability classes, based on *SI* and FoS_{min} values. For *SI* < 0.5, the location is classified unstable and stabilizing efforts are needed; while for *SI* values ranging from 0.5–1.0 and FoS_{min} values ranging from 1.0–1.25, the locations are classified as quasi-stable to moderately stable and slope destabilization factors are required for landsliding. For FoS_{min} values ranging from 1.25–1.5 and greater than 1.5, the area is classified as moderately stable and unconditionally stable respectively.

3.11.3. TRIGRS

TRIGRS (Transient Rainfall Infiltration and Grid-based Regional Slope-stability) (Baum *et al*., 2002; Savage *et al*., 2004; Baum *et al*., 2008) is a FORTRAN code developed for the purpose of evaluating the transient pore pressure response to rainfall infiltration, and thereby, simulate the temporal and spatial distribution of shallow, rainfall-induced landslides expressed as decrease in the Factor of Safety values. TRIGRS is capable of computing transient pore-pressure changes and changes in the factor of safety due to rainfall infiltration, combined with a simple runoff routing scheme. Complex rainfall histories can be implemented as time step function with varying intensity and duration. A detailed description of the TRIGRS model is presented in Chapter 6.

3.12. SUMMARY

The chapter presents a brief introduction of the study area along with rainfall induced landslide occurrence in the past. The climate, geomorphology and geological formation of the hill slope soil is shown. An overview of the methodology adopted for the study is also presented in form of a flow chart. A brief introduction of the various codes and software used in the study is also given.

Chapter 4. MATERIAL CHARACTERIZATION OF HILLSLOPE SOILS

4.1. INTRODUCTION

Soils of the hill slopes within Guwahati city is a product of physical and chemical weathering process on the parent rock vis., gneisses and granite. From field investigation of the hill slopes around Guwahati, two types of commonly found residual soils can be identified. A top laterite formation of reddish residual silty clay, of thickness varying from few centimeters to few meters which is then underlain by a saprolite formation of pale yellowish residual soil which can be classified as a poorly graded silty sand. Saprolite formation is isovolumetrically-weathered bedrock and retains much of the parent rock structure and fabric but with a much lower density (Selby, 1993). The resulting material is thus very porous and friable in nature and can easily crumble from the slightest disturbance (Armirza, 2004). Exposed saprolite formations are very prone to weathering and can easily loose the finer fraction through the seepage of water leading to loss in the cohesive component of shear strength (Durgin, 1977).

4.2. GEOTECHNICAL SOIL PROPERTIES

A proper understanding of the geology and the geotechnical characterization of the hill slope soil is important for meaningful analysis of rainfall-induced landslide phenomena and proper assessment of the hillslope stability of this region. Disturbed-representative and undisturbed soil samples have been collected from various locations of the hill areas of Guwahati. In-situ as well as laboratory test have been performed on the collected samples to assess the geotechnical characteristics. Test to determine grain size distribution, specific gravity, and Atterberg's limits, is done for classification of the soil types. In-situ bulk density, natural moisture content, dry density and void ratio or the porosity is determined from the undisturbed samples. Triaxial tests were conducted on the undisturbed and remolded samples to determine the shear strength parameters. Laboratory permeability test and in-situ infiltration test is conducted to determine the hydraulic conductivity and infiltration characteristics. The soil water-retention characteristic is determined in the laboratory using soil-suction and volumetric water content sensors and compared with that reported in literature. Such detailed characterization would provide the requisite understanding for an efficient analysis of the rainfall induced natural hill slope failure in this region

Figure 4.1 gives the cross-section of some undisturbed soil samples. Heterogeneities in the form of micro-fabric and mineralogical variations at the material scale (Aydin, 2006) can be most prominently observed in the samples.

Figure 4.1 Cross-section of the undisturbed soil samples.

4.2.1. Soil type and Classification

To determine the grain size distribution of the soil samples the sieve and hydrometer analysis as outlined in IS 2720 (Part – 4)-1985 is followed. The particle size distribution of a granular material is determined by allowing the material to pass through a series of sieves of progressively smaller mesh size and weighing the amount of material that is retained by each sieve, and is expressed as a fraction of the whole mass. Wet sieving is carried out for separating fine grains from coarse grains by washing the soil specimen on a 75-micron sieve mesh. Hydrometer analysis, also known as sedimentation analysis, is carried out to determine the grain size distribution for the fraction of soil finer than 75-micron are used. Soil particles are allowed to settle down from a suspension, which is based on the principle that in suspension, terminal velocity of particles is governed by the diameter of the particles and properties of the suspension. The density of the suspension medium is measured at different time intervals and from that the percentage finer is estimated. The results from the dry sieve and hydrometer analysis are combined and plotted between cumulative percent finer vs. log

size. Figure 4.2 shows the results of the grain size analysis of the soil samples collected from cut slopes at different locations of Noonmati and Sunsali hills, Fatasil hills and IITG hillock near Agyathuri hills at depth ranging from 0.5m to 1.5m from the surface of the slope. The test results are plotted together and it can be observed that the grain size distribution was similar and can be approximated as shown in Figure 4.2. Figure 4.2 also the shows the test results for the soil samples collected at depth of 1.5m to 2.5m at the above-mentioned sites. It can be observed the soil at this depth, had lesser fraction of fine content (<75-micron), and similar to the top soil layer the grain size distribution of the saprolite soil could be approximated as shown in Figure 4.2.

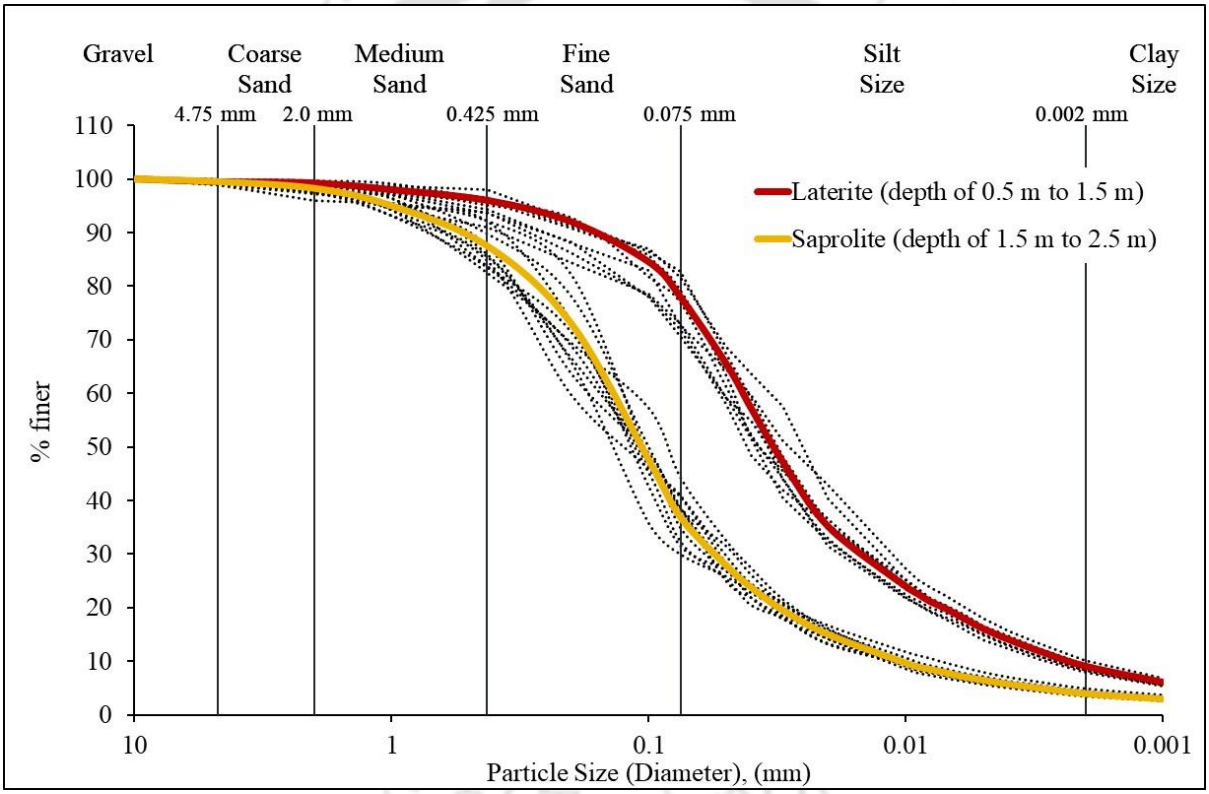

Figure 4.2 Grain-size distribution of hill-slope soil

The Plastic limit and Liquid limit of the soil samples as mentioned above were determined as per the procedure outlined in IS 2720 (Part – 5)-1985. Figure 4.3 shows the plasticity index of the soil samples collected from the top layer. Plasticity Index was observed to be nearer the A-line and the soil can be classified as clay with intermediate plasticity (CI).

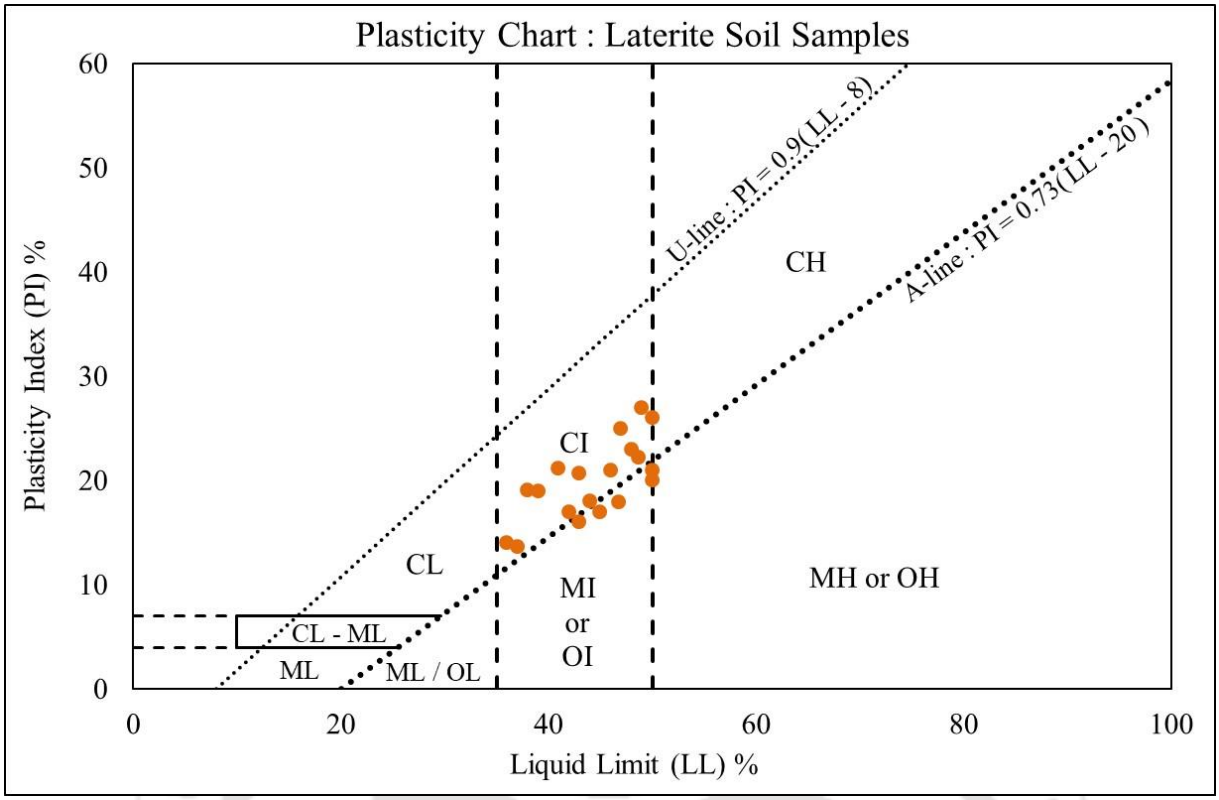

Figure 4.3 Plasticity Index of the laterite soil

The soil samples collected at depth of around 2.0m to 2.5 m were non-plastic sandy silt and as such could not be remoulded into threads of 3mm thickness for conducting the plastic limit test.

4.2.2. Hydraulic Conductivity

Constant head / Falling head Permeability test were conducted as per the procedure outlined in IS 2720 (Part – 17)-1986. Samples were collected from different depths of cut slopes (0.5 - 2.5 m), and the saturated permeability of the specimens was determined by laboratory permeability tests conducted on soil specimens compacted to in-situ density. The tests revealed that the saprolitic soil strata at lower depth is more permeable than the overlying mature lateritic soil. The permeability of the soil layers varied from 10^{-6} m/s approximately at the surface layers to 10^{-5} m/s at the lower layers.

4.2.3. Soil – Water Retention Characteristics

Soil Water Characteristic Curve is the relationship between the water content and matric suction. SWCC can be applied for quantifying unsaturated shear strength and derivation of unsaturated hydraulic conductivity. The SWCC for the soil was determined using Dielectric Water Potential Sensor, (Manifold Pressure Sensor - MPS–1) combined with

volumetric water content sensor (EC–5). The dielectric MPS uses the solid matrix equilibration technique to measure soil suction potential. The sensor is inserted into the soil and the two ceramic disks allowed attaining the state of hydraulic equilibrium with the surrounding soil water potential. The sensor measures the dielectric permittivity of the ceramic disks and gives the output in millivolts. The voltage output is then converted to suction head based on the calibration procedure given by the manufacturer (Decagon Devices, Pullman, WA, USA). The calibration curve is generated by measuring the Dielectric Potential of the ceramic plates and its water content and as such is not dependent on the type of soil into which the MPS-1 is installed. MPS can measure up to 500 kPa (Dielectric Water Potential Sensor, Operator's Manual 2008). The EC-5 sensor measures volumetric water content via the dielectric constant of the soil using capacitance technology. In soil, dielectric permittivity is directly related to the water content. The EC-5 probe outputs a voltage proportional to the dielectric permittivity, and therefore the water content of the soil. The EC-5 sensor needs to be calibrated for the particular type of soil texture and electrical conductivity for corresponding water content range (EC-5 Soil Moisture Sensor, User's Manual 2012). The experimental data is compared with that of literature (Chetia and Sreedeep, 2013) for similar soils of the same region obtained through same experimental procedure. Van Genuchten (1980) model for describing the soil water characteristics is fitted to the experimental data and the fitting parameters thus determined. Figure 4.4 gives the relation of the Volumetric Water Content, (θ) and the Matric Suction, (ψ kPa).

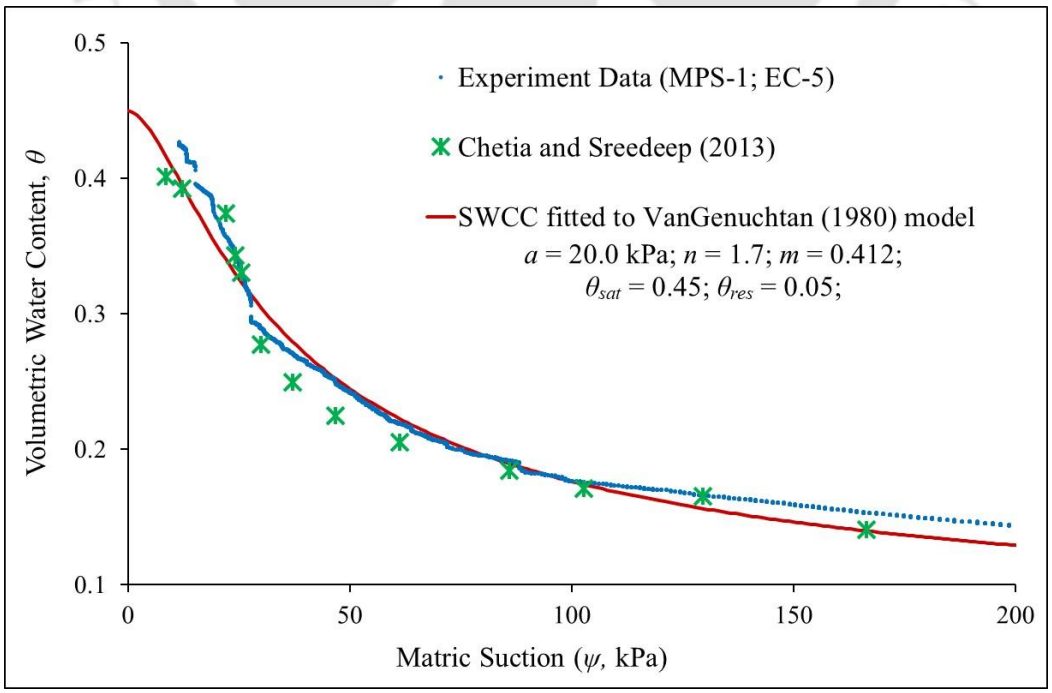

Figure 4.4 Soil water characteristic curve (SWCC)

4.2.4. In–Situ Infiltration Characteristics

In-situ tests, using Mini-disk infiltrometer and Guelph Permeameter, have been conducted for assessing the of in-situ infiltration characteristics.

The Mini-Disk infiltrometer is ideal for field measurements, due to its compact size and quick procedure. Significant number of observation spread across an area can be conducted. The Mini Disk Infiltrometer is a tension infiltrometer with an adjustable suction of 0.5 cm to 7 cm, and it measures the hydraulic conductivity of the medium it is placed on at different applied tensions (Figure 4.5).

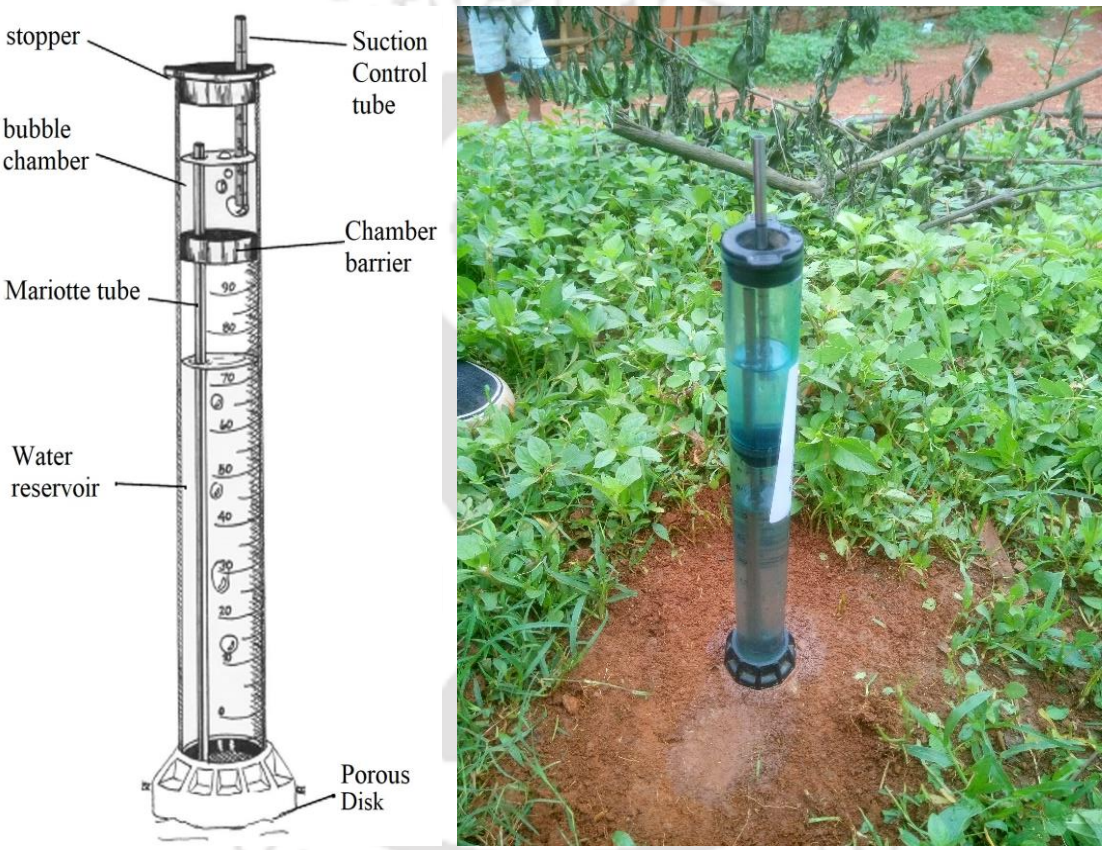

Figure 4.5 Mini-disk Infiltrometer

The upper and lower chambers of the Infiltrometer are both filled with water up to some level. The top chamber (or bubble chamber) controls the suction. The lower chamber contains a volume of water that infiltrates into the soil at a rate determined by the suction adjusted in the bubble chamber. The lower chamber is labelled like a graduated cylinder with volume shown in ml. The bottom of the infiltrometer has a porous sintered stainless-steel disk does not allow water to leak in open air. The small diameter of the disk allows for undisturbed measurements on relatively level soil surfaces. Once the Infiltrometer is placed on a soil surface, water begins to leave the lower chamber and infiltrate into the soil at a rate

determined by the hydraulic properties of the soil. As the water level drops, the volume is recorded at specific time intervals attuned to the rate of infiltration observed during the test. The method proposed by Zhang (1997) is used for estimating the hydraulic conductivity. The method requires the cumulative infiltration measurements versus time and fitting the results with the function as given by Equation (4.1)

$$I = C_1 t + C_2 \sqrt{t} \tag{4.1}$$

where, C_1 is the parameter related to hydraulic conductivity and C_2 is related to the soil sorptivity. The hydraulic conductivity for the soil (k) is then given by

$$k = \frac{C_1}{A} \tag{4.2}$$

where, C_1 is the slope of the curve of the cumulative infiltration versus the square root of time, and A is a value relating the van Genuchten parameters for a given soil type to the suction rate and radius of the Infiltrometer disk, and is given by

$$A = \frac{11.65\left(n^{0.1} - 1\right)\exp\left\{2.92\left(n - 1.9\right)ah\right\}}{\left(ar\right)^{0.91}} \tag{4.3}$$

or,
$$A = \frac{11.65\left(n^{0.1} - 1\right)\exp\left\{7.5\left(n - 1.9\right)ah\right\}}{\left(ar\right)^{0.91}} \tag{4.4}$$

where, n and a are the van Genuchten parameters for the soil (Fig 4.5), r is the disk radius (2.25 cm), and h is the suction at the disk surface (-1 cm and -2 cm). The formulation of the method is provided as a Microsoft Excel spreadsheet macro by the manufacturer of the Mini-disk infiltrometer, for different soil types and is used for the determination of the in-situ hydraulic conductivity.

95 tests are conducted in all around major 11 sites. Table 4.1 gives a summary of the test results.

Table 4.1 Summary of Mini-disk infiltrometer test results

Site name	**Maximum rate of infiltration {×10^{-6}(m/s)}**	**Minimum rate of infiltration {×10^{-6}(m/s)}**	**Average rate of infiltration {×10^{-6}(m/s)}**
Chunsali hill	8.68	4.42	6.55
Noonmati hill 1	3.51	0.21	2.01
Noonmati hill 2	3.06	1.41	2.23
Kailash Nagar hill 1	3.14	0.51	1.67
Kailash Nagar hill 2	0.81	0.61	0.43
Kailash Nagar hill 3	2.93	0.91	1.92
Punnya Nagar hill	6.33	1.52	4.84
Jyoti Ban	8.4	2.87	2.53
Indupur Kharghuli	12.9	3.08	7.82
Kamakhya hill	9.46	2.68	5.78
Shantipur hill	17.9	2.74	9.91

The Guelph Permeameter (Figure 4.6) is Constant-Head Permeameter (Guelph Permeameter Operating Instruction, 2008), employing the Marriotte Principle (McCarthy, 1934). As shown in the diagram (Figure 4.6), a stoppered reservoir is supplied with an air inlet and a siphon. The pressure at the bottom of the air inlet is always the same as the pressure outside the reservoir, i.e. the atmospheric pressure. If it were greater, air would not enter. If the entrance to the siphon is at the same depth, then it will always supply the water at atmospheric pressure and will deliver a flow under constant head height, regardless of the changing water level within the reservoir. The method involves measuring the steady-state rate of water recharge into unsaturated soil from a cylindrical well hole, in which a constant depth (head) of water is maintained. The constant head level in the well hole is maintained at the level of the bottom of the air tube by regulating the position of the bottom of the Air Tube, which is located in the centre of the Permeameter (Figure 4.6). As the water level in the reservoir falls, a vacuum is created in the air space above the water. The vacuum can only be relieved when air of ambient atmosphere pressure, which enters at the top of the air tube, bubbles out of the air inlet tip and rises to the top of the reservoir. Whenever the water level in the well begins to drop below the Air Inlet Tip, air bubbles emerge from the tip and rise into the reservoir air space. The vacuum is then partially relieved and water from the reservoir replenishes water in the well. The size of opening and geometry of the Air Inlet Tip is designed to control the size of air bubbles in order to prevent the well water level from fluctuating. When a constant height of water is established in the cored hole, a bulb region of soil surrounding the hole undergoes saturation. The outflow of water from the permeameter reaches a steady rate. The rate of this constant outflow of water, together with the diameter of

the hole, and the height of water maintained in the hole is used to determine the field hydraulic conductivity. The analysis of steady-state discharge from a cylindrical hole into unsaturated soil, measured using the Guelph Permeameter, accounts for the force for gravity, and the suction on the water out of the hole and into the surrounding soil.

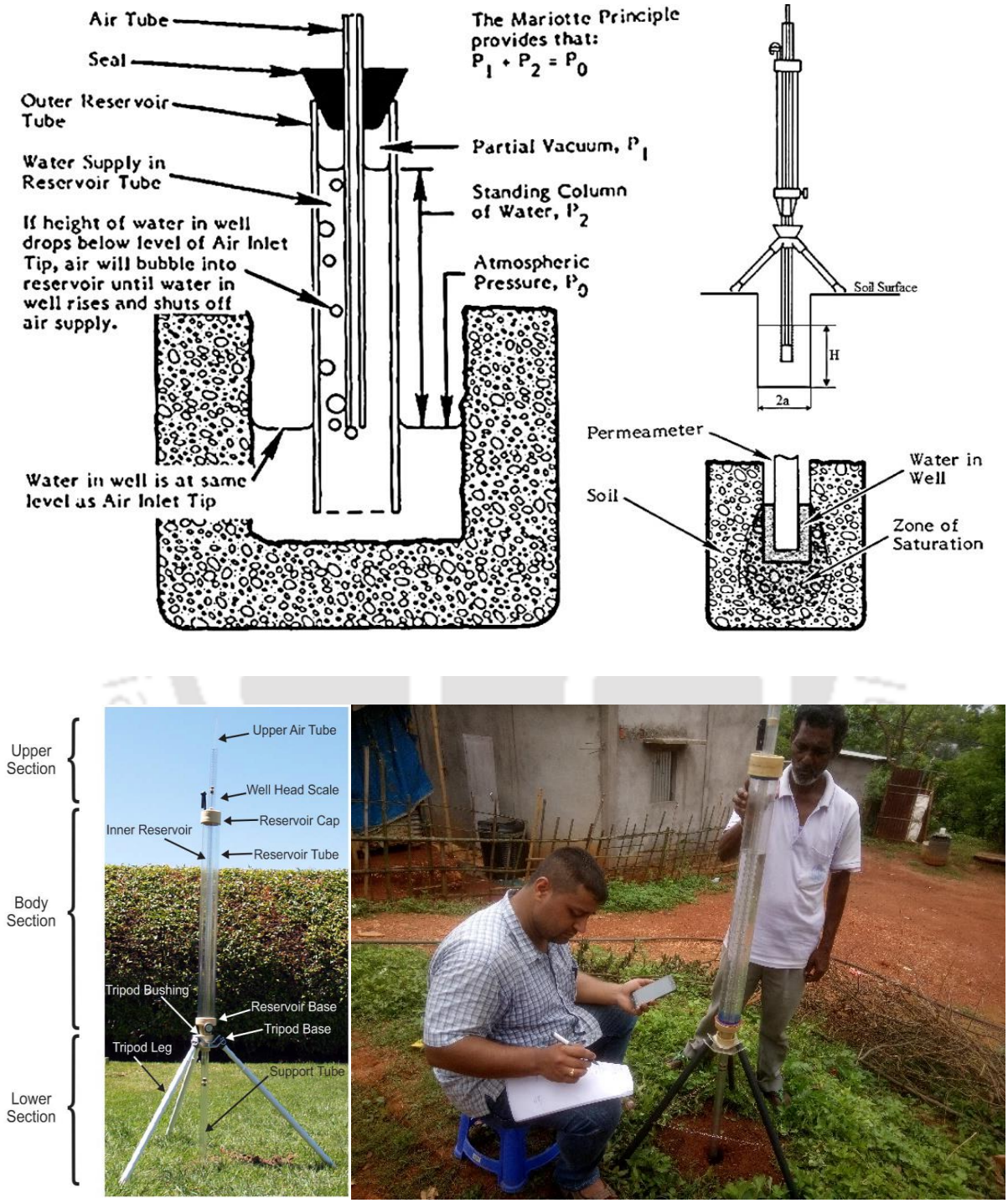

Figure 4.6 (a) Guelph Permeameter employing the Marriotte Principle (Guelph Permeameter Operating Instruction, 2008); (b) Guelph Permeameter test conducted in-situ

The field saturated hydraulic conductivity is calculated as given by

$$K_{saturated} = \frac{CQ}{2\pi H^2 + \pi r^2 C + 2\pi \frac{H}{\alpha^*}} \quad (4.5)$$

$$C = \left\{ \frac{\frac{H}{r}}{2.074 + 0.093\frac{H}{r}} \right\}^{0.754} \quad (4.6)$$

where, r is the hole radius in cm, C is shape factor parameter, Q is rate of outflow of water from the reservoir tube of the permeameter in cm3/min, α^* parameter depends on soil texture-structure categories (Elrick *et al.*, 1989).

The detailed methodology and the empirical equations adapted from Zhang *et al.*, 1998 is outlined in the manual, along with Microsoft Excel spreadsheet macro provided by the manufacturer for the determining the in-situ hydraulic conductivity of different types of soil.

Total 66 tests are conducted in and around major 11 sites. Table 2 gives a summary of the test results.

Table 4.2 Summary of Guelph Permeameter test results

Site name	Maximum rate of infiltration {$\times 10^{-6}$(m/s)}	Minimum rate of infiltration {$\times 10^{-6}$(m/s)}	Average rate of infiltration {$\times 10^{-6}$(m/s)}
Chunsali hill	0.96	0.87	0.91
Noonmati hill 1	1.75	0.16	0.95
Noonmati hill 2	7.36	6.70	4.02
Kailash Nagar hill 1	2.12	1.83	1.97
Kailash Nagar hill 2	0.83	0.64	0.72
Kailash Nagar hill 3	0.57	0.46	0.54
Punnya Nagar hill	4.59	4.48	4.53
Jyoti Ban	17.5	11.1	1.43
Indupur Kharghuli	11.3	9.00	10.1
Kamakhya hill	0.66	0.58	0.63
Shantipur hill	1.59	1.08	1.33

4.2.5. Shear Strength

Triaxial Tests were conducted on undisturbed samples as well as remoulded samples, compacted to in-situ dry density for evaluating the shear strength characteristics of the hill slope soils. Consolidated Drained (CD) Triaxial test as per ASTM D7181 – 11 were

conducted at effective confining stress of 50 kPa, 100 kPa and 200 kPa. Strain rate of 20%/hr i.e., 0.4667 mm/min was found sufficiently low to prevent any excess pore pressure generation in the consolidated drained test and hence was adopted for all further test. Consolidated Undrained (CU) Triaxial test were conducted as per IS 2720 (Part – 12)-1986 keeping the strain rate and effective confinement same as above. Figure 4.7 shows the stress-strain plot for CD test, while Figure 4.8 shows the same for CU test. Figure 4.9 shows the *p'*-*q* plot for the CU and CD Triaxial test conducted on the sample collected at IITG Cut Slope Site, along with the failure surface. Figure 4.10 shows the Mohr-Coulomb plot for the triaxial test conducted. Though some differences are observed at material scale of the soil samples, however, variations in the shear strength was not very significant. The angle of internal friction was observed to be around 27º to 30º, while the cohesion was varying from 10 kPa to 17 kPa.

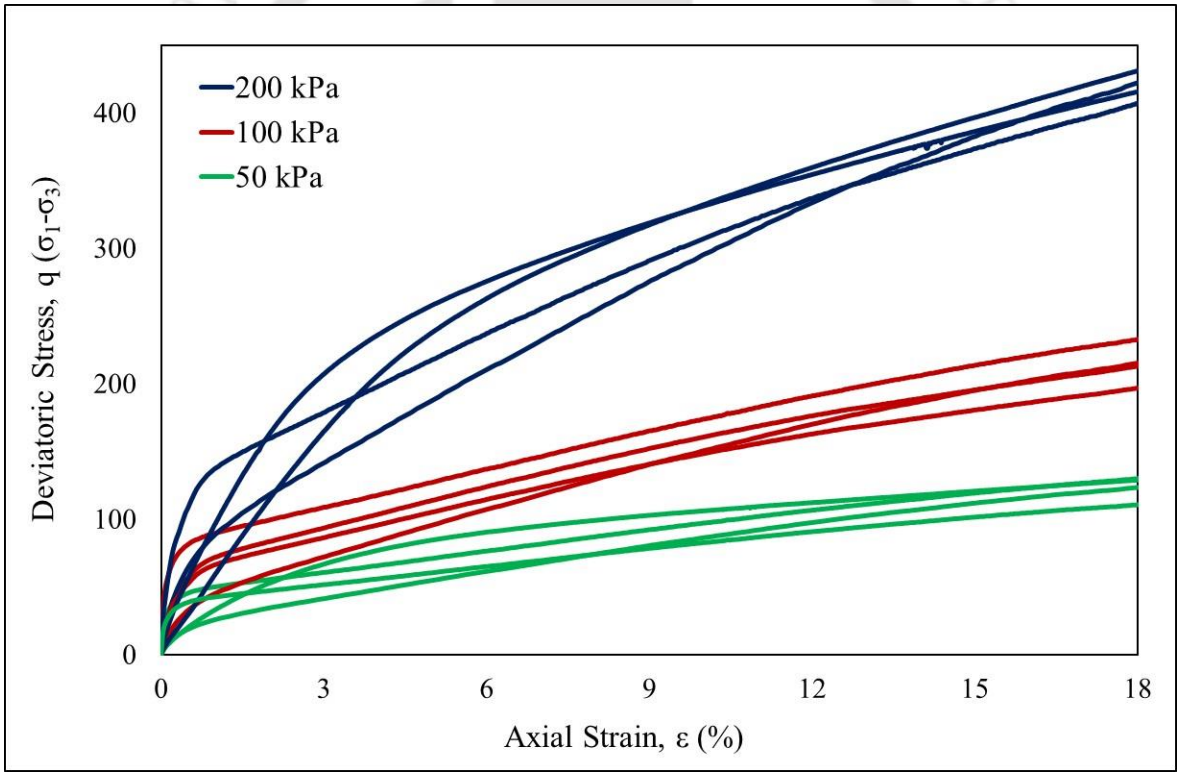

Figure 4.7 Deviatoric Stress vs. Strain (%) for CD Triaxial test

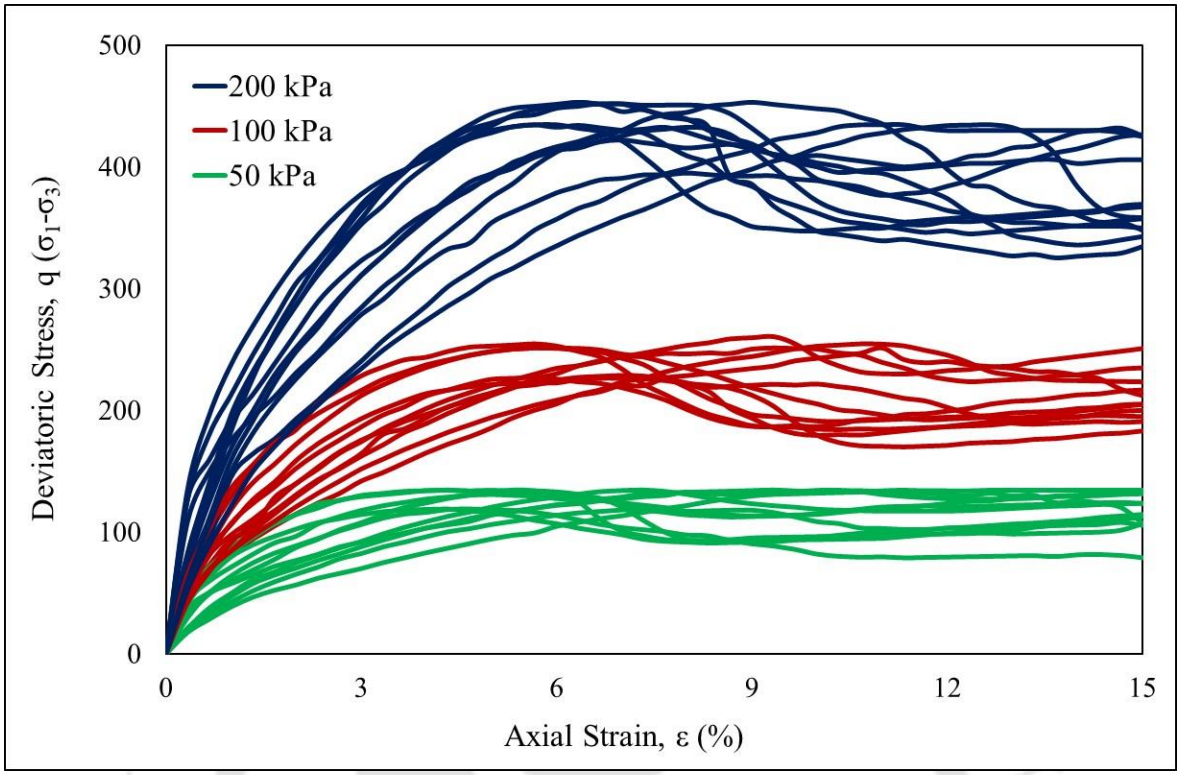

Figure 4.8 Deviatoric Stress vs. Strain (%) for CU Triaxial test

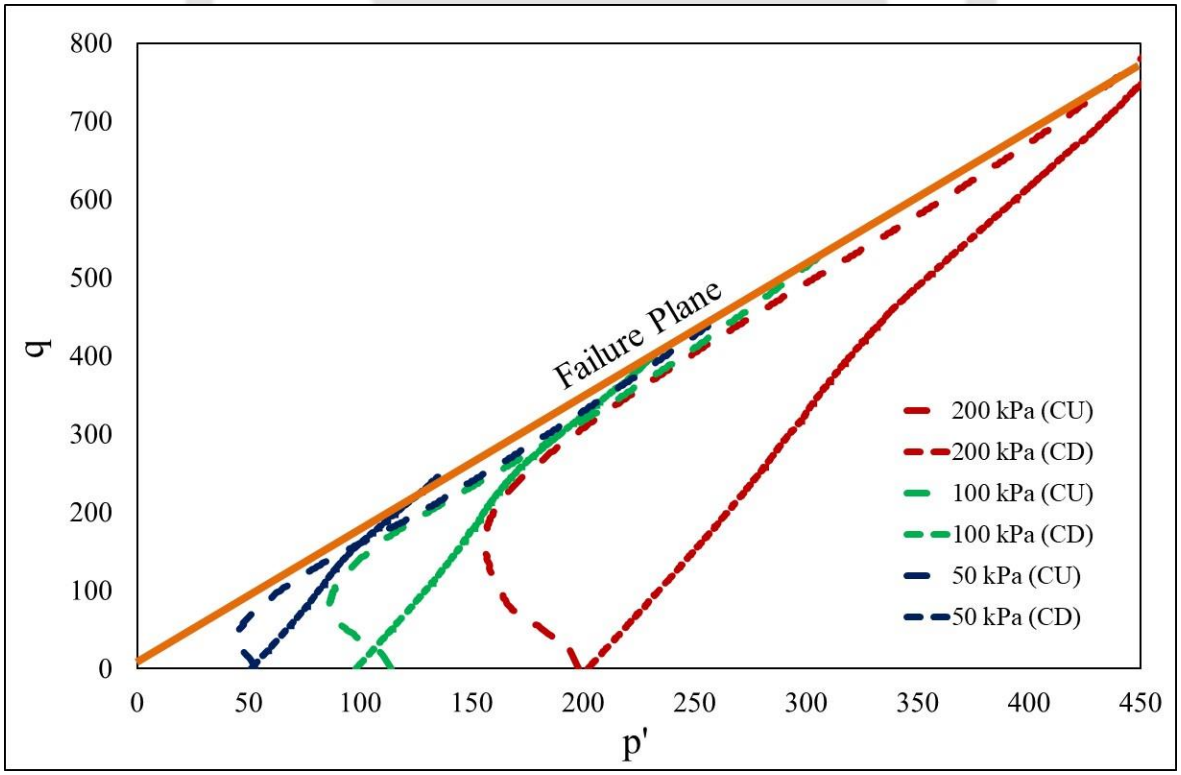

Figure 4.9 *p'*-*q* plot of CD and CU Triaxial tests

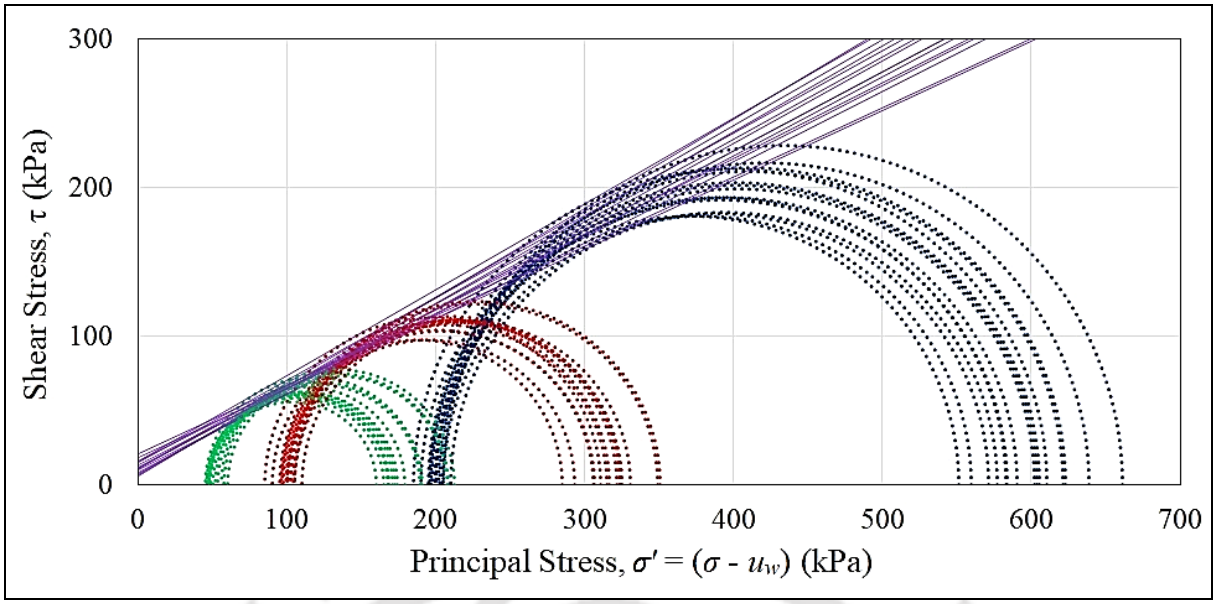

Figure 4.10 Mohr-Coulomb failure surface from triaxial tests

Figure 4.11 shows some typical sheared samples obtained after the triaxial test. The failure type can be observed to be predominantly shear failure with some bulging, a prevalent characteristic of the granular soils having fine content, as commonly obtained in this region. The samples behaved as normally consolidated specimen, with the pore pressure build up during undrained shearing and volume compression during drained shearing.

Figure 4.11 Sheared soil samples after triaxial test

4.3. RESULTS AND SUMMARY

Table 4.3 gives the summarised range of values for the soil parameters obtained from laboratory test and collated from that reported in various literature (Das 1992, 2003; Saikia *et al*, 1996; Saikia 2002; Das and Saikia 2010 & 2011; Yamsani *et al*, 2016).

Table 4.3 Range of soil properties from experimental data and various literature

Soil Property	Minimum reported value	Most common range	Maximum reported value
Cohesion, c' (kPa)	0	5 - 20	50
Angle of internal friction, φ'	14º	25º–30º	40º
Unit Weight of soil, γ_s (kN/m^3)	--	16.5 – 19.0	--
Saturated hydraulic conductivity k_s (m/s)	10^{-7}	10^{-6} – 10^{-5}	10^{-4}
Saturated Volumetric Water Content, θ_s	--	0.5 – 0.41	--
Residual Volumetric Water Content, θ_r	--	0.13 – 0.05	--

Chapter 5. LOCAL SLOPE STABILITY ANALYSIS

5.1. INTRODUCTION

Calculation of slope stability dates back to Coulomb (1776) and his work on stability of retaining walls and determination of the most likely shear surfaces with a wedge method. The basic concept of slope stability is built around the Coulomb friction model, and it still serves as the epicenter about which the theory of this particular topic revolves (Budhu, 2007). Terzaghi (1926), who established the fundamental concept of effective stress, made another important advance of slope stability calculation (Budhu, 2007). Therein, the effects of pore water pressure in slope stability are acknowledged. Water cannot sustain shear stress. Only the structure of solid particles at their contact points can, and thus slope stability decreases with increase in the pore-water pressure. The forces acting on a soil mass atop a slope can be illustrated by the vectors (Figure 5.1), where a mass (m) is subjected to acceleration due to gravity (g) which can be resolved into a downslope parallel or tangential component (T) and a force acting perpendicular to slope surface (N). P is the force on the soil mass due to seepage of water through the soil pores. The magnitude of the components depends on slope angle (β) and downslope force increases with higher slope angles, or with increase in P. The stability of slope is mostly expressed in the form of the Factor of Safety (FoS), which is the ratio of resisting forces (R) to the destabilizing forces (T+P) and within a slope (Crozier 1989). Figure 4.1 gives a simplified description of the Factor of Safety of the mass against sliding. The resisting force is the force due to friction, and depends on the materials involved and the type of friction represented by the coefficient of friction μ.

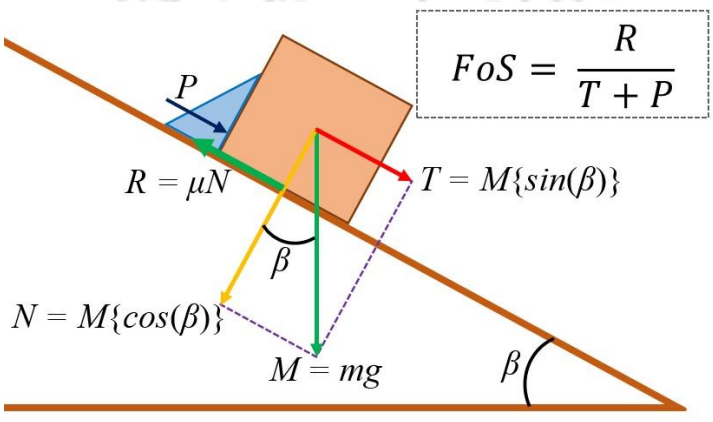

Figure 5.1 FoS of soil mass against sliding atop a slope (based on Budhu, 2007)

5.2. RAINFALL INDUCED SLOPE INSTABILITY ANALYSIS

Landslides occurrence is generally connected to some kind of triggering event. Many factors can act as triggers for landslides, human interaction in the form of loading or slope cutting can also trigger landslide events, though in majority of the cases it is the prime causal factor. The most important trigger of shallowest landslides however, is rainfall (Crosta and Frattini 2008). The impact of rainwater infiltration in causing landslides is widely recognized. Rainfall infiltration results in increase in the water content and decrease in the matric suction thereby raising the unit weight and reducing the shear strength of soil within the colluvium of the landslide (Fredlund and Rahardjo, 1993).

Hill slopes within the city of Guwahati consist of residual soils, often in unsaturated condition. Wesley (2010) gives an elaborate description of behavior of residual soils particularly pertaining to slope stability. Wesley (2010), notes that slopes composed of residual soil can stand stable at a much steeper angles (even greater than 45°) and at height greater than 10m. Slope failures in residual soils, even when steep slopes are involved are more likely to be shallow with slightly curved or planar surfaces. The cementation within the soil particles play an important role in the behavior of residual soils but, the shear strength arising from the zone of negative pore pressure above the water table contributes as a major factor in the stability of slopes. Landslides, in residual soils, are generally triggered by rainfall during a severe storm because of temporary increase of pore-water pressure in the topmost layers of the slope. This phenomenon highlights the importance of antecedent pore-water condition generated from seasonal effects. Studies concerning rainfall, infiltration and landslide mechanism are thoroughly addressed in the literature review (Section 2.6.1). Numerical models were developed to study how infiltration into a slope varied with respect to rainfall intensity and how this infiltration affected the stability of the slope.

Therefore, the conventional saturated soil mechanics approach to assessing the stability of these slopes is inadequate. To assess the potential susceptibility to rainfall-induced landslide an effective modeling of changes in water content and matric suction in response to rainfall infiltration is essential. The study involves two parts. The first part is transient seepage analysis to investigate the infiltration mechanism under different rate of infiltration and the simultaneous reduction in the matric suction with increase in the volumetric water content. The second part involves a slope stability analysis applying Limit Equilibrium Method to determine the degradation of the stability condition of the slope with time, due to the reduction in the soil suction.

For the following analysis, SLOPE/W and SEEP/W code within GeoStudio Software Suite (GeoSlope, 2007) is used. SLOPE/W includes several 2D limit equilibrium methods such as Ordinary Method of Slices, Bishop's Method, Janbu's method, Spencer, Morgenstern-Price, Generalized Limit Equilibrium and others. In addition, several soil strength models are available. Dynamic hydrological modelling of pore pressures is not included in SLOPE/W, but can be imported from SEEP/W, finite-element software within the same software suite. The infiltration is modeled using the seepage analysis module SEEP/W. The use of SLOPE/W, also in combination with SEEP/W is widely acknowledged in recent landslide research (Rahardjo *et al*, 2007; Cascini *et al*, 2008). In the following section, only the theoretical frameworks applied are briefly addressed while overlooking the numerical issues in the code itself.

5.2.1. Transient Seepage Analysis

SEEP/W is a code to perform numerical analysis of 2D steady state or transient seepage analyses within porous materials through the application of finite element method (FEM) (GEO-SLOPE International Ltd., 2010a). SEEP/W is capable of analysing isotropic or anisotropic seepage through a complex geometry, made up of either homogeneous or inhomogeneous material. In this section, the theory, meshing, necessary material properties, initial conditions, boundary conditions, and interpretation of results, associated with SEEP/W are briefly described in relation to transient seepage analyses.

Flow through soil

The formulation describing the flow of water through saturated and unsaturated soils in the SEEP/W code is based on Darcy's Equation of flow through saturated soil and can be represented by the following equation (GEO-SLOPE International Ltd., 2010).

$$[q] = [k][i] \tag{5.1}$$

where,

$[q] =$ Specific discharge matrix

$[k] =$ Hydraulic conductivity matrix

$[i] = \frac{\Delta h}{\Delta l};$ Unit hydraulic head gradient matrix

Richards (1931) modified the Darcy's Equation to be applied to the flow of water through unsaturated soil. Under the conditions of unsaturated flow, the hydraulic conductivity is expressed as a function of either the volumetric water content or the pore-water pressure (Childs and Collins-George, 1950). The general governing differential equation for two-dimensional seepage can thus, be expressed as:

$$\frac{\partial}{\partial x}\left\{k_x \frac{\partial h}{\partial x}\right\}+\frac{\partial}{\partial y}\left\{k_y \frac{\partial h}{\partial y}\right\}+q=\frac{\partial \Theta}{\partial t} \tag{5.2}$$

where,

$h=$ Hydraulic head

$k_x=$ Hydraulic conductivity in the *x*-direction

$k_y=$ Hydraulic conductivity in the *y*-direction

$q=$ Specific discharge or applied boundary flux

$\Theta=$ Volumetric water content

$t=$ Time

Equation 2 essentially states that the sum of the rate of flow changes in *x* and *y* directions and the external applied flux, is equal to the rate of change of the volumetric water content with respect to time.

The change in volumetric water content is then related to the change in pore-water pressure by the following expression

$$\partial\Theta = m_w \partial u_w \tag{5.3}$$

where,

$u_w = \gamma_w (h-y)$; Pore-water pressure

$m_w=$ Slope of the volumetric water storage curve

$\gamma_w=$ Unit weight of water

$y=$ Elevation head

Substituting the above in Equation 2;

$$\frac{\partial}{\partial x}\left\{k_x \frac{\partial h}{\partial x}\right\}+\frac{\partial}{\partial y}\left\{k_y \frac{\partial h}{\partial y}\right\}+q=m_w\gamma_w \frac{\partial(h-y)}{\partial t} \quad (5.4)$$

At an element, located at a particular position the elevation head will always remain constant and therefore the governing differential equation used in SEEP/W finite element formulation, is:

$$\frac{\partial}{\partial x}\left\{k_x \frac{\partial h}{\partial x}\right\}+\frac{\partial}{\partial y}\left\{k_y \frac{\partial h}{\partial y}\right\}+q=m_w\gamma_w \frac{\partial h}{\partial t} \quad (5.5)$$

However, changes in the stress state and the density or porosity of the soil affect the changes in volumetric water content. Fredlund and Morgenstern (1976 and 1977) stated regarding both condition of saturated and unsaturated, the stress state can be presented by two state variables as follow: $(\sigma - u_a)$ and $(u_a - u_w)$, where σ is the total stress, u_a is the pore-air pressure, and u_w is the pore-water pressure, $(u_a - u_w)$ is the matric suction.

Thus, while formulating the governing differential equation describing the flow of water through unsaturated soil, the following assumptions are made in the SEEP/W code.

a. $(\sigma - u_a)$ remains constant and has no effect on changes in volumetric water content.
b. The hydraulic conductivity is a function of the matric suction; changes in the hydraulic conductivity and the volumetric water content are consequently dependent only on changes in the matric suction.
c. With the pore-air pressure, (u_a) remaining constant, total stress is treated as constant and the change in volumetric water content is a function only of pore-water pressure changes.

SEEP/W uses the Backward Difference Method for the time integration, and thus in order to solve for the new head at the end of the time increment, it is necessary to know the head at the start of the increment. In other words, the initial conditions must be known or specified in order to perform a transient analysis. The simulations result is significantly affected by the initial conditions.

Soil Water Retention Characteristics

The main soil parameters required in the SEEP/W are the saturated hydraulic conductivity, the Soil Water Characteristic Curve (SWCC) and the Unsaturated Hydraulic

Conductivity Curve (UHCC). The SEEP/W has two method based on form equations by Fredlund and Xing (1994) and Van Genuchten (1980) respectively to define the SWCC.

Van Genuchten, (1980) ***SWCC model***

$$\Theta_w = \Theta_r + \frac{\Theta_s - \Theta_r}{\left[1+\left(\frac{\psi}{a}\right)^n\right]^m} \tag{5.6}$$

where,

$\psi =$ Negative pore-water pressure

$\Theta_w =$ Volumetric water content corresponding to ψ

$\Theta_s =$ Volumetric water content at saturated soil condition

$\Theta_r =$ Residual volumetric water content

$a, n, m =$ Curve fitting parameters

Fredlund and Xing, (1994) ***SWCC model***

$$\Theta_w = C_\psi \frac{\Theta_s}{\left\{\ln\left[e+\left(\frac{\psi}{a}\right)^n\right]\right\}^m} \tag{5.7}$$

where,

$C_\psi =$ Correction function

$a = \psi_i$; $e =$ The natural number (2.71828)

$$m = 3.67\ln\left(\frac{\Theta_s}{\Theta_i}\right), \quad n = \frac{1.31^{m+1}}{m\Theta_s} 3.72 s\psi_i$$

$\psi_i =$ The suction pressure corresponding to the water content occurring at the inflection point of the

$s =$ The slope of the line tangent to the function that passes through the inflection point

Apart from the above-mentioned empirical SWCC models, a predictive method using grain size data and Liquid limit of the soil as developed by Aubertin *et al*., (2003), modified from the method proposed by Kovacs (1981), is implemented in the SEEP/W code. Data points obtained through experimental procedure can be input into SEEP/W and interpolated to form the SWCC. Along with the above-mentioned methods, SEEP/W also has several "typical" sample water content functions for different types of soils in its database.

Unsaturated Hydraulic Conductivity

In a saturated soil, all the pore spaces between the solid particles are filled with water. Once the air-entry value is exceeded, air enters the largest pores and the air-filled pores than act as obstruction to the flow and increase the tortuosity of the flow path. As a result, the ability of the soil to transport water (i.e., the hydraulic conductivity) decreases. As pore-water pressures become increasingly more negative, more pores become air-filled and the hydraulic conductivity decreases further. The ability of water to flow through a soil profile depends on how much water is present in the soil, which is represented by the volumetric water content function. Actual measurement of the unsaturated hydraulic conductivity function is a very complex, time-consuming and expensive procedure. The unsaturated hydraulic conductivity function is therefore developed using one of several predictive methods that utilize either a grain-size distribution curve or a measured volumetric water content function and the saturated hydraulic conductivity. SEEP/W has built-in predictive methods that can be used to estimate the hydraulic conductivity function once the volumetric water content function and the saturated hydraulic conductivity value have been specified.

Van Genuchten (1980), *UHCC model*

Van Genuchten (1980) proposed the following closed form equation to describe the hydraulic conductivity of a soil as a function of matric suction; the hydraulic conductivity function of a soil can be estimated once the saturated conductivity and the two curve fitting parameters, *a* and n = 1/(1-*m*), are known.

$$k_w = k_s \frac{\left[1-\left(a\psi^{(n-1)}\right)\left\{1+\left(a\psi^{n}\right)^{-m}\right\}\right]^2}{\left\{\left(1+a\psi\right)^{n}\right\}^{\frac{m}{2}}} \qquad (5.8)$$

$k_w =$ The calculated conductivity for a specified water content or negative pore-water pressure (m/s),

$k_s =$ The measured saturated conductivity (m/s),

Fredlund *et al*., (1994) *UHCC model*

The method consists of developing the unsaturated hydraulic conductivity function by integrating along the entire curve of the volumetric water content function. The governing equation is:

$$k_w = k_s + \frac{\sum_{i=j}^{N} \frac{\Theta\left(e^{y}\right) - \Theta\left(\psi\right)}{e^{y_i}} \Theta'\left(e^{y_i}\right)}{\sum_{i=j}^{N} \frac{\Theta\left(e^{y}\right) - \Theta_s}{e^{y_i}} \Theta'\left(e^{y_i}\right)} \tag{5.9}$$

$\Theta' =$ The first derivative of the Fredlund and Xing, (1994) SWCC model

Apart from the above-mentioned UHCC model, SEEP/W also has the Green and Corey, (1971) UHCC model.

5.2.2. Slope Stability Analysis

Limit equilibrium analyses were performed by means of the SLOPE/W code (GeoSlope, 2007) referring to the methods proposed by Morgenstern & Price (1965), the pore pressures at different time steps are imported from SEEP/W. Soil shear strength and mobilized shear were related to soil suction through the extended Mohr-Coulomb criterion (Fredlund *et al*., 1978).

Shear strength of saturated / unsaturated soil

The SLOPE/W program considers unsaturated shear strength conditions by implementing the modification of the Mohr–Coulomb material model proposed by Krahn and Fredlund (1972), Fredlund *et al*., (1978) and Fredlund and Rahardjo (1993) (Figure 5.2) and is expressed in the following form (Eq. 5.10).

$$\tau_{ff} = c' + \left(\sigma_f - u_a\right)_f \tan\phi' + \left(u_a - u_w\right)_f \tan\phi^b \tag{5.10}$$

where c' is the effective cohesion of the soil, σ_f is the normal stress on the failure plain, u_a is pore-air pressure, u_w is pore-water pressure, ϕ' is the effective friction angle of the soil and ϕ^b is the angle defining the increase in strength with increase in matric suction.

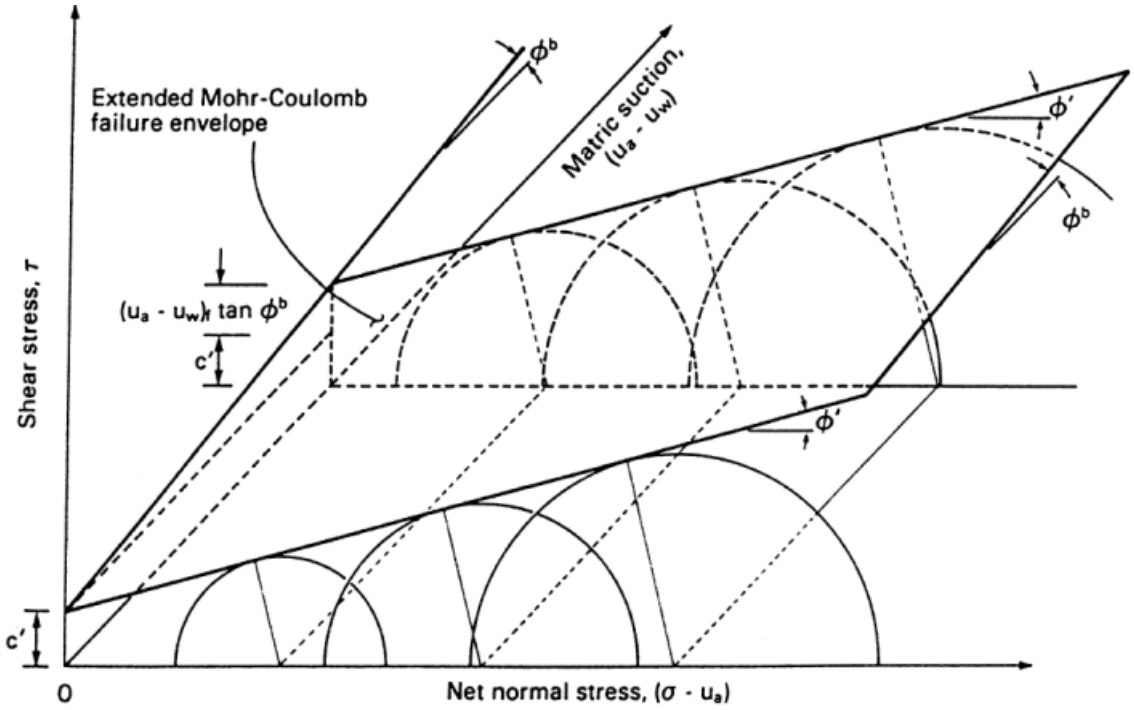

Figure 5.2 Failure envelope for unsaturated soil (Fredlund and Rahardjo, 1993)

Limit Equilibrium (Morgenstern–Price) method

For the slope stability analyses, Morgenstern-Price method of slices with a Half–sine inter slice force function was applied. Morgenstern-Price method satisfies both moment as well as force equilibrium. The pore–water pressures determined in the seepage analysis by SEEP/W are used as input data in the slope stability analysis. Limit equilibrium method is used in this study for stability determination of soil slopes. A failure surface is assumed (circular, non-circular or composite) and the soil mass is divided into a number of slices and each slice is checked for equilibrium of forces and moments. This method considers force and moment equilibrium of a mass of soil above a potential failure surface. The soil above the potential failure surface is assumed to be rigid (i.e., shearing can occur only on the potential failure surface). The available shear strength is assumed mobilized at the same rate at all points on the potential failure surface. Hence, the factor of safety is constant over the entire failure surface. A search procedure is used to find the critical slip surface giving the minimum factor of safety of the slope. Figure 5.3 show all the forces acting on a soil wedge considering a slip surface passing over a bedrock.

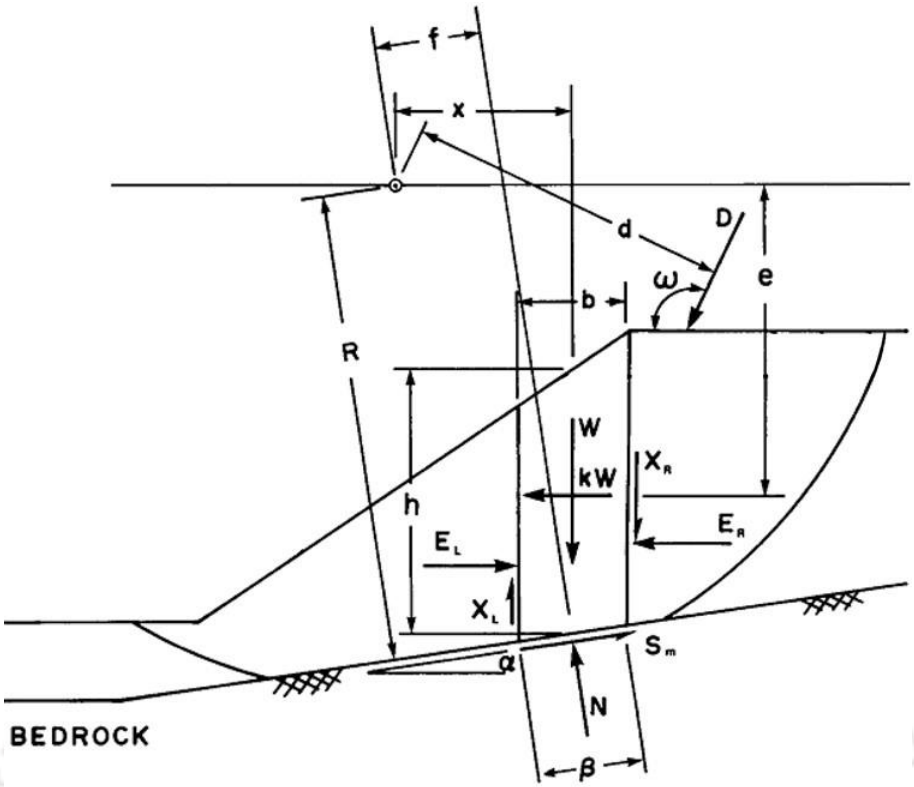

Figure 5.3 Forces acting on a slice through a sliding mass (GeoSlope, 2007)

The mobilized shear can also be written for unsaturated soil conditions.

$$s_m = \frac{b}{FoS}\left(c' + \left(\sigma_n - u_a\right)_f \tan\phi' + \left(u_a - u_w\right)_f \tan\phi^b\right) \tag{5.11}$$

SLOPE/W uses φ^b whenever the pore-water pressure is negative and φ' whenever the pore-water pressure is positive.

The normal at the slice base is:

$$N = \frac{W + \left(X_R - X_L\right) - \dfrac{\left\{c' + u_a\left(\tan\phi' - \tan\phi^b\right) + u_w \tan\phi^b\right\} b \sin\alpha}{FoS}}{\cos\alpha + \dfrac{\sin\alpha \tan\phi'}{FoS}} \tag{5.12}$$

The summation of forces in a horizontal direction can be written for each slice as:

$$E_R - E_L = \frac{\left\{c' - u_w \tan\phi'\right\} b \cos\alpha}{FoS} + N\left(\frac{\cos\alpha \tan\phi'}{FoS} - \sin\alpha\right) - kW \tag{5.13}$$

When only moment equilibrium is satisfied, the factor of safety equation is:

$$F_m = \frac{\sum\left(c'bR + R\tan\phi'\left[N - u_w b\frac{\tan\phi^b}{\tan\phi'} - u_a b\left\{1 - \frac{\tan\phi^b}{\tan\phi'}\right\}\right]\right)}{\sum W_x - \sum N_f + \sum kWe \pm \sum Aa} \quad (5.14)$$

The factor of safety equation with respect to horizontal force equilibrium is:

$$F_f = \frac{\sum\left(c'b\cos\alpha + \tan\phi'\cos\alpha\left[N - u_w b\frac{\tan\phi^b}{\tan\phi'} - u_a b\left\{1 - \frac{\tan\phi^b}{\tan\phi'}\right\}\right]\right)}{\sum N\sin\alpha + \sum kW \pm \sum A} \quad (5.15)$$

5.2.3. Validation of the numerical analysis

For the validation of the numerical analysis procedure to simulate rainfall induced instability, the analysis as presented by Tsaparas *et al*. (2002) is considered. Figure 2.6(a) shows the slope geometry. The slope is 10 m high and stands at an inclination of 26.6º (2H: 1V). The slope was discretized with a finite element mesh of combined 4-noded quadrilateral elements and 3-noded triangular elements with a fineness of 0.5 m. Surface elements of 0.1 m thickness were applied to define the ground surface of the slope. The slope is assumed composed of a homogenous and isotropic residual soil. The soil shear strength parameters as given by Tsaparas *et al*. (2002) are cohesion (c') of 1 kPa, an effective angle of internal friction (φ') of 25º, (φ^b) angle of 24º, soil unit weight of 19.0 kN/m^3. Four different values saturated hydraulic conductivity were considered, vis., 10^{-4} m/s, 10^{-5} m/s, 10^{-6} and finally 10^{-7} m/s. Figure 2.5 shows the (a) soil water characteristic curve and the (b) unsaturated hydraulic conductivity curves considered in the analysis. Initial groundwater level 1 (Figure 2.6a) with maximum soil suction limited to -25 kPa is considered (Tsaparas *et al*., 2002). Total rainfall of 240 mm is applied over a duration of 2 hours, 4 hours, 8 hours and 16 hours. The pore–water pressures determined in the seepage analysis by SEEP/W are used as input data in the slope stability analysis using SLOPE/W. The analysis results as plotted in Figure 5.4 can be observed to be matching with that of the published data (Figure 2.6b), thus validating the analysis procedure.

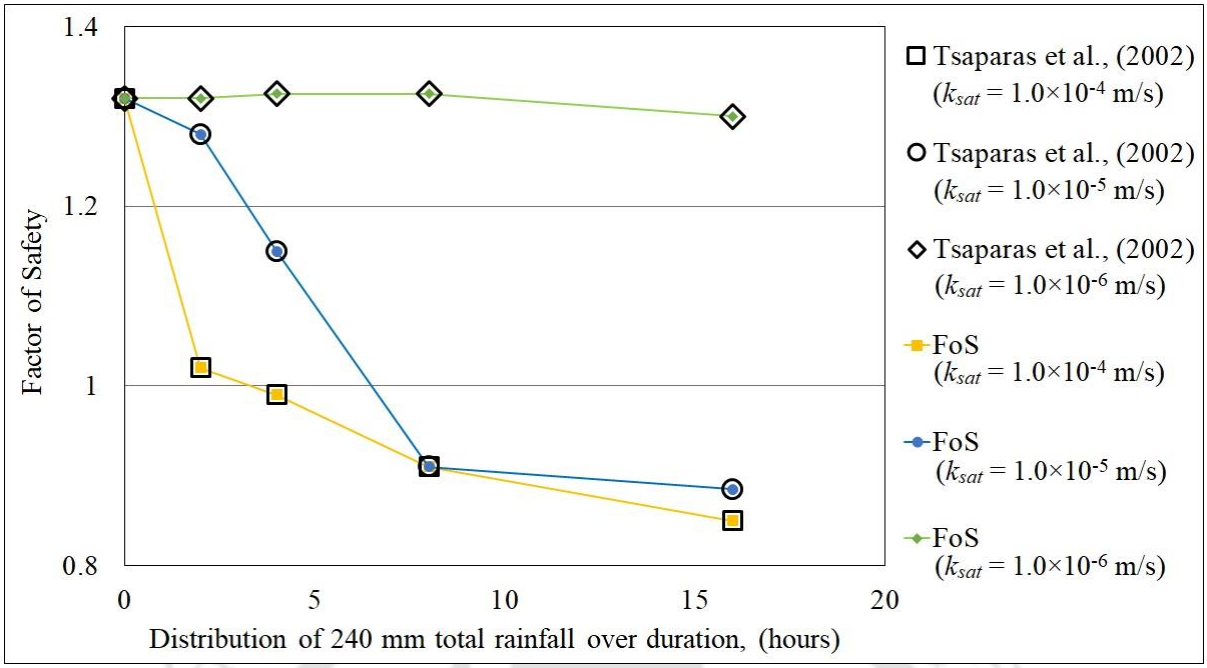

Figure 5.4 Factors of safety for the different values of saturated hydraulic conductivity (k_{sat}) for total of 240 mm rainfall

5.2.4. Description of the numerical model

Slope of height 30 m with an inclination of 45°, and composed of homogenous and isotropic residual soil was assumed (Figure 5.5). Das and Saikia (2010; 2011) presents an experimental data of the unsaturated soil properties of typical residual soils commonly found in the hill slopes of Guwahati and the same is been adopted in this study. One slope was assigned the Red Silty Clay (RS) properties and the other was assigned the Pale Yellow Silty Sand (PYS) properties (Table 5.1).

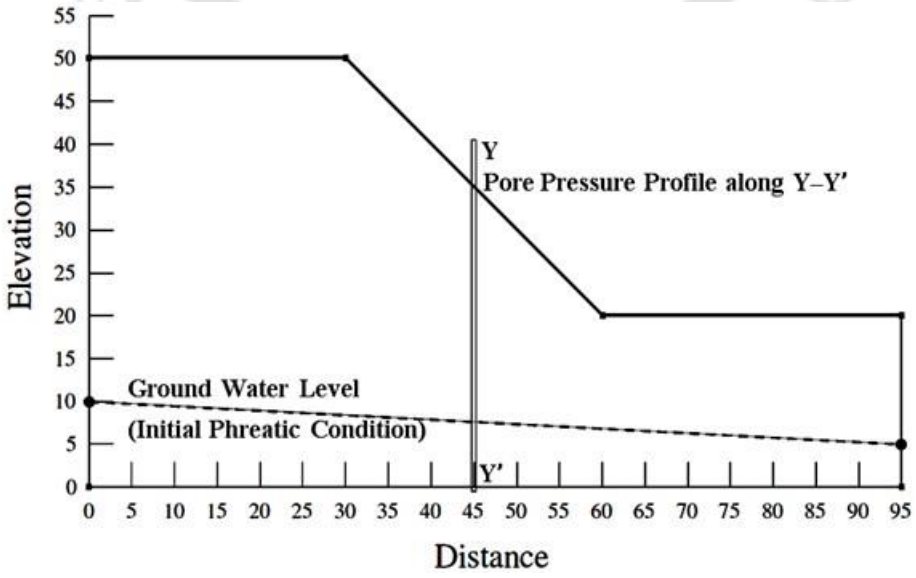

Figure 5.5 Slope Geometry used in this study

Table 5.1 Index Properties of the Soils used in this study (from Das and Saikia, 2010; 2011)

Property	**(RS)**	**(PYS)**
Classification	Silty Clay	Poorly Graded Silty Sand
Color	Reddish	Light Yellowish
Field Bulk Density	1.65 g/cm^3	1.79 g/cm^3
Field Dry Density	1.49 g/cm^3	1.63 g/cm^3
Liquid Limit	49%	39%
Plastic Limit	27%	Non-plastic
Fines Content	72.7%	7.45%
ϕ'	31^o	38.5^o
c'	10 kPa	0 kPa
ϕ^b	16.7^o	7.5^o
Residual Saturation	31 %	33 %
Co-efficient of permeability at saturation	1.86×10^{-6} m/s	1.21×10^{-5} m/s

The reported Soil Water Characteristic Curves (SWCC) for both type of soils is presented in Figure 5.6. The Unsaturated Hydraulic Conductivity Curve (UHCC) is derived empirically using the method proposed by Fredlund *et al*., (1994) and programmed within the SEEP/W (GeoSlope, 2007). Figure 5.7 presents the UHCC derived for both type of soils.

The idealized slope isolates the influence of complex hydro-geological conditions on the seepage analysis and enables to understand the individual response of each type of soil to a particular applied infiltration. The slope was discretized with a finite element mesh of combined 4-noded quadrilateral elements and 3-noded triangular elements with a fineness of 0.5 m. Surface elements of 0.1 m thickness were applied to define the ground surface of the slope. A time–step of 30 min. was found to be sufficient for efficient solution of the problem.

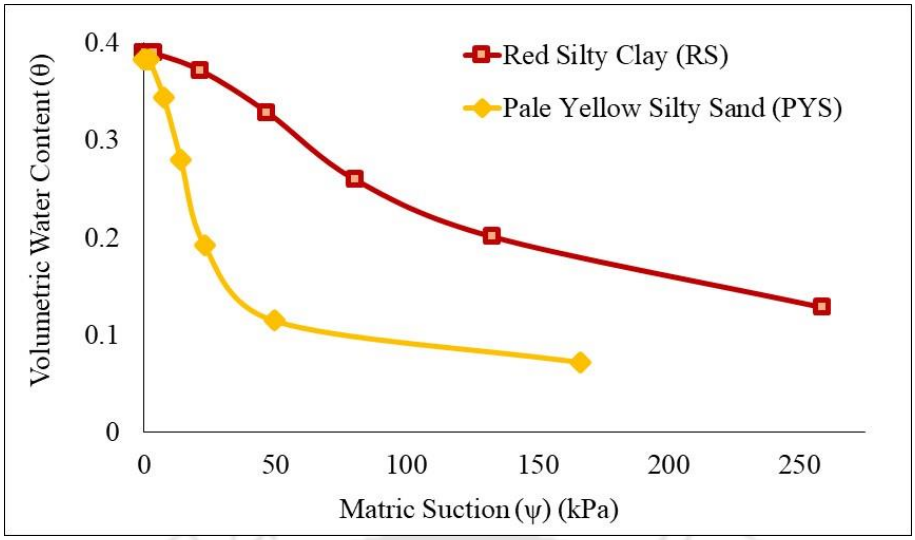

Figure 5.6 Soil Water Characteristic Curves (Das and Saikia, 2010; 2011)

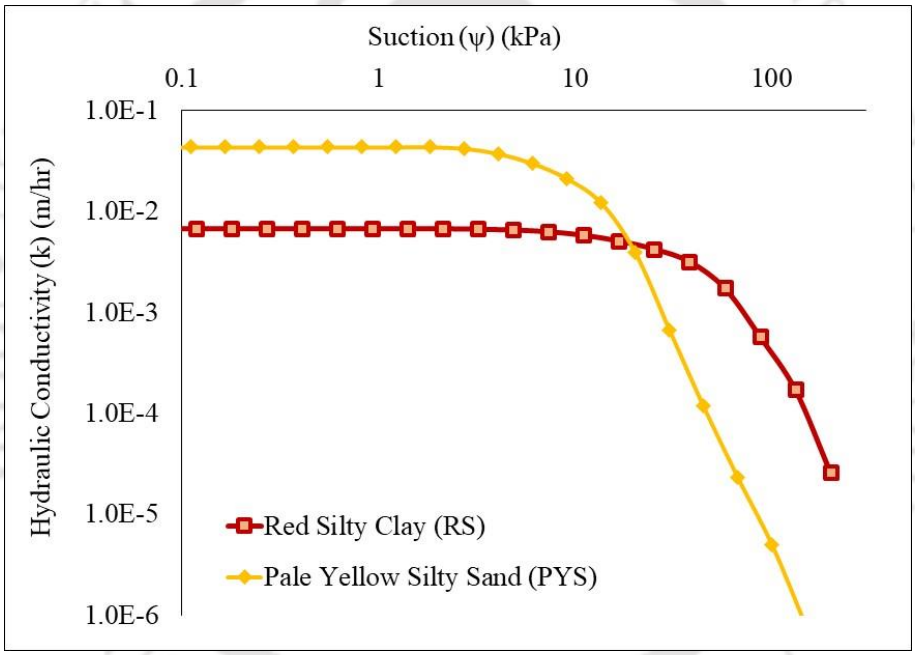

Figure 5.7 Unsaturated Hydraulic Conductivity Curves (UHCC)

Initial groundwater level and the initial pore–water pressure profile was defined by applying a phreatic line and restricting the maximum suction to a limit of 80 kPa (Figure 5.8). The maximum suction value is chosen to reflect the in-situ moisture content typical to the residual soils within the study area. The infiltration rate is modelled as a unit flux boundary (q) along the nodes at the ground surface. SEEP/W calculates the hydraulic head at each node based on the nodal boundary flux converted from the applied unit boundary flux. In case ponding, i.e., development of positive pore-pressure at a ground surface node occurs, the hydraulic head at those nodes are reset to the elevation of that node and the flux is determined

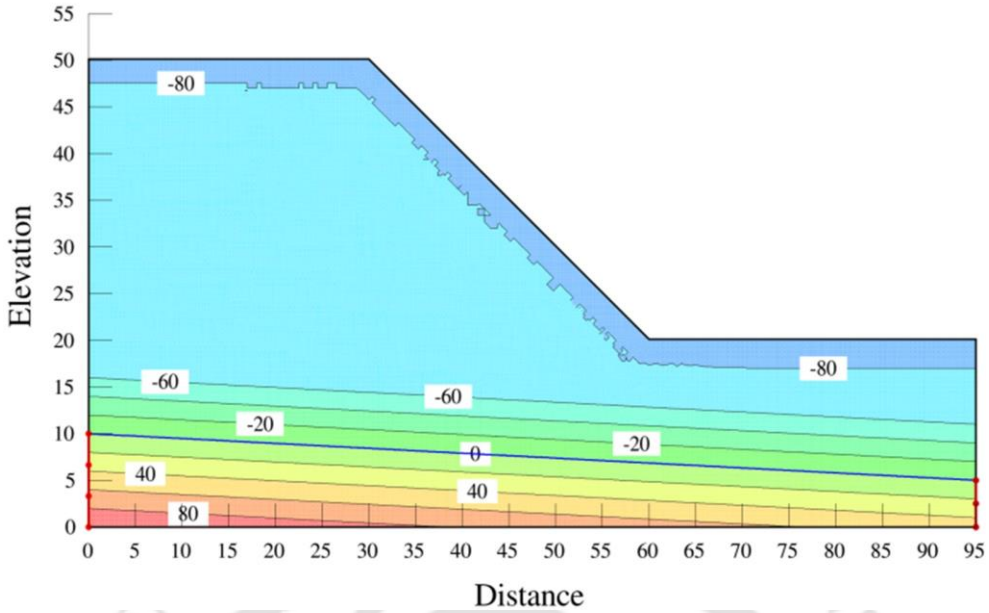

Figure 5.8 Initial pore pressure distributions

Five different rates of infiltration consistent to storm events prevalent in this region vis. 50 mm/day, 100 mm/day, 150 mm/day, 200 mm/day and 250 mm/day have been considered and applied for duration of 5 days. For the slope stability analyses, Morgenstern-Price method of slices with a Half–sine inter slice force function was applied. The pore–water pressures determined in the seepage analysis by SEEP/W are used as input data in the slope stability analysis.

5.2.5. Change in Factor of Safety with Rainfall Infiltration

Figure 5.9 (a) and (b) gives a graphical representation of the pore pressure scenario across the entire slope. The development of pore pressures along the profile X-Y as shown in Figure 5.5 are plotted for a particular rate of infiltration of 200 mm/day for increasing duration in Figure 5.10 (a) and (b). It is observed that the responses of the two types of soil are quite different for the same rate of infiltration applied.

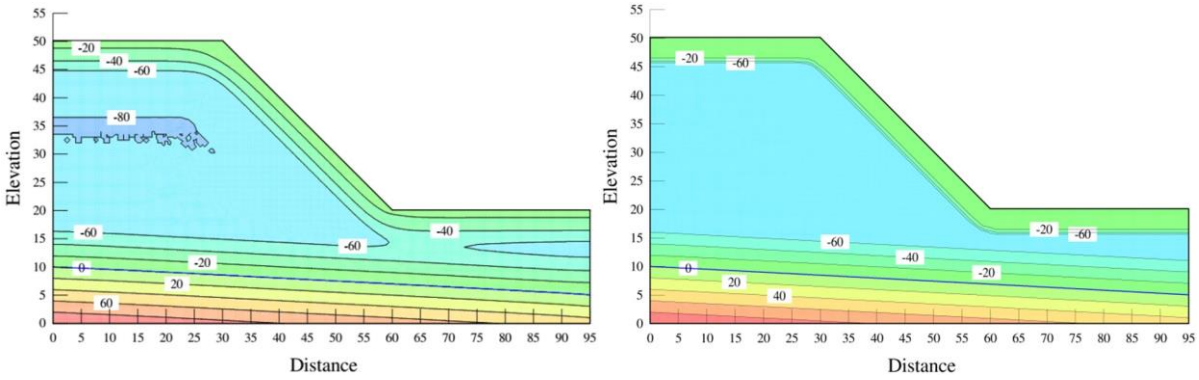

Figure 5.9 Pore Pressures (kPa) distribution within the slope composed of composed of (a) Red Silty Clay (RS) (b) Pale Yellow Silty Sand (PYS) after an infiltration of 200 mm/day for duration of 3 days

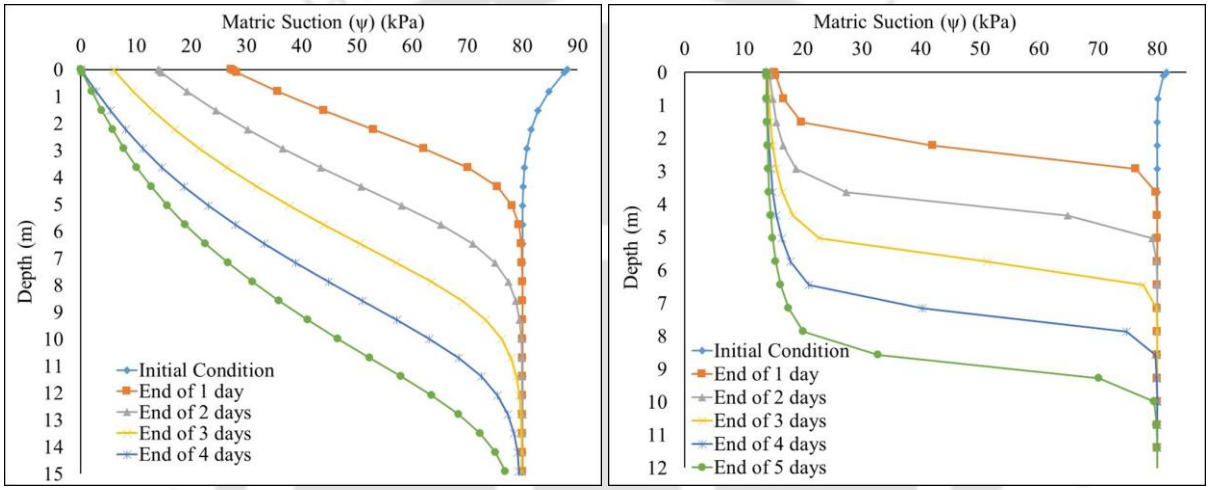

Figure 5.10 Development of pore pressure for an applied infiltration of 200 mm/day within the slope composed of (a) Red Silty Clay (RS) (b) Pale Yellow Silty Sand (PYS)

A gradual development of pore pressure can be observed within the slope composed of Red Silty Clay (RS). However for the Pale Yellow Silty Sand (PYS) a distinct zone of wetting can be observed, which can be attributed to the steep nature of the SWCC (Figure 5.6) due to high porosity of this type of soil amply reflected in the UHCC (Figure 5.7).

The factor of safety of the slopes are evaluated at an interval of 6 hours and plotted against time. Figure 5.11 (a), (b) gives the degradation of the Factor of Safety of the slope composed of the Red Silty Clay (RS) and the Pale Yellow Silty Sand (PYS) respectively.

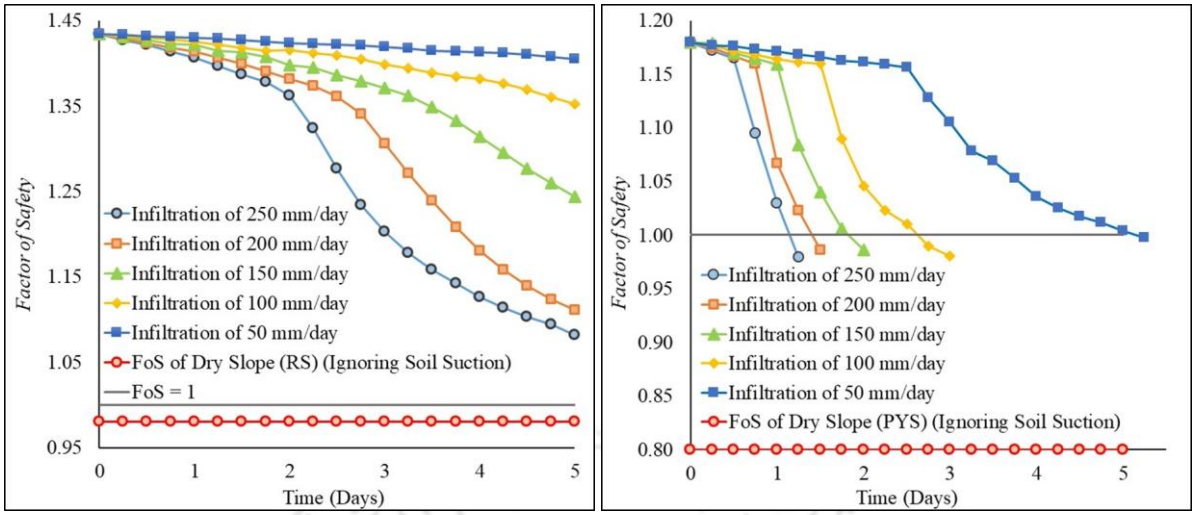

Figure 5.11 Factor of Safety vs. Time for slope composed of (a) Red Silty Clay (RS) (b) Pale Yellow Silty Sand (PYS)

The most prominent observation that can be made from figures is that slope analysis applying conventional soil mechanics deliberately ignoring soil suction gives an unrealistic estimate of the stability condition and thus fails completely to give an analytical description of the rainfall induced slope failure mechanism. Comparing both the figures, it can be understood that matric suction and the cohesion component plays a significant role in providing a much greater stability to the slope composed of the Red Silty Clay (RS). Figure 5.12 (a) and (b) gives the Factor of Safety for the corresponding slopes at a particular time step.

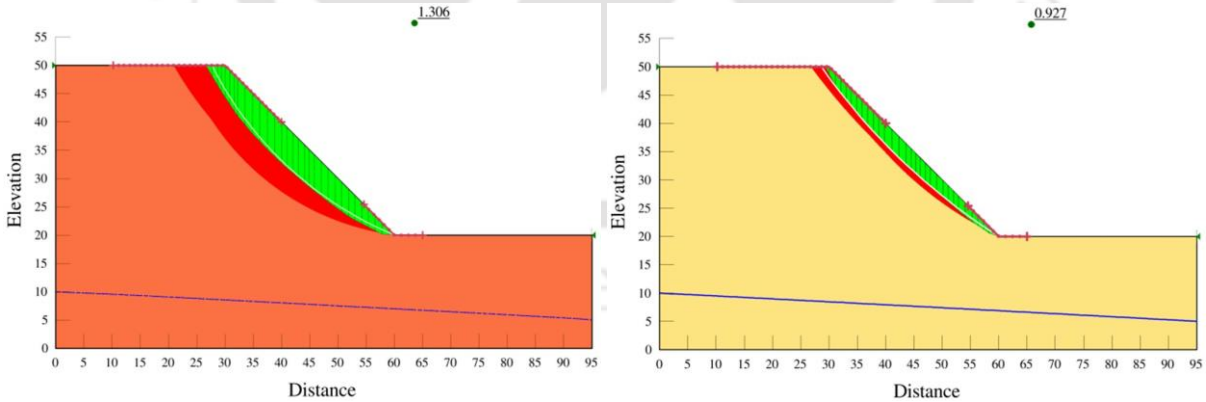

Figure 5.12 Factor of Safety of the slope composed of (a) Red Silty Clay (RS), (b) Pale Yellow Silty Sand (PYS) after an infiltration of 200 mm/day for duration of 3 days

For the slope composed of Pale Yellow Silty Sand (PYS), the Factor of Safety dips just below 1 indicating slippage. The shape and depth of the critical slip surface indicates a shallow translational slide that can be expected considering the shear strength properties

(Table 5.1) of the particular type of soil. A relatively deeper critical surface is observed, in case of the slope composed of the Red Silty Clay (RS), however the Factor of Safety is still sufficient enough to prevent failure of the slope, which can be attributed to the cohesive component and SWCC of the Red Silty Clay (RS). A close observation of Figure 5.12 (b) along with Figure 5.9 (b) gives a clear picture of the failure occurring within the wetting zone.

Following the fact that the slope composed of the Pale Yellow Silty Sand (PYS) had undergone failure, the pore pressure developed at the moment of the failure are plotted in Figure 5.13(a). The total cumulative rainfall required to initiate failure was calculated and plotted against rate of rainfall intensity in Figure 5.13(b).

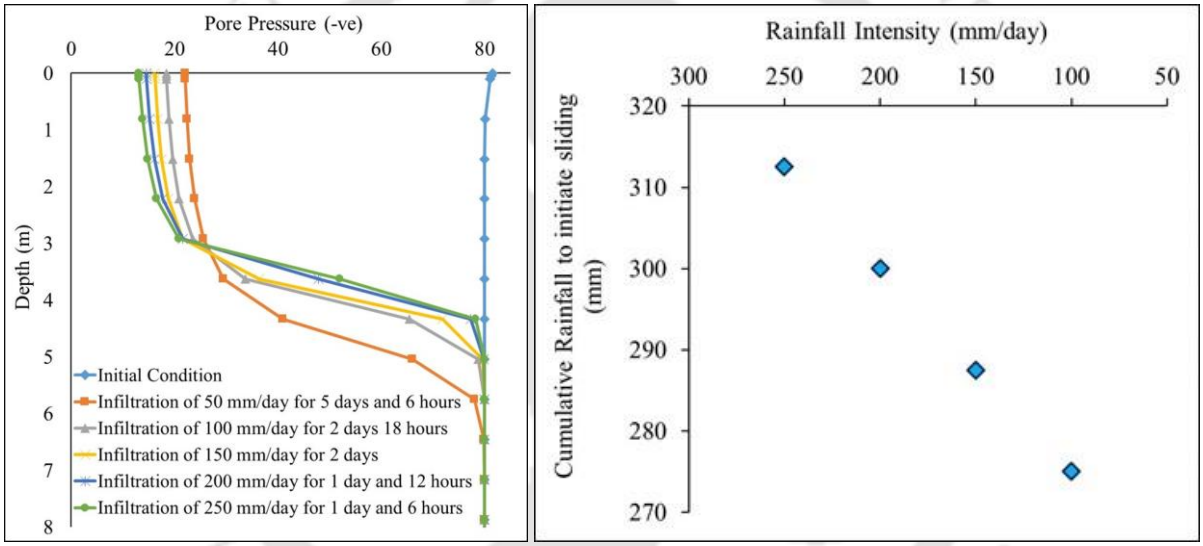

Figure 5.13 (a) Pore Pressure within the slope composed of Pale Yellow Silty Sand (PYS) at failure; (b) Total cumulative Rainfall required for initiating slipping within the slope composed of Pale Yellow Silty Sand (PYS) against the rate of applied infiltration

The depth of wetting as well pore pressure profiles are observed to be similar. A linear relation between rainfall intensity and cumulative rainfall required to initiate failure can be observed from Figure 5.13(b). The above two plots suggest that a similar wetting front needs to be developed to initiate slipping within the slope composed Pale Yellow Silty Sand (PYS). However, with decreasing rainfall intensity lesser amount cumulative rainfall is required to initiate failure. This from the fact that with decreasing rate of infiltration more amount rainwater can infiltrate into the slope minimizing the runoff.

Actual rainfall data was then input into the simulation to assess the response of the model to rainfall infiltration. The rainfall data used as input is obtained from the Tropical

Rainfall Measuring Mission (TRMM) 3-hourly rainfall estimate (3B42 V7) data set for the Guwahati city location. The time-series rainfall data for duration of 84 hours (3 days and 12 hours) from afternoon of 4th October to the midnight of 7th October 2004, for the analysis is obtained from Goddard Earth Sciences Data and Information Services Center (GES DISC) maintained web portal Giovanni (http://disc.sci.gsfc.nasa.gov/giovanni). Figure 5.14(a) gives the rainfall intensity versus time in hours, used in the simulation.

The factor of safety of the slopes are then calculated and plotted against time. It can observe in the Figure 5.14(b) that slope composed of the silty sand (PYS) is in near failure condition at around 76 hours and undergoes failure by 80 hours. The analysis shows that the stability condition of the slopes can be well predicted for actual rainfall condition with the application of such simulation techniques.

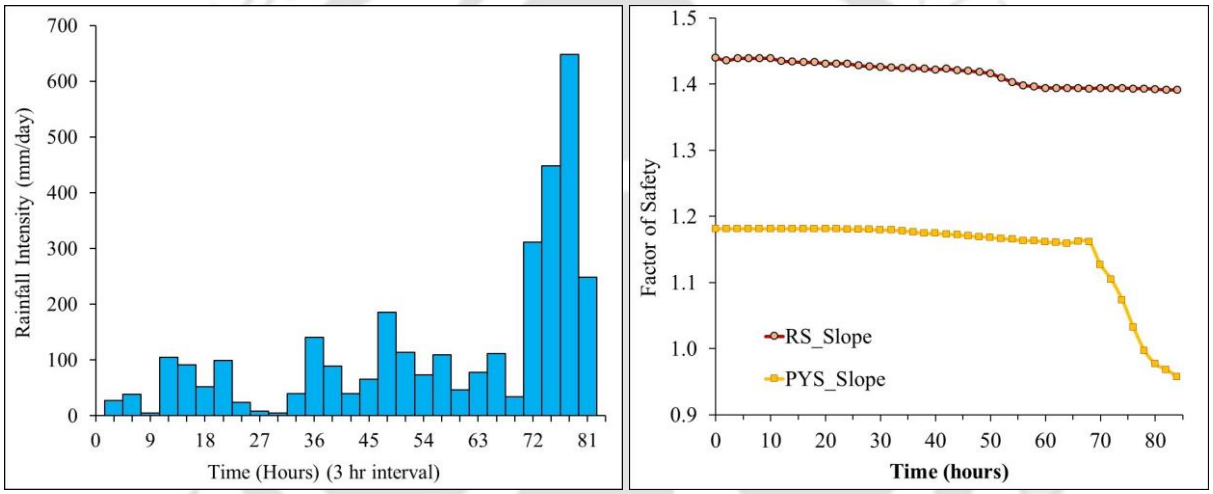

Figure 5.14 (a) Rainfall storm event history (afternoon of 4th October to the midnight of 7th October, 2004); (b) Factor of Safety vs. Time for actual rainfall infiltration

Coupling transient seepage analysis using the finite element method in SEEP/W and then using the output for slope stability analysis using the limit equilibrium method in SLOPE/W, a predictive model for rain-induced slope instability of natural residual soil slopes was developed to estimate the degradation of stability condition ultimately leading to failure. However, the analysis results depend greatly on the input parameters and thus extensive field investigations, laboratory soil testing, and rainfall data needs to be collected. The study suggests that slopes within the city of Guwahati thus have the potential of undergoing rainfall-induced landsliding, highlighting the observations made by previous researchers. However, the potential will vary depending on the type of soil and its response to infiltration.

5.3. PROBABILISTIC SLOPE STABILITY ANALYSIS

Even within an apparently homogenous soil layer, variability in geotechnical properties is a well-established fact. Such variability arises out of depositional and post depositional, geological and geo-morphological processes (Lee et al. 1983; Lacasse and Nadim, 1996). Uncertainty in geotechnical analysis or design arises essentially because a very insignificant portion of the total volume of soil is sampled, giving insufficient data for any conclusive inferences about the soil condition, on the other hand, investigating each and every point within a soil mass, would be economically unfeasible and rendered impractical (Baecher and Christian, 2003). Interestingly, ignoring such spatial variability, many conventional approaches rely on a deterministic analysis based on single-valued or equivalent soil parameters considering distinct geometry within the soil mass. A factor of safety (FoS), mostly based on experience and engineering judgment, is assumed to address different forms of uncertainty (Elkateb et al., 2002). Factor of safety has never been considered a reliable measure of risk (Li and Lumb, 1987). Slope stability analysis has always been acquiescent to probabilistic treatment and due attention towards this approach is available in literature (Alonso, 1976; Vanmarcke, 1977a&b; Cho, 2007). However, even if very sophisticated probabilistic analysis methods have been developed, mostly they have been combined with the classical slope stability analysis techniques vis., Limit Equilibrium methods (Griffiths et al., 2007).

Stability analysis of soil slopes, whether adopting a Limit Equilibrium method or utilizing Strength Reduction method using Finite Element/Finite Difference schemes, can be considered as numerical analysis techniques (Fredlund and Krahn, 1977). Adopting Finite Element or Finite Difference schemes gives a distinctive advantage over the conventional Limit Equilibrium methods. The most noticeable and important advantage is that the stress-deformation mechanism is allowed to develop automatically and seek out the most critical path to failure. Secondly, due to discretization of the slope into elements or zones, a platform for efficiently simulating spatial variability is offered (Fenton and Griffiths, 2008).

5.3.1. Slope Stability Analysis in FLAC^{2D}

FLAC is the abbreviation of “Fast Lagrangian Analysis of Continua” and is developed by ITASCA. The FLAC software is based on the explicit finite difference method, which can simulate the behaviour of many materials such as soils, rocks and structural elements. The dynamic equation applied in FLAC is very suitable to simulate slope failure, large

deformation and other such problems. A major advantage of FLAC is the built-in language FISH (ITASCA, 2005).

5.3.2. Random Variable and its Distribution

The Point Statistics are generally described by the Expected value, the Variance or Coefficient of variation and the governing probability distribution determined by unbiased estimation of sample statistics from 'n' number of data sets

$$\mathrm{E}[x] = \mu_x = \frac{1}{n}\sum_{i=1}^{n} x_i \tag{5.16}$$

$$\mathrm{Var}[x] = (\sigma_x)^2 = \frac{1}{(n-1)}\sum_{i=1}^{n} (x_i - \mu_x)^2 \tag{5.17}$$

$$\mathrm{CoV}[x] = \frac{\sigma_x}{\mu_x} \times 100\% \tag{5.18}$$

where E[x] is the Expected Value, Var[x] is the variance, σ_x is the Standard Deviation and, CoV[x] is the Coefficient of Variation of the variable x.

The statistics of the distribution is presented in Table 5.2 and is assumed constant for the purpose of this study. The soil cohesion (c) and angle of internal friction (φ) adopted from Chen (2007). The coefficient of variations for the corresponding soil properties is considered as reported by Baecher and Christian (2003). Changes in the probability of failure were evaluated for changing spatial correlation structure in the form of correlation length, for both isotropic and anisotropic random field. Figure 5.15 shows the probability (normal) distribution of the soil shear strength parameters.

Table 5.2 Statistics adopted for probabilistic slope stability analysis

Soil Property	Cohesion, c	Angle of Internal Friction, φ
Expected Value or Mean	12.38 kPa	20º
Coefficient of Variation	15 %	10 %
Standard Deviation	1.857 kPa	2º

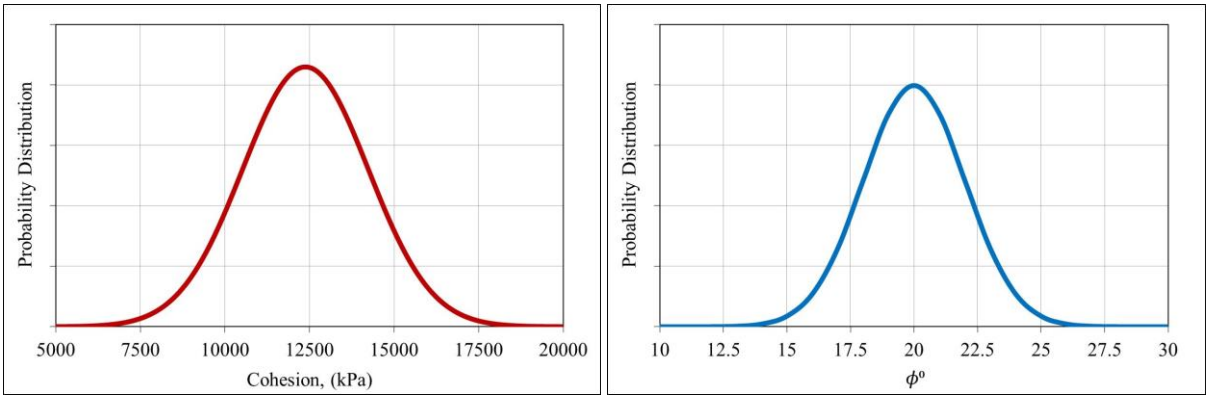

Figure 5.15 Probability distribution of the soil shear strength parameters (a) Cohesion; (b) Angle of internal friction

5.3.3. Spatial Variability – Random Field

The quantity of data required for characterizing the spatial variability of a soil deposit largely exceeds the amount than can be achieved in practice (Baecher and Christian, 2003). Therefore, a model is introduced for characterizing spatial variability, considering Variability at a Point and Spatial Dependence. Variability at a Point determines what could be the possible values the soil parameter can acquire at a particular point, given a probability density function, over which Spatial Dependence imposes a conditional probability, depending on the values of sur-rounding points and the corresponding distances, governed by a joint probability density function (Vanmarcke, 1983).

For further simplifying the characterization problem, the joint probability density function is assumed a Gaussian process i.e., a multivariate normally distributed random process. The second important assumption is that of statistical homogeneity, which implies that the joint probability distribution function is dependent only on relative position of points or in other words, the statistics of the soil parameter are constant over space and time. This assumption enables the spatial variability to be expressed as a summation of two quantities vis., the Deterministic trend and the Residual variability about that trend (Baecher and Christian, 2003; Fenton and Griffiths, 2008). The spatial variability at a point can then be defined by Equation 1 and the multivariate normal probability density function described by Equation 2

$$Z(\mathbf{x}) = T(\mathbf{x}) + U(\mathbf{x}) \tag{5.19}$$

where Z(x) is the value of the soil parameter at position (x), T(x) is the trend at (x), and U(x) is the residual variation.

$$f_{(\mathbf{X})}(\mathbf{x}) = \frac{1}{\sqrt{|\mathbf{C}|(2\pi)^k}} \exp\left\{-\frac{1}{2}(\mathbf{X}-\boldsymbol{\mu})^{\mathrm{T}}\mathbf{C}^{-1}(\mathbf{X}-\boldsymbol{\mu})\right\} \tag{5.20}$$

where C is the Covariance Matrix, μ is the vector of Expected Values, X is the random variable, and (x) is the position vector for k dimensions.

Under the above stated simplifying assumptions, the random field can be characterized based on three parameters (i) the Field Mean, (ii) Variance and (iii) Correlation Length.

5.3.4. Covariance – Correlation

Covariance dictates how the value of a parameter will be correlated depending on the relative spatial location and the corresponding values of the surrounding field. For a Gaussian random field, the Covariance function can be expressed as

$$\begin{aligned}\mathbf{C}[\mathbf{x}_1,\mathbf{x}_2] &= \mathrm{Var}[\mathbf{X}(\mathbf{x}_1),\mathbf{X}(\mathbf{x}_2)] \\ \mathbf{C}[\mathbf{x}_1,\mathbf{x}_2] &= \mathrm{E}[\mathbf{X}(\mathbf{x}_1),\mathbf{X}(\mathbf{x}_2)] - \boldsymbol{\mu}_x(\mathbf{x}_1)\boldsymbol{\mu}_x(\mathbf{x}_2)\end{aligned} \tag{5.21}$$

where x_1 and x_2 are the position vectors and X is the random variable.

Covariance function is expressed as a Correlation function in non-dimensional form as

$$\boldsymbol{\rho}[\mathbf{x}_1,\mathbf{x}_2] = \frac{\mathbf{C}[\mathbf{x}_1,\mathbf{x}_2]}{\boldsymbol{\sigma}_x(\mathbf{x}_1)\boldsymbol{\sigma}_x(\mathbf{x}_2)} \tag{5.22}$$

Assuming the statistics independent of position i.e., a stationary random field, the correlation function can be expressed as

$$\boldsymbol{\rho}[\boldsymbol{\tau}] = \frac{\mathbf{C}[\boldsymbol{\tau}]}{\boldsymbol{\sigma}_x^{\,2}} \tag{5.23}$$

where $\tau = x_1 - x_2$, is the relative position vector.

Once the Correlation Matrix with the prescribed co-variance structure

$C(\tau_{ij}) = C(|x_i - x_j|)$, where i,j = 1,2,3,…..,n

is obtained, the correlation matrix is de-composed into the product of a lower triangular matrix and its transpose by Cholesky's decomposition, such that

$$LL^{\mathrm{T}} = [\mathbf{C}] \tag{5.24}$$

The Gaussian random field is then generated according to

$$X(x) = LU \tag{5.25}$$

where U is column vector of 'n' numbers of independent Gaussian random variables, and 'n' is the total numbers of element or zones in the numerical model.

For the present study, an Ellipsoidal Markovian Correlation Structure is assumed and is expressed as

$$\boldsymbol{\rho}(\tau) = \exp\left\{-\sqrt{\left(\frac{2\tau_x}{\theta_x}\right)^2 + \left(\frac{2\tau_y}{\theta_y}\right)^2}\right\} \tag{5.26}$$

where τ_x, τ_y are relative position vectors and θ_x, θ_y are the Correlation Lengths in the *x* and *y* direction respectively.

The Ellipsoidal Markovian Correlation function is quadrant symmetric and results in properly conditioned symmetric covariance matrix. Both isotropic and anisotropic random field can be generated with equal ease. However, the variance function cannot be obtained in a closed form solution and, thus, the variance reduction over the zone space needs to be calculated by numerical integration of Equation 13. The effect of correlation length on the correlation structure is illustrated graphically in Figure 5.16 (a), (b) and Figure 5.17.

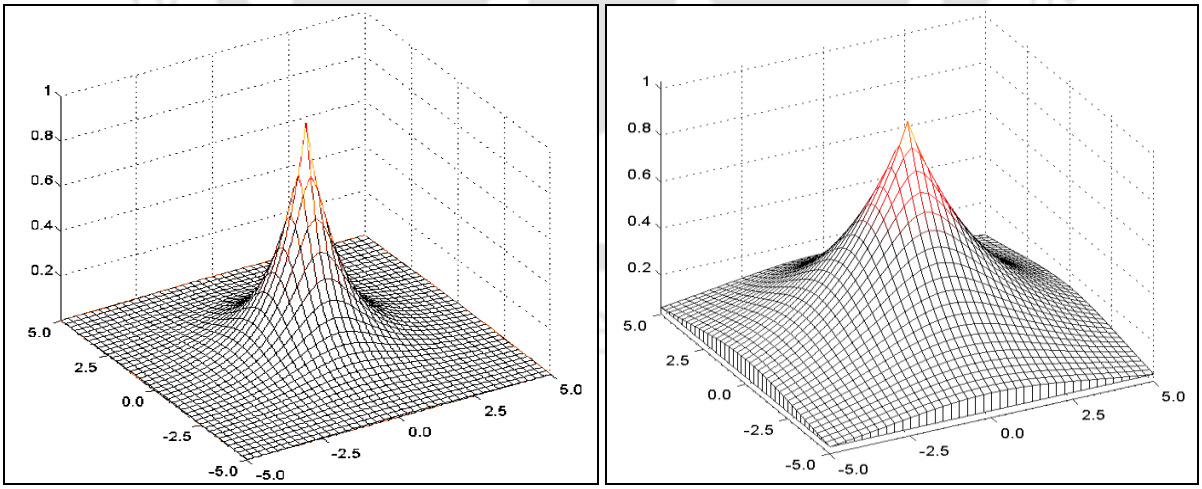

Figure 5.16 Isotropic Correlation Structure for Correlation Length $\theta_x = \theta_y$ = (a) 3.0m; (b) 10m.

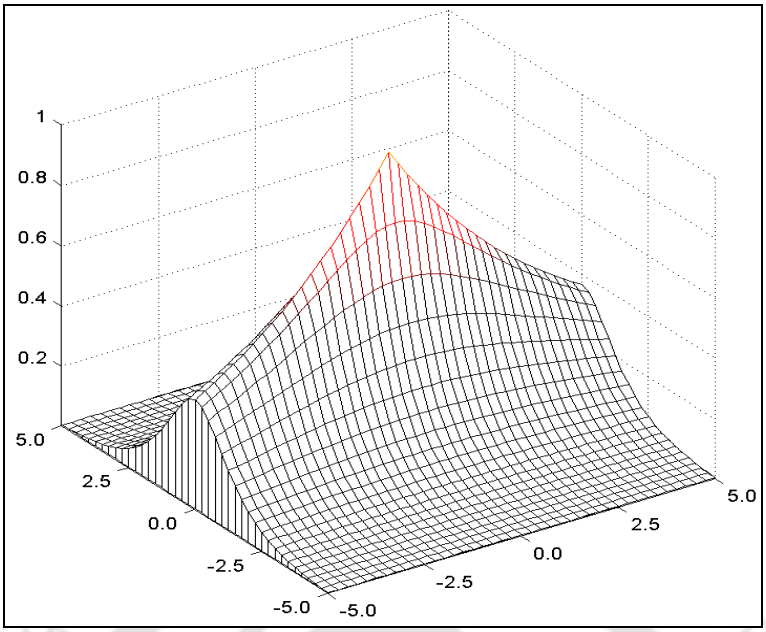

Figure 5.17 Anisotropic Correlation Structure for Correlation Length θ_x = 10.0m in the x – direction and $\underline{\theta}_y$ = 2.0m in the y – direction

5.3.5. Local Averaging within a Zone

Random field is defined as a continuous process and are characterized by their point statistics. However, while simulation the values are generated at discrete points, mostly at the centroids of the elements or zones. Therefore, the variance needs to average over the zone size, and for this purpose, a variance function needs to be introduced (Fenton and Vanmarcke, 1990) such that

$$\mathrm{Var}\left[\mathbf{X_T(x)}\right] = \mathrm{Var}\left[\mathbf{X(x)}\right]\gamma(\mathrm{T}) \tag{5.27}$$

where, Var[$\mathbf{X}_\mathrm{T}$(**x**)] is the reduced variance over the zone space given the point variance Var[**X**(**x**)] of the random variable **X** at position (**x**) and γ(T) is the variance function defined as

$$\gamma(\mathrm{T}) = \left(\frac{\sigma_{\mathbf{x}}}{A}\right)^2 \int_0^{T_1}\int_0^{T_1}\int_0^{T_2}\int_0^{T_2} \rho(x-\zeta, y-\eta)\,dx\,dy\,d\zeta\,d\eta \tag{5.28}$$

where T_1 and T_2 is the zone or element dimension, A is the averaging domain or space, x and y defines the point over which the variance reduction is integrated for the zone dimensions and ζ and η represents a local coordinate defined over the particular zone.

5.3.6. Cross – Correlation

Determination of complete spatial cross-correlation structure is unlikely due to the requirement of dense spatially distributed data. Cross-correlation is therefore defined at a point and estimated by statistically comparing the soil properties in pairs obtained from number of samples assumed to be from the same population (Fenton and Griffiths, 2008). For a stationary random field, the cross-correlation reduces to the just the constant coefficient $\rho_{c\varphi}$. Stationary point wise correlated fields can thus be described by the correlation functions $\rho_c(\tau)$ and $\rho_\varphi(\tau)$ and the cross-correlation coefficient $\rho_{c\varphi}$. The point wise covariance structure can then be expressed in matrix form as

$$\rho(\tau = 0) = \begin{bmatrix} \rho_c & \rho_{c\phi} \\ \rho_{\phi c} & \rho_\phi \end{bmatrix} \tag{5.29}$$

For the presented analysis the cohesion and angle of internal friction is assumed normally distributed random variable, and negatively cross-correlated with a cross-correlation coefficient of -0.7 (Wolff, 1985; Cherubini, 2000) which implies that high values of cohesion are associated with low values of friction angle and vice versa.

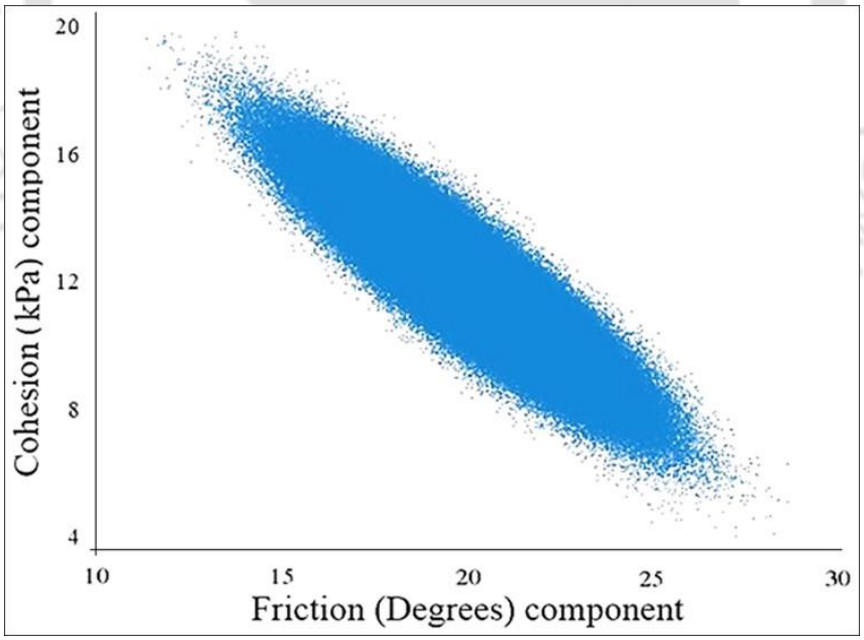

Figure 5.18 Covariance structure of random parameters – cohesion and angle of internal friction

5.3.7. Spatial distribution of C-φ

The presented problem is adopted from Chen (2007). The slope geometry and parameters are shown in Figure 5.19. Using limit analysis, Chen (2007) evaluated the factor of safety of this particular slope to be exactly 1.0. Figure 5.19 compares the factor of safety obtained by various methods considering the same parameters.

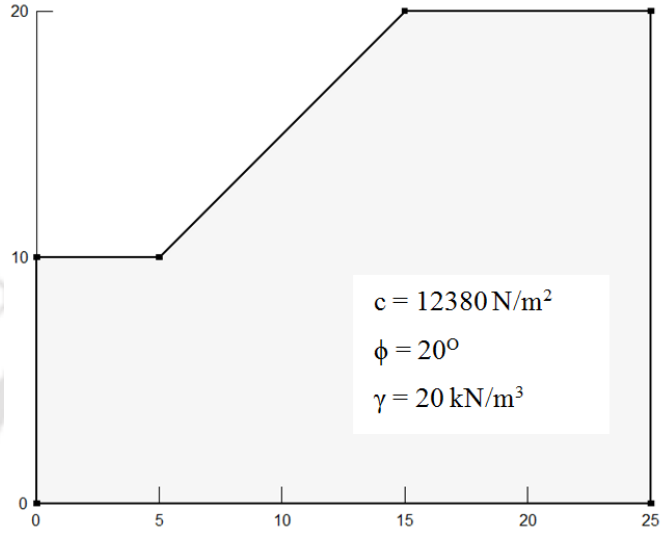

Figure 5.19 Geometry of the slope with assumed parameters

Table 5.3 Factor of safety from various methods

Method adopted	**Factor of Safety**
Limit Analysis (Chen, 2007)	1.0
Ordinary Method of Slices	0.987
Bishop's Simplified	1.025
Janbu's Simplified	0.98
Spencer's Method	1.022
Morgenstern-Price Method	1.022
Strength Reduction Method in FLAC^{2D}	1.01

A probabilistic slope stability analysis of the same slope considering spatial variability within the soil mass is conducted. The slope is discretized into 3150 number of zones. However, random field is simulated for 10m depth from slope surface to reduce the size of the covariance matrix. This simplification does not affect the results as the failure zone is well within this region. The number of zones over which the random field is simulated thus reduces to 2250. The size of the covariance matrix is therefore 2250×2250. Monte Carlo simulation approach is applied in the generation of the 2D normal random field. For realization of the random field (Vanmarcke, 1983) the covariance matrix is decomposed

according to Equation 9 and the lower triangular matrix is multiplied with a Gaussian random column vector of 2250 statistically independent elements according to Equation 10.

Isotropic random field is generated for correlation length $\theta_x = \theta_y$ = 1m, 2m, 3m, 5m, 7m & 10m. Figure 5.20 shows the distribution of cohesion and angle of internal friction as randomly distributed and cross-correlated parameter isotropic random field of correlation length of 1.0m. It can be observed that zones where the cohesion value is greater, the angle of internal friction is lesser and vice versa. Figure 5.21 shows the random distribution of the cohesion parameter for correlation length of 5.0m and 10.0m respectively.

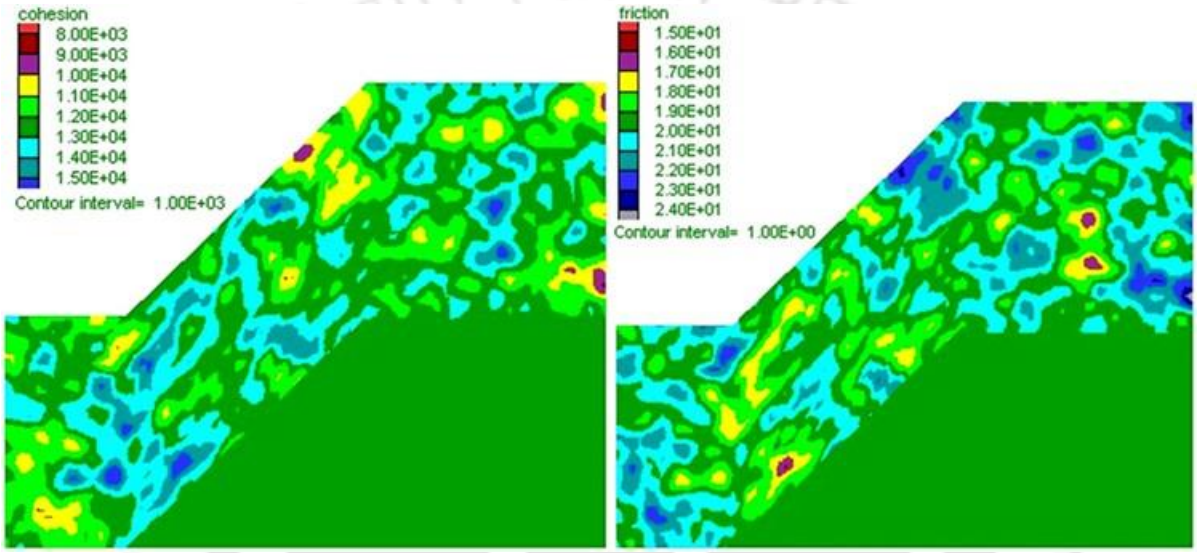

Figure 5.20 Cross-correlated isotropic random field for cohesion and friction; $\theta_x = \theta_y$ = 1.0m.

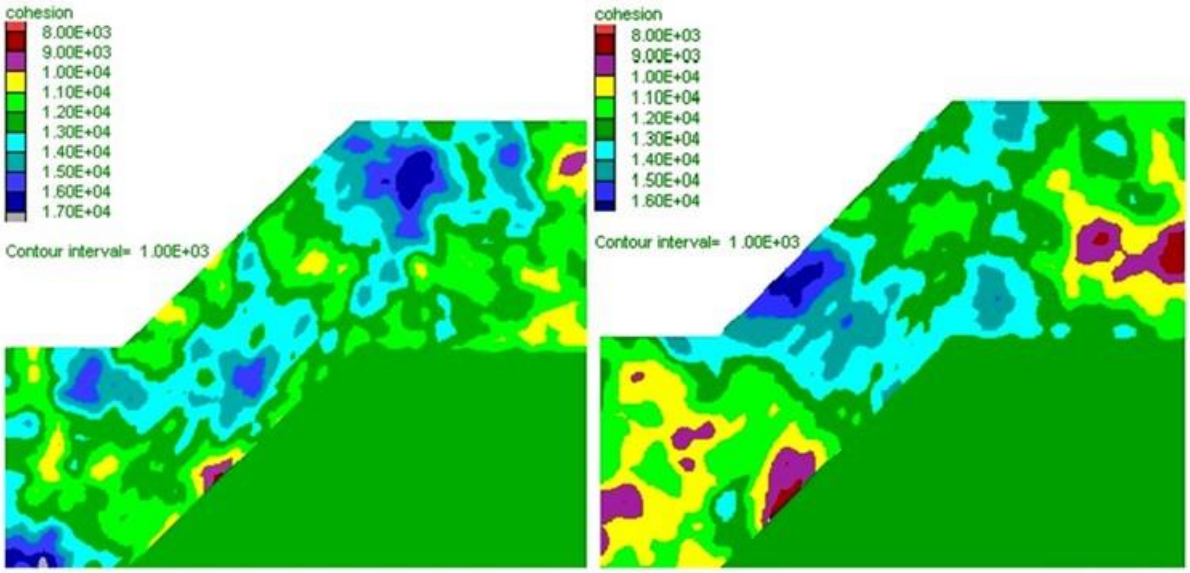

Figure 5.21 Isotropic random field for $\theta_x = \theta_y$ = (a) 5.0m; (b) 10.0m

Table 5.4 gives the combination of correlation length used for generation of anisotropic random field.

Table 5.4 Combination of correlation length for anisotropic random field

θ_y	1	1	1	2	2	3	3
θ_x	5	10	20	10	20	15	30

Figure 5.22 shows the distribution of soil parameter within the soil mass for anisotropic random field. The variation trend within the soil mass can be clearly observed with the change in correlation structure.

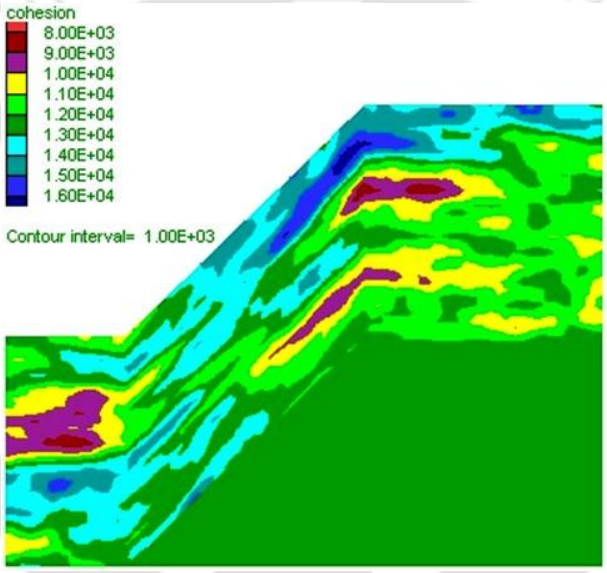

Figure 5.22 Anisotropic random field for θ_x = 15.0m and θ_y = 3.0m

5.3.8. Probability of Failure (*PoF*)

1000 random field realization is generated for each combination of correlation length and probability of failure evaluated. For reducing the time consumption, only the deformation-based stability situation of the slope is estimated according to the convergence criterion for each numerical simulation, instead of calculating the factor of safety using strength reduction method. Elastic-perfectly plastic Mohr-Coulomb material model governs the failure criterion.

The probability of failure, *PoF* can then be evaluated as

$$PoF = \frac{m}{n} \times 100\% \tag{5.30}$$

where, m is the number times solution fails to reach steady state (Itasca, 2008) implying constant plastic deformation, and n is the total number of simulations.

5.3.9. Effect of Correlation Length on *PoF*

Figure 5.23 shows the results obtained from the analysis for isotropic random field. Increase in probability of failure was observed with increase in spatial correlation length for the initial portion of the curve up to about θ = 3, however with further increase in correlation length the probability of failure increases and approaches an asymptotic behaviour. This is attributed to the fact that with increase in the correlation length, the soil parameter tend to vary smoothly over large distances and larger zones of near valued parameters are formed(Figure 5.21). Beyond a specific size of the zonation, the probability of failure remains unaffected.

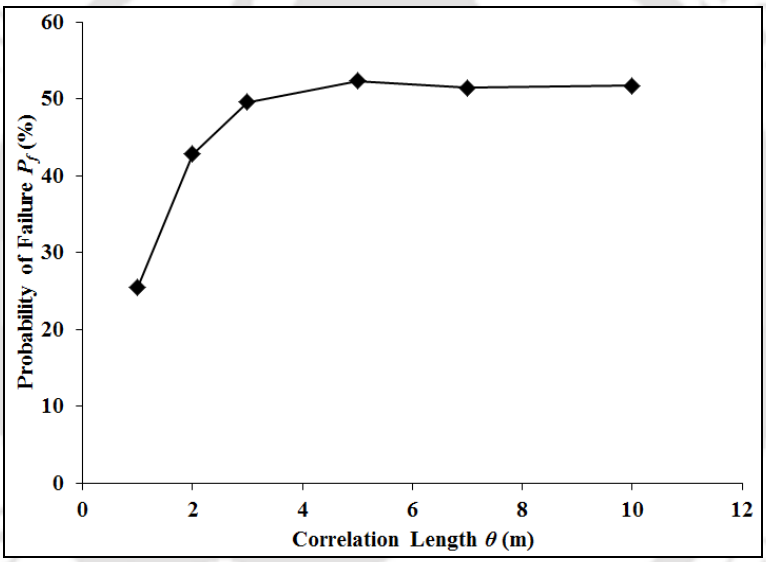

Figure 5.23 Probability of Failure vs. Correlation Length for isotropic random field.

Table 5.5 Probability of failure for anisotropic random field

θ_y (m)	θ_x (m)	*PoF* (%)
1	5	43.2
	10	45.1
	20	46.3
2	10	45.7
	20	48.5
3	15	47.5
	30	53.1

Table 5.5 reveals that for anisotropic random field probability of failure increases, the magnitudes of which were comparatively higher than that obtained for isotropic condition.

Formation of larger zones of near-valued parameters has been observed to occur with increasing width for the anisotropic random field, thereby increasing the probability of failure.

Covariance Matrix Decomposition method combined with Monte Carlo Simulation can serve to be an intuitive tool for simulating spatial variability. With help of software such as FLAC2D and MATLAB, spatial variability can be efficiently simulated. Realizations of both isotropic and anisotropic random field can be attained with equal ease for an Ellipsoidal Markovian Correlation Structure. For all the cases, increasing the correlation length exhibited an increase in the probability of failure of the system. The present study shows that a slope with a given factor of safety can have different probability of failure depending on the spatial correlation structure, and therefore will be associated with different risk levels.

5.4. SUMMARY

To assess the potential susceptibility to rainfall-induced landslide an effective modeling of changes in water content and matric suction in response to rainfall infiltration is essential. Seepage analysis is performed using SEEP/W (Geo-Slope International, 2007) for transient/steady state conditions considering saturated/ unsaturated material model, and the computed pore-water pressure are then used in SLOPE/W (Geo-Slope International, 2007) to evaluate the changes in stability with time applying Limit Equilibrium method. It is observed that the matric suction is closely related to slope stability, and is significantly affected by the effective degree of saturation controlled by rainfall events. Permeability parameters of the soil, including the variation of permeability with suction along with the intensity and duration of rainfall event are a critical factor in controlling the seepage behavior. The simulation was able to quantify the effect of infiltration on the stability of such natural slopes with time.

The probabilistic slope stability analysis considering spatial variations for soil properties attempts to identify the effect of spatial correlation structure on the probability of slope failure. Covariance Matrix Decomposition method based on Monte Carlo Simulation (MCS) is used for the generation of spatial variability and evaluating the probability of failure. Finite difference numerical code FLAC2D and numerical computing programming language MATLAB have been utilized for this purpose. This study shows that a slope with a given factor of safety can exhibit different probability of failure depending on the spatial variation.

5.5. CONCLUSIONS

The most important conclusion that can be drawn from the above analysis is that suction within a soil layer plays a very significant role in stabilizing a slope. Deliberately ignoring suction in the stability analysis can not only give an unrealistic result of Factor of Safety but also fail to explain how such steep natural slopes can remain stable during the dry season. The study shows that numerical seepage and slope stability analysis was able to quantify the effect of infiltration on the stability of the residual soil slope.

The strength parameters as well as response of soil to infiltration dependent on the SWCC and UHCC play a very significant role in determining the potential of slope towards failure. The Red Silty Clay (RS) due to its cohesion component of shear strength and higher suction values at comparable volumetric water content showed greater resilience than the slope composed of Pale Yellow Silty Sand (PYS). The study suggests that slopes within the city of Guwahati thus have the potential of undergoing rainfall-induced landsliding, highlighting the observations made by previous researchers. However, the potential will vary depending on the type of soil and its response to infiltration.

To take into account the variability in the various parameters the problem of slope stability analysis needs to be addressed from within a probabilistic framework. Therefore, with this aim, a probabilistic model for slope stability analysis was developed. The study shows that a slope with a given factor of safety can have different probability of failure depending on the spatial correlation structure, and therefore will be associated with different risk levels. Covariance Matrix Decomposition method combined with Monte Carlo Simulation can serve to be an intuitive tool for simulating spatial variability. With help of software such as FLAC2D and MATLAB, spatial variability can be efficiently simulated.

The study also highlights the fact that the Probability of Failure is a much better quantification of the stability of a slope as it is capable of taking into account the variability of the different significant factors. The level of uncertainty in the factor of safety is quantified through the variance of the factor of safety and the probability of failure under in-situ conditions. Therefore, combining conventional deterministic slope analysis and probabilistic analysis will be beneficial to slope engineering practice and will enhance the decision making process

Chapter 6. TRIGRS MODEL FOR GUWAHATI CITY

6.1. INTRODUCTION

The Transient Rainfall Infiltration and Grid-Based Regional Slope-Stability Model (TRIGRS) is a code program. The infinite slope stability model forms the theoretical basis of the code. A one-dimensional analytical transient flow model is implemented for modelling the infiltration process into a partially unsaturated surface layer above the water table and computing transient pore-pressure changes as response to complex storm histories. The program operates on a gridded elevation model or the DEM of a map area.

Analyses using TRIGRS are applicable to areas that are prone to shallow precipitation-induced landslides and that satisfy other model assumptions reasonably well. These assumptions include a well-documented initial water table and steady background flux, and relatively isotropic, homogeneous hydrologic properties.

6.2. SURFACE HYDROLOGY

The program, TRIGRS, uses a simple method for routing of surface runoff from cells that have excess surface water to adjacent downslope cells where it can either infiltrate or flow farther down slope. Runoff at a particular cell is assumed to occur when the precipitation and runoff supplied from upslope cells exceed the infiltration capacity or the rate of actual infiltration estimated at that cell for a particular time step.

The saturated hydraulic conductivity is generally considered the limiting case for the infiltration capacity for saturated and tension-saturated soils (Hillel, 1982; Iverson, 2000). Tension-saturated state represents the in-situ condition wherein the pore-water pressure is less than the atmospheric pressure (i.e., considered negative) while the soil being in a saturated state. This condition generally prevails in the capillary zone of the soil, just above the water table. The hydraulic conductivity is considered constant and equal to the saturated permeability. The purpose of routing the surface runoff is to prevent the loss of excess precipitation that cannot infiltrate at the cell of application. Simple runoff routing model allows diverting excess water from impervious areas onto more permeable downslope areas.

6.2.1. Runoff

The infiltration at each cell is computed as the sum of the precipitation plus any runoff from upslope cells with the limitation that infiltration cannot exceed the saturated hydraulic conductivity. The excess, if any, is considered runoff and is diverted to adjacent downslope cells.

$$Q_{in} = \begin{cases} RI + R_{ru} & ; \quad RI + R_{ru} \le k_{sat} \\ k_{sat} & ; \quad RI + R_{ru} > k_{sat} \end{cases} \tag{6.1}$$

where, Q_{in} is the rate of infiltration,

RI is the applied rainfall intensity,

R_{ru} is the run-off from upslope cells, (≥ 0),

k_{sat} is the saturated hydraulic conductivity,

$$R_{rd} = \begin{cases} RI + R_{ru} - k_{sat} & ; \quad RI + R_{ru} > k_{sat} \\ 0 & ; \quad RI + R_{ru} \le k_{sat} \end{cases} \tag{6.2}$$

where, R_{rd} is the run-off from the cell, diverted to adjacent downslope cells.

The run-off between adjacent cells is assumed to occur instantaneously and is not modelled as overland flow. The runoff from one-time step is not carried over to the next. Thus, excess water that runs off a cell during any given time step will either infiltrate at another cell or reach the edge of the model within that time step. The routing method enforces mass balance for each time step at individual cell level. The total precipitation at all the cells therefore is equal to the water that infiltrates at all the cells and the water that flows to edges of the problem domain without infiltrating within that particular time step.

In addition to runoff from cells where precipitation exceeds the infiltration capacity, water is assumed to run off from any cells where the water table is initially at the ground surface and the initial (steady) rate of infiltration is negative. TRIGRS is capable of modelling exfiltration from such cells using the mass balance calculations. Water from such cells runoffs to the adjacent downslope cell(s).

TRIGRS avoids iteration for satisfying mass balance for the entire problem domain. Therefore, to ascertain that the runoff routing is efficient TRIGRS computes the infiltration

and runoff at cells in order from the topographically highest cell(s) to the lowest. Hence, the topographic data have to be properly indexed. The digital elevation model (DEM) should be adjusted in GIS software to be hydrologically consistent. This adjustment is a selective smoothing process accomplished by raising the elevation of single-cell closed depressions to match surrounding cells, and slightly raising or lowering the elevation of cells in flat areas to produce flow directions that are consistent with surrounding topography.

6.2.2. Topographic Indexing and Flow Routing

TopoIndex (Topographic Index) is a companion utility program with the TRIGRS code that prepares a group of data files for the runoff-routing calculations. The TRIGRS program uses these data to control the order of runoff routing calculations as described above. TRIGRS will compute infiltration based on the rainfall input without routing any excess surface water if this step is skipped.

The program TopoIndex uses a two-step process to index the cells from highest to lowest elevation. The first step, sorting the cell elevations, consists of defining an index using the 'Heapsort' algorithm (Press *et al*., 1986). The second step corrects the index by comparing the indices of neighboring cells to their relative positions along downslope paths. The output files of TopoIndex also contain a list of grid cells and their downslope neighbors, along with a list of weighting factors that determine what proportion of the runoff is transferred to each neighboring downslope cell.

Thus, the output of the TopoIndex defines a continuous runoff flow path from upslope cell to downslope cell and the ratios by which the runoff of one cell will be divided into the adjacent downslope cells. TopoIndex provides the user several options for determining how excess water will be distributed among the downslope cells. Figure 6.1 shows the distribution weights of the various methods alongside the DEM. Figure 6.1 (a) shows the DEM of 9 cells, with the elevation value of each cell. The runoff is considered to occur from the shaded cell marked 'C' to adjacent downslope cells. Figure 6.1 shows the weighting factors for the (b) D-∞ method, (c) uniform distribution to all adjacent downslope cells, (d) D-8 method, (e) slope proportional distribution and (f) weighting factor proportional to square of slope. Comparing the weights with the elevation values, the distribution pattern of the runoff can be observed.

The D-∞ method assumes that water flows down the steepest slope, and computes the direction of steepest slope and attempts to direct flow in that direction by partitioning the flow between the two cells nearest to the steepest slope direction. The weighting factors are

proportional to the angles between the grid directions and the dip direction of the facet as described by Tarboton (1997). D-∞ method is physically more realistic than any of the other methods implemented in TopoIndex, and is used in the steady-state regional slope stability program SINMAP (Pack *et al*., 1998).

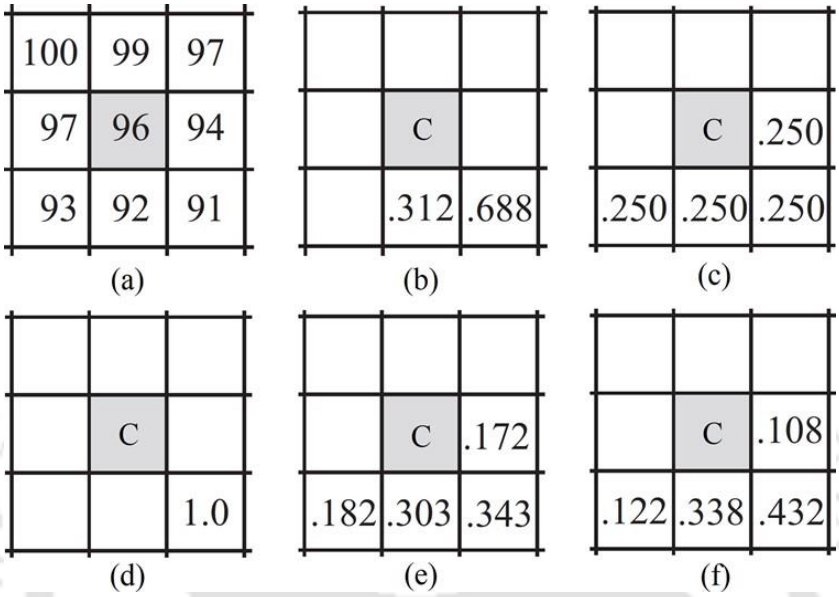

Figure 6.1 (a) DEM elevation values; (b), (c), (d), (e) and (f) Weighting factors for runoff distribution from the arbitrary cell marked C.

6.3. INFILTRATION MODEL AND PORE PRESSURE ESTIMATION

Infiltration over saturated initial condition

Iverson (2000) applied coordinate transformation to the Richards' (1931) equation as shown by researchers (Freeze and Cherry, 1979; Hurley and Pantelis, 1985) and proposed one-dimensional equation describing steady, near-surface groundwater flow in the vertical direction. The formulation considers the effects of a sloping ground surface and vertical infiltration into unsaturated soil.

$$\frac{\partial \theta}{\partial t} = \frac{\partial}{\partial z}\left[k(\psi)\left\{ \frac{1}{\cos^2 \beta}\frac{\partial \psi}{\partial z} - 1 \right\} \right] \tag{6.3}$$

where, z is depth in the vertical direction, t is time, θ is the volumetric water content, ψ is the negative pressure head (suction) in the soil, β is the slope angle, and $k(\psi)$ is the unsaturated hydraulic conductivity as a function of ψ

Iverson (2000) assumed initial wet condition (i.e., tension saturated soil condition). The hydraulic conductivity was assumed constant and equal to k_{sat} and the change in volumetric water content per unit change in pressure head was assumed constant over the range of volumetric water content. The infiltration model thus applies to saturated or tension-saturated initial conditions, so that flow is in the linear range for Darcy's law and the hydraulic diffusivity is approximately constant. Consequently, the fundamental infiltration equation is then expressed in the following form;

$$\frac{\partial \psi}{\partial t} = D_0 \cos^2 \beta \frac{\partial^2 \psi}{\partial z^2} \tag{6.4}$$

where, $D_0 = \frac{k_{sat}}{C_0}$ is the maximum characteristic diffusivity, and

C_0 is the rate of change of volumetric water content per unit change in pressure head for saturated soil, analogous to coefficient of volume compressibility.

Soil diffusivity defines how the pressure is equilibrated over soil layer from one point to other. Soil diffusion marks the transformation of the flow equation (involving volumetric water content) to pressure head. Iverson (2000) further provided an analytical solution for the above equation to estimate the infiltration into tension saturated soil, considering the following initial boundary conditions to hold true;

$$\psi(z,0) = (z-d)\left\{\cos^2\beta - \frac{I_B}{k_{sat}}\right\} \qquad \frac{\partial \psi}{\partial z}(\infty,t) = \left\{\cos^2\beta - \frac{I_B}{k_{sat}}\right\}$$

$$\frac{\partial \psi}{\partial z}(0,t) = \begin{cases} \left\{\cos^2\beta - \frac{I_B}{k_{sat}}\right\} - \frac{I_n}{k_{sat}} & ;t \le T \\ \left\{\cos^2\beta - \frac{I_B}{k_{sat}}\right\} & ;t > T \end{cases}$$

where, I_B is the steady-state background flux,

I_n is the rainfall intensity,

The solution of the initial boundary value problem posed by the above conditions is then expressed as:

$$\psi(z,0<t\le T)=(z-d)\left\{\cos^2\beta-\frac{I_B}{k_{sat}}\right\}$$
$$-\frac{I_n}{k_{sat}}\left[\left(\frac{D't}{\pi}\right)^{\frac{1}{2}}\exp\left(-\frac{z^2}{D't}\right)-z\left\{erfc\left(\frac{z^2}{D't}\right)^{\frac{1}{2}}\right\}\right] \quad (6.5)$$

$$\psi(z,t>T)=\psi(z,t\le T)$$
$$-\frac{I_n}{k_{sat}}\left[\left(\frac{D'(t-T)}{\pi}\right)^{\frac{1}{2}}\exp\left(-\frac{z^2}{D'(t-T)}\right)-z\left\{erfc\left(\frac{z^2}{D'(t-T)}\right)^{\frac{1}{2}}\right\}\right] \quad (6.6)$$

where, $D'=4D_0\cos^2\beta$ is termed as the effective hydraulic diffusivity (Iversion, 2000),

T is the duration of the rainfall,

erfc is complementary error function.

Equation 6.5 gives the pore pressure change with depth z and time t for the rainfall continuing within duration T, Equation 6.6 gives the pore pressure change after the rainfall stops at time $t = T$, and $t > T$.

Normalizing the time as;

$$t'=\frac{t}{(z^2/D')};\qquad T'=\frac{T}{(z^2/D')}$$

Subsequently, Iversion (2000) derives a pressure head response function as

$$R(t')=\sqrt{\frac{t'}{\pi}}\exp\left(-\frac{1}{t'}\right)-\mathrm{erfc}\left(\frac{1}{\sqrt{t'}}\right) \quad (6.7)$$

The formulation can be described graphically (Figure 6.2) as given by Iverson (2000)

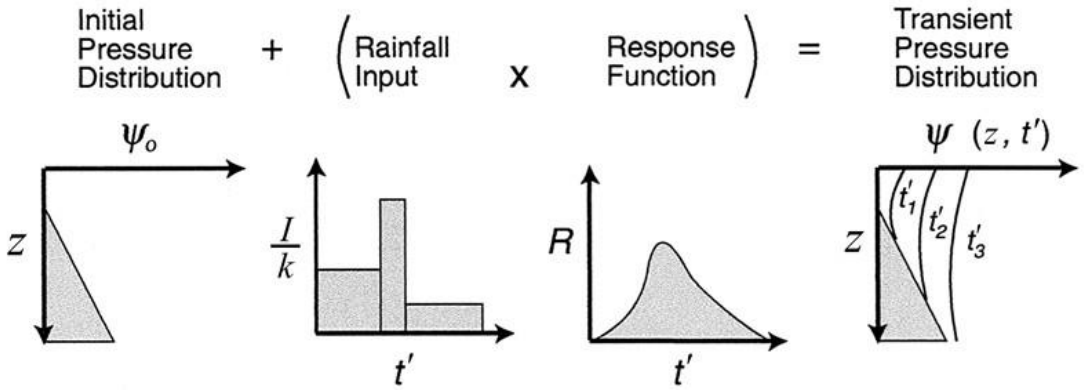

Figure 6.2 Schematic of rainfall input and pressure head response (Iverson, 2000)

Thus, as can be observed from the Figure 6.2, the infiltration model defines the location of a saturated wetting front that travels downwards analogous to a kinematic wave, similar to that conceived by Green and Ampt (1911) infiltration model. Iverson's (2000) solution consists of a steady (background) component and a transient component. The steady seepage component depends on the initial depth to the water table and a steady infiltration rate. The steady infiltration rate, the saturated hydraulic conductivity, and the slope angle determine the steady (background) flow direction in the plane of the infinite slope. The steady vertical hydraulic gradient is a function of the slope, the initial (steady or background) infiltration rate, and the saturated hydraulic conductivity. Model results are very sensitive to the steady-seepage initial condition. The transient component assumes one-dimensional, vertical downward flow, with a simple specified time-varying flux of fixed duration and intensity at the ground surface and a zero-flux condition for times greater than the starting time at an infinitely deep basal boundary.

Baum *et al*. (2002) extended the Iverson's (2000) infiltration model for tension saturated initial conditions and infinite depth basal boundary (Savage *et al*., 2004). Heaviside step functions is used in TRIGRS to implement Iverson's (2000) suggested summation of the original solution for rainfall of constant intensity to represent a general time-varying sequence of surface fluxes of variable intensities and durations. The Heaviside step function, or the unit step function, is a discontinuous function whose value is zero for negative arguments and one for positive arguments. The generalized solution used in TRIGRS is:

$$\psi(z,t) = (z-d)\left\{\cos^2\beta - \left(\frac{I_B}{k_{sat}}\right)\right\}$$

$$+2\sum_{n=1}^{N}\frac{I_n}{k_{sat}}\left\{H(t-t_n)\left[D'(t-t_n)\right]^{\frac{1}{2}}\,\text{ierfc}\left[\frac{z}{2\left[D'(t-t_n)\right]^{\frac{1}{2}}}\right]\right\} \qquad (6.8)$$

$$-2\sum_{n=1}^{N}\frac{I_n}{k_{sat}}\left\{H(t-t_{n+1})\left[D'(t-t_{n+1})\right]^{\frac{1}{2}}\,\text{ierfc}\left[\frac{z}{2\left[D'(t-t_{n+1})\right]^{\frac{1}{2}}}\right]\right\}$$

The function 'ierfc' is of the from

$$\text{ierfc}(\eta) = \frac{1}{\sqrt{\pi}}\exp\left(-\eta^2\right) - \eta\,\text{erfc}(\eta)$$

where, erfc(η) is the complementary error function,

H is the Heaviside step function.

Baum *et al*., (2002) further modified the infiltration model to include an alternative option of finite depth impermeable basal boundary (Savage *et al*., 2004). Infiltration model for estimating the infiltration through tension saturated soil profile for finite depth basal boundary is given as:

$$\psi(z,t) = (z-d)\left\{\cos^2\beta - \left(\frac{I_B}{k_{sat}}\right)\right\}$$

$$+2\sum_{n=1}^{N}\frac{I_n}{k_{sat}}H(t-t_n)\left[D'(t-t_n)\right]^{\frac{1}{2}}\sum_{m=1}^{\infty}\left\{\begin{array}{l}\text{ierfc}\left[\dfrac{(2m-1)d_{Lz}-(d_{Lz}-z)}{2\left[D'(t-t_n)\right]^{\frac{1}{2}}}\right] \\ +\text{ierfc}\left[\dfrac{(2m-1)d_{Lz}+(d_{Lz}-z)}{2\left[D'(t-t_n)\right]^{\frac{1}{2}}}\right]\end{array}\right\}$$

$$-2\sum_{n=1}^{N}\frac{I_n}{k_{sat}}H(t-t_{n+1})\left[D'(t-t_{n+1})\right]^{\frac{1}{2}}\sum_{m=1}^{\infty}\left\{\begin{array}{l}\text{ierfc}\left[\dfrac{(2m-1)d_{Lz}-(d_{Lz}-z)}{2\left[D'(t-t_{n+1})\right]^{\frac{1}{2}}}\right] \\ +\text{ierfc}\left[\dfrac{(2m-1)d_{Lz}+(d_{Lz}-z)}{2\left[D'(t-t_{n+1})\right]^{\frac{1}{2}}}\right]\end{array}\right\} \quad (6.9)$$

where, d_{Lz} is the depth to the impermeable basal boundary.

Equations 6.8 and 6.9 represent two different subsurface conditions. Equation 6.8 applies where hydraulic properties are uniform with depth and Equation 6.9 applies where a well-defined decrease in hydraulic conductivity exists at a finite depth. Therefore, Equation 6.9 would apply where loose relatively permeable slope deposits overlie relatively impermeable bedrock. Note that only one solution (either Equation 6.8 or 6.9) can be applied to all cells in a particular simulation analysis.

Infiltration over unsaturated initial condition

To model infiltration through unsaturated soil layer, TRIGRS applied the analytical solution of Equation 6.3 as proposed by Srivastava and Yeh, (1991) (Savage *et al*., 2004). Srivastava and Yeh (1991) showed that the exponential hydraulic parameter model of Gardner (1958) could be used to linearize Equation 6.3 and provide an analytic solution for transient infiltration through the unsaturated zone. This option treats the soil as an unsaturated zone that extends from the surface to the capillary fringe above the water table underlain by saturated soil zone where the pore water pressure is positive.

Gardner's (1958) unsaturated conductivity model is generally considered appropriate for coarse-grained soils. In this model, dependence of hydraulic conductivity, $k(\psi)$, and the volumetric water content, θ, on pressure head in the Richards' equation is given by the following formulas

$$k(\psi) = k_{sat} \exp(\alpha\psi'); \qquad \psi' = \psi - \psi_0$$

$$\theta(\psi) = \theta_r + (\theta_s - \theta_r)\exp(\alpha\psi') \tag{6.10}$$

where, $k(\psi)$ is the hydraulic conductivity function,

θ_s is the volumetric water content at saturated state,

θ_r is the residual volumetric water content,

α is fitting parameter, obtained by fitting equation to the SWCC,

$1/\alpha$ is the height of the capillary fringe above the water table (Gardner, 1958)

TRIGRS has the option to consider $\psi_o = -1/\alpha$, which lead to $k(\psi) = k_{sat}$ and $\theta = \theta_s$ at the top of capillary fringe. Thus, the hydraulic conductivity is constant and independent of pressure head, and is equal to the saturated hydraulic conductivity within the capillary fringe and below the water table. The other option being $\psi_o = 0$, which implies $k(\psi) = k_{sat}$ and $\theta = \theta_s$ at the ground water table.

The flux at the base of the unsaturated zone is given by;

$$q(d_u, t) = I_n - 4(I_n - I_B)\exp\left(\frac{\alpha' d_u}{2}\right)\exp\left(-D_\psi \frac{t}{4}\right)\sum_{m=1}^{\infty}\frac{\Lambda_m \sin(\Lambda_m \alpha' d_u)}{1 + \frac{\alpha' d_u}{2} + 2\Lambda_m^2 \alpha' d_u}\exp\left[-\Lambda_m^2 D_\psi t\right] \tag{6.11}$$

where, $D_\psi = \dfrac{\alpha' k_{sat}}{(\theta_s - \theta_r)}$ is the is the soil-water diffusivity (Freeze and Cherry, 1979)

$\alpha' = \alpha\cos^2\beta$: considering the coordinate transformation for the sloping ground surface

d_u is the vertical depth to the top of the capillary fringe for $\psi_o = -1/\alpha$ or the vertical depth to the ground water table for $\psi_o = 0$

The parameters $D_\psi t$ and $\alpha' d_u$ in the Equation 6.11 are analogous to the non-dimensional time and non-dimensional depth respectively, as used by Srivastava and Yeh (1991) (Savage *et al.*, 2004).

The initial distribution of the unsaturated hydraulic conductivity with depth is given by;

$$k(z)_{T=0} = I_B - \left[I_B - k_{sat} \exp(\alpha' \psi_o) \right] \exp\left\{ -\alpha' (d_u - z) \right\} \tag{6.12}$$

The variation of the unsaturated hydraulic conductivity in the unsaturated zone with time and depth as the rainfall continues is given by:

$$\begin{aligned} k(z,t) &= I_n - \left[I_n - k_{sat} \exp(\alpha' \psi_o) \right] \exp\left\{ -\alpha' (d_u - z) \right\} \\ &-4(I_n - I_B) \exp\left[\frac{\alpha' z}{2} \right] \exp\left(-D_\psi \frac{t}{4} \right) \sum_{m=1}^{\infty} \frac{\sin\left[\Lambda_m \alpha' (d_u - z) \right] \sin(\Lambda_m \alpha' d_u)}{1 + \frac{\alpha' d_u}{2} + 2\Lambda_m^2 \alpha' d_u} \exp\left[-\Lambda_m^2 D_\psi t \right] \end{aligned} \tag{6.13}$$

The values of Λ_m are the positive roots of the pseudo-periodic characteristic equation, $\tan(\Lambda \alpha' d_u) + 2\Lambda = 0$ and are obtained by a combination of bracketing, bisection, and Newton-Raphson iteration coded within TRIGRS.

To accommodate the time-varying input at the upper boundary, such as would occur during a rainstorm with varying intensity, Heaviside series expansions of the generalized form of Srivastava and Yeh's (1991) solution (Equation 6.11) is formulated to estimate the basal flux arriving at the base of the unsaturated zone;

$$\begin{aligned} q(d_u, t) = &\sum_{n=1}^{N} H(t - t_n) \left\{ \begin{array}{l} I_n - 4(I_n - I_B) \exp\left(\frac{\alpha' d_u}{2} \right) \exp\left(-D_\psi \frac{t - t_n}{4} \right) \\ \sum_{m=1}^{\infty} \frac{\Lambda_m \sin(\Lambda_m \alpha' d_u)}{1 + \frac{\alpha' d_u}{2} + 2\Lambda_m^2 \alpha' d_u} \exp\left[-\Lambda_m^2 D_\psi (t - t_n) \right] \end{array} \right\} \\ &- \sum_{n=1}^{N} H(t - t_n) \left\{ \begin{array}{l} I_n - 4(I_n - I_B) \exp\left(\frac{\alpha' d_u}{2} \right) \exp\left(-D_\psi \frac{t - t_{n+1}}{4} \right) \\ \sum_{m=1}^{\infty} \frac{\Lambda_m \sin(\Lambda_m \alpha' d_u)}{1 + \frac{\alpha' d_u}{2} + 2\Lambda_m^2 \alpha' d_u} \exp\left[-\Lambda_m^2 D_\psi (t - t_{n+1}) \right] \end{array} \right\} \end{aligned} \tag{6.14}$$

Similarly, the hydraulic conductivity varying with depth and time, $k(z,t)$ is formulated and is given as:

$$k(z,t)=\sum_{n=1}^{N}H(t-t_n)\left\{\begin{array}{l} I_n-\left[I_n-k_{sat}\exp(\alpha'\psi_o)\right]\exp\left\{-\alpha'(d_u-z)\right\}-4(I_n-I_B)\exp\left[\dfrac{\alpha' z}{2}\right] \\ \exp\left(-D_\psi\dfrac{t-t_n}{4}\right)\displaystyle\sum_{m=1}^{\infty}\frac{\sin\left[\Lambda_m\alpha'(d_u-z)\right]\sin(\Lambda_m\alpha' d_u)}{1+\dfrac{\alpha' d_u}{2}+2\Lambda_m^2\alpha' d_u}\exp\left[-\Lambda_m^2 D_\psi(t-t_n)\right] \end{array}\right\} \quad (6.15)$$

$$-\sum_{n=1}^{N}H(t-t_{n+1})\left\{\begin{array}{l} I_n-\left[I_n-k_{sat}\exp(\alpha'\psi_o)\right]\exp\left\{-\alpha'(d_u-z)\right\}-4(I_n-I_B)\exp\left[\dfrac{\alpha' z}{2}\right] \\ \exp\left(-D_\psi\dfrac{t-t_{n+1}}{4}\right)\displaystyle\sum_{m=1}^{\infty}\frac{\sin\left[\Lambda_m\alpha'(d_u-z)\right]\sin(\Lambda_m\alpha' d_u)}{1+\dfrac{\alpha' d_u}{2}+2\Lambda_m^2\alpha' d_u}\exp\left[-\Lambda_m^2 D_\psi(t-t_{n+1})\right] \end{array}\right\}$$

The pressure head in the unsaturated zone is given by:

$$\psi(z,t)=\frac{\cos\beta}{\alpha'}\ln\left[\frac{k(z,t)}{k_{sat}}\right]+\psi_o \quad (6.16)$$

where, ψ_o can be initialised as $-1/\alpha$ or 0, as mentioned above.

Water-table rise

Water-table rise occurs in response to vertical infiltration when the amount of infiltrating water reaching the water table exceeds the maximum amount that can be drained by gravity. To compute the water-table rise, the excess flux accumulating at the water table or top of the capillary fringe is compared to the available pore space directly above the water table or capillary fringe. Complete saturation below the rising water table is assumed in all computations that follow. The excess flux arriving at the water table is integrated over time to compute the volume of water (per plan-view unit area) accumulating at the base of the unsaturated zone, $V_A(t)$, the limits of integration being from t = 0 to any time, t_n, that is of interest during the simulated infiltration event. The fillable volume (available pore space) per unit (plan-view) area, $V_F(z,t)$ above the water table is computed by integrating the fillable porosity $\theta_f = \theta_s - \theta$ from the initial top of the saturated zone up to various equally spaced heights above it in the unsaturated zone as:

$$V_F(z,t)=(\theta_s-\theta_r)\left[d_u-z+\frac{1}{k_s}\int_{d_u}^{z}k(z,t)\,dz\right] \quad (6.17)$$

The numerical integration of Equation 6.17 is done to compute the water-table rise.

Pressure Diffusion below the Water Table

Once the water-table rise has been computed at a grid cell for a particular time increment, pressure head applied by the newly accumulated water above the initial water table is given by:

$$\psi_{hn} = \left\{ \cos^2 \beta - \left(\frac{I_B}{k_{sat}} \right) \right\} h_n \tag{6.18}$$

where, h_n is computed water-table rise.

For relatively homogeneous hillsides with impermeable basal boundary at infinite depth, the head changes below a rising water table is computed using the pressure-diffusion expression given as:

$$\psi(z-d,t) = \sum_{n=1}^{N} \psi_{hn} H(t-t_n) \operatorname{erfc}\left[\frac{z-d}{2\sqrt{D'(t-t_n)}} \right] - \sum_{n=1}^{N} \psi_{hn} H(t-t_{n+1}) \operatorname{erfc}\left[\frac{z-d}{2\sqrt{D'(t-t_{n+1})}} \right] \tag{6.19}$$

Similarly, for hillsides that have a strong permeability contrast at shallow depth, a model that has an impermeable boundary at finite depth is used for estimating pressure-diffusion below the water table, and is given as:

$$\begin{aligned} \psi(z-d,t) = & \sum_{n=1}^{N} \psi_{hn} H(t-t_n) \left\{ 1 - \frac{4}{\pi} \sum_{m=1}^{\infty} \frac{(-1)^{m-1}}{2m-1} \exp\left[-\frac{(2m-1)^2 \pi^2 D'(t-t_n)}{4 d_{sat}^2} \right] \right. \\ & \left. \cos\left[\frac{\pi}{2}(2m-1)\left(\frac{z-d}{d_{sat}} - 1 \right) \right] \right\} \\ & - \sum_{n=1}^{N} \psi_{hn} H(t-t_{n+1}) \left\{ 1 - \frac{4}{\pi} \sum_{m=1}^{\infty} \frac{(-1)^{m-1}}{2m-1} \exp\left[-\frac{(2m-1)^2 \pi^2 D'(t-t_{n+1})}{4 d_{sat}^2} \right] \right. \\ & \left. \cos\left[\frac{\pi}{2}(2m-1)\left(\frac{z-d}{d_{sat}} - 1 \right) \right] \right\} \end{aligned} \tag{6.20}$$

6.4. SLOPE–STABILITY MODEL

The TRIGRS program uses a simple infinite-slope model to compute factor of safety on a cell-by-cell basis. Therefore, the infinite slope stability model demands a mention at the onset since the deterministic model that have been applied in this study is particularly based

on this stability concept. This model compares the destabilizing stresses and restorative strength of the material on an infinite plane parallel to the soil surface (Figure 6.3). No slope can be considered infinite in extent; as such, Infinite slope is purely conceptual. However, when the depth of the slip surface is much less compared to the areal extent of the landslide and the field condition remains nearly identical, then such a mathematical model can be applied for estimating a fairly close approximation of the stability condition (Bromhead, 1992). The other most advantageous feature of this model is that, it is readily applicable to the grid-based GIS framework for determination of the stability condition on a spatially distributed setting. The FoS can be calculated for each cell of the grid and the results presented in the form of a FoS–map.

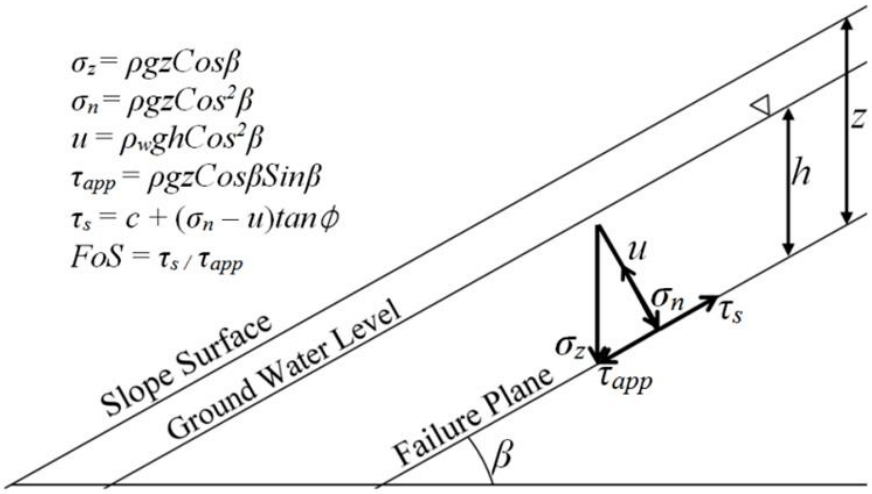

Figure 6.3 Infinite Slope Model

Factor of Safety based on Limit-equilibrium concept is defined as ratio of the shear strength of the material to the destabilizing stresses along an assumed failure plane, and is expressed as:

$$FoS = \frac{Shear\ strength\ \ of\ \ hill-slope\ soil}{Applied\ shear\ stress} = \frac{\tau_s}{\tau_{app}} \tag{6.22}$$

Mohr–Coulomb failure criterion (Equation 6.23) gives the shear strength of the material as a function of the soil cohesion and frictional resistance due to the effective normal stress on the failure plane

$$\tau_s = c' + (\sigma_n - u)tan\phi' \tag{6.23}$$

where, τ_s is the shear strength of the soil,

c' is the soil cohesion,

φ' is the effective angle of internal friction,

σ_n is the total normal stress,

u is pore-water pressure on the failure plane.

TRIGRS applies extended Mohr–Coulomb failure criterion based on Bishop's (1959) effective stress expression to account for the soil shear strength in the unsaturated zones (Equation 6.24)

$$\tau = c' + \{(\sigma_n - u_a) + \chi(u_a - u_w)\}\tan\phi' \tag{6.24}$$

where, u_a is the pore air pressure considered equal to atmospheric pressure,

u_w is the pore water pressure.

The parameter χ is approximated according to Vanapalli and Fredlund (2000), as:

$$\chi = \frac{\theta - \theta_r}{\theta_s - \theta_r} \tag{6.25}$$

The suction component in this expression is obtained from the soil water characteristic curve function, and for any particular depth is given by Equation 6.26

$$(u_a - u_w) = \psi(z,t)\rho_w g \tag{6.26}$$

The FoS is thus calculated as in Equation 6.27 (Baum *et al*., 2002)

$$FoS = \frac{\tan\phi}{\tan\beta} + \frac{c - \chi\psi(z,t)\gamma_w \tan\phi}{\gamma_s z \sin\beta\cos\beta} \tag{6.27}$$

where, γ_w is unit weight of water,

γ_s *is* bulk unit weight of partially saturated (in-situ) soil,

A depth-averaged soil unit weight is considered in Equation 6.27 to account for the unit weight of partially saturated soil above the water table and the increased unit weight of saturated soil below the water table.

The Factor of Safety is calculated at predetermined depth intervals. The slope is considered to be stable if the FoS ≥ 1.0 at all depths. Failure is assumed to occur when FoS < 1. The depth z where FoS first drops below 1 is the depth of landslide initiation. This initiation depth depends on soil shear strength, rainwater infiltration characteristics and the time and depth variation of the pressure head, which, in turn, depend on rainfall history.

6.5. INPUT – PARAMETERS FOR GUWAHATI HILLSLOPES

Input data required for TRIGRS simulation includes topographic parameter vis., the 'Digital Elevation Model' (DEM) of the study area, the 'Slope' map and the 'Aspect' map derived from the DEM, and the Depth of Basal-boundary map. The soil parameters include Mohr-Coulomb shear strength parameters (Cohesion – c and Angle of Internal Friction – φ), soil unit weight (γ), saturated hydraulic conductivity (k_{sat}), saturated and residual volumetric water content (θ_s and θ_r) and soil diffusivity (D_o).

6.5.1. Digital Elevation Model (DEM)

The primary input for TRIGRS or any such GIS-based models is the Digital Elevation Model (DEM). The DEM represent the topography of the area and thus is an important data from which all other input parameters such as the slope map, drainage pattern or runoff routing etc. as required are derived. There are few DEM available publically for the study area, vis., Indian Space Research Organization (ISRO) CartoSat-DEM (1/3 and 1 arc sec), Advanced Land Observing Satellite ('ALOS-DAICHI') AW3D30-DEM (1 arc sec), Shuttle Radar Topography Mission SRTM-DEM (1 arc sec and 3-arc sec), Advanced Space Borne Thermal Emission and Reflection Radiometer – Global DEM ASTER-GDEM (1 arc sec). The study utilizes all of the DEM's as mentioned above to assess the suitability of any particular DEM over the others for assessing the predictability of rainfall-induced landslide scenario of the Guwahati region with the application of TRIGRS, (the study is presented in Chapter 7).

Figure 3.6 shows the general topography and geomorphology of the study area. Figure 6.4 shows the color-shadow representation of the 'ALOS-DAICHI' AW3D30-DEM (1 arc sec), and is overlaid RVS-points (3.3).

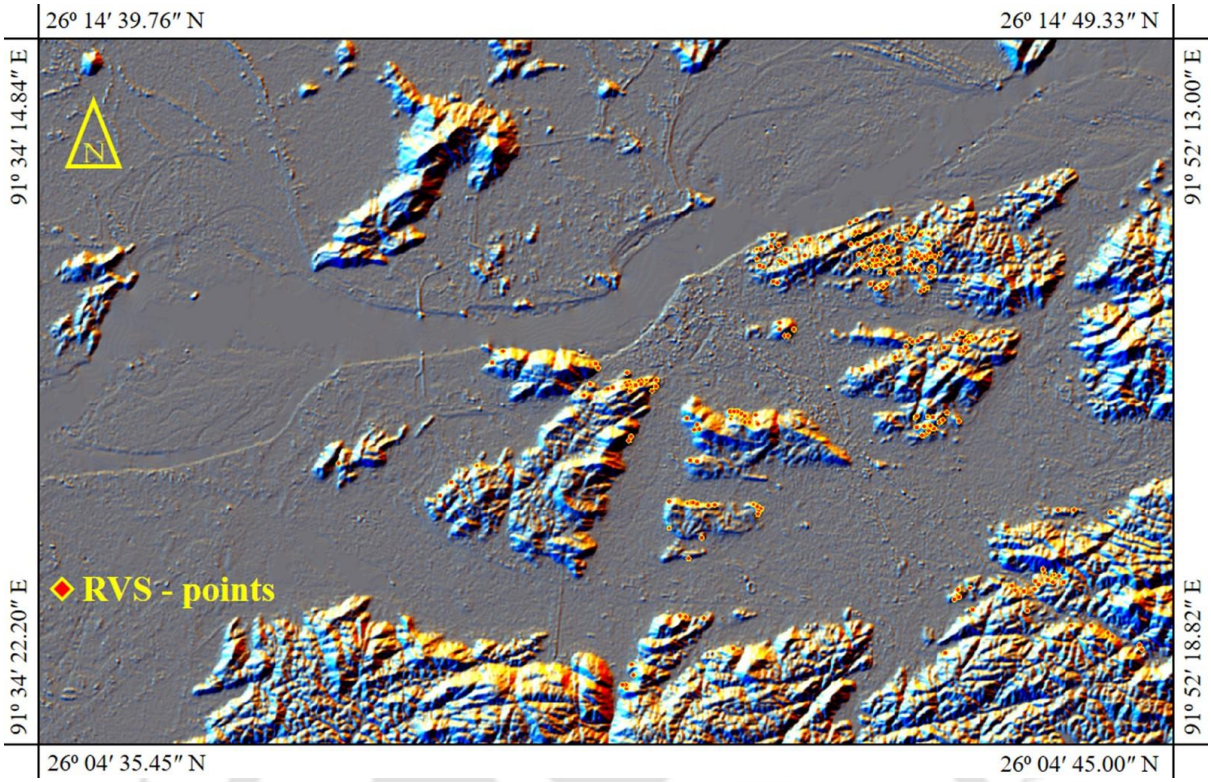

Figure 6.4 Color-shadow representation of the AW3D30-DEM with overlaid RVS-points

6.5.2. Slope Map

Topographic input parameter vis., the slope map (Figure 6.5) and the aspect map, required as input for the analysis, are extracted from the DEM. The slope and the aspect map are obtained using the SAGA-GIS (Conrad et al., 2015) slope, aspect, curvature module (Cimmery, 2010) applying the Zevenbergen and Thorne (1987) method which applies a second-order finite difference algorithm using 9 polynomial parameters to calculate the slope or the maximum gradient along the aspect direction at a particular cell.

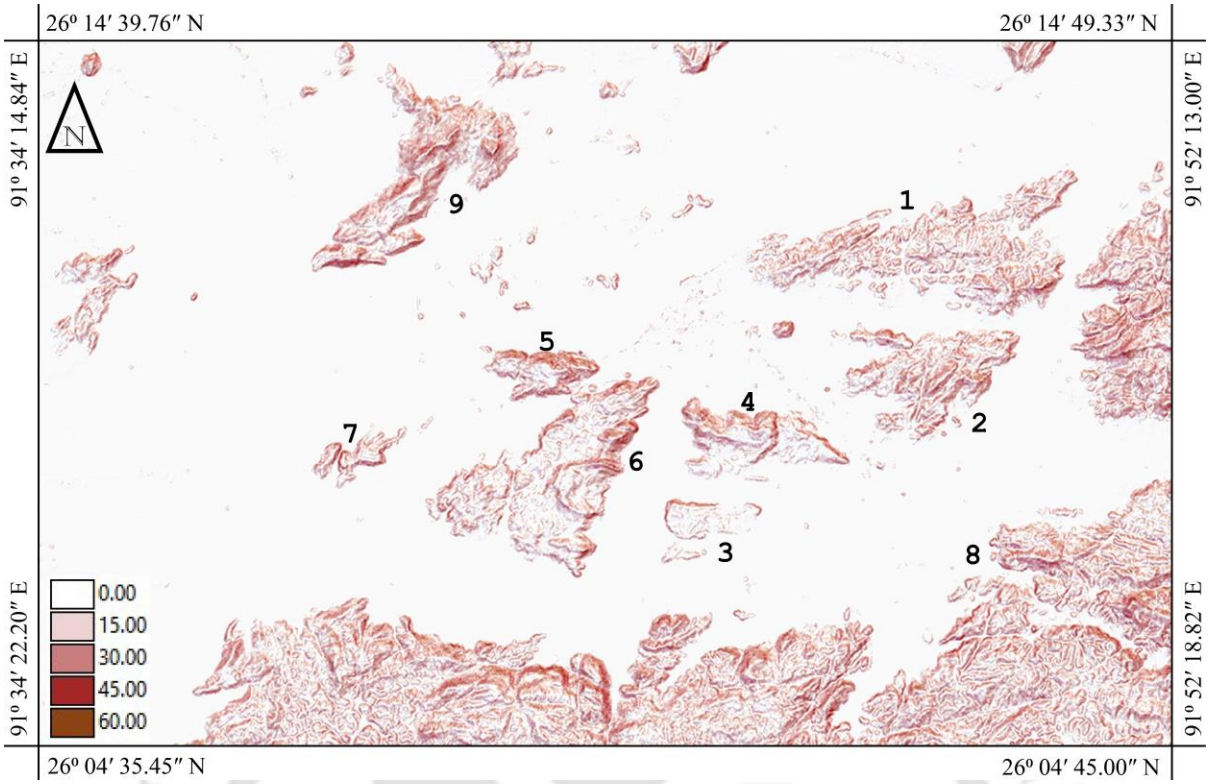

Figure 6.5 Slope map (in degrees) of Guwahati city

6.5.3. Depth of Basal Boundary and Initial Ground Water Level

The weathered soil thickness is affected by many factors including the vegetation cover, the underlying lithology, the climate, rainfall, the angle and curvature of slope, and land use. However, it is very difficult to quantify the relation among so many variables. From available literature, it is observed that the slope angle is the prime factor affecting the thickness of residual soil formation, and, therefore, it is more convenient to assume a simple exponential relationship between the soil thickness and the slope angle (Delmonaco *et al*., 2003; Salciarini *et al*., 2006; Tan *et al*., 2008).

Based on the borehole reports obtained across Guwahati city, the soil thickness (z) and slope angle (β) is related as per Equation 6.28. Figure 6.6 shows the soil depth map derived from the slope map (Figure 6.5) using Equation 6.28

$$z = 22.0e^{-0.074\beta} \tag{6.28}$$

where, z is the depth of soil above the (assumed) impermeable basal strata,

β is the slope angle.

Figure 6.6 Depth (m) of basal boundary map

The alluvial plains of this region remain saturated all year round, owing to the ground water table (GWT) being controlled by the mighty Brahmaputra River flowing through the city. However, detailed data on the ground water table in the hills of the study area does not exist. Observing the wells dug for obtaining drinking water and from the few in-situ borehole investigation data, it can be assumed that the basal rock strata remain saturated at all times. Thus, in the TRIGRS analysis, the initial ground water table is considered same as the depth of the basal rock. Finite depth basal boundary is considered and the ground water table is allowed to rise due to the rainwater infiltration.

6.6. TRIGRS – SEEP/W COMPARATIVE ANALYSIS

To arrive upon the input values of the parameters vis., the saturated hydraulic conductivity k_s, the saturated volumetric water content θ_s, the residual volumetric water content θ_r, Gardner fitting parameter α and the soil diffusivity D_o, a comparative (trial-error) analysis involving SEEP/W and TRIGRS was done.

A model of a typical slope was created in SEEP/W as shown in Figure 6.7. The slope angle of 29° was considered, being the mean of the hill slope angles affected most by landslides, as observed from the Rapid Visual Screening (RVS) study. The soil depth was

considered 2.57 m, as that given by Equation 6.28. The soil strata is considered composed of two layers. The top soil layer is assigned with saturated hydraulic conductivity, k_s = 1.0×10^{-6} m/s while the bottom soil layer is assigned with k_s = 1.0×10^{-5} m/s, the basal boundary is considered impermeable. The initial ground water table is considered to be at the interface of the soil and basal boundary. The soil layers of the slope were discretized with a finite element mesh of combined 4-noded quadrilateral elements with a fineness of 0.1 m and the sizes of the mesh gradually increased in the basal strata to reduce the total number of elements and decrease the computational time requirement. Surface elements of 0.1 m thickness were applied to define the ground surface of the slope. Figure 4.4 shows the SWCC and the van Genuchten (1980) parameters used to define the SWCC in the SEEP/W analysis. The unsaturated hydraulic conductivity curve is derived with the van Genuchten (1980), UHCC model coded in SEEP/W. The SEEP/W model was developed to represent the closest generalized approximation of the in-situ condition.

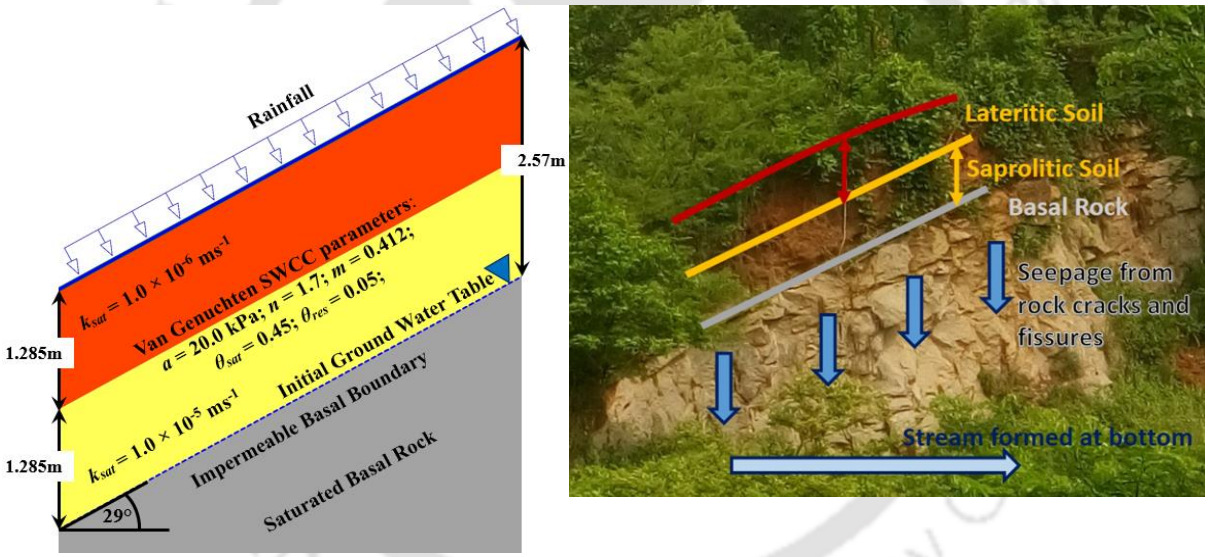

Figure 6.7 (a) Slope model as developed in SEEP/W (b) Cut-slope at Fatasil hill showing close resemblance to developed model

In the SEEP/W model, the SWCC is defined using the van Genuchten (1980) four parameter model, while the Richards' (1931) flow equation is solved using the finite element method to evaluate the pore pressure distribution within the slope. The soil parameters obtained through laboratory and in-situ testing were used as input to define the soil characteristics. The model comprises two soil layers with different permeability giving a much closer approximation to the in-situ condition. TRIGRS uses the Gardner's (1958) exponential hydraulic parameter model to define the SWCC and the unsaturated hydraulic conductivity, while applying analytically derived one dimensional infiltration model to

estimate the transient pore pressure changes. Modelling of layered soil profile is therefore, not possible in TRIGRS. The pore pressure distribution obtained from SEEP/W is likely to be a much closer approximation of the in-situ condition and different from that obtained with TRIGRS. To define the values of TRIGRS input parameters an analysis consisting of a finite element numerical model and TRIGRS simulation were conducted.

Unsaturated infiltration condition and finite depth boundary condition was considered and the ground water level was allowed to rise with infiltration of rainwater in TRIGRS simulation. Pore pressure profiles obtained for the above considered slope angle and depth of basal boundary from the TRIGRS model were compared with that obtained from SEEP/W model, for identical intensity of rainfall, as shown in Fig. 6.8. From the in-situ observation of landslides occurrences reported in the morning of 26th June 2012 at various locations in the Guwahati city, the landslides were inferred to occur along the soil-basal rock interface, with depth of slip surface ranging from 2.0 m to 2.5 m. The reported landslides were accompanied by profuse interfacial seepage indicating saturation of basal rock and landslide soil mass (Goswami, 2013). The numerical modeling conducted in the present study efficiently illustrated that the rise of water table led to the saturation and loss of strength of the overlying soil, leading to landslides that were conforming to those actually occurred in the field. Hence, the rise of water table is adjudged as the predominant condition leading to the widespread landslides in the region. It is worth mentioning that the rise of water table is not a field observation, as there were no subsoil instrumentations available yet in the landslide-affected areas to recognize the rise of water table. The TRIGRS parameters are so attuned such that the temporal rise in water table simulated by TRIGRS is in closest possible similitude to that obtained from SEEP/W, and that the corresponding location of slope instability, along with its time of occurrence, matched with that of in-situ conditions. The values of the parameters themselves should be consistent with that of experimentally observed values. Thus, for the present study, instead of focusing on the pore pressure profile itself, emphasis is given on the location and time of triggering of slope failure due to rising water table. Table 6.1 and Table 6.2 gives the values of the hydraulic soil parameters and soil shear strength parameters respectively, considered for conducting the rainfall induced landslide hazard analysis of the study area.

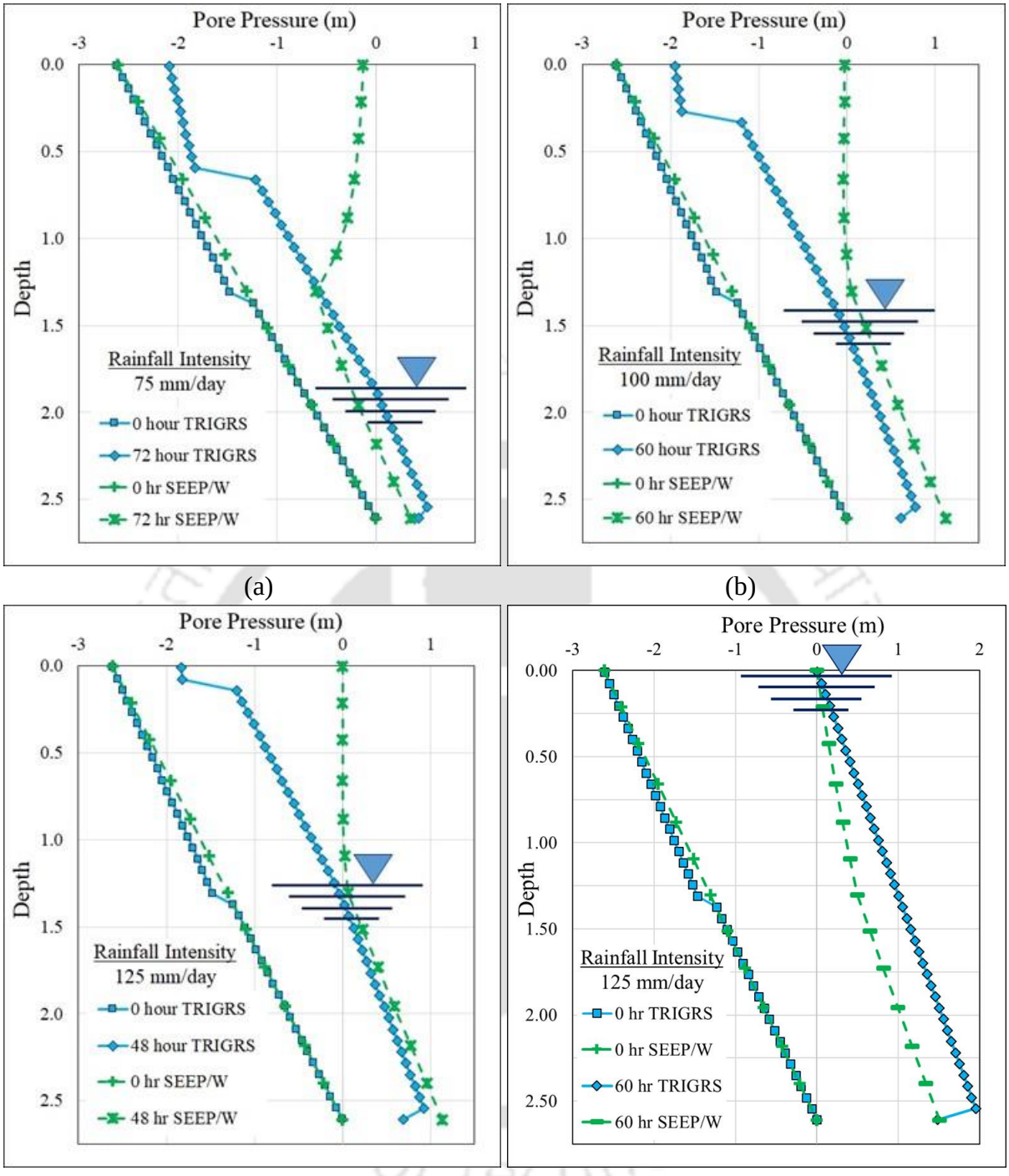

Figure 6.8 Pore pressure profiles and Ground Water Table for different rainfall intensities: (a) 75 mm/day for 72 hours duration; (b) 100 mm/day for 60 hours duration; (c) 125 mm/day for 48 hours duration; and (d) 125 mm/day for 60 hours duration

6.6.1. Sub–Surface Flow Parameters

Table 6.1 gives the hydraulic parameters used in the TRIGRS analysis. Previous studies report the soil diffusivity (D_o) values ranging approximately 5–500 times that of the hydraulic conductivity (Iverson, 2000; Liu and Wu 2008; Baum *et al.*, 2010; Kim *et al.*,

2010; Viet *et al*., 2018). The general trend being with increase in saturated permeability (k_{sat}) the ratio of D_o to k_{sat} also increases. For this study, the soil diffusivity (D_o) is assumed to be 10 times the saturated permeability (k_{sat}) (Baum *et al*., 2010). Figure 6.9 shows the soil water characteristics curve applied in the analysis and the corresponding unsaturated hydraulic conductivity curve. As can be observed from the figure the unsaturated hydraulic conductivity is highly sensitive to the soil moisture and can vary by an order for change in volumetric water content of only 0.1. The soil water characteristic has a significant effect on the hydraulic conductivity and soil shear strength.

Table 6.1 Hydraulic parameters used in TRIGRS analysis

k_s (m/s)	D_o (m/s)	θ_s	θ_r	α
2.5×10^{-6}	2.5×10^{-5}	0.45	0.05	0.8

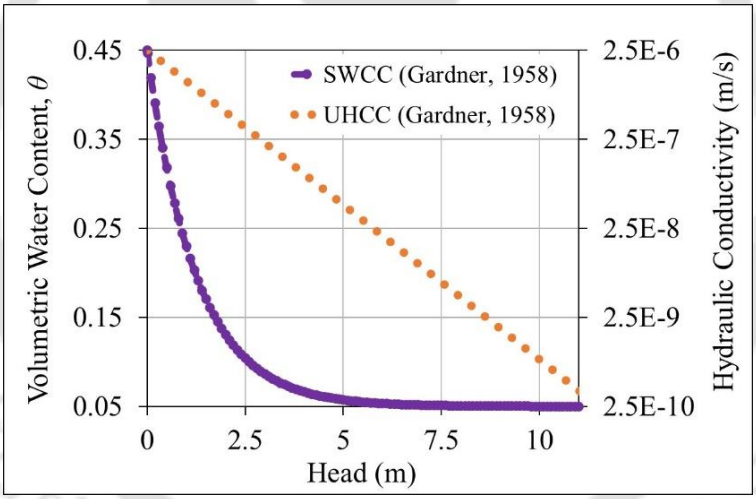

Figure 6.9 Soil water Characteristics Curve (SWCC) and corresponding Unsaturated Hydraulic Conductivity Curve (UHCC) as used in the TRIGRS analysis

6.6.2. Shear Strength Parameters

Table 6.2 shows the Mohr-Coulomb shear strength parameters and the unit weight used as input for the TRIGRS analysis. The shear strength parameters were so adjusted such that the corresponding location of slope instability, along with its time of occurrence, due to the rise in water table, matched with that of in-situ conditions. The values of the parameters, consistent with that of experimentally observed values, were only considered for the analysis.

Figure 6.10 shows the factor of safety (FoS) profile with depth, output from TRIGRS corresponding to the pore pressure changes as shown in Figure 6.8 (c) and (d).

Table 6.2 Soil shear strength parameters used in TRIGRS analysis

c' (kPa)	φ' (°)	γ_s (kN/m^3)
10	27°	18.5

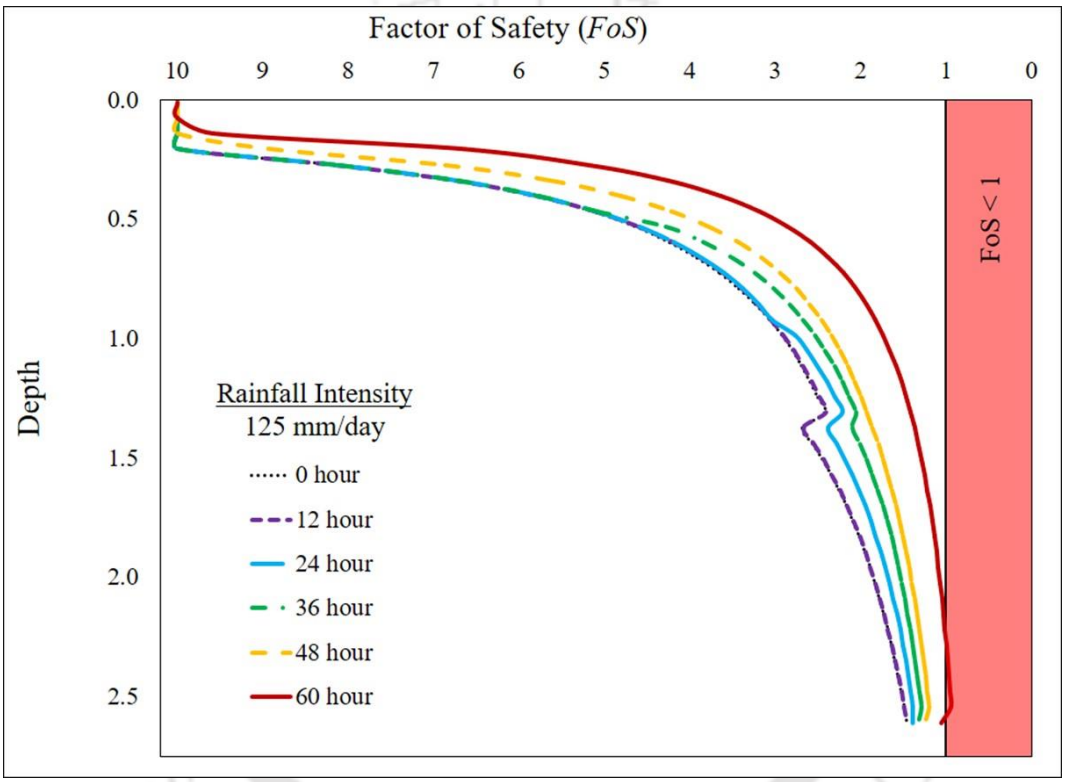

Figure 6.10 Factor of safety profile for rainfall intensity of 125 mm/day

6.7. EVALUATION AND VALIDATION OF TRIGRS OUTPUT

The most important output of a TRIGRS simulation is the FoS–map. FoS–map is representation of areal distribution the factor of safety across the cells of the entire gridded study area. Figure 6.11 shows the FoS-map for the initial condition, or the beginning of the simulation representative of the dry season. As can be observed from Figure 6.11, TRIGRS predicts a very stable initial condition. Most of the hillslopes were predicted to have a FoS of 1.5 and higher, with only few very steep slopes having FoS in the range of 1.3 to 1.5. This

prediction relates well to the observed in-situ condition during the dry season, when the suction within the unsaturated soil renders very high shear strength to the hillslopes.

Figure 6.12 show the stability condition of hill slopes of the study area in the form of the FoS–map after the application of a landslide triggering rainfall event, in this case the rainfall of 28th May – 8th June 1998 as shown in Figure 6.16. At the end of the rainfall event, the stability condition changes drastically. The FoS drops to < 1.0, at the location of landslide prone areas of the hilly region. Across large areas, the FoS drops to marginally stable condition of 1.0 to 1.25.

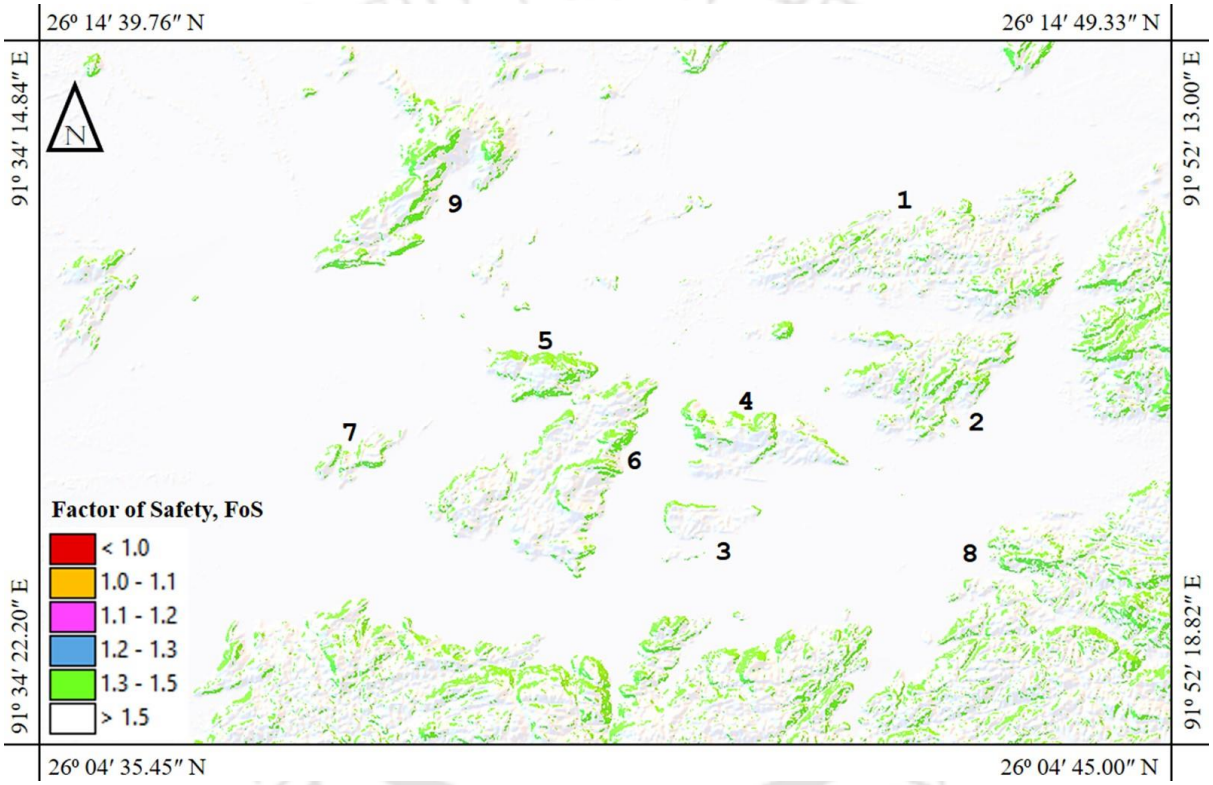

Figure 6.11 Factor of safety (FoS) map – initial condition (TRIGRS output)

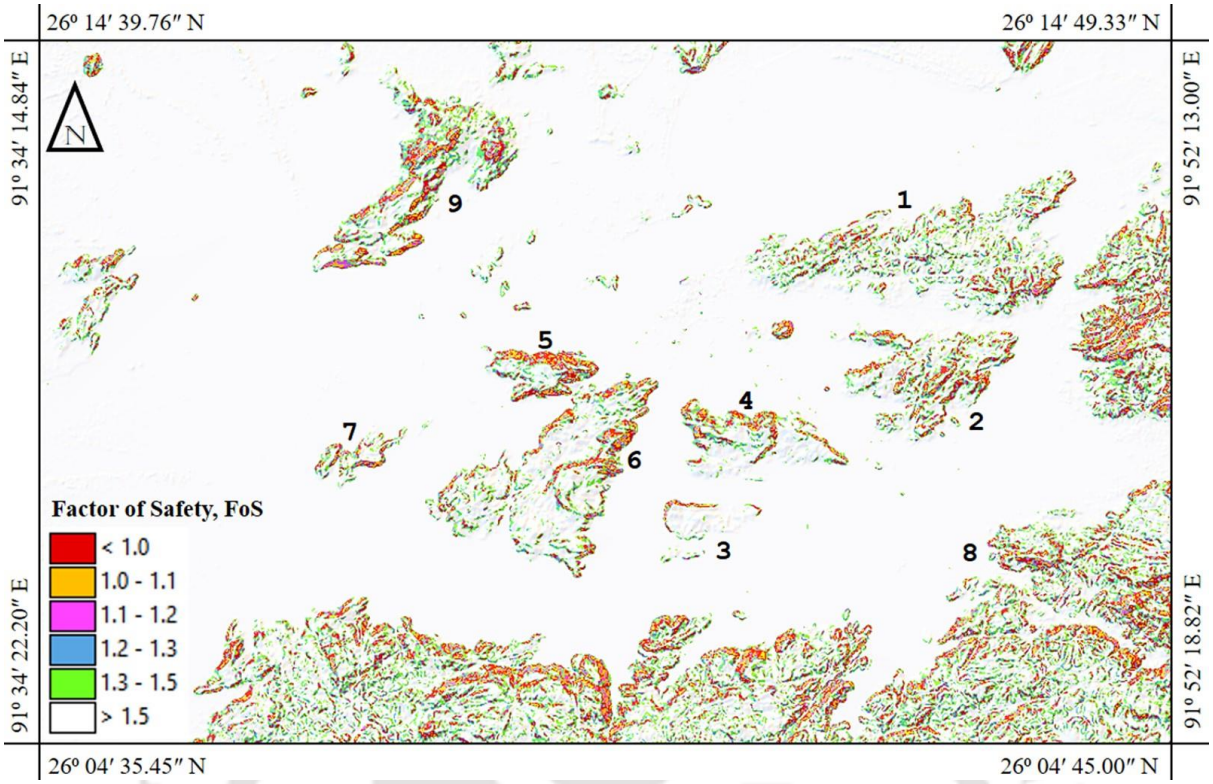

Figure 6.12 FoS–map for 8th June 1998 after the application of a landslide triggering rainfall event (28th May – 8th June, 1998)

The effectiveness of landslide predicting models, such as TRIGRS, is mostly evaluated based on a statistical classifier such as Receiver Operating Characteristics (ROC) using confusion matrix (Godt *et al*., 2008; Montrasio *et al*., 2012; Raia *et al*., 2014), Success Index and Error Index (Sorbino *et al*., 2010) or Scar Concentration and Landslide Potential (Vieira *et al*., 2010). The underlying concept of such classifier models is primarily involved in comparing the locations of observed landslides with the predicted results. In the present study, the GPS (Latitude/Longitude) coordinates of the RVS locations were used in the ROC model to establish a comparison of the TRIGRS output to in-situ condition. Figure 6.13 shows the RVS-points marked with black triangles and overlaid on the FoS–map. Figure 6.14 shows the enlarged view of the Noonmati-Sunsali hill (1) from the FoS – map (Figure 6.13). Similarly, Figure 6.15 shows the enlarged view of the Narakashur hill (4). The states or classes considered are; stable (i.e., FoS ≥ 1.0) or unstable (i.e., FoS < 1.0). If the grid cell is simulated by TRIGRS to be unstable and is coincident with a mapped landslide in the inventory it is counted as a true positive; if it falls outside a mapped landslide, it is counted as a false positive. If the grid cell is modelled to be stable and it falls outside a mapped slide, it is counted as a true negative; if it falls within a mapped slide, it is counted as a false negative.

The comparison counts can be entered in a 2×2 contingency table that is the confusion matrix (Table 6.3).

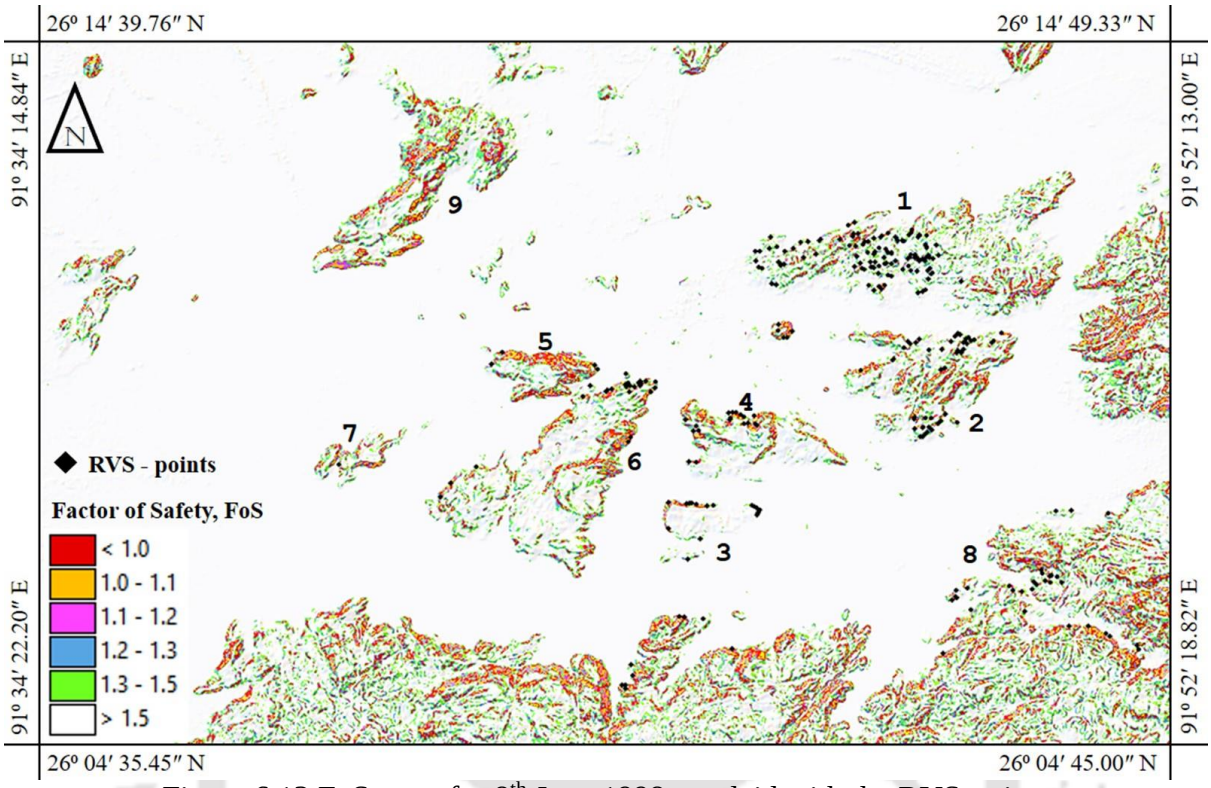

Figure 6.13 FoS–map for 8th June 1998 overlaid with the RVS-points

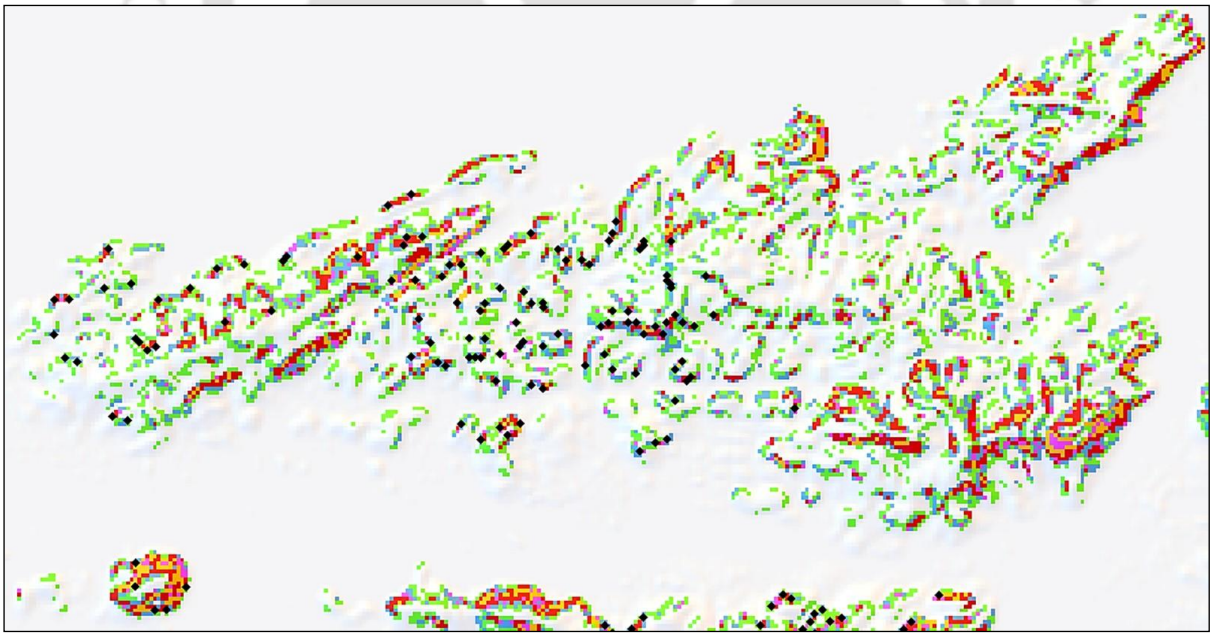

Figure 6.14 FoS–map of the Noonmati-Sunsali hill (1) overlaid with the RVS-points

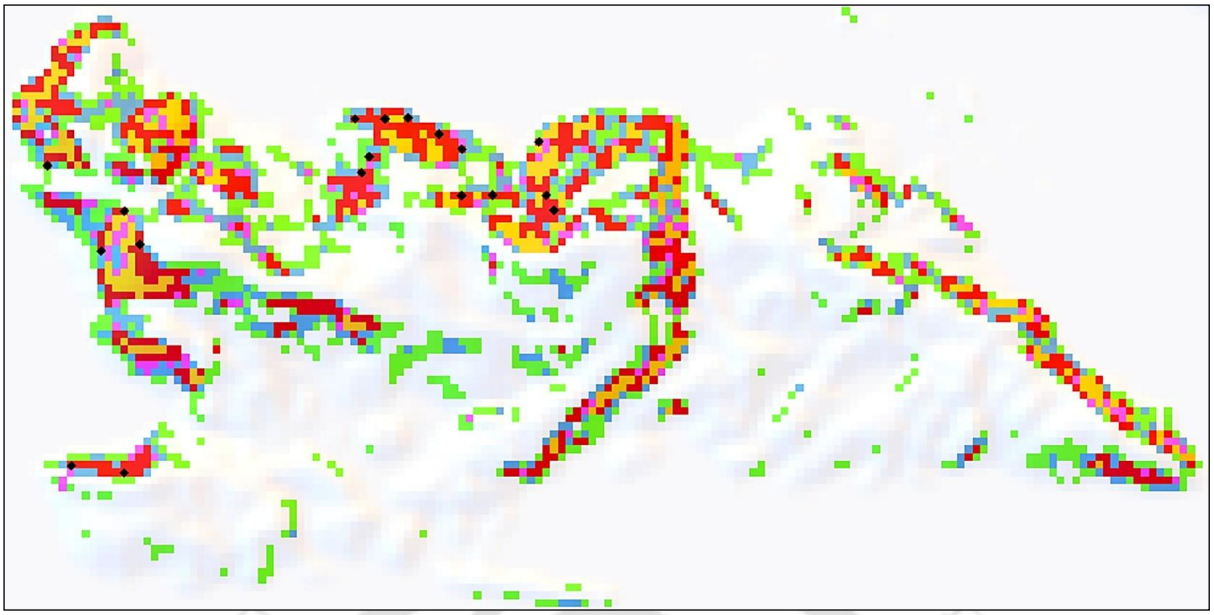

Figure 6.15 FoS–map of the Narakashur hill (4) overlaid with the RVS-points

Complex rainfall events of varying duration and intensity can be input into TRIGRS. The output of TRIGRS includes the FoS map, which can be obtained at the desired time steps corresponding to input rainfall event. For the present study, the daily rainfall data is input into TRIGRS in time steps of 24 hours. The FoS maps corresponding to each day are thus obtained. For example considering the rainfall event of June 1998 (28-5-1998 to 8-6-1998) the daily rainfall is input into TRIGRS as shown in Figure 6.16. The figure gives a time-series plot of FoS during the rainfall event. The plot shows the daily rainfall as clustered columns with the magnitude of rainfall intensity on the secondary vertical axis (on the right). Thus from the analysis 12 FoS maps corresponding to each consecutive day of the rainfall event is obtained. Figure 6.12 shows the FoS map obtained from TRIGRS corresponding to the scenario of 8th June 1998, taking into consideration the cumulative effect of the entire rainfall event. Figure 6.13 shows the RVS-points overlaid on the FoS map. Similarly the FoS maps of the previous days of the rainfall event are also obtained. The FoS for each time step (i.e., each day) at the RVS-points are extracted out and the average, maximum, minimum and the standard deviation are plotted (Viet *et al*., 2016). Figure 6.16 shows the daily rainfall along with the average of FoS across the RVS-points for each day throughout the rainfall event of June, 1998. The average of the FoS at all 347 RVS-points is shown as marker for each time step (daily), along with the standard deviation of the dataset as error bars. The area plot in the background gives the range of maximum and minimum range of FoS values of the set, for each time step. Before the rains began on 28th of May, the FoS values were significantly high for the entire study area indicating stable slopes throughout. Gradually the

FoS values decreased with rainfall infiltration leading to increase in pore water pressure. As can be observed from Figure 6.16, TRIGRS predicts rainfall occurrences on 8th June 1998. The FoS reached the minimum value on the 8th of June. The maximum-minimum area plot converges to a FoS value lesser than 1.0 on 8th June, indicating that the FoS < 1.0 at all of the RVS points. The gradual deterioration of the slope stability over a period of an entire month can also be clearly observed from Figure 6.16. The landslides occurred after a total cumulative rainfall of 681 mm over a duration of 12 days.

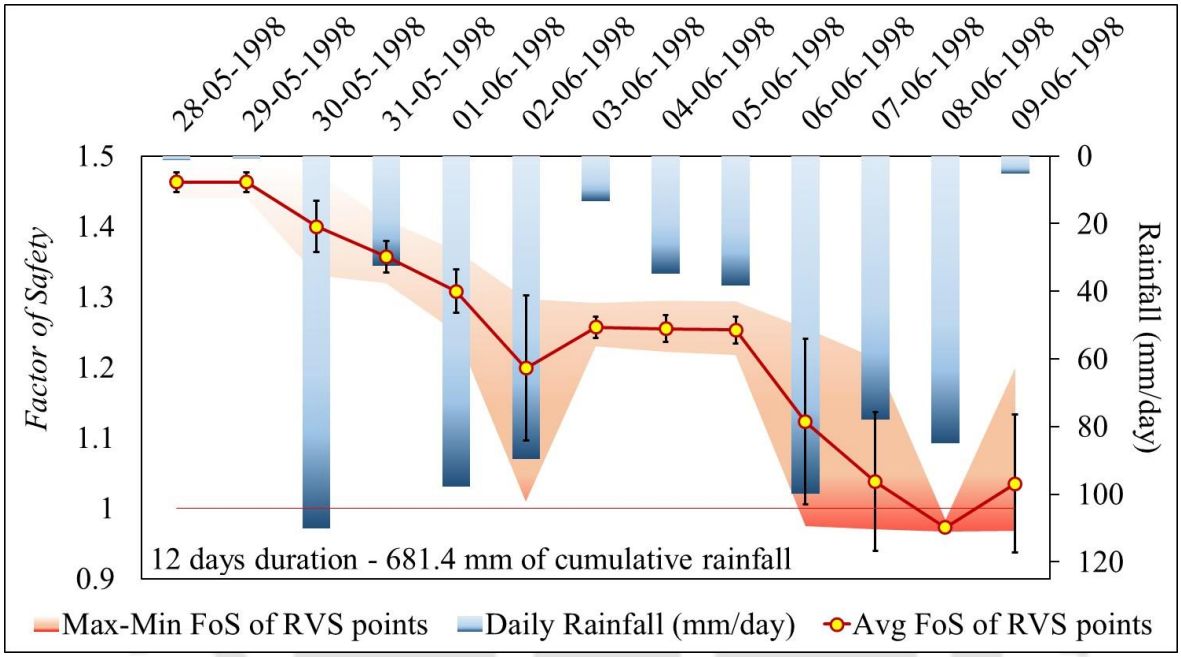

Figure 6.16 Statistics of FoS at the RVS-points as response to rainfall event of 25th May – 8th June, 1998, with TRIGRS predicting landslide occurrence on the 8th of June

Once the RVS-points are overlaid on the FoS-map, the ROC of the TRIGRS FoS–maps are calculated in terms of the True Positive (TPR) and False Positive Rates (FPR), as shown in Table 6.3. The classes considered are; stable (i.e., FoS ≥ 1.0) and unstable (i.e., FoS < 1.0), compared with, whether RVS-points are located; (Yes and No). If a particular grid cell is modelled by the TRIGRS simulation to be unstable and a mapped landslide is coincident with that geographical location it is counted into the true positive (*a* of Table 6.3); if it does not coincide with a mapped landslide, it is counted into the false positive (*c* of Table 6.3). If the grid cell is modelled to be stable and there is no landslide mapped within that location, it is counted as a true negative (*d* of Table 6.3); and if TRIGRS simulated a grid cell to be stable, but in in-situ condition there was a landslide occurrence, it is counted into the false negative (*b* of Table 6.3). The comparison counts are then entered into the 2×2 contingency table (Table 6.3) which is the confusion matrix.

The assessment of landslide occurrences would be considered ideal when when the ROC of the output FoS-map is located in top-leftmost corner of the ROC plot (Figure 6.17), indicating a 100% TPR and 0% FPR, i.e., TRIGRS predicts FoS < 1.0 exactly at the RVS-points while at all other cells it predicts FoS ≥ 1.0. However, such a scenario would never be achieved from a practical perspective. The output of TRIGRS can be considered satisfactory as long as the ROC plots on the upper left region as shown Figure 6.17.

Table 6.3 Receiver Operating Characteristics (ROC) for the TRIGRS simulation results

		RVS – points located	
		Yes	**No**
TRIGRS prediction *FoS* < 1.0	**Yes**	**(*a*)** No. of cells where RVS – points are located and TRIGRS predicts *FoS* < 1.0	**(*c*)** No. of cells where TRIGRS predicts *FoS* < 1.0 excluding **(*a*)**
	No	**(*b*)** No. of cells where RVS – points are located but TRIGRS predicts *FoS* ≥ 1.0	**(*d*)** No. of cells where TRIGRS predicts *FoS* ≥ 1.0 excluding **(*b*)**
		True Positive Rate (TPR) $= \frac{(a)}{(a)+(b)}$	False Positive Rate (FPR) $= \frac{(c)}{(c)+(d)}$

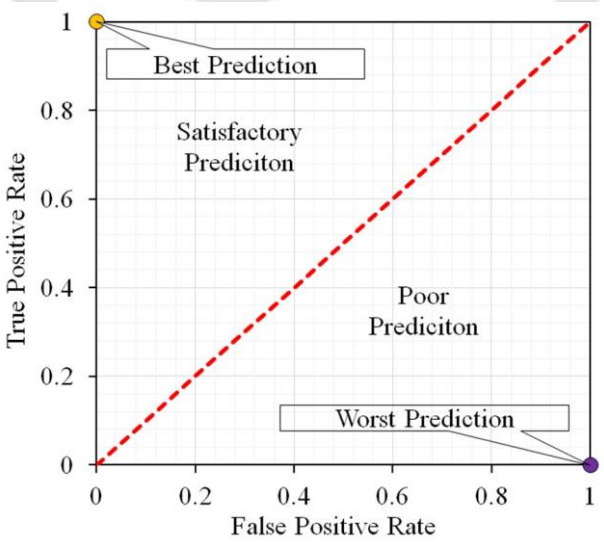

Figure 6.17 A typical ROC plot used for validation of TRIGRS output FoS-map comparing with the RVS-points location

6.8. LIMITATIONS

All numerical and analytical models of ground water flow and slope stability are subject to limitations imposed by simplifying assumptions, approximations, and other shortcomings in the underlying theories. The TRIGRS program therefore also has limitations. TRIGRS assumes flow in homogeneous, isotropic soil; thus, as has been highlighted in this chapter the parameters are calibrated to match the rise in the ground water table.

Along with the limitations in TRIGRS, there are limitation in defining the soil parameters as well. The soil parameters are considered constant throughout the study area, which a simplified assumption. The values of the input parameters considered for the analysis contain uncertainties. With increasing number of soil samples and laboratory tests, the representation of parameter variability over the study area can be increased; however, the description can never be made exact. This is because only a very insignificant portion of the total volume of soil can be sampled in reality, and the subsurface conditions that dictate pore water pressure evolution and material strength can never be conclusively inferred.

6.9. SUMMARY

The chapter gave a brief description of the TRIGRS model. The procedure of application of TRIGRS to study area was elaborated. The various input parameters were described. The methodology for calibrating the input parameters for efficient modelling of rainfall-induced landslide within the study area was shown. Finally, the methodology based on Receiver Operating Characteristics for validation of the TRIGRS output FoS-map with in-situ data, i.e., the RVS-points is presented.

Chapter 7. LANDSLIDE ANALYSIS OF GUWAHATI CITY USING TRIGRS

7.1. INTRODUCTION

This chapter reports the application of TRIGRS (Transient Rainfall Infiltration and Grid based Regional Slope-stability), to investigate the rainfall-induced landslide hazard scenario for Guwahati city, India.

The gradual changes of hill slope leading to triggering of rainfall-induced landslide is analyzed as response to actual rainfall events known to have triggered landslides within the study in the past. The effect of antecedent condition and triggering rainfall is elucidated in detail through the analysis results. The intricate equilibrium of the various factors namely; rainfall intensity and duration, soil water characteristics, the unsaturated hydraulic conductivity as a function of the saturated hydraulic conductivity and soil suction (soil moisture) and of course the shearing resistance or shear strength of the soil, in triggering of landslide is brought forth.

The accuracy of the TRIGRS simulation outcomes are largely dependent on the Digital Elevation Model (DEM), which is the primary input of any such GIS-based approaches. The DEM represents the topography of the area and used to derive all other topographic input parameters, which are subsequently used in the prediction simulations. There are several DEM available for the study area, vis., CartoDEM, ALOS-AW3D30-DEM, SRTM-DEM, and ASTER-GDEM. The influences of various types of DEMs for accurate prediction of the rainfall-induced landslides in the hillslopes of the municipal precinct of Guwahati city are study. Based on various rainfall events considered for the study area, ALOS-3D DEM provided the best agreements with the actual reported landslides in the area for the corresponding events.

ALOS World 3D-30m (AW3D30) is adopted as the digital elevation model (DEM) for the present study. The rainfall Intensity-Duration-Frequency (IDF) relationships are evaluated for the region based on the regional rainfall data. The IDF relations are used to select the rainfall intensity corresponding to the particular return period and rainfall duration, and the selected events are considered as input into TRIGRS simulation to generate the Factor of Safety (FoS) maps for the region. The FoS maps corresponding to various such rainfall events are further combined to form the landslide hazard map of the study area. The

Receiver Operating Characteristic (ROC) of the FoS maps is subsequently evaluated by overlaying the point-based RVS (Rapid visual screening) landslide locations and the efficacy of the simulation results is assessed. The agreeable match of the analyses outcome with those of actually detected landslide locations showed that TRIGRS is efficiently applied to assess the landslide susceptibility and hazard of the selected region. The response in terms of the stability of a hill slope region subjected to different rainfall pattern is analyzed. From the analysis results, it was observed that the rainfall pattern could significantly affect the widespread landsliding especially for moderate to low permeable soil.

7.2. RAINFALL EVENTS

To find a relation of rainfall events and landslide as a first step the rainfall statistics is compared with the reports of landslide occurrences. It can be observed from Figure 3.8 that the landslide occurrences is not always related to the wettest years in terms of the yearly cumulative rainfall. For example, in the year 2003 and 2014, the cumulative rainfall was lower than average and yet there were many landslide incidences reported. Whereas in the year 2010 the cumulative rainfall was on the higher side, but still no landslides incidences were reported. To have a better understanding of the effect of rainfall on landslides occurrences the rainfall statistics are extracted and presented in Table 7.6Table 7.1.

Table 7.1 gives the maximum daily rainfall (70 – 223 mm), maximum cumulative rainfall that occurred within a duration of 48 hours (101 – 347 mm) and 72 hours (124 – 363 mm), number of days with rainfall, and the cumulative rainfall (1973 – 3647 mm) for various years. As can be observed from Table 7.1, the different values vary significantly for different years. Rainfall events in some years are characterized by low intensity long duration rainfall while in some years they are of shorter durations but with higher intensity. As can be observed from Table 7.1 in the year 2010 majority of rainfall was with rate lower than 80 mm/day with only one day in the whole year when the intensity exceeded 100 mm/day, but still there was a cumulative rainfall of 3356 mm. On the contrary, in 2014, the yearly cumulative rainfall was only 2513 mm, and out of which 347 mm fell within just 48 hours. In addition, there are years where there have been incessant rainfall in the monsoon season such as in the year 2004, 2007 and 2012. Table 7.1 also presents the number of days where the rainfall intensity was in between a particular range and tries to draw a correlation of the above-mentioned parameters to the occurrence of landslides. It can be observed that the cumulative rainfall exceeding 202 mm in 48-hour durations is the parameter directly

correlated to the landslide occurrences. There were no other parameters which could be directly correlated to landslide occurrence.

Table 7.1 Rainfall statistics from 1998 to 2015

Year	No of days with Rainfall	Cumulative Rainfall (mm)	No of days for Daily Rainfall (10mm - 25 mm)	No of days for Daily Rainfall (25mm-50mm)	No of days for Daily Rainfall (50mm - 80mm)	No of days for Daily Rainfall (80mm - 100mm)	No of days for Daily Rainfall > 100mm	Max Daily Rainfall (mm)	Max Cumulative Rainfall within 48 hours (mm)	Max Cumulative Rainfall within 72 hours (mm)	Landslides Reported
1998	170	3185	39	20	6	8	**4**	148	**238**	263	**y**
1999	179	2978	47	32	11	0	1	106	144	190	
2000	171	3058	26	26	9	2	5	144	157	169	
2001	178	2404	43	25	8	0	0	70	101	138	
2002	178	2878	44	26	7	2	2	104	158	180	
2003	179	2881	51	15	7	3	**4**	147	**237**	313	**y**
2004	167	3647	38	27	9	7	**4**	223	**316**	363	**y**
2005	180	2977	42	22	15	2	1	106	153	186	
2006	159	1973	41	16	6	0	1	108	109	124	
2007	169	3466	38	24	8	4	**6**	185	**202**	254	**y**
2008	182	2731	47	34	6	1	0	91	122	152	
2009	148	2265	29	14	10	2	2	119	136	141	
2010	171	3356	46	29	11	5	1	105	181	226	
2011	156	2229	51	19	6	1	1	101	185	202	
2012	152	2877	34	28	10	1	**2**	131	**209**	212	**y**
2013	151	2457	38	25	9	0	1	104	150	185	
2014	146	2513	33	29	3	3	**2**	190	**347**	362	**y**
2015	143	2547	37	22	8	1	3	111	173	234	
Maximum	182	3647	51	34	15	8	6	223	347	363	
Average	166	2801	40	24	8	2	2	127	184	216	
Minimum	143	1973	26	14	3	0	0	70	101	124	

7.3. TRIGRS – SIMULATIONS

Based on the observation made from Table 7.1, it can be noted that only certain rainfall events trigger landslides. Therefore, to understand the influence of the rainfall patterns on the triggering of landslide and to apprehend the hydro-geotechnical mechanism that leads to the occurrence of the slope failure, different rainfall patterns (Table 7.2) are identified and chosen for input into the TRIGRS simulations.

Table 7.2 Rainfall events selected for TRIGRS analysis

Case	Period of rainfall	Duration (No. of Days)	Cumulative Rainfall (mm)	Average Rainfall Intensity (mm/day)
I	28th May to 9th June 1998	13	371.4	92.75
II	3rd to 8th October 2004	6	417.2	83.44
III(a)	20th to 26th June 2012	7	284.8	47.47
III(b)	1st to 26th June 2012	26	818.4	47.47
IV	20th to 25th September 2014	6	681.4	56.78
V	24th March to 4th May 2010	42	887.3	21.12

The rainfall events of 1998 (28-05-1998 to 09-06-1998) (Figure 6.16), 2004 (03-10-2004 to 08-10-2004) (Figure 7.1) 2012 (20-6-2012 to 26-6-2012) (Figure 7.2) and 2014 (20-9-2014 to 25-9-2014) (Figure 7.3) were input into the TRIGRS and the analysis was run. The FoS-map corresponding to each day was obtained. The RVS-points are then overlaid on the FoS-maps and the FoS values at the RVS-points are extracted. The average, maximum and minimum of the FoS values at RVS-points are then plotted along with rainfall event. The procedure is described in detail in Section 6.7.

In Figure 7.1, it can be seen the FoS remains almost constant until 5th October 2004 and starts to drop on the 6th and further drops on the 7th to the state of slope failure in some locations of the RVS points as marked by the red colored zone in the plot. Similarly, in the Figure 7.3, it can be seen the FoS remains constant until the 22nd of September, 2014 and starts to drop on the 23rd and further drops on the 24th to state of slope failure covering all locations of the RVS points unleashing landslides across many locations of the Guwahati

hillslopes. The red color area plot constricts at a point establishing that at all locations of RVS points it is FoS < 0.99. The other point of importance is the difference in response to landslide triggering for the rainfall events. On October 7, 2004, the rainfall amounted to 223 mm compared to 157 mm on September 24, 2014. The difference was made by the rainfall on the previous day. Rainfall of only 93 mm on 6 October 2004 could not provide enough infiltration as compared to 190 mm rainfall on 23 September 2014. This difference lead to widespread landsliding across the study area on 24 September 2014 as compared to the landsliding on 7th of October 2004. However, it was observed that the TRIGRS predicted no landslide as a response to rainfall event of 2012 (20-6-2012 to 26-6-2012) (Figure 7.2). However, contrary to TRIGRS prediction there were landslide occurrences reported on 26 June 2012.

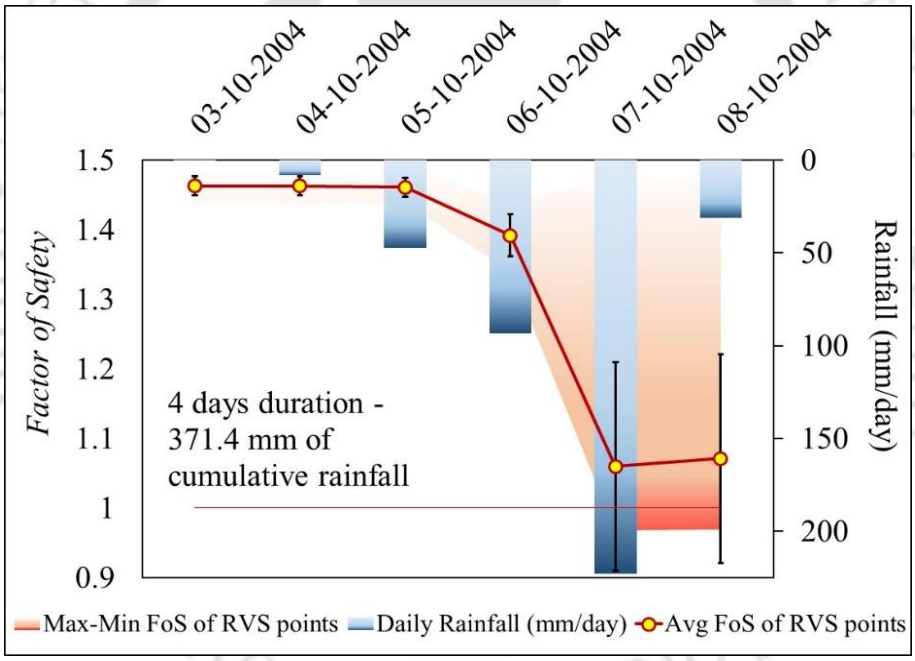

Figure 7.1 Rainfall event of October 2004, (3-10-2004 to 8-10-2004) and FoS distribution across the RVS-points

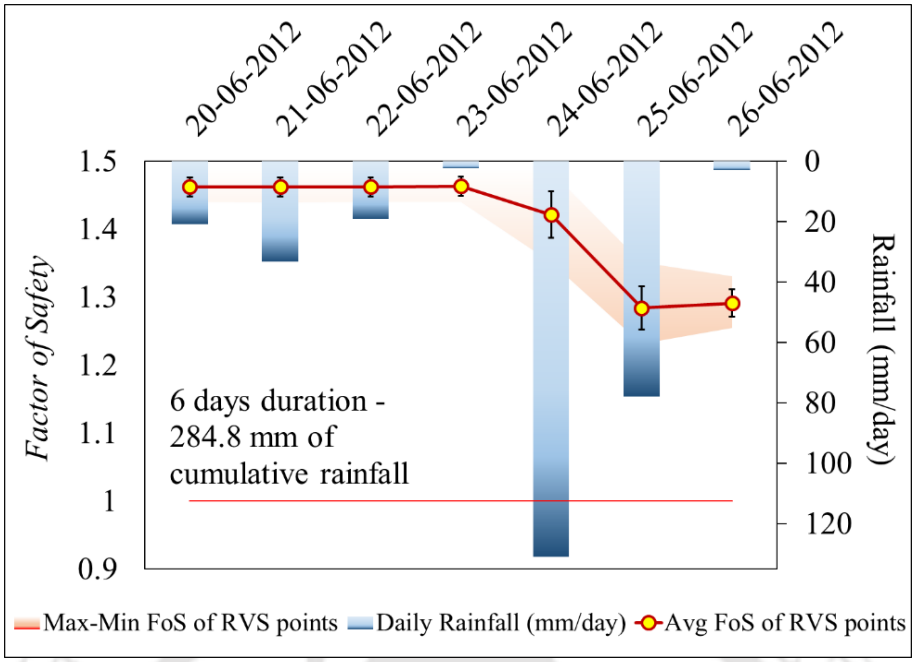

Figure 7.2 Rainfall event of June 2012, (20-06-2018 to 26-06-2018) and FoS distribution across the RVS-points

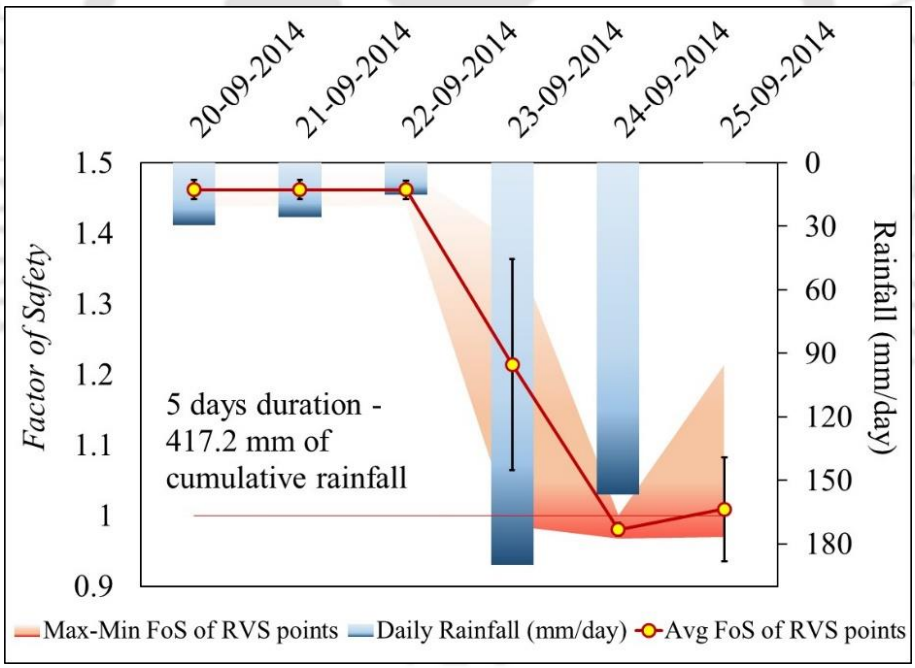

Figure 7.3 Rainfall event of September 2014, (20-09-2014 to 25-09-2014) and FoS distribution across the RVS-points

7.3.1. Effect of Antecedent Conditions

For understanding the effect of antecedent condition on the landslide occurrence on the 26th June 2012, the analysis was then rerun for considering the rainfall of the entire month of June 2012 (01-06-2012 to 26-06-2012). Figure 7.4 shows the rainfall for the month of June 2012 and the degradation of the FoS over the entire month. As can be seen from Figure 7.4

TRIGRS analysis now predicts rainfall occurrences on 25 June 2012. In field conditions, the landslides occurred at the night of 25th June, and were subsequently reported in the morning of 26th June 2012. Thus, TRIGRS was able to predict accurately the timing of the occurrence. The gradual deterioration of the slope stability over a period of an entire month can also be clearly observed from Figure 7.4. The process to landslide started from the 3rd day of June, the next fall in FoS happened on the 14th, the highest intensity of rainfall occurred on 24th, but as is observed the landslide occurred at night of the next day, 25th of June or in the early morning hours of 26th June. Thus, the high the intensity rainfall on 24th June is not the only triggering factor. It is the intricate combination of the antecedent rainfall over entire month and the triggering rainfall of 24th and 25th June 2012. The simulation showed that TRIGRS suitably simulated the time of landslide triggering.

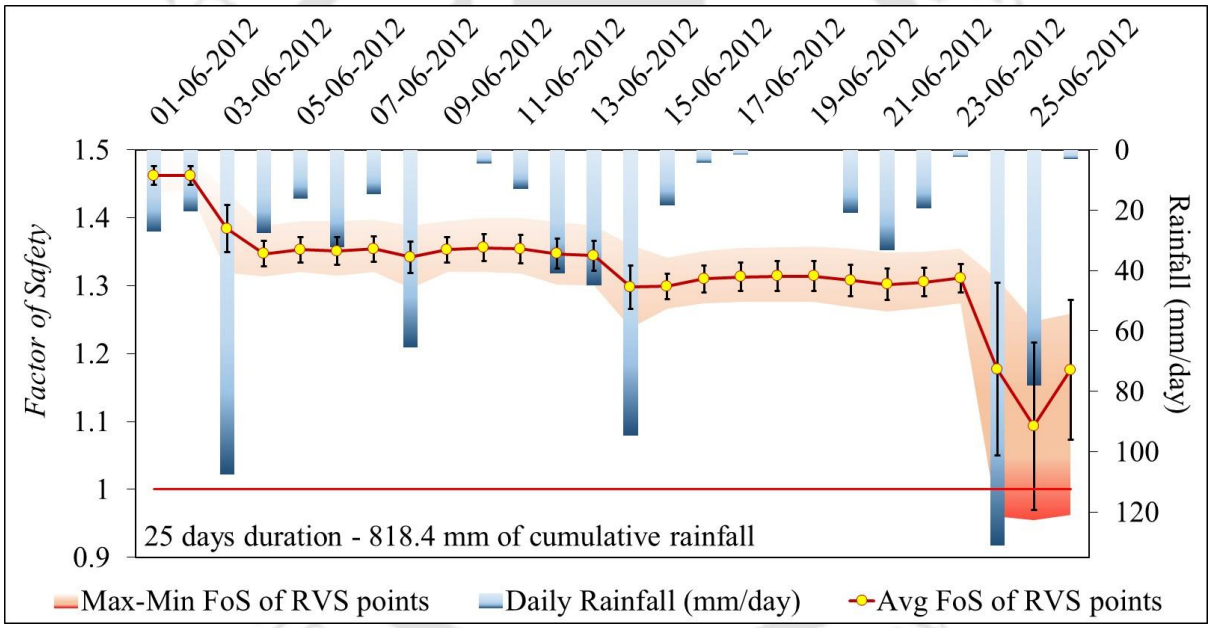

Figure 7.4 Rainfall event of June 2012, (01-06-2018 to 26-06-2018) and FoS distribution across the RVS-points

Several landslides occurrences were reported in the morning of 26th of June 2012 at various locations in the Guwahati city. In all the cases, the landslides have been reported to occur along the interface of the soil and the underlying rock, accompanied by profuse interfacial seepage (Goswami, 2013). In each of the landslide incidences, there has been loss of life and damage to properties. Figure 7.5 exhibits the location of some landslides overlaid on the FoS map obtained from TRIGRS corresponding to the scenario of 25th June 2012. It can be observed that TRIGRS was able to predict location of landslides with that of the observed landsliding.

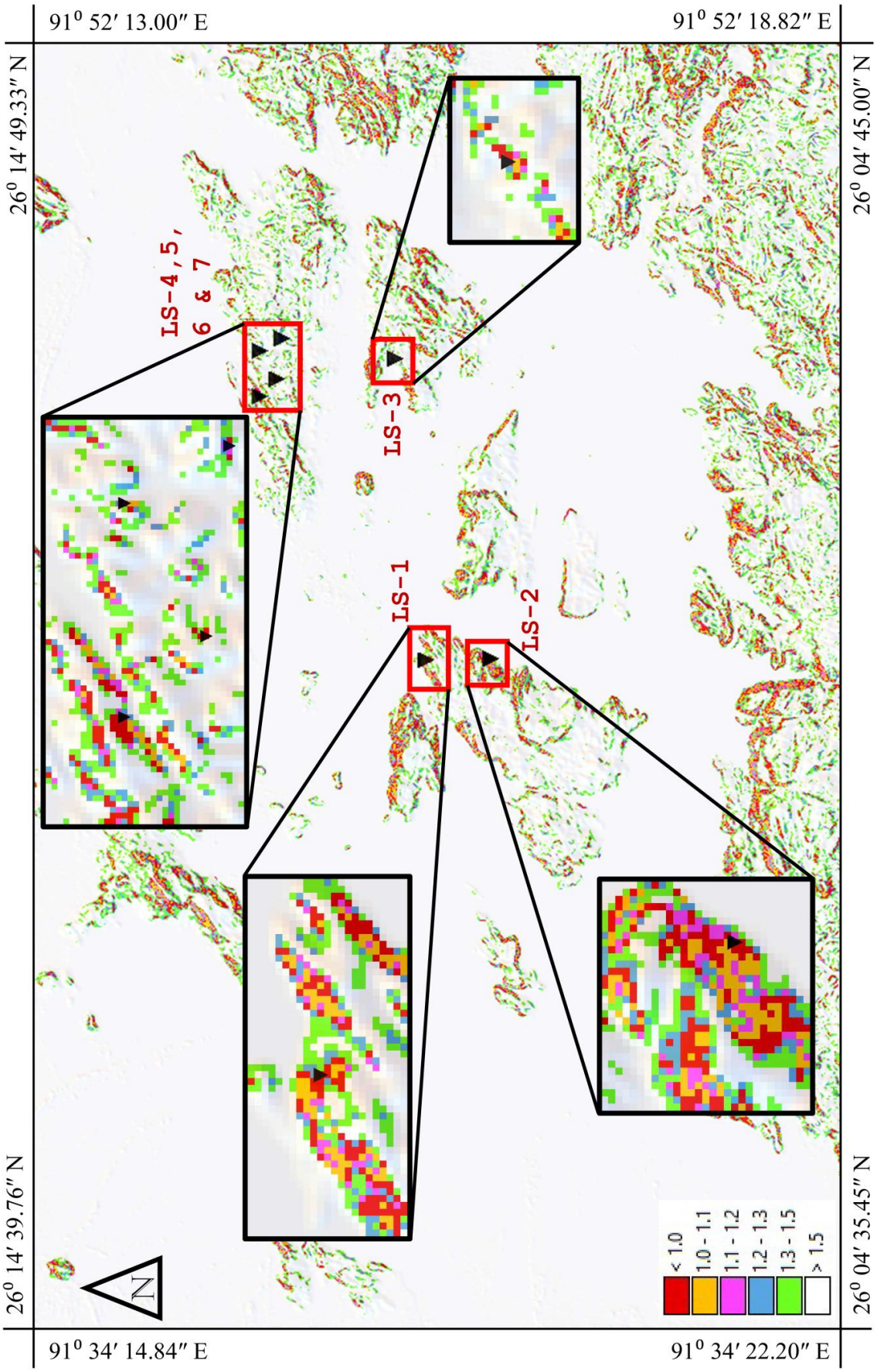

Figure 7.5 Location of some observed landslides overlaid on the FoS map obtained from TRIGRS corresponding to that of 25th June 2012

As can be observed from Table 7.2 in the year 2010, the cumulative rainfall was greater than that of 2012. Daily rainfall data for the years 2010 and 2012 have been presented in Figure 7.6. The figure also shows the daily variations of the cumulative rainfall for both the years. The landslide triggering rainfall event in the month of June 2012 is demarcated in the figure. It is also to be noted that though the cumulative rainfall for the year 2010 was more landslides were not reported. So to compare the TRIGRS analysis the rainfall event of highest cumulative rainfall within a period of approximately a month is chosen from 2010. It was observed that the highest rainfall occurred in the month of April 2010. The rainfall was then input into TRIGRS, and the simulation was run.

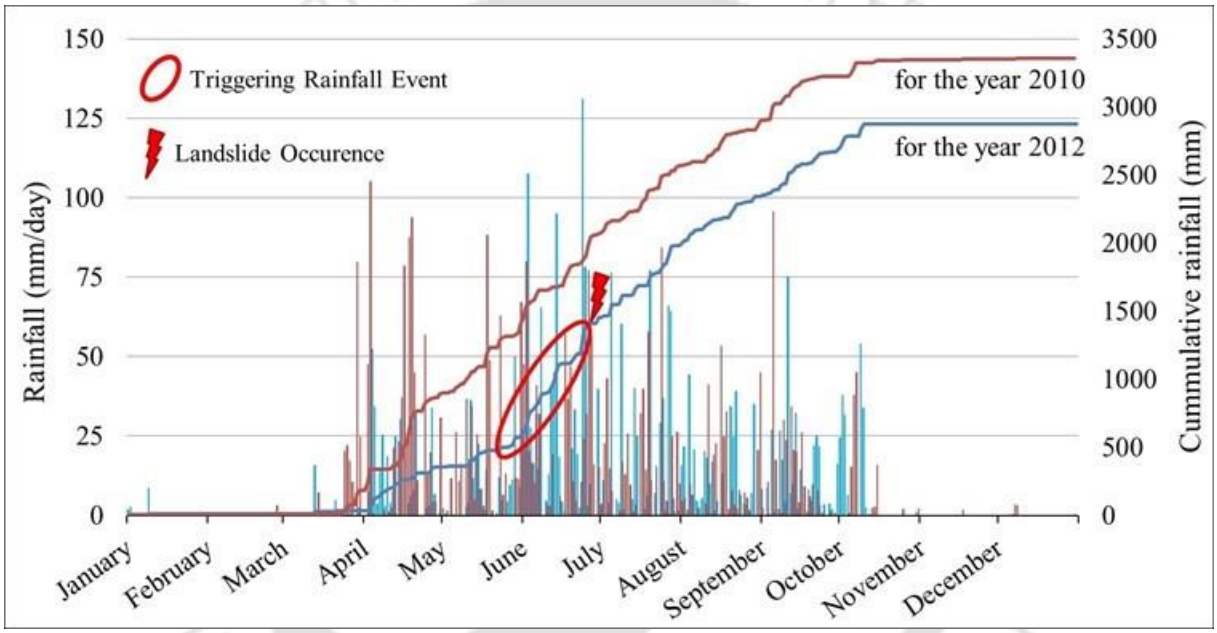

Figure 7.6 Rainfall of 2010 and 2012

Figure 7.7 shows the analysis results for FoS in response to rainfall of March-April 2010. Similar to the occurrence of June 2012, the FoS starts degrading from 30 March; slowly it degrades over the month to the lowest value on 20 April. However, contrary to occurrence of 2012, in 2010 the rainfall intensity on the 19th, 20th and 21st were not sufficient to trigger the landslide. The comparison highlights the intricate equilibrium of the antecedent rainfall or soil moisture condition, the intensity and duration of the triggering rainfall and the soil hydraulic properties. The slightest difference between the rainfall conditions prevailing in June 2012 and the rainfall event of March-April 2010 resulted in landslide occurrence, and is shown in Figure 7.4, Figure 7.6 and Figure 7.7.

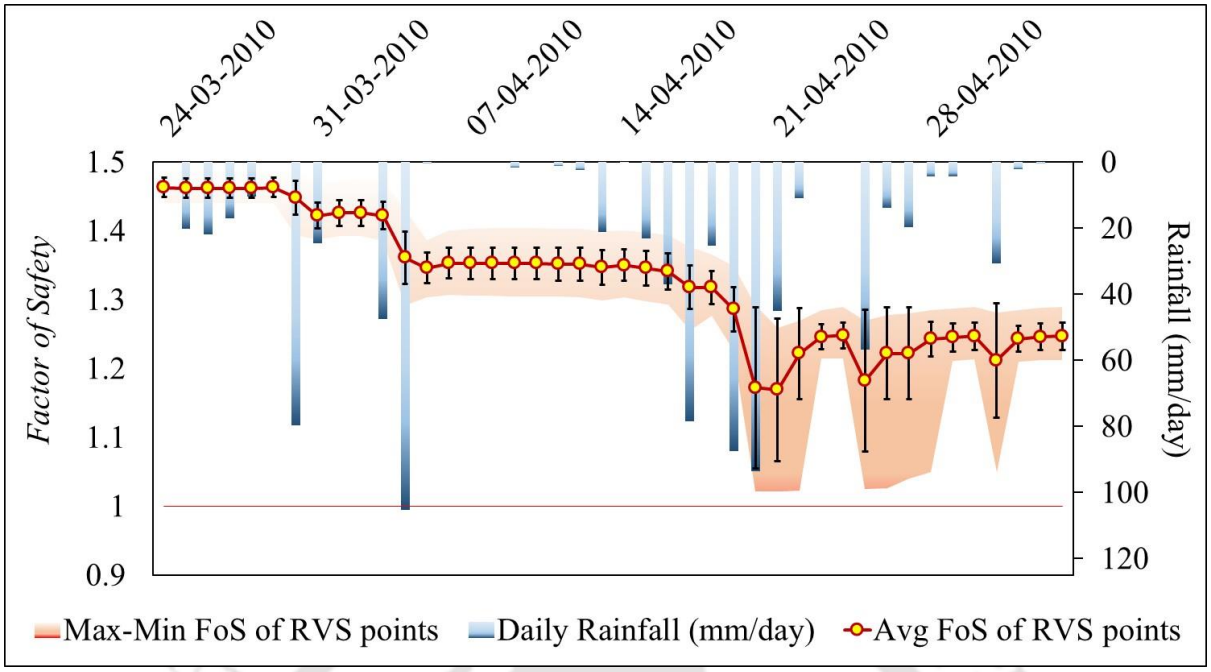

Figure 7.7 Rainfall event of March-April 2010 and FoS distribution across the RVS-points

Similarly, the rainfall event of June 1998 (28-05-1998 to 09-06-1998) was considered and TRIGRS analysis was run. Figure 6.16 gives the analysis results. It can be observed that the highest intensity rainfall was on 30 May 1998 and yet the FoS drops by a marginal amount. As can be observed in Figure 6.16 the rainfall intensity drops to 32 mm/day on 31 May, but still the FoS is deteriorating and then again, on 3rd June, the rainfall intensity drops to 13 mm/day and the FoS increases. Had the rainfall stopped from 4th June, the FoS would have increased and there would have been no landslides. On the other hand, had there been no rainfall from 28th May to 2nd June, the stability situation would been very much better and the rainfall from 4th June to 8th June may not have been able to trigger such devastating landslides across the region.

7.3.2. Discussion

The analysis result showed that TRIGRS is able to describe the gradual degradation of the stability condition of the hill slopes of the study area as response to the rainwater infiltration over the entire duration of the rainfall event. TRIGRS simulation result was able to bring out the effect of the intricate equilibrium of the antecedent rainfall or soil moisture condition, the intensity and duration of the triggering rainfall and the soil hydraulic properties on the triggering of landslides. As is observed the slightest of difference between the rainfall conditions prevailing in June 2012 to that of the rainfall event of March-April, 2010 have resulted in landslide occurrence.

7.4. EFFECT OF THE DIGITAL ELEVATION MODEL

The primary input for any such GIS-based quantification approaches is the Digital Elevation Model (DEM). DEM is an important data representing the topography of the area, which is subsequently used to derive all other input parameters including the slope map and drainage pattern. Some of the researchers have elucidated the effect of choice of DEM on the landslide hazard assessment (Claessens *et al*., 2005; van Westen *et al*., 2008; Viet *et al*., 2016). It has been highlighted that correct or precise representation of the topography of the study area by the chosen DEM is of paramount importance to derive meaningful outcomes. Achieving a satisfactory representation of the topography by a DEM based on satellite-data becomes even more difficult when the hilly terrain is substantially undulating and tortuous with frequently changing gradient.

Studies can be found in literature that have reported about the evaluation of the relative accuracy of the chosen DEMs and their corresponding advantages and disadvantages in representation of different geomorphological features (Dhakal *et al*., 2000; Jain *et al*., 2018). Several researchers have shown that finer resolution does not necessarily result in higher predictive accuracy in landslide mapping. The appropriate grid size selection, for certain cases, are dependent on the area, geomorphology and topography characteristics of study region. There are instances where 20-30 m resolution DEMs provided better landslides susceptibility mapping than their finer counterparts. It is highlighted that the source of the data sets is more important and have significant influence on the accuracy of a landslide susceptibility analysis.

Several researchers have used DEMs of varying resolutions for studying the aspects of rainfall-induced landslides across the world. It is emphasized that the selection of DEM of a specific resolution largely depends on the availability of corresponding data for the study region (Li and Zhou, 2003; Lee *et al*., 2004; Claessens *et al*., 2005; Pawłuszeka *et al*., 2017; Wang et al., 2017; Mahalingam and Olsen, 2015). CartoDEM is reported to be having a marginally higher accuracy than TanDEM-X DEM, while sufficiently accurate than SRTM and ASTER DEM (Bothale and Pandey, 2013; Deo *et al*., 2016; Lakshmi and Yarrakula, 2018). Vaze *et al*. (2010) specifically pointed out that very high resolution DEMs also comprise artefacts due to layout and shadow effects that pose difficulties in understanding and analysis of the terrain, and may not provide better output in comparison to lower resolution DEMs.

Li and Zhou (2003) modelled the susceptibility of landslides in Hong Kong (Latau) with DEMs of varying resolutions (5 m, 10 m, 20 m, 40 m and 80 m) using various parameters such as condition factors, the slope, aspect, type of vegetation, geology, altitude and distance to the water line. The appropriate grid size selection for the studies were found to be dependent on the area of pilot region, user requirement, as well as the geomorphology and topography characteristics of the study region. Based on the study, the 20 m resolution DEM was best suitable for the assessment of study region. Lee et al. (2004) used DEMs of 5 m, 10 m, 30 m, 100 m and 200 m resolution, for evaluating the landslide susceptibility to landslide at Bour (Korea), and observed that similar outcomes were observed with 5, 10 and 30 m resolution DEMs. It was concluded that DEMs with less than 30 m resolution is need for landslide analysis in Korea where most of the available maps are in the range 1:5000−1:50000. Claessens *et al*. (2005) used DEMs of four different resolutions (10 m, 25 m, 50 m and 100 m) to assess the landslide susceptibility of 12 km^2 area in New Zealand. It was concluded that the selection of DEM according to its resolution is strongly dependent on the data availability and scale of analysis. Mahalingam and Olsen (2015) illustrated that finer resolution does not necessarily result in higher predictive accuracy in landslide mapping. The source of the datasets used is an important consideration and has significant influence on the accuracy of a landslide susceptibility analysis.

Hence, it is understandable that the accuracy of the simulation results strongly depends on the chosen DEM, and it is necessary to define the best suitable DEM for a particular region.

The hilly terrains of Guwahati city are extremely tortuous and undulating, which calls a thorough study about the influence of DEM on the landslide susceptibility and hazard in the study area. There are quite a few DEM available for the study area, namely Indian Space Research Organisation (ISRO) CartoSat-DEM, Advanced Land Observing Satellite (‘DAICHI’), AW3D30-DEM (ALOS-3D), Shuttle Radar Topography Mission (SRTM-DEM), and the Advanced Space Borne Thermal Emission and Reflection Radiometer- Global DEM (ASTER-GDEM).

TRIGRS simulation is run by considering all the available DEMs for the study area as the base map for the analysis, and their suitability is assessed in predicting rainfall-induced landslide scenarios of the Guwahati region with as much accuracy as possible. The primary aim of the analysis is to evaluate the applicability of various available DEMs in predicting the landslide hazard scenarios of Guwahati city to the best possible accuracy.

In this regard, the DEMs as above mentioned are collected, and thereafter applied for the analysis. Before providing the discussion about the analyses result, these forthcoming sections provide a brief introduction about the collected DEMs.

7.4.1. ALOS – 3D

ALOS World 3D – 30m (AW3D30) is a global digital surface model (DSM) dataset, distributed publically by the Japan Aerospace Exploration Agency (JAXA), having a horizontal resolution of approximately 30 m mesh (1×1 arc second). The AW3D30 dataset is generated by down sampling the commercial version of the precise global digital 3D map, having 5 m resolution, to 1 arc-sec resolution of DSM dataset. The commercial 5-meter mesh global DSM dataset is generated through optical photogrammetry, using 3 million scene archives acquired by the PRISM panchromatic stereo mapping sensor on the Advanced Land Observing Satellite "DAICHI" (ALOS) that operated from 2006 to 2011. DAICHI was equipped with the Panchromatic Remote-sensing instrument for Stereo Mapping (PRISM) that enabled its observations with a high-resolution three-dimensional view. PRISM consisted of three radiometers viewing forward, nadir and backwards with 35 km swath-width, producing three sets of stereoscopic images. The developed digital 3D map consists of digital elevation model (DEM) or digital surface model (DSM) that can represent land terrains with an approximate 5 m spatial resolution and 5 m target height accuracy (standard deviation) (Tadono *et al*., 2014; Takaku *et al*., 2014; Takaku *et al*., 2016; Tadono *et al*., 2016; Takaku and Tadono, 2017; EORC–JAXA–ALOS, 2018).

7.4.2. CartoDEM

The Cartosat-1 Digital Elevation Model (CartoDEM) is a National DEM developed by the Indian Space Research Organization (ISRO). The CartoDEM is a surface model of elevation and covers land surfaces of India. The Cartosat-1 has a pair of panchromatic cameras having an along-the-track stereoscopic capability that uses its near-nadir viewing and forward viewing telescopes to acquire the stereo image data. The spatial resolution is 2.5 m in the horizontal plane. The CartoDEM is generated from strip stereo pairs through stereo-strip triangulation using high precision ground control points, interactive cloud masking, and automatic dense conjugate pair generation using matching approach. The irregular DEM is processed using TIN (Triangular Irregular Network) modelling and interpolating for generating a regular DEM, and then automatic strip-to-strip mosaicking is done to produce a seamless homogeneous DEM. These generated DEM tiles are evaluated for quality and

edited to remove anomalies. The primary output data is a DEM of resolution 1/3 arc-sec, along with co-registered ortho-image of resolution 1/12 arc-sec. As per the design of CartoDEM, the DEM accuracy is 8 m at LE90 and 15 m at CE90 for ortho data. The DEM of 1 arc-sec resolution generated by sub sampling the original 1/3 arc-sec data is available publically on Bhuvan portal of NRSC/ISRO.

7.4.3. ASTER – GDEM

The Ministry of Economy, Trade, and Industry (METI) of Japan and the United States National Aeronautics and Space Administration (NASA) jointly released the Advanced Spaceborne Thermal Emission and Reflection Radiometer (ASTER) Global Digital Elevation Model Version 2 (GDEM V2) on October 17, 2011. The ASTER GDEM is generated using stereo-pair images collected by the ASTER instrument on-board TERRA satellite. The ASTER sensor takes images of the earth with 14 different bands ranging from ultraviolet to infrared. The Thermal Emission and Reflection Radiometer collects in-track stereo pairs using nadir-pointing and aft looking near-infrared cameras. These stereo pairs are used to produce single-scene (60 x 60 km) digital elevation models having vertical accuracies generally between 10 m and 25 m. The ASTER-GDEM is released publically to users worldwide as a contribution to the Global Earth Observing System of Systems (GEOSS) and is available through United States Geological Survey (USGS) Earth Explorer.

7.4.4. SRTM DEM

The Shuttle Radar Topography Mission (SRTM) is an international research effort spearheaded by the United States National Geospatial-Intelligence Agency (NGA) and the United States National Aeronautics and Space Administration (NASA) to generate digital elevation model on a near-global scale. SRTM consisted of a specially modified radar system that flew on board the Space Shuttle Endeavour for an 11-day mission in February 2000. The NASA SRTM obtained elevation data on a near-global scale using interferometric synthetic aperture radar. The shuttle used the reflection of emitted radar signals in the C-band (wavelength ≈ 5.6 cm) for the SIR-C (Spaceborne Imaging Radar C-band Synthetic Aperture Radar) sensor. The C-band could penetrate through the canopy cover penetration, and reflected mostly at the ground surface. Interferometric synthetic aperture radar (InSAR) is a radar technique used in geodesy and remote sensing. This geodetic method uses two or more synthetic aperture radar (SAR) images to generate maps of surface deformation or digital elevation, using differences in the phase of the waves returning to the satellite. For the

present study, the SRTM DEM V3.0 of 1 arc-sec resolution and SRTM DEM V4.1 of 3 arc-sec resolution are used which are available publically on the USGS Earth Explorer. The data voids in the SRTM V3.0 has been eliminated with fill primarily from ASTER GDEM2 (Global Digital Elevation Model Version 2), and secondarily from USGS GMTED2010 (Global Multi-resolution Terrain Elevation Data, 2010). The SRTM 90 m resolution DEM is significantly coarse and is expected to produce results with limited accuracy. The same is used and shown only for a comparison purpose, while the 90 m DEM is not used for TRIGRS simulations since the output is not likely to produce any meaningful output with respect to the study area.

7.4.5. TRIGRS – simulation and results

TRIGRS simulations were carried out considering the rainfall of June 1998, July 2007 and June 2012, for the five different DEMs as formerly mentioned. The FoS-maps are obtained for each day of the rainfall event and the RVS-points were overlaid on the FoS-maps. The FoS values at the RVS-points were extracted out and the average, maximum, minimum and the standard deviation are plotted for the entire duration of the rainfall event. The exact same procedure is followed for all of the DEMs.

Figure 7.8 shows the gradual decreasing trend of the average of FoS at the RVS-point locations obtained from the different DEMs as the base map, correponding to the rainfall event of June 1998. Only the analysis, conducted with ALOS 3D as the base DEM, was successful in providing the exact timing of the occurrence of landslides i.e. 8th June 1998. The FoS values from ALOS-3D and CartoDEM (1/3 arc-sec) were in close agreement until 6th June 1998, exhibiting a magnitude of 1.2, while deviating in the further days for the simulation with the latter DEM. A similar exercise was conducted considering the July 2007 rainfall and landslide events (Figure 7.9). In this case also the simulation results considering the ALOS 3D as the base DEM, prevailed over the others. Only the results derived from the ALOS 3D DEM could successfully predict that landslide may occur in sites of the RVS points trigerred by the above mentioned rainfall events.

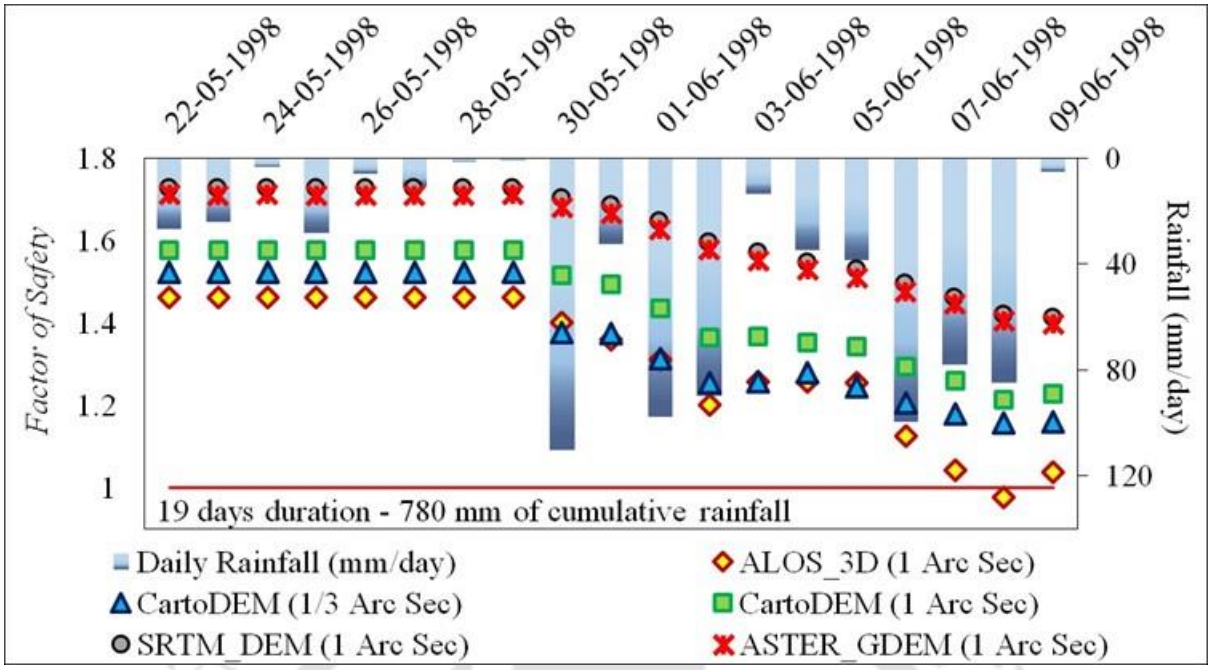

Figure 7.8 Average of FoS at the RVS-points as a response to rainfall event of June 1998

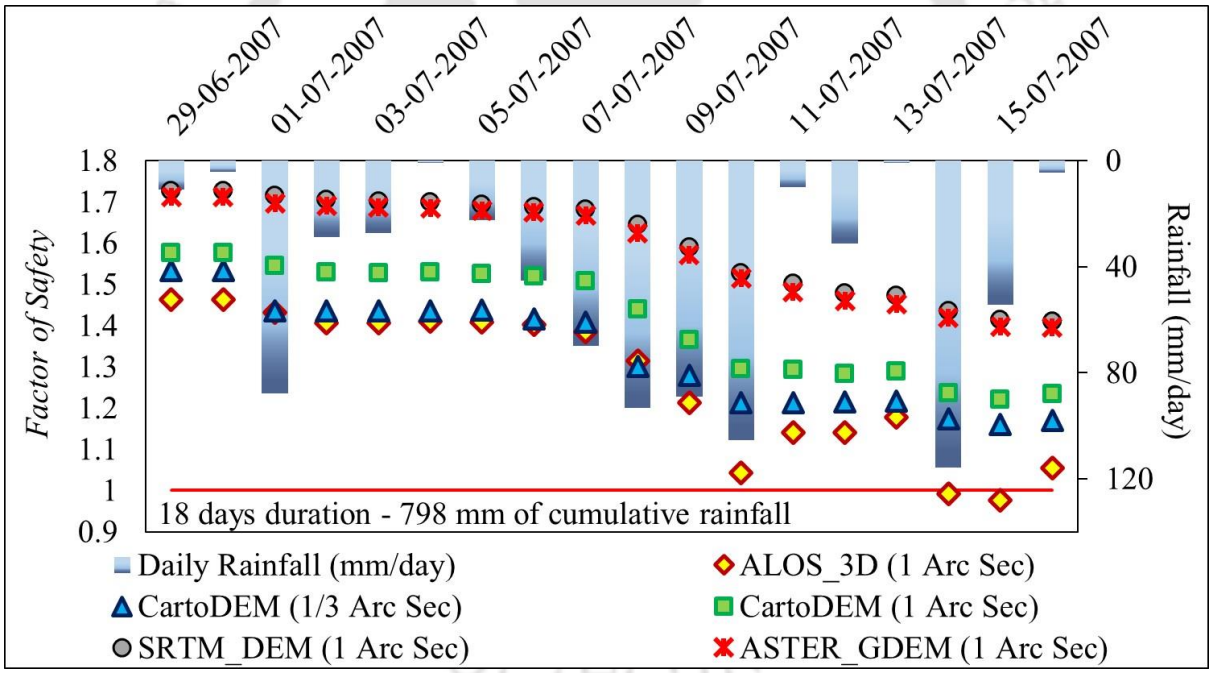

Figure 7.9 Average of FoS at the RVS-points as a response to rainfall event of July 2007

Figure 7.10 shows the distribution of the FoS at the RVS-points in detail along with the daily rainfall through the month of June, 2012. The plot shows the daily rainfall as clustered columns with the magnitude of rainfall intensity on the vertical axis on the right. The average of the FoS at all location of the 347 RVS-points is shown as marker for each time step (daily), along with standard deviation of the set as error bars. The area plot in the background gives the maximum and minimum FoS value of each (24-hour time-step) set.

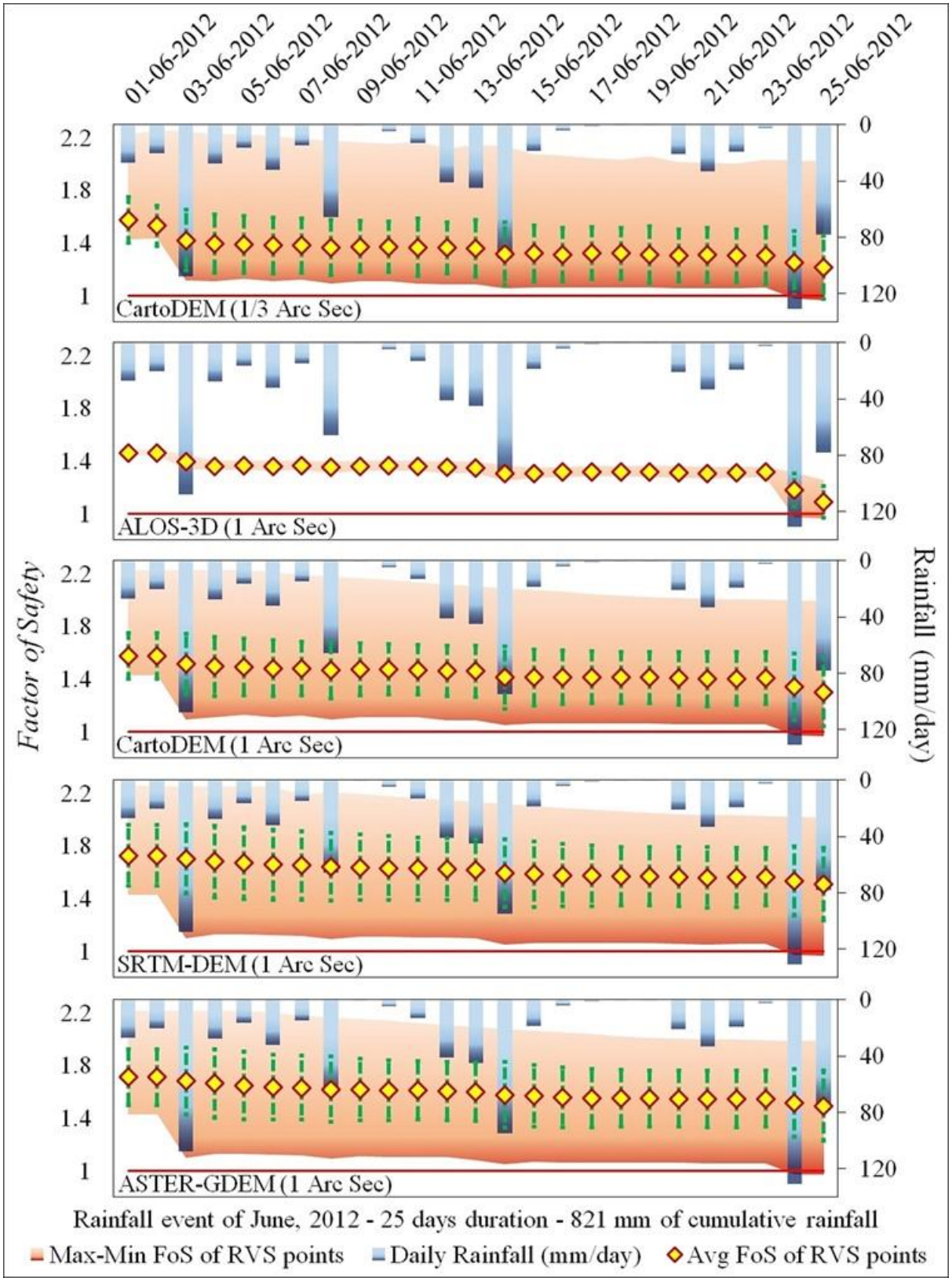

Figure 7.10 Distribution of the FoS at the RVS-points as a response to rainfall event of June 2012

The most impotant observation from the Figure 7.10 is the difference in the response when different DEMs are considered as the base map for the rainfall-induced landslide

analysis. The trend of the FoS distribution across the RVS-points over the rainfall event duration as obtained using ALOS-3D DEM is significantly different from the outcome of the other DEMs. The trend of the average FoS obtained from the ALOS-3D was closely followed by that obtained from CartoDEM 1/3 arc sec, followed by the outcome from CartoDEM 1 arc sec, yet the FoS values obtained from these DEMs were highly scattered as can be observed from Figure 7.10. However, the results obtained from TRIGRS simulation using the SRTM-DEM (1 arc sec) and the ASTER-GDEM deviated significantly away from that of ALOS-3D.

7.4.6. Evaluation of the simulation result

The effectiveness of landslide predicting models, are then evaluated based on the Receiver Operating Characteristics (ROC) using confusion matrix (Table 6.3) as described in Section 6.7. Subsequently, the True Positive Rate (TPR) are plotted against the False Positive Rate (FPR) for the FoS-maps obtained from the various DEMs and for a particular rainfall event, as shown in Figure 7.11.

As can be observed from Figure 7.11, the results obtained from using ALOS-3D as the base map have the highest True Positive Rate as compared to the other DEMs. The TPR is observed to be almost 1 for the rainfall events of 1998 and 2007, encompassing all of the RVS points i.e., at all of the RVS-points TRIGRS predicted FoS < 1.0. The rainfall event of June 1998 and July 2007 triggered wide spread landsliding, and simultaneously the TRIGRS solutions showed more areas of the region to be destabilized (represented by FoS<1.0).

The outcome of CartoDEM was observed to be comparatively poorer than the ALOS 3D DEM. Further, it is noted that the demarcation of the CartoDEM of two different resolutions (1 arc-sec and 1/3rd arc-sec) are nearly overlapping, thereby indicating negligible influence of the resolution of the CartoDEM on the ROC of the FoS-maps. The ROC of the FoS-maps obtained from the SRTM-DEM and ASTER-GDEM showed a very poor correlation to landslide occurrences within the study area. Thus, from the ROC plot of Figure 7.11, the TRIGRS FoS-maps obtained using the ALOS-3D DEM can be graded as the best possible outcome of the rainfall-induced landslide analysis of the in-situ scenario of the Guwahati region.

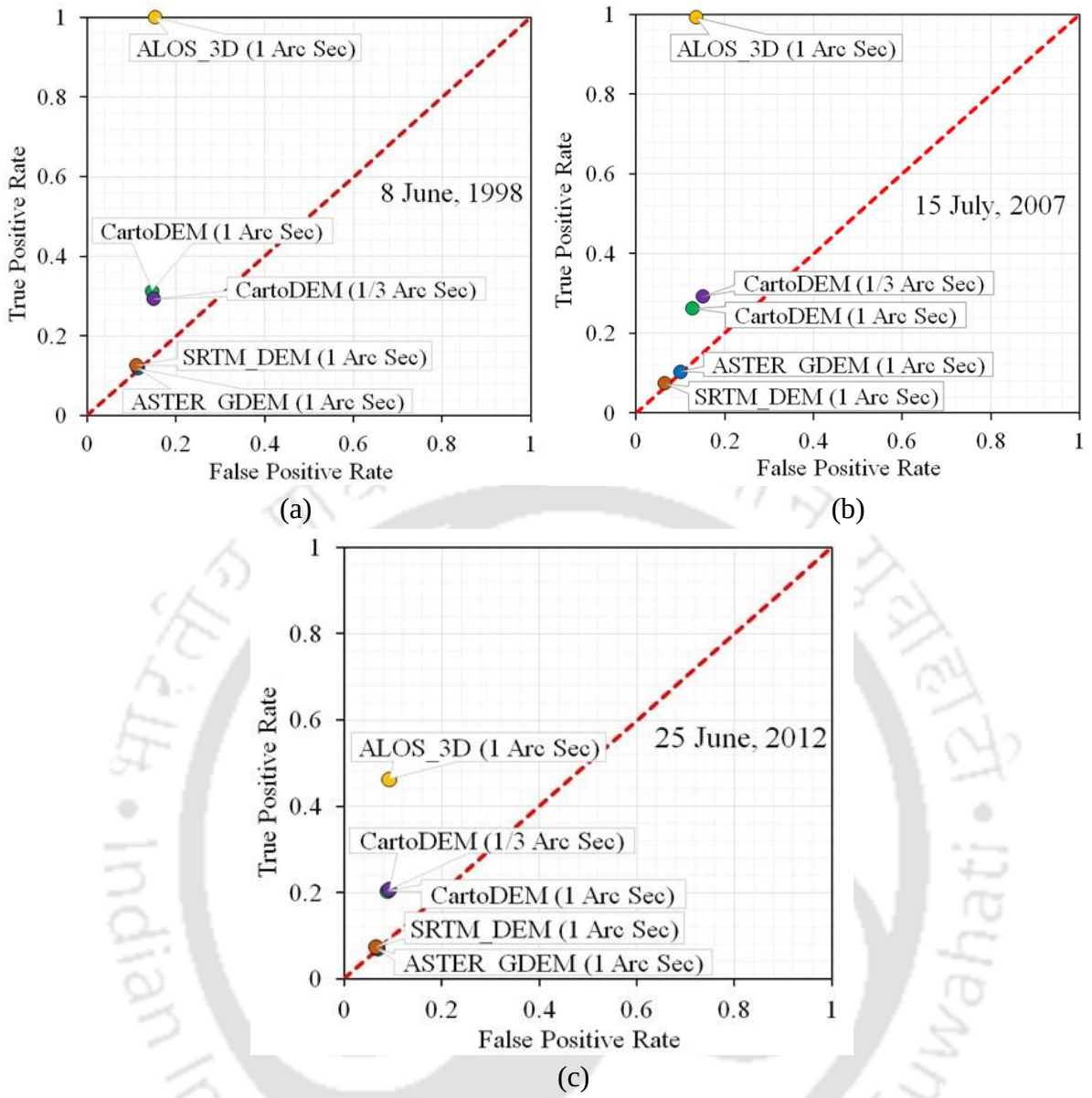

Figure 7.11 ROC for the TRIGRS simulation results using the different DEMs

To provide with a precise and detailed description of the TRIGRS simulations, the LR_{class} evaluation method as proposed by Park *et al*., (2013) is employed. The efficiency of this evaluation method, especially for geographical point-location based landslide occurrence data, have been verified by previous researchers (Park *et al*., 2013, Viet *et al*., 2017). LR_{class} is the ratio of the percentage of landslide locations (out of the total number of considered landslide locations), within a particular range of Factor of Safety class, to the percentage area under the same range of Factor of Safety values. LR_{class} is a quantitative measure of the percentage chance of accurately predicting a slope failure occurrence by the TRIGRS simulation. The results of LR_{class} are presented in Table 7.3, Table 7.4 and Table 7.5 for the TRIGRS simulation results corresponding to rainfall of June 1998, July 2007 and June 2012.

The RVS-points are distributed into Factor of Safety classes and the number of RVS-points under a particular FoS class is shown under column (a) of Table 7.3, Table 7.4 and Table 7.5. Column (*c*) shows the percentage of area under a particular FoS class. For comparison purpose, the '% of predicted area excluding the Stable areas' is presented alongside '% of predicted area considering the entire study area'. The percentage predicted area are almost comparable for CartoDEM (1 arc-sec and 1/3rd arc-sec) and ALOS 3D DEM, with small variation for SRTM – DEM and ASTER – GDEM. However, when it comes to inclusions of the observed landslide locations within the predicted areas, the results vividly bring out the differences of the various DEMs. CartoDEM 1 arc-sec and 1/3rd arc-sec have similar percentage LR_{class}, followed by SRTM – DEM and ASTER – GDEM with even lower percentage LR_{class}. A higher value of percentage LR_{class} indicates higher accuracy in the prediction by the simulations in terms of lower over-prediction by the model (Park *et al*., 2013, Viet *et al*., 2017). ALOS 3D DEM stands out with the highest count of percentage LR_{class}. The 'Stable' area represents the grid cells where the slope angle is supposed less than 15º by the respective DEMs, along with those regions where the FoS unconditionally remains greater than 2.0, and therefore are not included in the analysis for evaluation of the LR_{class}. The TRIGRS simulation using CartoDEM 1 arc-sec and 1/3rd arc-sec DEMs predicts that in 9 and 15 numbers of sites, out of the 347 landslide locations, respectively, there should be no landslide. The count considerably increases to 36 for simulation using SRTM – DEM, and astonishingly to 66 for the ASTER – GDEM. The results obtained with ALOS 3D DEM showed significant agreement between the simulated and the documented landslide point locations. Comparing the simulation results from ALOS 3D DEM corresponding to the rainfall of June 1998 and July 2007, to June 2012, the effect of the variations in the rainfall pattern on the FoS distribution across the RVS-point locations and in general, across the study area can be distinctly observed. Corresponding to the June 2012, the FoS classes are seen to be distributed across the RVS-point locations, with FoS < 1.0 at 161 sites, 1.0 ≤ FoS < 1.1 at 55 sites, 1.1 ≤ FoS < 1.2 at 60 sites and 1.2 ≤ FoS < 1.3 at the remaining 71 sites. While for the rainfall event of June 1998 and July 2007, the FoS at 344 and 340 sites respectively, out of the total 347 sites is simulated to be below 1.0. Consequently the '% of predicted area' under FoS<1.0 class also increases for the rainfall event of June 1998 and July 2007, compared to that of June 2012.

Table 7.3 LR_{class} evaluation of the TRIGRS model results on 8 June 1998 for the simulation with rainfall of June 1998

FoS distribution on the 8th June, 1998 Factor of Safety classes	Landslide (RVS-point) locations (*a*)					% of the sites (*b*) = 100 × (*a*)/347				
	CartoDEM (1/3 arc-sec)	ALOS – 3D	CartoDEM (1 arc-sec)	SRTM – DEM	ASTER – GDEM	CartoDEM (1/3 arc-sec)	ALOS – 3D	CartoDEM (1 arc-sec)	SRTM – DEM	ASTER – GDEM
FoS < 1.0	102	344	105	44	41	29.3	99.1	30.4	12.6	11.9
1.0 ≤ FoS < 1.1	78	0	41	14	12	22.6	0.0	11.9	4.1	3.3
1.1 ≤ FoS < 1.2	41	3	24	9	4	11.9	0.9	7.0	2.6	1.1
1.2 ≤ FoS < 1.3	55	0	64	42	45	15.9	0.0	18.5	12.2	13.0
1.3 ≤ FoS < 1.4	23	0	33	51	46	6.7	0.0	9.6	14.8	13.3
1.4 ≤ FoS < 1.5	12	0	22	44	30	3.3	0.0	6.3	12.6	8.5
1.5 ≤ FoS < 1.7	14	0	15	39	54	4.1	0.0	4.4	11.1	15.6
1.7 ≤ FoS < 2.0	13	0	26	68	50	3.7	0.0	7.4	19.6	14.4
Stable	9	0	15	36	66	2.6	0.0	4.4	10.4	18.9
	% of predicted area (*c*) [excluding the Stable areas]					% of predicted area [considering the entire study area]				
FoS < 1.0	15.0	15.5	14.7	11.1	11.3	3.3	3.1	2.7	1.6	2.0
1.0 ≤ FoS < 1.1	8.5	6.5	6.1	4.2	5.0	1.9	1.3	1.1	0.6	0.9
1.1 ≤ FoS < 1.2	5.5	4.3	4.1	3.2	3.6	1.2	0.9	0.8	0.5	0.6
1.2 ≤ FoS < 1.3	13.4	12.9	12.5	11.0	10.5	3.0	2.6	2.3	1.6	1.8
1.3 ≤ FoS < 1.4	13.1	14.6	14.4	13.8	13.0	2.9	2.9	2.7	2.0	2.2
1.4 ≤ FoS < 1.5	11.8	10.0	10.0	10.7	10.0	2.6	2.0	1.9	1.6	1.7
1.5 ≤ FoS < 1.7	10.6	14.5	15.1	17.0	16.5	2.3	2.9	2.8	2.5	2.9
1.7 ≤ FoS < 2.0	22.2	21.5	23.0	29.0	30.0	4.9	4.2	4.3	4.3	5.2
Stable						77.9	80.3	81.4	85.2	82.8
	LR_{class} (*d*) = *b*/*c*					% of LR_{class} = 100 × *d*/*e*				
FoS < 1.0	1.9	6.4	2.1	1.1	1.0	20.9	96.9	22.8	15.0	16.0
1.0 ≤ FoS < 1.1	2.7	0.0	1.9	1.0	0.7	28.7	0.0	21.2	12.8	10.2
1.1 ≤ FoS < 1.2	2.2	0.2	1.7	0.8	0.3	23.3	3.1	18.7	10.6	4.7
1.2 ≤ FoS < 1.3	1.2	0.0	1.5	1.1	1.2	12.7	0.0	16.3	14.7	18.8
1.3 ≤ FoS < 1.4	0.5	0.0	0.7	1.1	1.0	5.5	0.0	7.4	14.1	15.6
1.4 ≤ FoS < 1.5	0.3	0.0	0.6	1.2	0.9	3.0	0.0	6.9	15.4	13.0
1.5 ≤ FoS < 1.7	0.4	0.0	0.3	0.7	0.9	4.1	0.0	3.2	8.6	14.3
1.7 ≤ FoS < 2.0	0.2	0.0	0.3	0.7	0.5	1.8	0.0	3.5	8.9	7.3
Sum (*e*)	9.3	6.6	9.1	7.6	6.6	100	100	100	100	100

Table 7.4 LR_{class} evaluation of the TRIGRS model results on 15 July 2007 for the simulation with rainfall of July 2007

FoS distribution on the 15th July, 2007 Factor of Safety classes	Landslide (RVS-point) locations (*a*)					% of the sites (*b*) = 100 × (*a*)/347				
	CartoDEM (1/3 arc-sec)	ALOS – 3D	CartoDEM (1 arc-sec)	SRTM – DEM	ASTER – GDEM	CartoDEM (1/3 arc-sec)	ALOS – 3D	CartoDEM (1 arc-sec)	SRTM – DEM	ASTER – GDEM
FoS < 1.0	102	340	91	35	33	29.3	98.0	26.3	10.0	9.6
1.0 ≤ FoS < 1.1	78	0	41	14	14	22.6	0.0	11.9	4.1	4.1
1.1 ≤ FoS < 1.2	35	7	30	12	8	10.0	2.0	8.5	3.3	2.2
1.2 ≤ FoS < 1.3	55	0	69	48	39	15.9	0.0	20.0	13.7	11.1
1.3 ≤ FoS < 1.4	30	0	39	53	55	8.5	0.0	11.1	15.2	15.9
1.4 ≤ FoS < 1.5	12	0	21	49	35	3.3	0.0	5.9	14.1	10.0
1.5 ≤ FoS < 1.7	19	0	23	40	60	5.6	0.0	6.7	11.5	17.4
1.7 ≤ FoS < 2.0	8	0	18	62	37	2.2	0.0	5.2	17.8	10.7
Stable	9	0	15	36	66	2.6	0.0	4.4	10.4	18.9
	% of predicted area (*c*) [excluding the Stable areas]					% of predicted area [considering the entire study area]				
FoS < 1.0	15.0	13.6	12.8	9.6	9.9	3.3	2.7	2.4	1.4	1.7
1.0 ≤ FoS < 1.1	8.5	6.6	6.2	4.3	5.0	1.9	1.3	1.2	0.6	0.9
1.1 ≤ FoS < 1.2	2.6	4.4	4.2	3.2	3.6	0.6	0.9	0.8	0.5	0.6
1.2 ≤ FoS < 1.3	15.3	14.0	13.6	11.8	11.3	3.4	2.8	2.5	1.7	2.0
1.3 ≤ FoS < 1.4	14.1	16.0	15.7	15.1	14.2	3.1	3.2	2.9	2.2	2.5
1.4 ≤ FoS < 1.5	11.8	10.1	10.2	10.9	10.2	2.6	2.0	1.9	1.6	1.8
1.5 ≤ FoS < 1.7	14.4	16.7	17.5	19.9	19.3	3.2	3.3	3.2	2.9	3.3
1.7 ≤ FoS < 2.0	18.3	18.6	19.8	25.3	26.4	4.1	3.7	3.7	3.8	4.6
Stable						77.9	80.3	81.4	85.2	82.8
	LR_{class} (*d*) = *b*/*c*					% of LR_{class} = 100 × *d*/*e*				
FoS < 1.0	1.9	7.2	2.1	1.0	1.0	17.9	94.0	21.9	13.4	14.3
1.0 ≤ FoS < 1.1	2.7	0.0	1.9	1.0	0.8	24.5	0.0	20.2	12.2	12.0
1.1 ≤ FoS < 1.2	3.9	0.5	2.0	1.0	0.6	35.3	6.0	21.7	13.4	9.0
1.2 ≤ FoS < 1.3	1.0	0.0	1.5	1.2	1.0	9.5	0.0	15.6	15.0	14.5
1.3 ≤ FoS < 1.4	0.6	0.0	0.7	1.0	1.1	5.5	0.0	7.5	13.0	16.5
1.4 ≤ FoS < 1.5	0.3	0.0	0.6	1.3	1.0	2.6	0.0	6.2	16.5	14.5
1.5 ≤ FoS < 1.7	0.4	0.0	0.4	0.6	0.9	3.5	0.0	4.1	7.4	13.3
1.7 ≤ FoS < 2.0	0.1	0.0	0.3	0.7	0.4	1.1	0.0	2.8	9.0	6.0
Sum (*e*)	10.9	7.7	9.4	7.8	6.8	100	100	100	100	100

Table 7.5 LR_{class} evaluation of the TRIGRS model results for the simulation with rainfall of June 2012

FoS distribution on the 25th June, 2012 Factor of Safety classes	Landslide (RVS-point) locations (*a*)					% of the sites (*b*) = 100 × (*a*)/347				
	CartoDEM (1/3 arc-sec)	ALOS – 3D	CartoDEM (1 arc-sec)	SRTM – DEM	ASTER – GDEM	CartoDEM (1/3 arc-sec)	ALOS – 3D	CartoDEM (1 arc-sec)	SRTM – DEM	ASTER – GDEM
FoS < 1.0	72	161	71	27	24	20.7	46.4	20.4	7.8	7.0
1.0 ≤ FoS < 1.1	73	55	28	9	10	21.1	15.9	8.1	2.6	3.0
1.1 ≤ FoS < 1.2	49	60	10	4	4	14.1	17.3	3.0	1.1	1.1
1.2 ≤ FoS < 1.3	36	71	68	30	24	10.4	20.5	19.6	8.5	7.0
1.3 ≤ FoS < 1.4	41	0	49	35	27	11.9	0.0	14.1	10.0	7.8
1.4 ≤ FoS < 1.5	28	0	30	42	48	8.1	0.0	8.5	12.2	13.7
1.5 ≤ FoS < 1.7	18	0	44	84	77	5.2	0.0	12.6	24.1	22.2
1.7 ≤ FoS < 2.0	21	0	32	81	67	5.9	0.0	9.3	23.3	19.3
Stable	9	0	15	36	66	2.6	0.0	4.4	10.4	18.9
	% of predicted area (*c*) [excluding the Stable areas]					% of predicted area [considering the entire study area]				
FoS < 1.0	9.3	9.3	8.8	6.5	6.8	2.1	1.8	1.6	1.0	1.2
1.0 ≤ FoS < 1.1	7.3	5.5	5.1	3.5	4.3	1.6	1.1	1.0	0.5	0.7
1.1 ≤ FoS < 1.2	4.9	2.7	2.5	1.8	2.4	1.1	0.5	0.5	0.3	0.4
1.2 ≤ FoS < 1.3	8.8	9.8	9.5	7.4	7.5	2.0	1.9	1.8	1.1	1.3
1.3 ≤ FoS < 1.4	11.7	10.2	9.9	8.7	8.2	2.6	2.0	1.8	1.3	1.4
1.4 ≤ FoS < 1.5	11.4	12.6	12.3	11.7	11.0	2.5	2.5	2.3	1.7	1.9
1.5 ≤ FoS < 1.7	17.5	23.2	23.6	25.3	23.9	3.9	4.6	4.4	3.7	4.1
1.7 ≤ FoS < 2.0	29.2	26.6	28.3	35.1	36.0	6.5	5.2	5.3	5.2	6.2
Stable						77.9	80.3	81.4	85.2	82.8
	LR_{class} (*d*) = *b*/*c*					% of LR_{class} = 100 × *d*/*e*				
FoS < 1.0	2.2	5.0	2.3	1.2	1.0	19.5	30.4	22.8	15.9	15.3
1.0 ≤ FoS < 1.1	2.9	2.9	1.6	0.7	0.7	25.4	17.7	15.7	9.8	10.2
1.1 ≤ FoS < 1.2	2.9	6.4	1.2	0.6	0.5	25.3	39.1	11.6	8.1	6.8
1.2 ≤ FoS < 1.3	1.2	2.1	2.1	1.1	0.9	10.3	12.7	20.4	15.3	13.8
1.3 ≤ FoS < 1.4	1.0	0.0	1.4	1.2	0.9	8.9	0.0	14.1	15.4	13.9
1.4 ≤ FoS < 1.5	0.7	0.0	0.7	1.0	1.2	6.2	0.0	6.9	13.9	18.4
1.5 ≤ FoS < 1.7	0.3	0.0	0.5	1.0	0.9	2.6	0.0	5.3	12.7	13.7
1.7 ≤ FoS < 2.0	0.2	0.0	0.3	0.7	0.5	1.8	0.0	3.2	8.8	7.9
Sum (*e*)	11.5	16.4	10.1	7.5	6.8	100	100	100	100	100

7.4.7. Discussions

Based on the ROC plots and the LR_{class}, it can be well recognized that the choice of DEM of various types and resolution have varying effect on the efficacy of the prediction regional rainfall-induced landslides. The parameter that mostly affects the FoS at particular location can be identified to be the slope angle that is derived from the corresponding DEMs. The slope angles, corresponding to the RVS-point locations, are extracted from the corresponding slope maps derived from the five DEMs, respectively, and are plotted against the site location number (Figure 7.12). Significant scatter in the slope angle values is seen for the slope maps derived from the different DEMs, except those derived from ALOS-3D. For the latter case, the slope angles at the corresponding RVS locations were observed to be concentrated in the range 26º-31º. which compares reasonably well with the observations made by previous researchers (Goswami and Singh, 2008; Bhusan *et al*., 2014) and reaffirmed with in-situ visual reconnaissance. The statistics of the scatter is plotted in Figure 7.13, which illustrates the average of the slope angles (derived from DEMs) along with their standard deviation, as well as the maximum-minimum range of slope angles at the RVS-point locations.

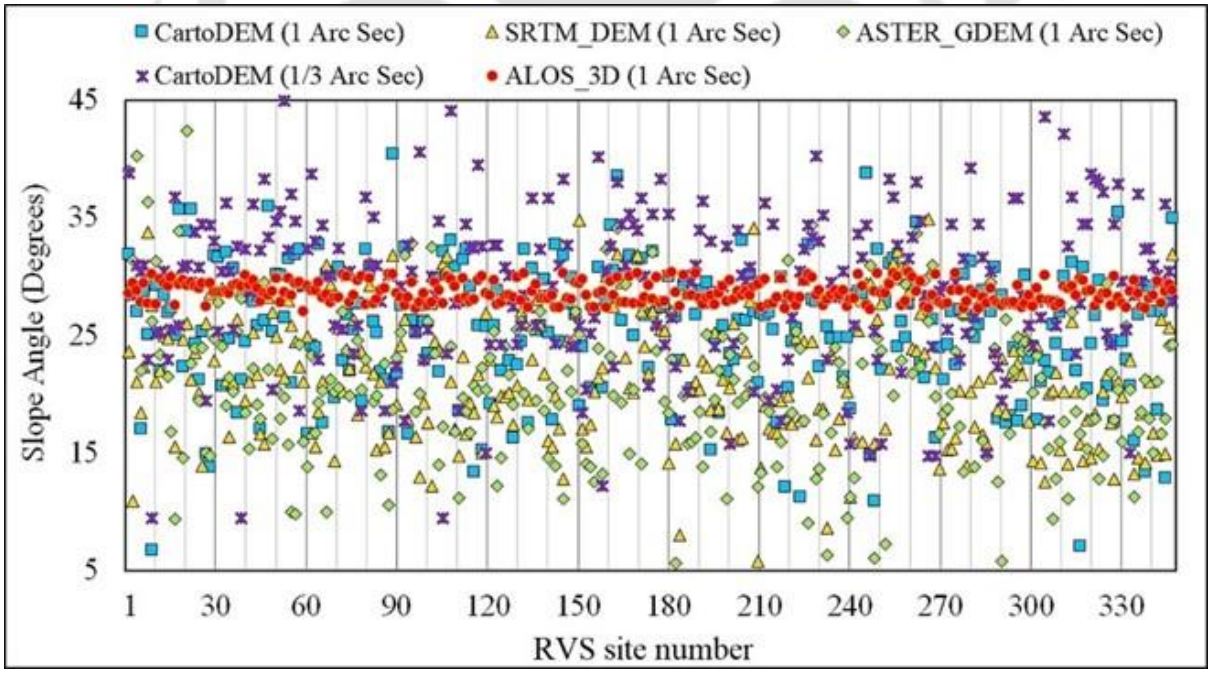

Figure 7.12 Slope angles derived from the DEMs at the RVS-point locations

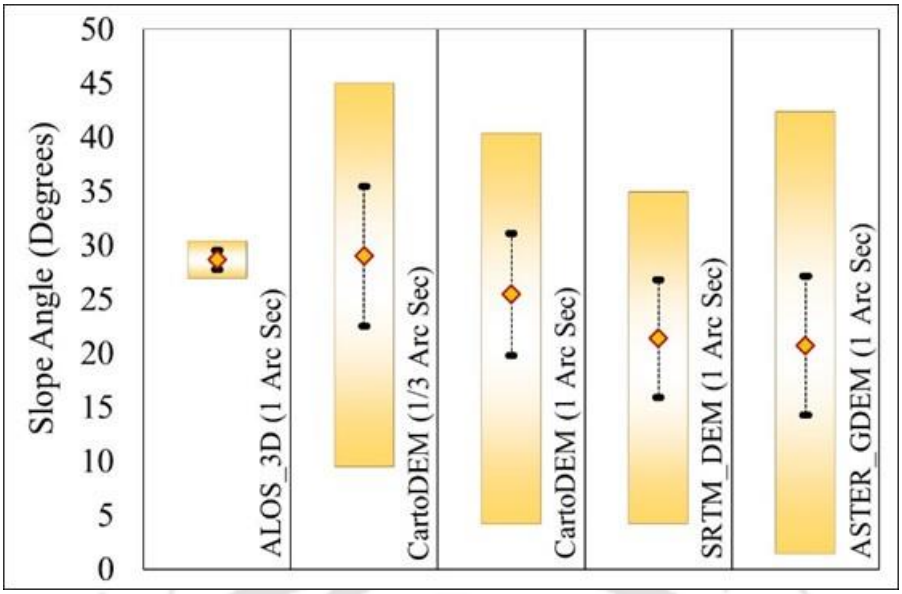

Figure 7.13 Statistics of the slope angle values considering the RVS-point locations

It can be observed that both ALOS 3D and CartoDEM 1/3rd arc-sec exhibit nearly similar average slope angle, however the latter DEM exhibits notably higher standard deviation and maximum-minimum range. The rest of the DEMs not only reveal a lower value of average slope angle, at the same time they exhibit a significantly high standard deviation and a very high maximum-minimum range. This scatter of the slope angle explains the variations in the trend of FoS values over the rainfall duration as shown in Figure 7.8, Figure 7.9 and Figure 7.10. Due to similar average slope angle values the initial average FoS as obtained from ALOS-3D and CartoDEM 1/3rd arc-sec DEM were of similar magnitude. However, with proceed of rainfall the FoS deviated resulting from the scatter of slope angle values for the CartoDEM 1/3rd arc-sec DEM.

It is observed from Figure 7.12 and Figure 7.13 that at the RVS site location, the slope angles derived from the various above-mentioned DEMs are considerably different from each other, which ultimately lead to incorrect representation of the topography. To further assess whether different DEMs manifest different slope angles for the entire study area, the cumulative percentage area against the slope angle is evaluated for each DEM and plotted, as shown in Figure 7.14. The cumulative percentage area represents that fraction of the entire study area that have slope angle lesser than a particular value. Figure 7.14 showed a significant difference in the representation of the topography by the various DEMs considered in the present study. It can be observed that the SRTM - DEM (3 arc sec) has the lowest fraction of area under slope angle of 20º- 40º, followed by SRTM - DEM (1 arc sec) and ASTER - GDEM (1 arc sec), while the CartoDEM (1/3 arc sec) showed the highest

fraction. As the total area of the study region is approximately 556 sq. km, it can be naturally deduced that even a meagre difference of 1% in the topographic representation would mean a notable difference in the field area by approximately 5.5 sq. km.

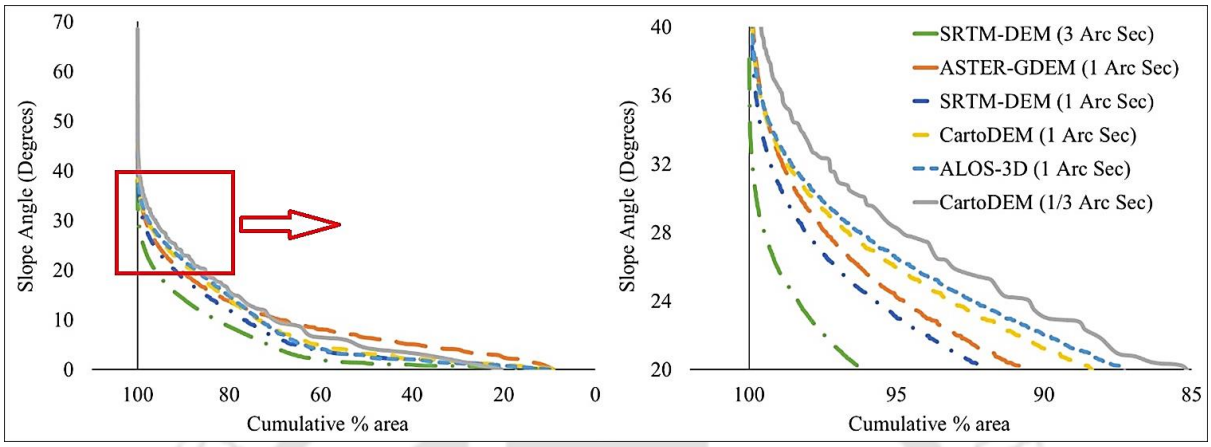

Figure 7.14 Cumulative percentage area vs. the slope angle for the entire study area

To understand the implications of this disparity, the in-situ slope maps of the Nabagraha-Sunsali-Noonmati hill series (marked as 1 in Figure 3.6) derived from various DEMs are plotted in Figure 7.15. This particular area is chosen as it is most severely affected by rainfall-induced landslide occurrences and the topography of this particular hill series exhibits the most tortuous conditions with indubitably undulating terrain. There seems to be considerable similarity in the slope map of ALOS-3D and CartoDEM (1 arc sec and 1/3 arc sec), however keen scrutiny of the same aids in highlighting their differences, as already revealed in Figure 7.12 and Figure 7.13. In contrary, the slope maps obtained from ASTER-GDEM and SRTM (1 arc sec and 3-arc sec) DEM are significantly different from the other and poor in representing the topography of the region. Based on the observations, it can be inferred that ALOS-3D DEM gave the best correlation to the landslide location, and that the other DEMs are observed to be notably different. In this regard, ALOS-3D DEM is recommended to be used to studying the future landslide scenarios for Guwahati city. The other important parameter affecting the landslide occurrences is the drainage pattern of the hill regions. The gully regions, which receive relatively higher surface drainage and sub-surface seepage water, are more prone to landslides. Landslides in such regions can also be caused because of erosion by the surface runoff draining from the upslope areas. To understand the influence of the DEM data on the drainage pattern of the hillslopes, the upslope catchment area is delineated from the DEMs, and is plotted for the Nabagraha-Sunsali-Noonmati hill series, as shown in Figure 7.16.

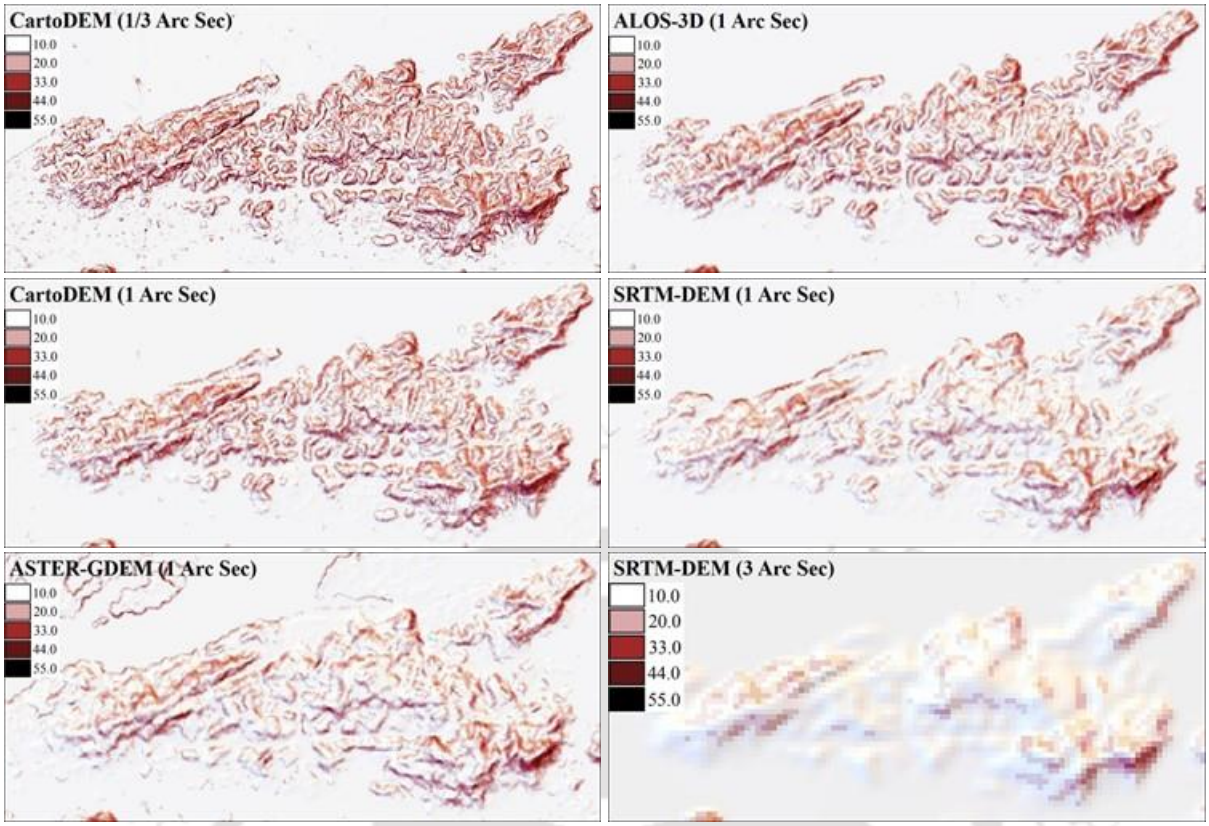

Figure 7.15 Slope Map of Nabagraha-Sunsali-Noonmati hill series derived from the corresponding DEMs

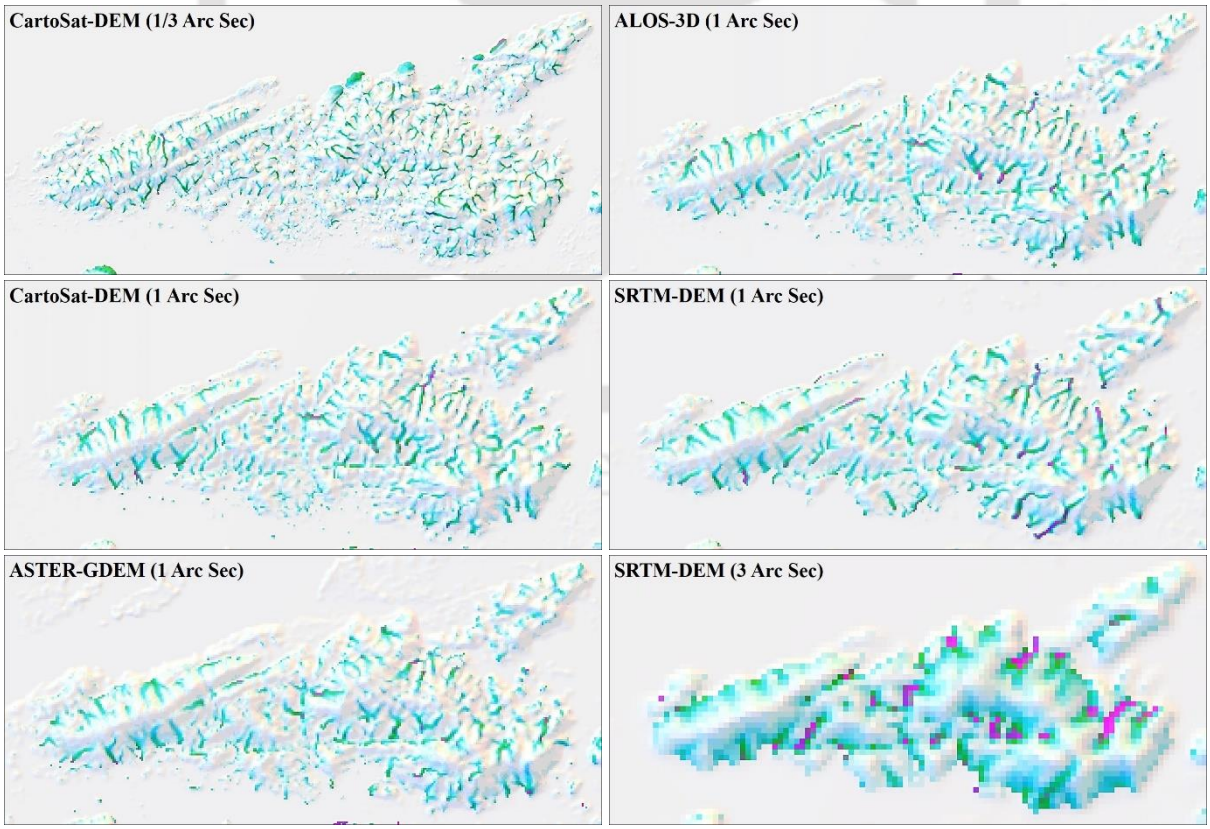

Figure 7.16 Drainage pattern of Nabagraha-Sunsali-Noonmati hill series derived from the corresponding DEMs

The drainage pattern derived from CartoDEM (1/3 arc sec) is the most intricate owing to the finer resolution of the base DEM, which allowed identifying and mapping of the gullies up to the maximum details. The CartoDEM (1 arc sec) and ALOS-3D yielded a similar drainage map. However, as for the slope maps, the drainage maps obtained from ASTER-GDEM and SRTM (1 arc sec and 3-arc sec) DEM were significantly different.

7.4.8. Remarks

The main purpose of this study was to assess the impact of the resolution of the DEMs and its choice on the subsequent performance of TRIGRS in predicting the location of shallow rainfall-induced landslide occurrences in the hillslopes of Guwahati region. The rainfall events of June 1998, July 2007 and June 2012 were reported to have triggered several landslides and therefore were selected as event scenarios for the present study. RVS-points obtained from corresponding reconnaissance surveys were adopted as in-situ data for validating and comparing the TRIGRS simulation results. The input parameters describing the mechanical and hydrological properties of the overburden soil layer was adopted as shown in section 6.6, and was maintained constant for the all the simulations conducted with different DEMs.

The study showed that the choice of DEM could make a significant impact on the results obtained from the TRIGRS simulation. It is worth recapitulating that the study is not to idealize the superiority and accuracy of one chosen DEM over the other. There can be several factors that can possibly affect the accuracy of the prediction; namely, the reliability of input data, the limitations imposed by simplifying assumptions, and the approximations and shortcomings in the underlying theory (Baum et al. 2008). However, based on the present study, it can be concluded that the resolution of the DEM is secondary to the accuracy of the DEM in predicting the landslide scenarios in a region, which is also reported in various earlier researches. With respect to the present study area (Guwahati region), it can be concluded that the TRIGRS predicted location of landslides based on ALOS-3D DEM, were in maximum agreement to those actually observed RVS locations. The next better agreement to the RVS landsliding locations were obtained using the CartoDEMs (1 arc sec and 1/3 arc sec). However, for the output obtained from these DEMS, the value of the True Positive Rate was considerably low, while the False Positive Rate were comparable to that obtained from ALOS-3D DEM. This is indicative that CartoDEMs wrongly predicted several RVS locations would not exhibit rainfall-induced shallow landslides, in contrary to the fact that there may be landslides actually triggered at many of those specific locations, which is never a preferable

outcome. The results obtained from ASTER-GDEM and SRTM DEM as the base maps showed the poorest agreement with the in-situ condition. This is attributed to fact that the ASTER-GDEM and SRTM DEM represents the lowest cumulative percentage of the study area in the slope angles ranging from 26º to 31º, which, in reality, is the range exhibiting highest possibility of landslides. Hence, based on the present study, ALOS-3D DEM was found to the best suitable DEM to be used for the study of rainfall-induced landslides in the municipal precinct of Guwahati, and the same is recommended for any further studies related to landslide hazards in the city.

7.5. LANDSLIDE RECURRENCE - HAZARD

TRIGRS is capable of simulating the change in slope stability condition and the landslide triggering as response to rainfall events for particular intensity and duration. Utilizing this advantage, various rainfall events are represented in terms of Intensity–Duration–Frequency (IDF) curves, selected rainfall intensity for particular duration and concerned return period are applied into TRIGRS (Salciarini *et al*., 2008). Thus, the output obtained from TRIGRS gives the landslide recurrence as a response to applied rainfall intensity representing the return period. Therefore, the landslide recurrence is quantified and landslide hazard of the study area determined. The area averaged-time series of the TRMM 3-hourly rainfall estimate and daily (24–hour) rainfall dataset for the study region, spanning from 1998 to 2016, is used for the analysis.

7.5.1. Rainfall Intensity–Duration–Frequency

An IDF curve provides the expected rainfall intensity of a given duration and having a particular frequency of occurrence. The frequency is expressed in terms of return period (T), which is referred as the average time duration between the successive rainfall events (of particular intensity and duration) that equal or exceed a particular chosen magnitude. The most common practice of developing IDF relationships is to use Gumbel's Extreme Value Type-I distribution (Apel *et al*., 2006; Devkota *et al*., 2018), and the same is adopted for the present study. The rainfall intensity for a given return period is expressed as:

$$I_T = I_{mean} + f_T \sigma \tag{7.1}$$

where, I_{mean} is the mean rainfall intensity, σ is standard deviation and f_T frequency factor for return period T is calculated as:

$$f_T = -\frac{\sqrt{6}}{\pi}\left\{0.5772 + \ln\left[\ln\left(\frac{T}{T-1}\right)\right]\right\} \quad (7.2)$$

Table 7.6 shows the maximum rainfall intensity corresponding to the duration of the rainfall event over the years from 1998 to 2015. The mean and the standard deviation of the rainfall intensity corresponding to a particular duration are shown at the bottom row of Table 7.6. Using the mean and the standard deviation in Equation 7.2, the rainfall intensity corresponding to the rainfall duration for a particular return period is obtained. Changing the frequency factor, the rainfall intensity for returns periods are obtained. The data - points are plotted in Figure 7.17 and fitted with an exponential curve. Figure 7.17 presents the rainfall intensity-duration curves of the Guwahati city region and shows the expression of the rainfall intensity corresponding to duration and the return period.

Table 7.6 Yearly Maximum Rainfall Intensity (mm/hour)

Year	Duration (hours)											
	3	6	9	12	15	18	21	24	27	30	33	36
1998	41.40	23.09	16.48	12.36	9.89	8.25	7.07	6.54	5.97	6.16	5.67	6.22
1999	21.04	12.73	8.52	6.39	5.20	4.68	4.49	4.42	4.23	4.08	4.11	3.77
2000	25.51	18.98	12.91	9.80	9.50	8.01	6.86	6.01	5.57	5.01	4.58	4.20
2001	17.40	9.63	6.59	5.66	4.67	3.89	3.48	3.15	2.80	2.52	2.44	2.58
2002	32.66	17.40	11.60	9.34	7.48	6.29	5.79	5.36	4.79	5.15	4.68	4.29
2003	35.12	22.62	16.53	14.04	11.49	10.40	9.77	8.68	7.71	7.13	7.40	7.15
2004	37.53	22.82	19.53	17.23	14.06	12.49	11.17	10.01	9.41	8.77	8.40	8.35
2005	25.38	12.89	10.95	10.07	9.28	7.73	6.72	5.98	5.49	5.04	4.70	4.53
2006	36.16	18.08	12.05	9.04	7.23	6.03	5.17	4.52	4.02	3.62	3.29	3.03
2007	43.99	25.42	17.67	14.86	12.33	10.27	8.80	7.95	7.50	6.75	6.13	5.62
2008	19.75	12.68	8.45	7.43	5.94	5.00	5.15	4.60	4.09	3.68	3.35	3.07
2009	27.06	18.82	14.31	11.26	9.01	7.51	6.43	5.63	5.00	4.51	4.12	3.79
2010	34.84	17.53	11.69	8.77	7.01	5.84	5.32	5.53	5.63	5.09	4.63	4.24
2011	22.93	13.45	9.37	8.07	6.87	5.96	5.17	4.83	5.18	5.18	5.15	5.05
2012	18.52	13.13	10.44	8.90	7.12	6.16	6.24	5.46	4.99	5.02	5.06	4.67
2013	17.68	10.20	7.11	6.36	6.00	5.77	4.94	4.32	4.03	3.63	4.13	4.17
2014	25.41	15.53	14.67	14.68	13.94	12.45	10.95	9.87	9.54	9.35	8.96	8.37
2015	35.22	18.07	12.47	10.49	9.07	7.92	7.44	6.51	5.79	5.21	4.79	4.97
I_{mean}	28.76	16.84	12.30	10.26	8.67	7.48	6.72	6.08	5.65	5.33	5.09	4.89
σ	8.49	4.65	3.68	3.25	2.82	2.51	2.18	1.92	1.83	1.77	1.71	1.68

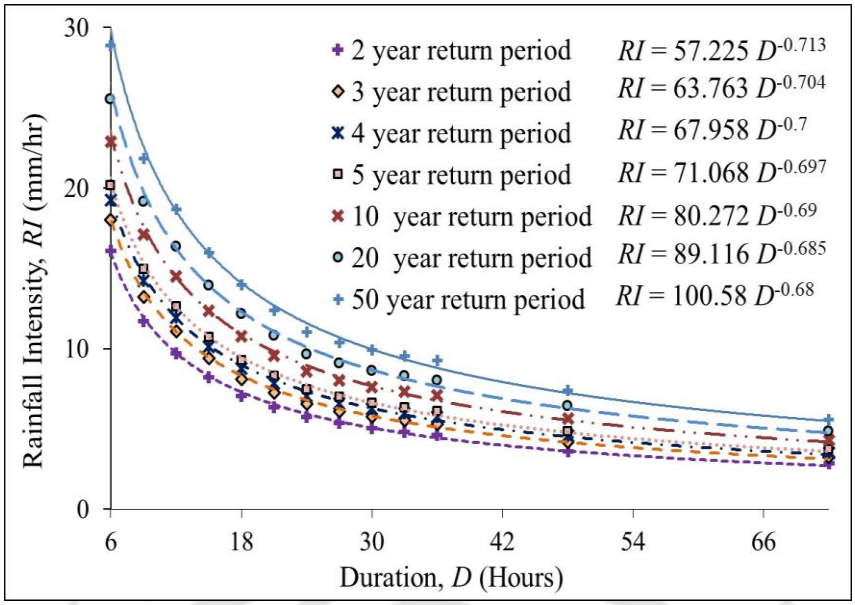

Figure 7.17 Rainfall Intensity–Duration–Frequency (IDF) curve for Guwahati region

Based on seven different durations and return periods of rainfall, Table 7.7 lists the forty-nine different intensities of rainfall (mm/hr) that are selected for the present study to be implemented into the TRIGRS model. The applied rainfall intensity is considered constant for the particular duration. As the dataset comprises area-averaged rainfall magnitudes, the applied rainfall intensity is assumed uniform over the entire study area.

Table 7.7 Rainfall intensity corresponding to rainfall duration and return period selected for applying in the TRIGRS model

Rainfall intensity (mm/hr) corresponding to -		**Return period in years**						
		3	**4**	**5**	**10**	**20**	**50**	**100**
Duration of a single rainfall event (hours)	**6**	18.1	19.4	20.4	23.3	26.1	29.7	32.5
	12	11.1	11.9	12.6	14.5	16.2	18.6	20.3
	24	6.8	7.3	7.8	9.0	10.1	11.6	12.7
	36	5.1	5.5	5.8	6.8	7.7	8.8	9.6
	48	4.2	4.5	4.8	5.6	6.3	7.2	7.9
	60	3.6	3.9	4.1	4.8	5.4	6.2	6.8
	72	3.1	3.4	3.6	4.2	4.8	5.5	6.0

Based on the selected rainfall intensities, 49 *FoS* maps were obtained that represented the stability of the hillslopes of Guwahati region for the corresponding rainfall durations and return periods. The *FoS* magnitudes at all the RVS – points were subsequently extracted and their conglomerated average, maximum and minimum magnitudes were plotted against the return period, as shown in Figure 7.18.

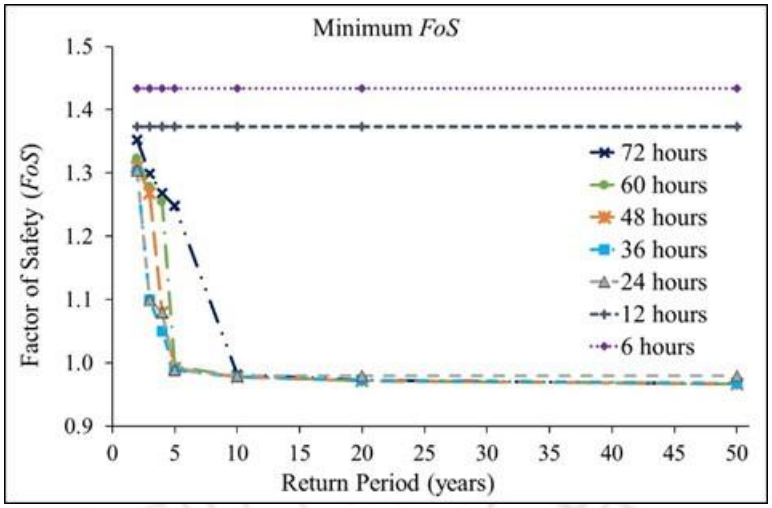

(a)

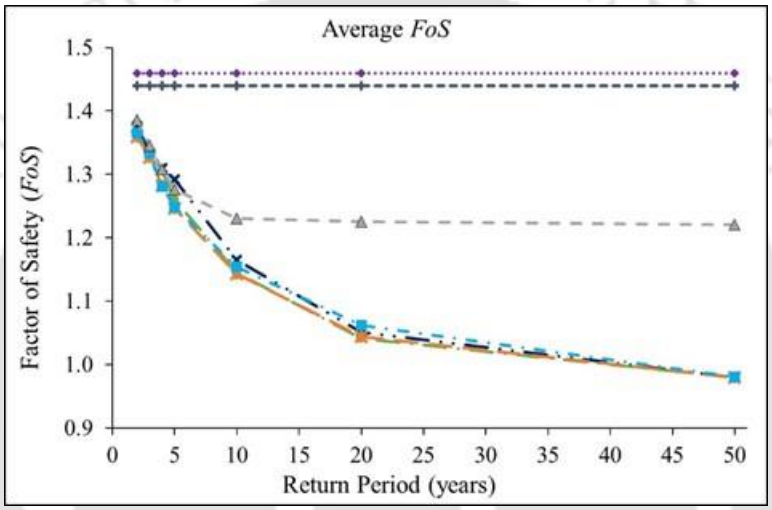

(b)

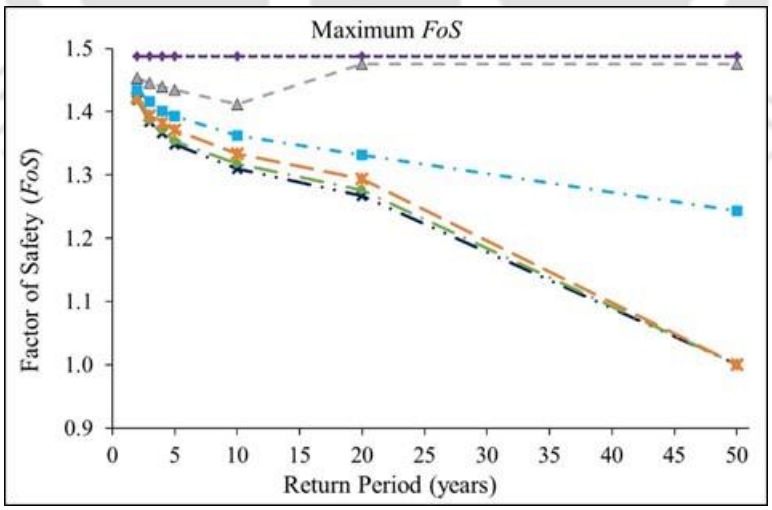

(c)

Figure 7.18 (a) Minimum, (b) Average and (c) Maximum FoS across the RVS-points with increasing return period

From Figure 7.18(b), it can be observed that for any return period greater than 20 years, as highlighted by the low average of FoS across the RVS-points, a significant area of

the region is susceptible to landslides. Irrespective of the rainfall intensity, shorter duration rainfall (< 24 hours) does not instill any recognizable effect on the stability of the slopes. Such response is attributed to the fact that under such conditions, a major portion of the rainwater is lost as runoff and the infiltrated portion is not adequate enough to raise the level of ground water to trigger landslides. Considering a return period of 40 years, the average FoS of the hillslopes drops below 1.0, indicative of widespread landslides across the hillslopes of Guwahati region. The difference in the maximum and minimum FoS indicates that some areas are highly prone to landslides. As governed by the exponential relationship between slope angle and residual soil cover, a higher slope angle automatically results in lesser thickness of overburden soil, thereby requiring lesser amount of infiltrated water to raise the ground water level. On the other hand, larger upslope catchment area results in higher volumes of runoff water draining in to a lower elevation. The gully regions, having higher slope angles and larger upslope catchment area, are very much prone to landslides, and are characterized by minimum magnitudes of FoS. From Figure 7.18 it can be inferred that, there are certain areas where the return period of landslide recurrence is observed to be as narrow as 4 years, while extensive landslide occurrences can be expected in the hillslopes of Guwahati city over a return period of 50 years. The duration of a rainfall event has a significant effect on the slope stability. Controlled by the moderate to low permeability of the hill slope soils, it is observed that landslides in Guwahati region is mostly triggered by longer duration rainfall. This is attributed to the fact that such longer duration rainfalls lead to enough infiltration of rain water within the soil, thereby raising the ground water table to a sufficient extent to trigger landslide. The critical rainfall intensity can be considered approximately equal to the saturated permeability of the soil. If the rainfall intensity is significantly lower than the critical intensity, the infiltrated water flows out through the soil as basal flux, and the ground water level does not rise. As the rainfall intensity increases to the critical magnitude, the rate of infiltration exceeds the rate of basal flux and as a result, the water accumulates within the soil domain leading to a rise in the ground water table. Finally, beyond the critical rainfall intensity, the rate of infiltration remains constant approximately at the saturated permeability of the soil, while the excess rainwater is lost as runoff.

7.5.2. Landslide Hazard Map

Presenting FoS maps for each and every rainfall scenario is not practically feasible, and, thus, all the results are combined to produce a landslide hazard map. Figure 7.19 depicts the Landslide Hazard Map of Guwahati city that highlights the return period of rainfall-

induced landslide occurrences in the study region. As a response to the rainfall intensity and duration corresponding to 4 years return period, the locations in the study region having the predicted FoS less than 1.0 are marked as areas of similar recurrence return period of landslide occurrences. With increasing return period (for example, 5 years), the rainfall intensities increase and, accordingly, the areal extent highlighting FoS<1 also increases. Compared to the areal extent corresponding to the preceding return period, the additional locations of landslide occurrences are marked as landslide areas for the successive return period (5 years in this case). Based on the same approach, the landslide recurrences for various ranges of return period were predicted and presented in the form of landslide hazard map, thereby indicating the locations of probable landslides in terms of the chosen return period.

As shown in section 6.7 the magnitude of TPR and FPR are obtained for various return periods and exhibited in Figure 7.20. The rates for the 2012 rainfall induced landslide event is included in the plot as well. It can be noted that for the rainfall events up to 4-year return period, there were no occurrences of landslide and thus the point is located at the origin of the plot. As the return period increases, larger extent of the region become susceptible to landslides (represented by FoS < 1.0), leading to an increase in the TPR. For a 50-year return period, all the RVS – points match with the TRIGRS prediction of FoS < 1.0, and accordingly the TPR reaches the magnitude of 1.0. It is observed that the results fall on the better side of the ROC plot (TPR > FPR), thereby indicating a very satisfactory prediction of landslide occurrences from TRIGRS simulations against the actual in-situ occurrence of the phenomenon. As can be observed from Figure 7.20, the extent of the areas characterized to be unstable (FoS < 1.0) progressively increases with the increase in the rainfall return period, providing enhanced agreement between the known (RVS-points) and predicted locations of landslides (TRIGRS simulations predicting FoS<1.0). However, at the same time, the rate of false alarm (i.e. the FPR) also increases owing to the greater number of grid cells being marked as unstable where the actual RVS points are not located (which may be due to insufficient field reconnaissance and survey). It can be intuitively perceived that the model output with more false alarms (relatively higher FPR) is better than the underestimated results, since, in many cases, the probable occurrences of landslides may lead to catastrophic situation rather than a mere scientific exercise, and it is better to be prepared with a prediction rather than facing it in reality.

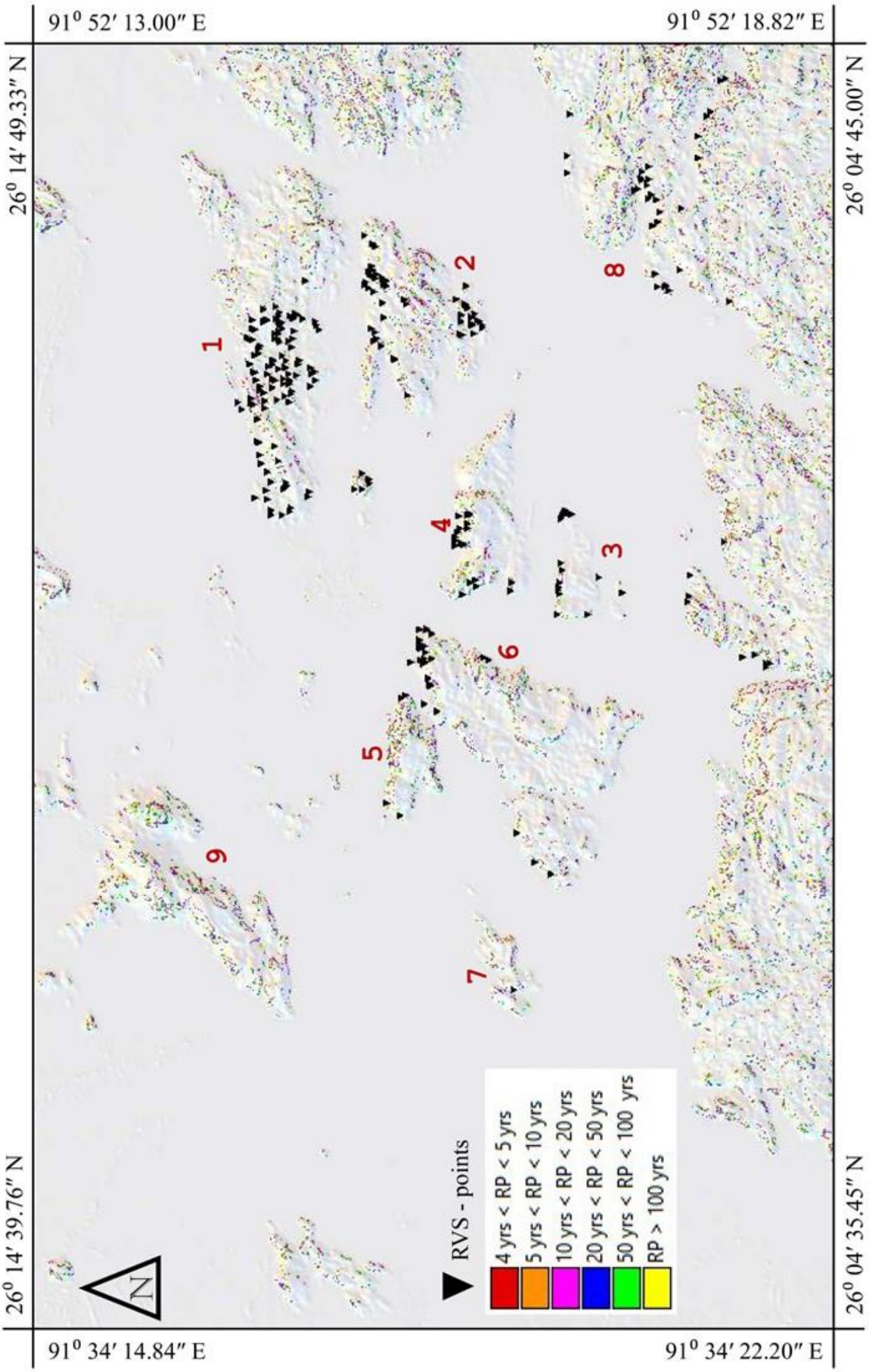

Figure 7.19 Landslide Hazard Map of Guwahati city

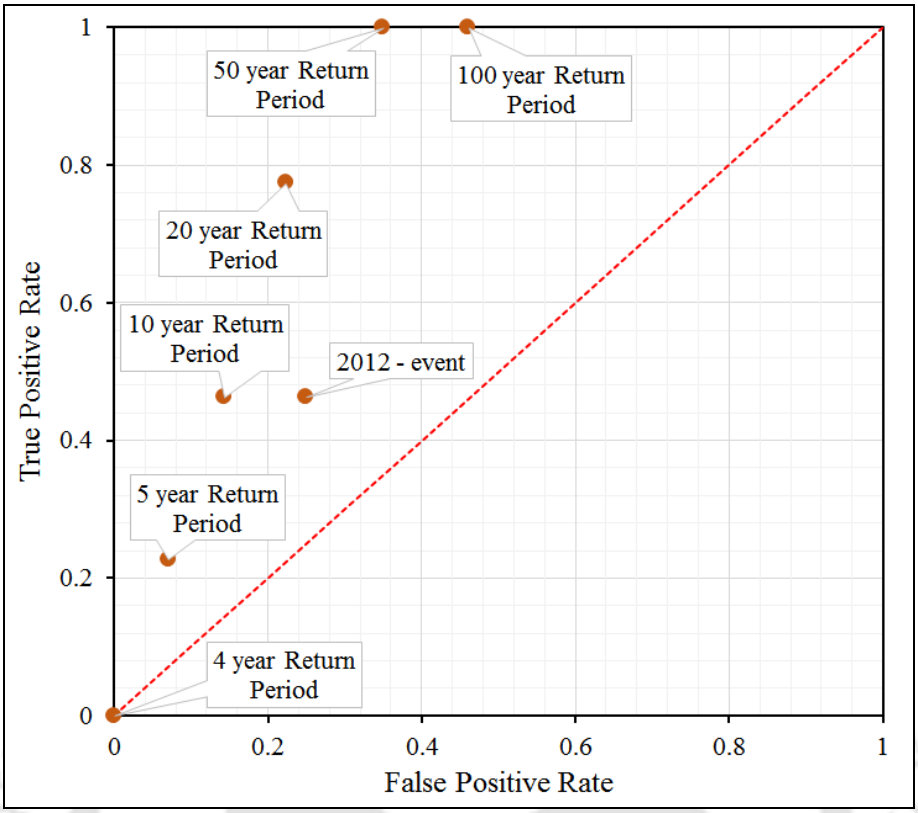

Figure 7.20 ROC for the TRIGRS simulation results for various rainfall-event return periods

The results of LR_{class} are presented in Table 7.8 for the TRIGRS simulation results corresponding to rainfall return periods and compared with that of the June 2012 event. From observation of the '% of predicted area excluding the Stable areas' along with the '% of predicted area considering the entire study area' it can be noted, that for the rainfall events up to 4-year return period, 0 % area were simulated to be under the FoS < 1.0 class, indicative of stable hills slopes all throughout the study area. With increasing return period, the rainfall intensity increases for a particular duration, leading to more infiltration and destabilization of the previously stable slopes, and with that the area under FoS < 1.0 class increases. The '% of predicted area considering the entire study area' increases from 0% for a 4-year return period to 3.2% for 100-year return period. The other point to observe is that with increase in return period, the FoS at RVS-points decreases. The FoS was higher than 1.0 at all of the RVS-point location considering a 4-year return period rainfall, while for a rainfall event with 50-year return period, 346 points out of the total 347 points moves into the FoS<1.0 class, which is also aptly reflected in the ROC plot. The percentage of LR_{class} also increases up to 99.2% for a 50-year return period indicating good prediction rate by the TRIGRS simulations.

Table 7.8 LR_{class} evaluation of the TRIGRS model results for the simulation with rainfall of June 2012

Rainfall Return Periods / Factor of Safety classes	Landslide (RVS-point) locations (*a*)							% of the sites (*b*) = 100 × (*a*)/347						
	4 year	5 year	10 year	June, 2012	20 year	50 year	100 year	4 year	5 year	10 year	June, 2012	20 year	50 year	100 year
FoS < 1.0	0	79	161	161	268	346	346	0.0	22.8	46.4	46.4	77.2	99.6	99.6
1.0 ≤ FoS < 1.1	39	43	49	55	31	1	1	11.2	12.4	14.1	15.9	8.9	0.4	0.4
1.1 ≤ FoS < 1.2	51	46	56	60	21	0	0	14.7	13.3	16.1	17.3	6.1	0	0
1.2 ≤ FoS < 1.3	72	125	57	71	27	0	0	20.7	36.0	16.4	20.5	7.8	0	0
1.3 ≤ FoS < 1.4	161	54	24	0	0	0	0	46.4	15.6	6.9	0	0	0	0
1.4 ≤ FoS < 1.5	24	0	0	0	0	0	0	6.9	0	0	0	0	0	0
1.5 ≤ FoS < 1.7	0	0	0	0	0	0	0	0	0	0	0	0	0	0
1.7 ≤ FoS < 2.0	0	0	0	0	0	0	0	0	0	0	0	0	0	0
Stable	0	0	0	0	0	0	0	0	0	0	0	0	0	0
	% of predicted area (*c*) [excluding the stable area]							% of predicted area [considering the entire study area]						
FoS < 1.0	0.0	1.2	5.6	9.3	8.7	13.2	16.4	0.0	0.2	1.1	1.8	1.7	2.6	3.2
1.0 ≤ FoS < 1.1	3.8	4.2	4.9	5.5	5.7	6.4	7.9	0.7	0.8	1.0	1.1	1.1	1.3	1.6
1.1 ≤ FoS < 1.2	6.3	6.7	5.9	2.7	5.6	5.2	4.5	1.2	1.3	1.2	0.5	1.1	1.0	0.9
1.2 ≤ FoS < 1.3	7.3	7.2	8.4	9.8	8.8	7.3	6.3	1.4	1.4	1.6	1.9	1.7	1.4	1.2
1.3 ≤ FoS < 1.4	13.1	12.5	10.3	10.2	8.4	7.8	6.7	2.6	2.5	2.0	2.0	1.7	1.5	1.3
1.4 ≤ FoS < 1.5	9.7	9.9	9.4	12.6	10.1	10.7	10.1	1.9	2.0	1.9	2.5	2.0	2.1	2.0
1.5 ≤ FoS < 1.7	23.6	21.4	20.3	23.2	18.3	15.8	15.5	4.6	4.2	4.0	4.6	3.6	3.1	3.0
1.7 ≤ FoS < 2.0	36.2	36.9	35.3	26.6	34.5	33.6	32.7	7.1	7.3	6.9	5.2	6.8	6.6	6.4
Stable								80.3	80.3	80.3	80.3	80.3	80.3	80.3
	LR_{class} (*d*) = *b*/*c*							% of LR_{class} = 100 × *d*/*e*						
FoS < 1.0	0.0	18.9	8.3	5.0	8.9	7.6	6.1	0.0	62.8	50.3	30.4	71.5	99.2	99.2
1.0 ≤ FoS < 1.1	3.0	3.0	2.9	2.9	1.6	0.1	0	23.9	9.9	17.3	17.7	12.7	0.8	0.8
1.1 ≤ FoS < 1.2	2.3	2.0	2.7	6.4	1.1	0	0	18.9	6.6	16.4	39.1	8.7	0	0
1.2 ≤ FoS < 1.3	2.8	5.0	2.0	2.1	0.9	0	0	23.0	16.6	11.9	12.7	7.1	0	0
1.3 ≤ FoS < 1.4	3.5	1.2	0.7	0	0	0	0	28.5	4.1	4.1	0	0	0	0
1.4 ≤ FoS < 1.5	0.7	0	0	0	0	0	0	5.7	0	0	0	0	0	0
1.5 ≤ FoS < 1.7	0	0	0	0	0	0	0	0	0	0	0	0	0	0
1.7 ≤ FoS < 2.0	0	0	0	0	0	0	0	0	0	0	0	0	0	0
Sum (*e*)	12.4	30.1	16.6	16.4	12.5	7.6	6.1	100	100	100	100	100	100	100

7.5.3. Remarks

The study presented herein highlights the effectiveness of physically based TRIGRS model towards the predictability of spatiotemporal rainfall induced landslide occurrences in the hills of Guwahati city, thereby addressing regional landslide hazard assessment. Based on the TRMM dataset, the rainfall IDF curves for Guwahati city were developed. The rainfall intensities, represented by its duration and return period, were applied into TRIGRS simulation to assess the scenario of landslide recurrences. The results of all the rainfall scenarios were combined to form the landslide hazard map of Guwahati city. The efficiency of the TRIGRS simulations were assessed through the ROC plot, which indicated the TRIGRS predictions of rainfall-induced landslides for various return periods to be located on the better side of the plot, i.e. TPR > FPR. A very narrow return period of 4 years did not trigger landslides (as indicated by its location in the origin of the ROC plot), while a 50-year return period highlighted a likely widespread occurrence of landslides across the region.

7.6. EFFECT OF THE RAINFALL PATTERN

Considering the duration of rainfall events capable of triggering landslides, it can be inferred that the intensity of the rainfall does not remain constant over the entire duration as is deliberated in the analysis. Therefore, the question arises that whether the trend of rainfall or the pattern of rainfall over such a duration have an effect on the landslide occurrence.

So, to check the effect of the rainfall pattern on the landslide triggering, two rainfall events reflecting the rainfall intensity and duration prevalent within the study region is chosen. Figure 7.21 shows a cumulative rainfall of 400 mm distributed over 5 days, being applied in increasing intensity (I-RP), constant intensity over the duration (C-RP) and decreasing intensity (D-RP). Figure 7.22 shows the degradation in the stability condition of the slope, in the form of decreasing FoS as response to I-RP, C-RP and D-RP.

Average FoS shown in the Figure 7.22 represents the average; across the RVS point locations or cells for each of the time step as shown in the x-axis. The maximum and minimum FoS evaluated at the locations are also plotted in the form of the strip demarcating the distribution of FoS in these locations.

By comparing the FoS response from the three rainfall patterns, it can be easily observed that the rainfall pattern makes a significant variation in the FoS distribution over the region. The average FoS drops below 1.0 indicating widespread landsliding for the rainfall event of increasing rainfall intensity. While for the same amount of cumulative rainfall when

applied constant throughout the duration, considering the average rainfall intensity gives a significantly different output and landslide is predicted in the most susceptible areas only. While if the rainfall unfolds in a decreasing trend, the FoS falls to a low value but then with time the slope stabilizes.

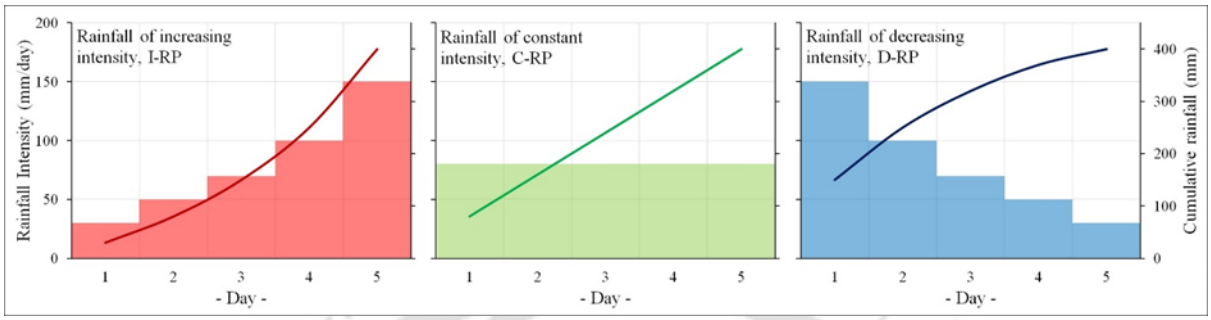

Figure 7.21 Rainfall pattern for cumulative rainfall of 400mm distributed over 5 days; area plot shows the rainfall intensity (mm/day) applied in TRIGRS simulation while the line plot shows the cumulative rainfall (mm) over the duration

To explain this phenomenon, it is required to look into the characteristic behavior of unsaturated soil. The soil water characteristic has a significant effect on the hydraulic conductivity and soil shear strength. It is a well-established fact that the hydraulic conductivity of partially saturated soil is a function of the matric suction within the soil, which in turn is a function of the volumetric water content of the soil. Figure 6.9 shows the soil water characteristics curve applied in the analysis and the corresponding unsaturated hydraulic conductivity curve. As can be observed from the figure the unsaturated hydraulic conductivity is highly sensitive to the soil moisture and can vary by an order for change in volumetric water content of only 0.1.

Figure 7.23 shows the variation in rate of infiltration at the surface of the slope for I-RP, C-RP and D-RP. As can be observed the rate of infiltration slowly increases as the soil wets with rainwater infiltration. It can be inferred that the increase in rate of infiltration is dependent more on the soil parameter namely the SWCC and the UHCC than the intensity of rainfall, but. Thus, in the first two days, the loss of water as runoff has been maximum for D-RP followed by C-RP and least for I-RP. On the third and fourth day, the soil is wetted enough but there is not enough rain intensity for D-RP and C-RP. However, the situation is opposite for the case of I-RP. With time, the saturation and permeability of the soil increases with the rainfall intensity, thus allowing more water to be infiltrated into the soil slope. The loss of rainwater as runoff has been the minimum, and therefore the ground water table rises to such a level to be able to trigger landslide contrary to that of C-RP and D-RP.

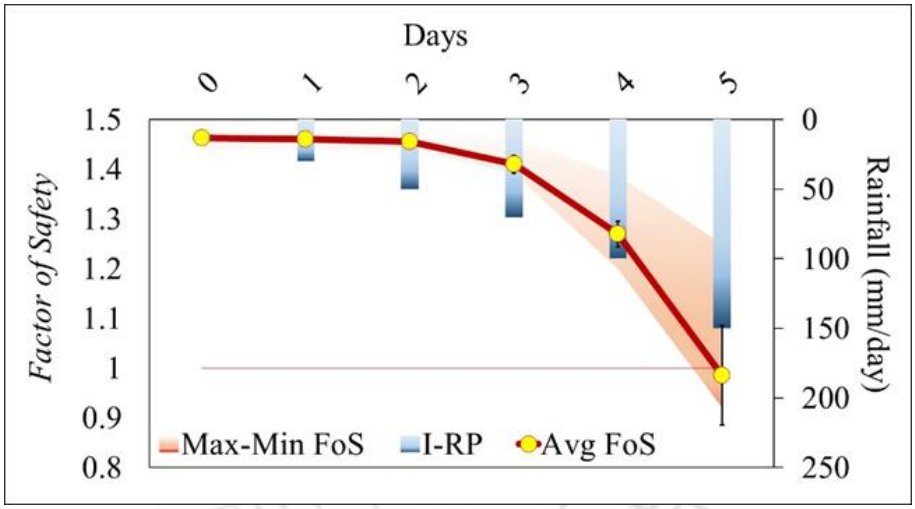

(a)

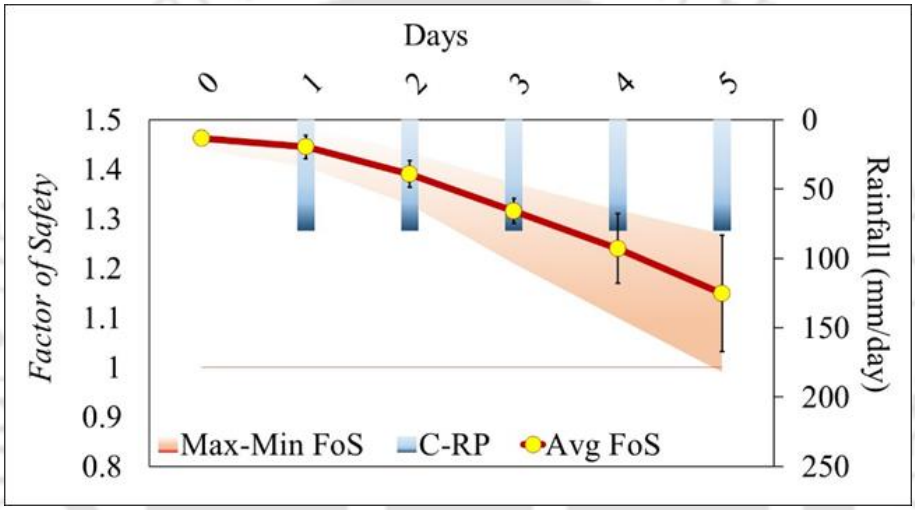

(b)

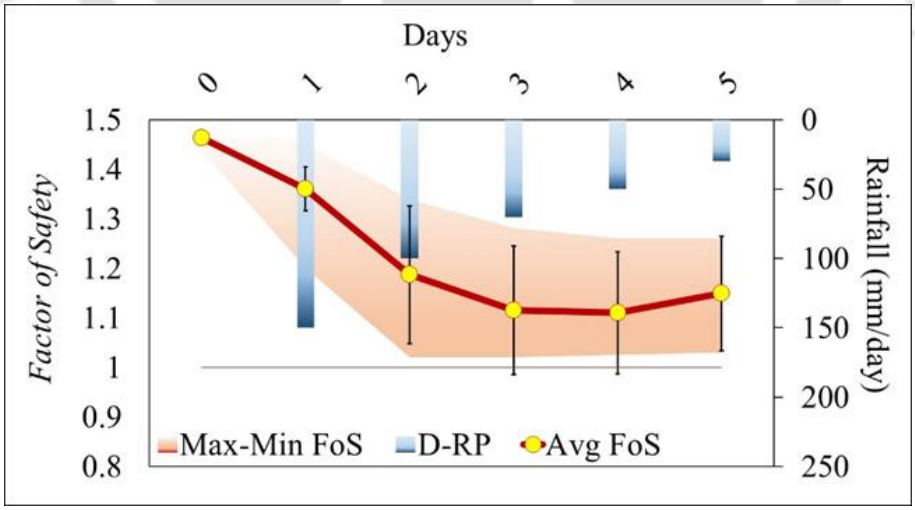

(c)

Figure 7.22 FoS of the RVS points as response to rainfall event (a) I-RP; (b) C-RP; (c) D-RP

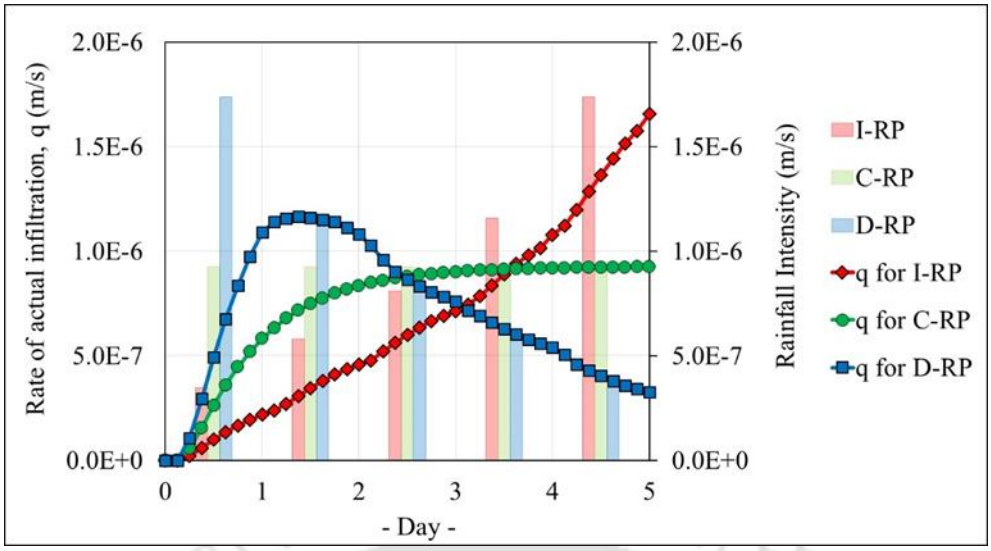

Figure 7.23 Actual rate of infiltration through slope surface for I-RP, C-RP and D-RP

Figure 7.24 shows the development of pore pressure and the reduction of FoS with time along the failure plane, as a response to rainfall patterns. The trend in rise in the pore water pressure is observed as mirror image to the decrease in FoS.

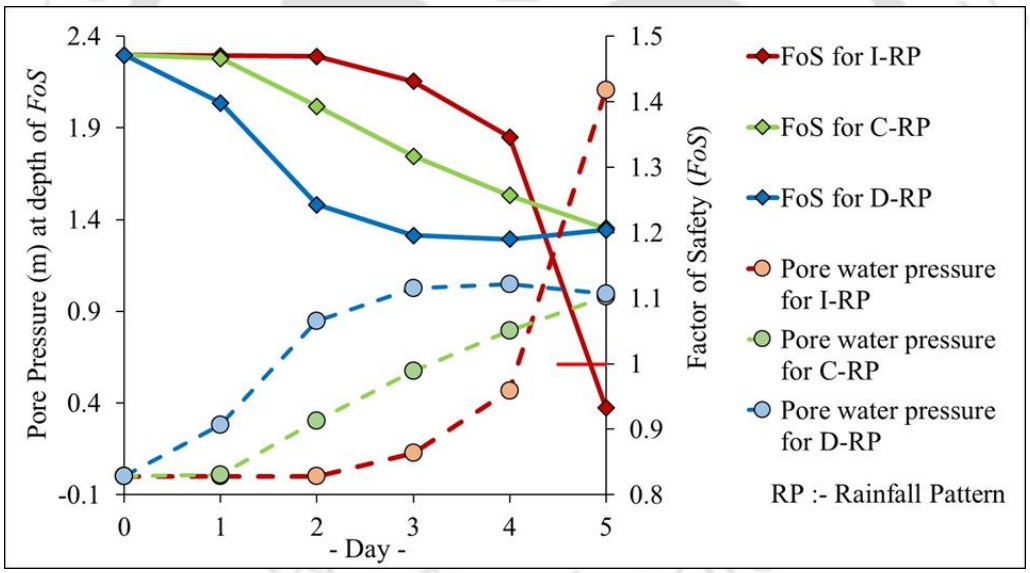

Figure 7.24 Development of pore water pressure and the reduction of FoS with time for the different rainfall patterns

7.6.1. Discussion

To analyse the effect of the rainfall pattern on the landslide triggering, a rainfall event of cumulative rainfall of 400 mm rainfall of 5-day duration was adopted and applied as three patterns each as I-RP, C-RP, D-RP respectively. It was seen, from the results of the simulation that the rainfall pattern had a significant effect on the response of the model.

Considering all the simulation results and their thorough analysis, it can be converged that the triggering of rainfall-induced landslides is subjected to the realisation of an intricate equilibrium of certain significant parameters. The parameters include rainfall intensity and duration, soil water characteristics, the unsaturated hydraulic conductivity as a function of the saturated hydraulic conductivity and soil suction (soil moisture) and the shearing resistance or shear strength of the soil.

From the above analysis, it is clearly understood that the rise of pore water pressure rising beyond a certain threshold value ultimately triggers the sliding of the soil mass. While considering a column of soil mass of a unit area, the rise in pore water pressure (or the rise in the ground water) can be considered as the water fraction retained. The relation can be expressed as: Water within the soil column at a certain time = Actual quantity of water infiltrating through the soil surface – Water flowing out through the base of the soil column at a particular moment of time.

The rate of actual infiltration at a particular instant is dependent on the hydraulic conductivity and the suction in the soil at the top, which are again functions of the soil saturation. Now at a particular instant if the rainfall intensity is greater than the rate of actual infiltration than the extra amount of water is lost as runoff. As rain wets the slope surface gradually, the hydraulic conductivity increases up to the maximum of the saturated hydraulic conductivity. Along with it, the rate of actual infiltration also increases.

Then again, the rate of basal flux or sub-surface flow that is dependent on the hydraulic head at the basal layers of the soil and increases proportionately up to a certain threshold beyond which the rate then becomes constant. Therefore, as can be realised from the above inference, at a particular instant if the rate of infiltration exceeds the rate of basal outflow, there is build-up of pore water pressure and the ground water table rises. In case of the rainfall event with increasing trend in the rainfall intensity, soil hydraulic conductivity also increases simultaneously with time, as the soil slowly wets. The rainfall intensity increases and so thus the rate of actual infiltration and the loss of rainwater as runoff is the least.

In case of I-RP (rainfall with gradually increasing intensity) the rate of actual infiltration goes on increasing till the end of the rainfall event, and while on the later halves of the events the infiltration increases beyond the rate of basal outflow and the ground water table rises to such an extent as to be able to trigger landsides. While in case of D-RP (rainfall

with gradually decreasing intensity), most of the rainwater drains along the surface as runoff and by the time the soil permeability increases there is not enough rainfall intensity to be able to make the water table rise. Similarly, in the case of C-RP (rainfall with constant intensity) the rainfall intensity is not sufficient to trigger landslides. In nature, most rainfall events are of increasing pattern similar to I-RP.

7.7. SUMMARY

The study shows that it is not only rainfall intensity and duration, but also several other factors that has devastating effect on the landslide triggering. The event of June 2012 and June 1998 shows the gradual decrease in slope stability over long duration rainfall spanning 25 days and 12 days respectively and highlights the significant impact of the antecedent conditions. The event October 2004 and September 2014 shows the triggering effect of high intensity, shorter duration rainfall event.

The study showed that the DEM could make a significant impact on the results obtained from the TRIGRS simulation. The location of landslides was in maximum agreement between the simulated scenario and the observed sliding locations for ALOS-3D DEM.

To predict the landslide hazard of the Guwahati hill slopes the prevalent methodology was adopted wherein the rainfall intensity-duration-frequency (IDF) were evaluated and the landslide recurrence was simulated by the rainfall intensities of particular duration concerning a particular return period.

In case of the rainfall event with increasing trend in the rainfall intensity, soil hydraulic conductivity also increases simultaneously with time, as the soil slowly wets. The rainwater infiltration is maximum and therefore such rainfall events are able to trigger widespread landsliding.

Chapter 8. PROBABILITY OF FAILURE (*PoF*) MAP OF GUWAHATI CITY USING TRIGRS

8.1. INTRODUCTION

The analysis so far conducted, showed the gradual degradation of the stability condition of the hill slopes with rainfall infiltration. The study showed that application of physically based models could consider the hydrogeological factors such as soil characteristics, rainfall, slopes and topography of the contribution area in a quantitative manner. The methodology employed, can provide results that can assist in gaining a different perspective to the problem for Guwahati region, especially in determining areas of instability from a geotechnical viewpoint, within a GIS framework. However, the outcome of the TRIGRS simulations are significantly affected by the input parameters. As can be observed from Section 4.3 there is range of values of the various parameters as is used for input into the TRIGRS model. From the range of values of the parameters, some input values of the soil parameters have been selected which gave a sufficiently close description of the rainfall-induced landslide occurrence in the hill slope of Guwahati.

Therefore, the values of the input parameters considered for the analysis contain uncertainties. With increasing number of soil samples and laboratory tests, the representation of parameter variability over the basin can be increased; however, the description can never be made exact. This is because only a very insignificant portion of the total volume of soil can be sampled in reality, and the subsurface conditions that dictate pore water pressure evolution and material strength can never be conclusively inferred.

Probabilistic simulations offer a means for dealing with such uncertainty in a quantified manner and estimate the likelihoods of occurrence of different outcomes. Researchers previously have attempted to modify the TRIGRS code to include probabilistic analysis. Raia *et al.*, (2014), introduced the TRIGRS-P code considering a probabilistic Monte Carlo approach to the distributed modelling of rainfall-induced shallow landslides. TRIGRS-P copes with the natural variability inherent to the mechanical and hydrological properties of the slope materials by allowing values of the TRIGRS model input parameters to be sampled randomly from a given probability distribution.

However, TRIGRS-P has only two options of probability density functions (pdf) for generating the random modelling parameters, vis., the normal distribution function or the

uniform distribution function. The geotechnical and hydrological properties were treated explicitly as independent i.e., uncorrelated variables and that there is no spatial correlation of the individual variables. The researchers themselves notes that it is a simplified assumption and that in reality some dependence (correlation) as well as spatial correlation exists between the different geo-hydrological properties.

In this study, an attempt is made to run the TRIGRS simulation within the MatLab environment with Monte Carlo simulation techniques. A set of random values for the TRIGRS input parameters are generated with a MatLab code. Another MatLab code generates the input file for TRIGRS by changing the values of the input parameters one set at a time, runs the TRIGRS simulation, and stores the FoS-map. Therefore, a number of FoS-map are generated each corresponding to a particular set of values of the input parameters. A third MatLab code then reads the FoS-map, and counts the number of times the FoS drops below 1.0 at a particular cell of the grid and then calculates the Probability of Failure as the total number of times, FoS<1.0 at that cell divided by the total number of simulations in percentage. The code then generates the Probability of Failure map that is then imported into the ILWIS GIS software and is presented as is shown below.

8.2. DISTRIBUTION OF THE RANDOM PARAMETERS

For the present probabilistic analysis, the cohesion and the angle of internal friction are considered as log-normally distributed random parameters, as in nature the soil parameters in most general cases follow a lognormal distribution (Lee *et al.* 1983; Lacasse and Nadim, 1996; Baecher and Christian, 2003; Griffiths *et al.*, 2007). Using a MatLab code, random values of the soil parameters vis., the soil cohesion, angle of internal friction, saturated hydraulic permeability and the Gardner (1958) α-parameter are generated.

Figure 8.1 shows the random distribution of the cohesion parameter which is used as input the TRIGRS simulation, in the form of histogram plot. Similarly, Figure 8.2 shows the distribution of the angle of internal friction used in the analysis. Figure 8.3 and Figure 8.4 shows the random saturated hydraulic conductivity and the Gardner (1958) α parameter respectively. Figure 8.1 and Figure 8.2 shows the mode and mean of the random distribution. The data is so generated such that the mode (which is the most frequently occurring value in case of lognormal distribution) corresponds to the values used for the deterministic analysis as shown in the previous chapters. In case of the saturated hydraulic conductivity and the α-

parameter, the distribution is considered normal for simplifying the analysis, and the mean of the distribution corresponds to the values used for the deterministic analysis.

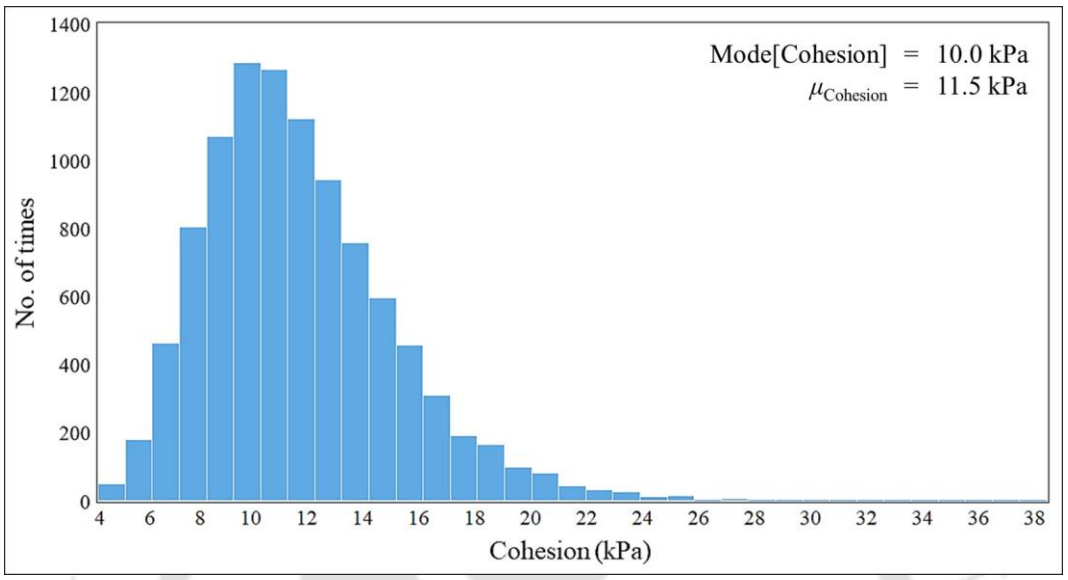

Figure 8.1 Random distribution of the soil cohesion, *c*

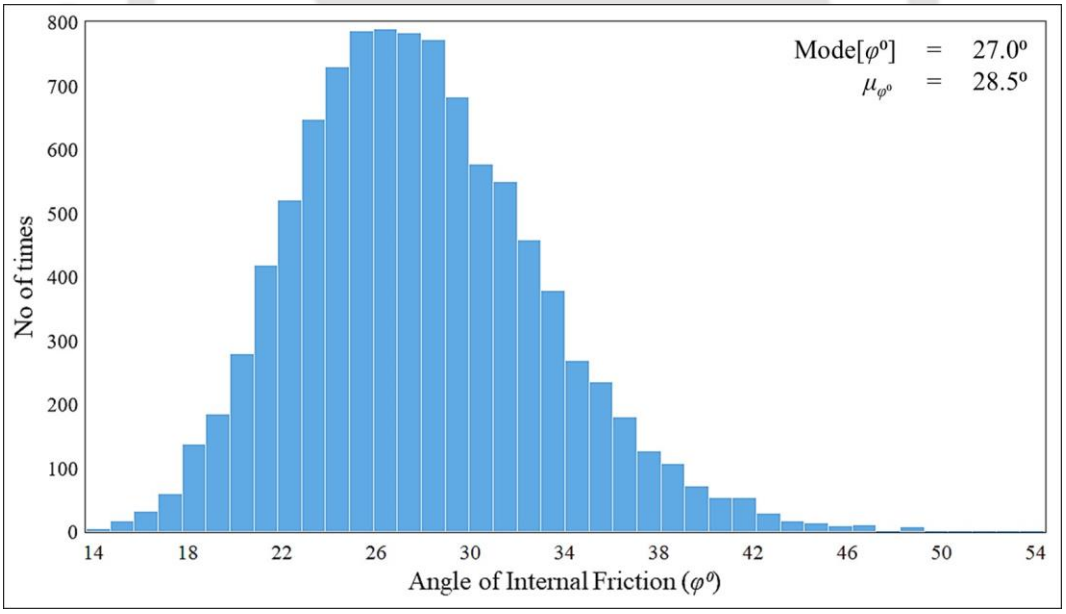

Figure 8.2 Random distribution of angle of internal friction (φ^o)

Establishing a complete cross-correlation structure between the various parameters will require significant quantity of test result data, which would require huge quantity of soil sampling and testing. Cross-correlation for the present analysis is therefore defined based on recommendation as provided in literature. For the present analysis, the cross-correlation is defined for stationary random field. The cross-correlation then reduces to the just the constant

coefficient $\rho_{c\varphi}$. Stationary point wise correlated fields can thus be described by the correlation functions $\rho_c(\tau)$ and $\rho_\varphi(\tau)$ and the cross-correlation coefficient $\rho_{c\varphi}$ (Fenton and Griffiths, 2008). The point wise covariance structure can then be expressed in matrix form as

$$\rho(\tau = 0) = \begin{bmatrix} \rho_c & \rho_{c\phi} \\ \rho_{\phi c} & \rho_\phi \end{bmatrix}$$

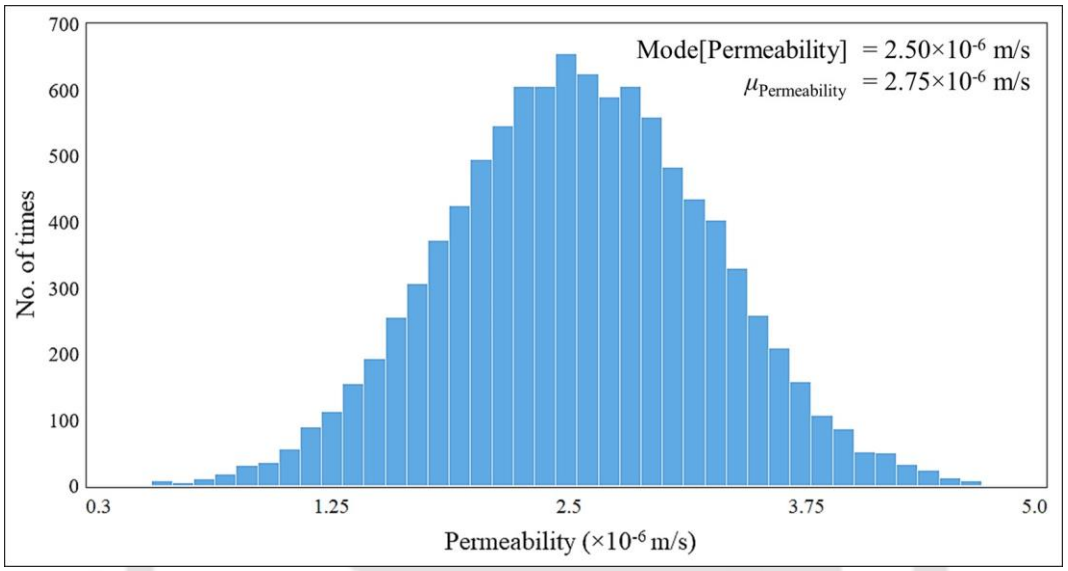

Figure 8.3 Random distribution of the saturated hydraulic conductivity

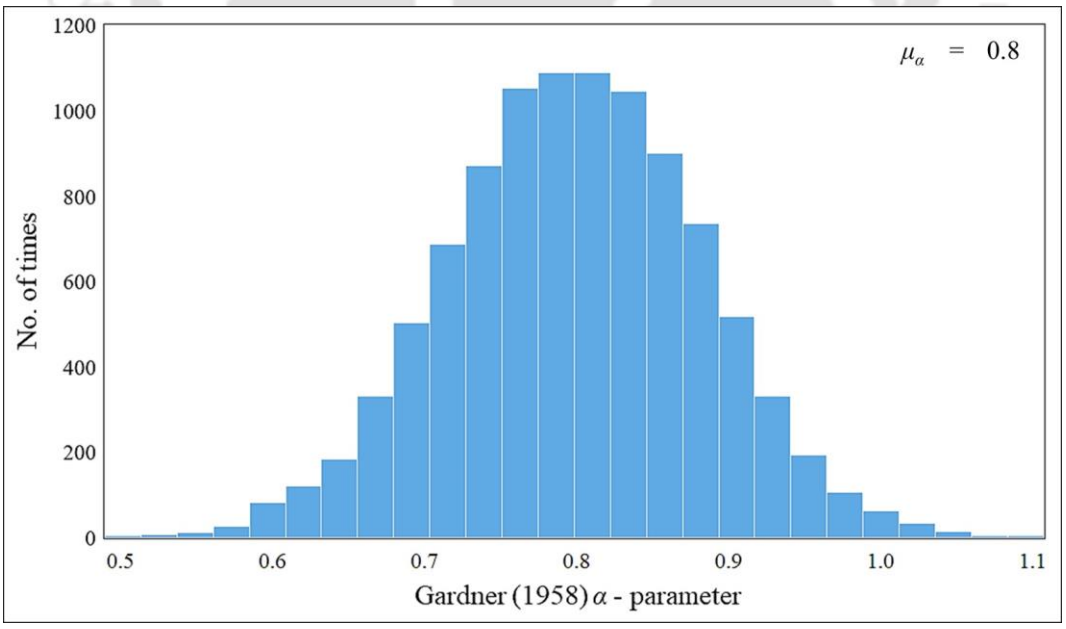

Figure 8.4 Random distribution of the Gardner (1958) α parameter

For the present analysis the cohesion and angle of internal friction is assumed to be negatively cross-correlated with a cross-correlation coefficient of -0.7, implying that high values of cohesion are associated with low values of friction angle and vice versa. Similarly, the saturated hydraulic conductivity is negatively cross-correlated to the cohesion, implying with increase in cohesion the saturated permeability decreases, while the α-parameter is positively cross-correlated to the angle of internal friction (φ) (Wolff, 1985; Cherubini, 2000; Baecher and Christian, 2003).

Figure 8.5 shows the cross-correlation of the soil cohesion to the angle of internal friction. Figure 8.6 shows the cross-correlation of the saturated hydraulic conductivity to the soil cohesion. Figure 8.7 shows the cross-correlation of the Gardner (1958) α-parameter to the angle of internal friction (φ). From Figure 8.5 the distribution of the soil cohesion can be overserved to vary randomly but within a certain range defined by the cross-correlation for a particular value of angle of internal friction (φ). Similar nature of cross-correlation can be observed from the other figures as well.

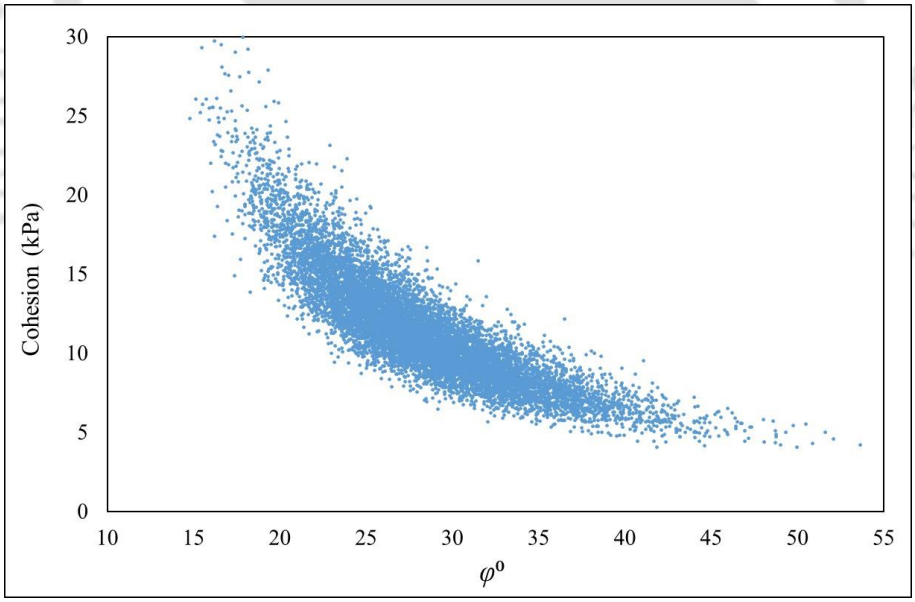

Figure 8.5 Cross-correlation of the soil cohesion (c) to the angle of internal friction (φ)

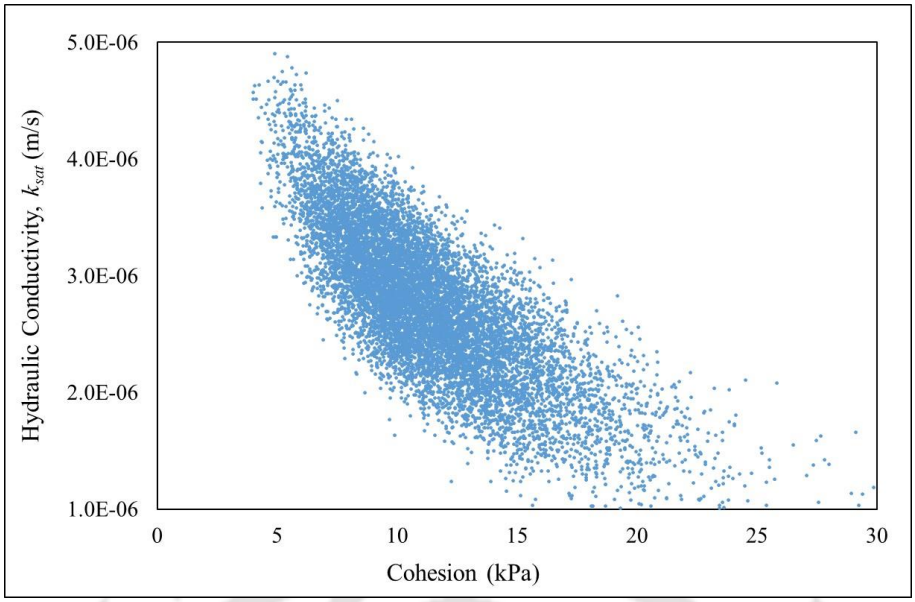

Figure 8.6 Cross-correlation of the saturated hydraulic conductivity (k_{sat}) to the soil cohesion (c)

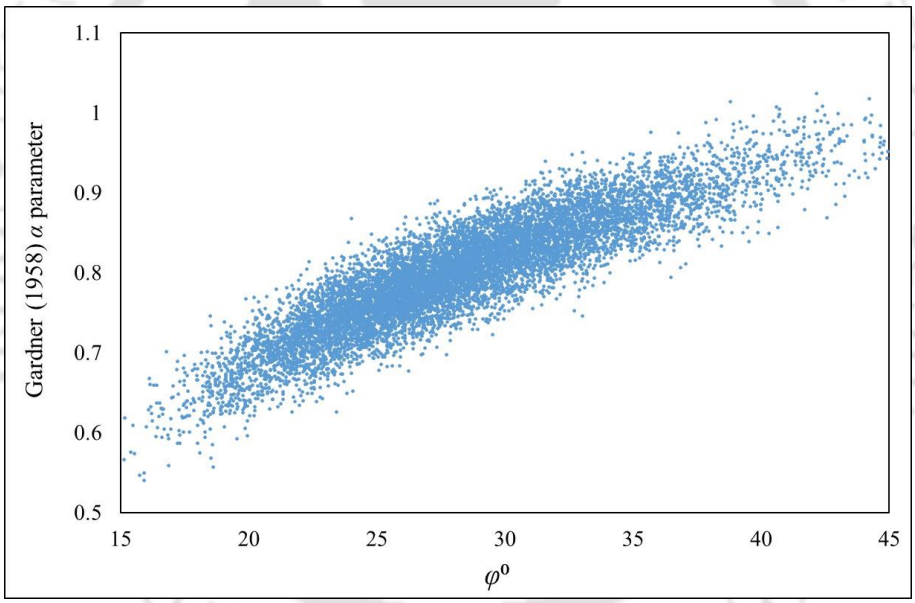

Figure 8.7 Cross-correlation of the Gardner (1958) α-parameter to the angle of internal friction (φ)

The cross-correlation are chosen based on field observation. The saturated permeability of the soil is generally observed to decrease with the soil becoming more clayey, while the capillary rise of the soil generally decreases. The shape of the SWCC shifts to more steep asymptotic shape from a smooth curve due to the increase in the α-value, with the soil becoming granular characterized by the increase in the φ value.

8.3. PROBABILITY OF FAILURE MAP

Within MatLab, the input file for TRIGRS analysis is generated each time with a new set of parameters. Subsequently, TRIGRS is executed and the FoS-map is obtained and stored. A rainfall intensity of 116 mm/day for a duration of 3 days is applied in the probabilistic TRIGRS simulations. The chosen rainfall intensity corresponds to a return period of 20 years for the specified 3 days duration. The chosen rainfall intensity is approximately equivalent to the intensity of rainfall events that have triggered landslide within the study area. For the present analysis the depth of initial ground water is considered to coincide with the soil depth (or, the depth of basal boundary), where the depth is decided as per Equation 6.28 and as shown in Figure 6.6. The soil unit weight is also considered as constant for the entire study.

Figure 8.8 shows the FoS distribution over the study area for a prefixed value assigned to the soil parameters, c = 10 kPa, φ = 27º, k_{sat} = 2.5×10-6 m/s, α = 0.8. Similarly, Figure 8.9 shows the FoS distribution considering the soil parameters as c = 13.3 kPa, φ = 19.96º, k_{sat} = 1.88×10^{-6} m/s, α = 0.67. Similarly, Figure 8.10 gives the FoS-map for c = 9.55 kPa, φ = 32.74º, k_{sat} = 3.46×10^{-6} m/s, α = 0.855, while Figure 8.11 shows the FoS-map for c = 18.04 kPa, φ = 21.32º, k_{sat} = 2.29×10^{-6} m/s, α = 0.72. In all the simulations, the rainfall intensity and duration is maintained constant as defined earlier. It can be observed that the variation of soil properties over the study area makes a significant difference to the outcome of TRIGRS simulation. Figure 8.8 and Figure 8.9 showed that slope failure should have occurred across a significant area of the hillslopes, while on the contrary Figure 8.10 and Figure 8.11 predicted stable slopes across the study area. The soil properties are therefore varied randomly to take into account the uncertainty of the slope stability condition across the hillslopes of the study area.

10,000 simulations with varying parameters is executed and subsequently 10,000 FoS-maps were obtained. The number of times the FoS drops below 1.0 at a particular cell is counted and probability of failure is calculated. Accordingly, combining all the outcomes, the probability of failure map is generated. Figure 8.12 shows the probability of failure map generated for the study area after combining all the FoS maps. Figure 8.13 shows the RVS-points overlaid on the probability of failure map.

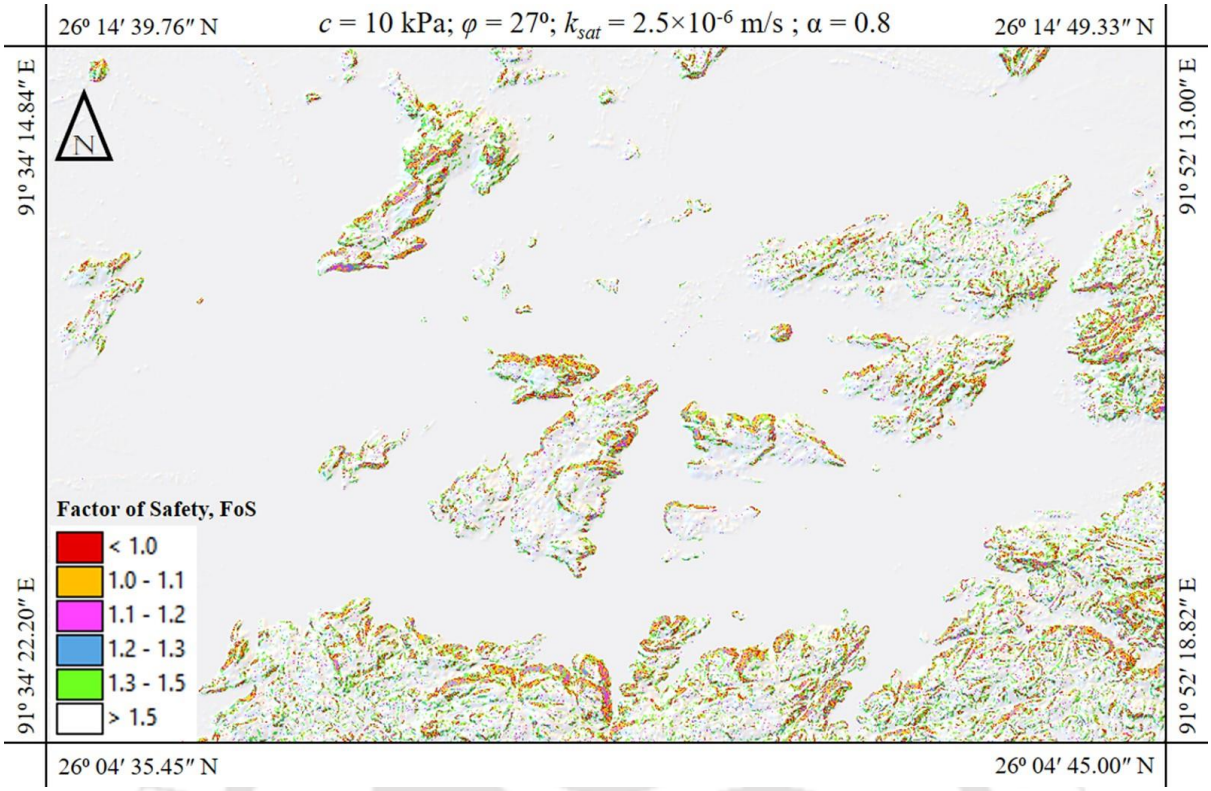

Figure 8.8 FoS–map for soil parameters, c = 10 kPa, φ = 27º, k_{sat} = 2.5×10-6 m/s, α = 0.8 for rainfall intensity of 116 mm/day applied for duration of 3 days

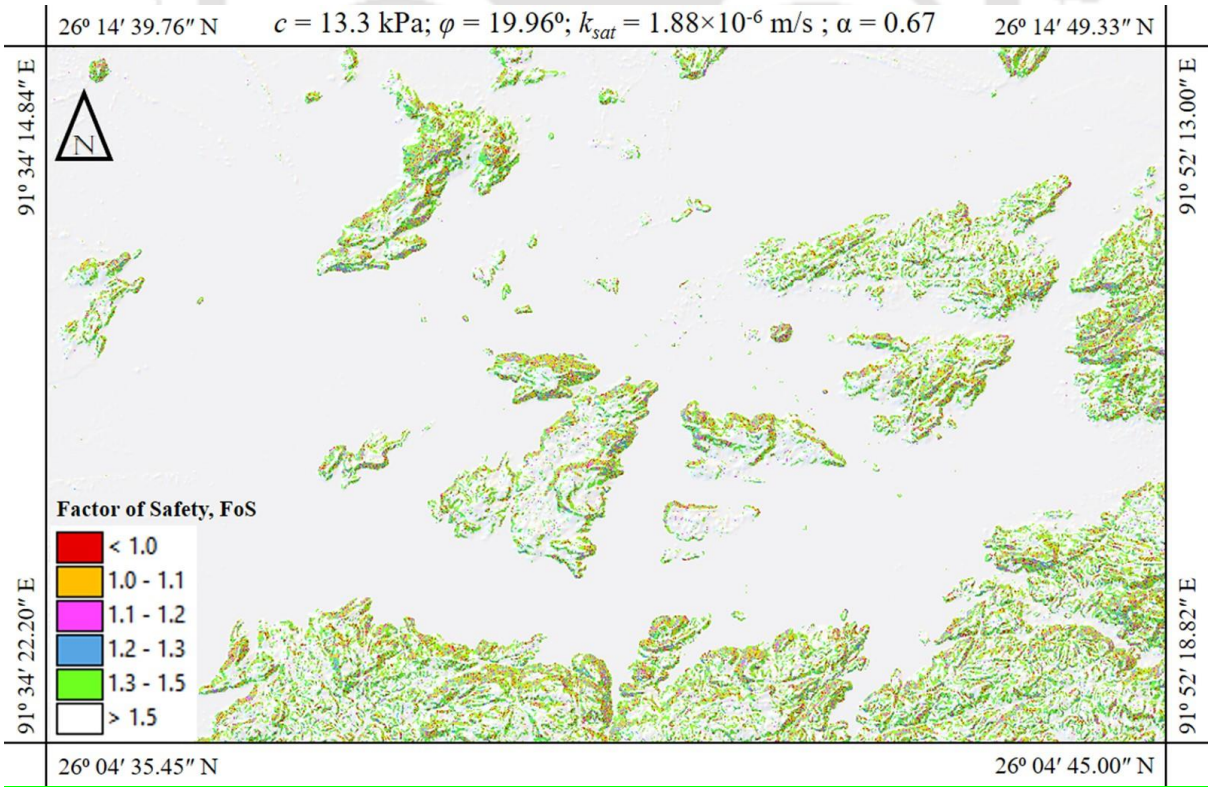

Figure 8.9 FoS–map for soil parameters, c = 13.3 kPa, φ = 19.96º, k_{sat} = 1.88×10^{-6} m/s, α = 0.67 for rainfall intensity of 116 mm/day applied for duration of 3 days

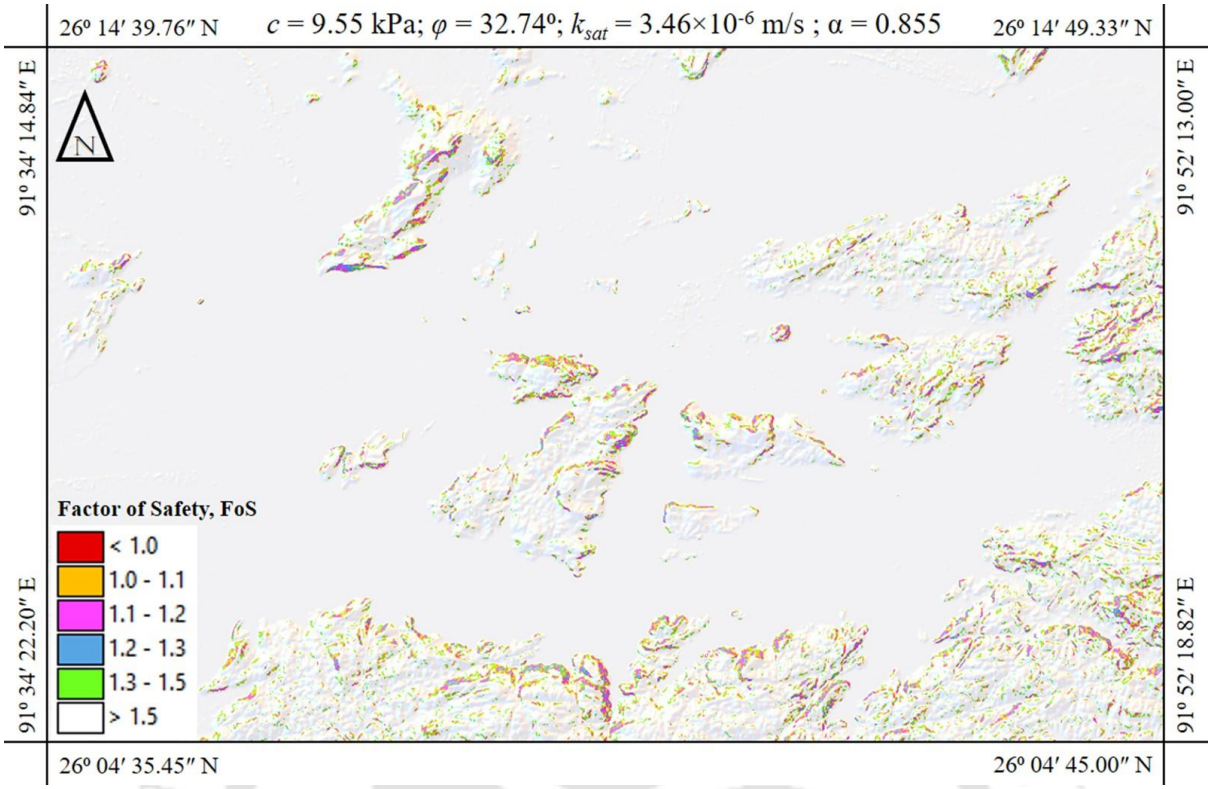

Figure 8.10 FoS–map for soil parameters, c = 9.55 kPa, φ = 32.74º, k_{sat} = 3.46×10^{-6} m/s, α = 0.855 for rainfall intensity of 116 mm/day applied for duration of 3 days

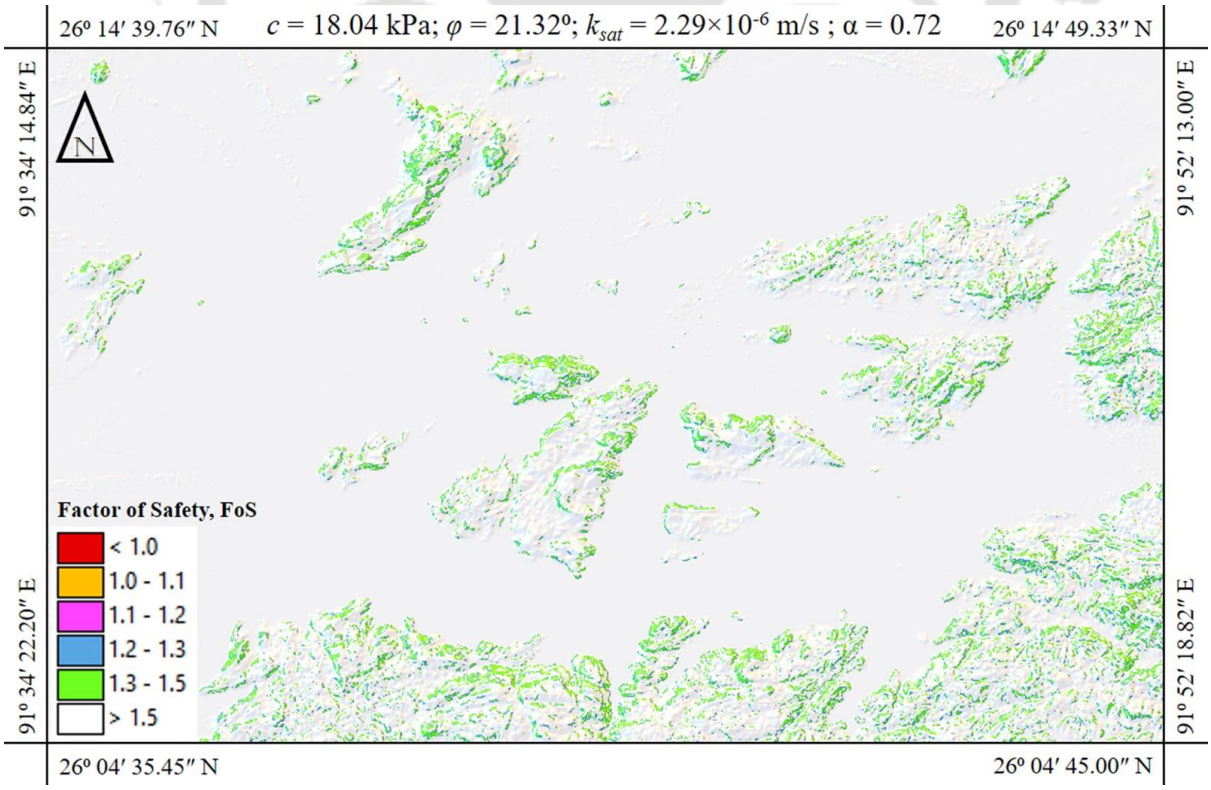

Figure 8.11 FoS–map for soil parameters, c = 18.04 kPa, φ = 21.32º, k_{sat} = 2.29×10^{-6} m/s, α = 0.72 for rainfall intensity of 116 mm/day applied for duration of 3 days

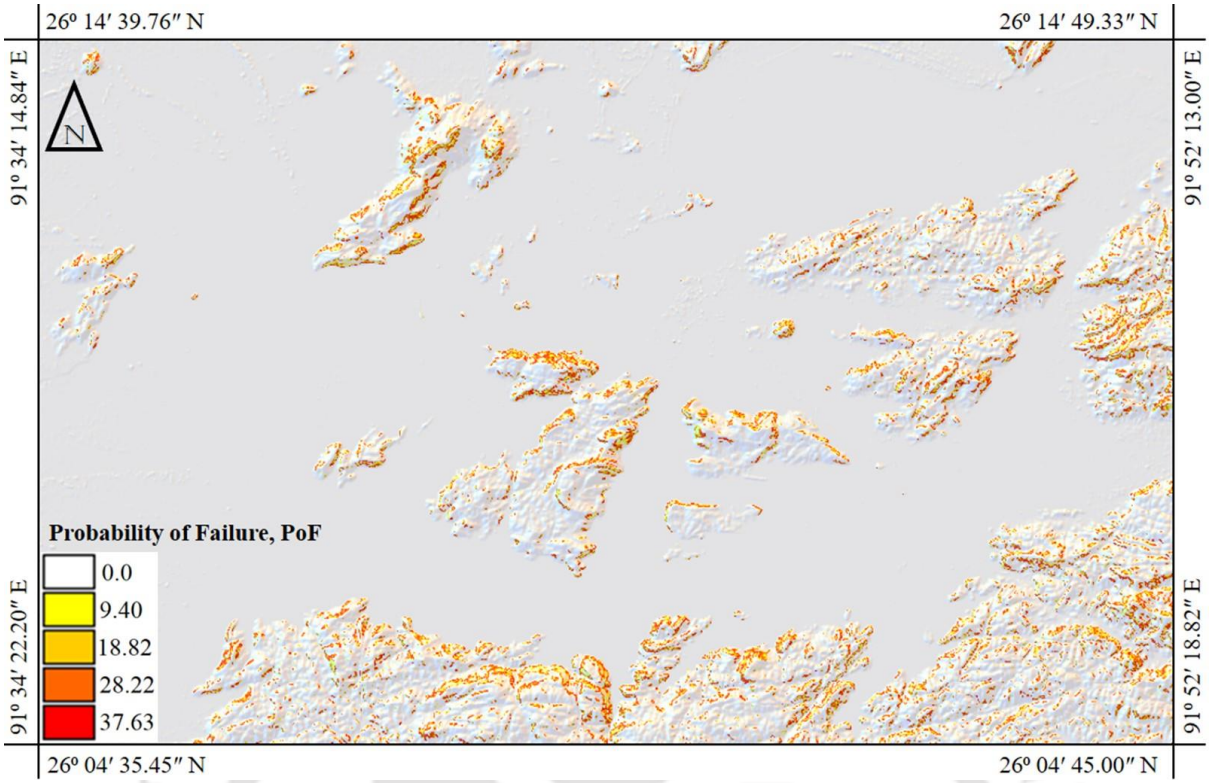

Figure 8.12 Probability of failure (PoF) map of the study area corresponding to rainfall event of 3 days duration and with return period of 20 years

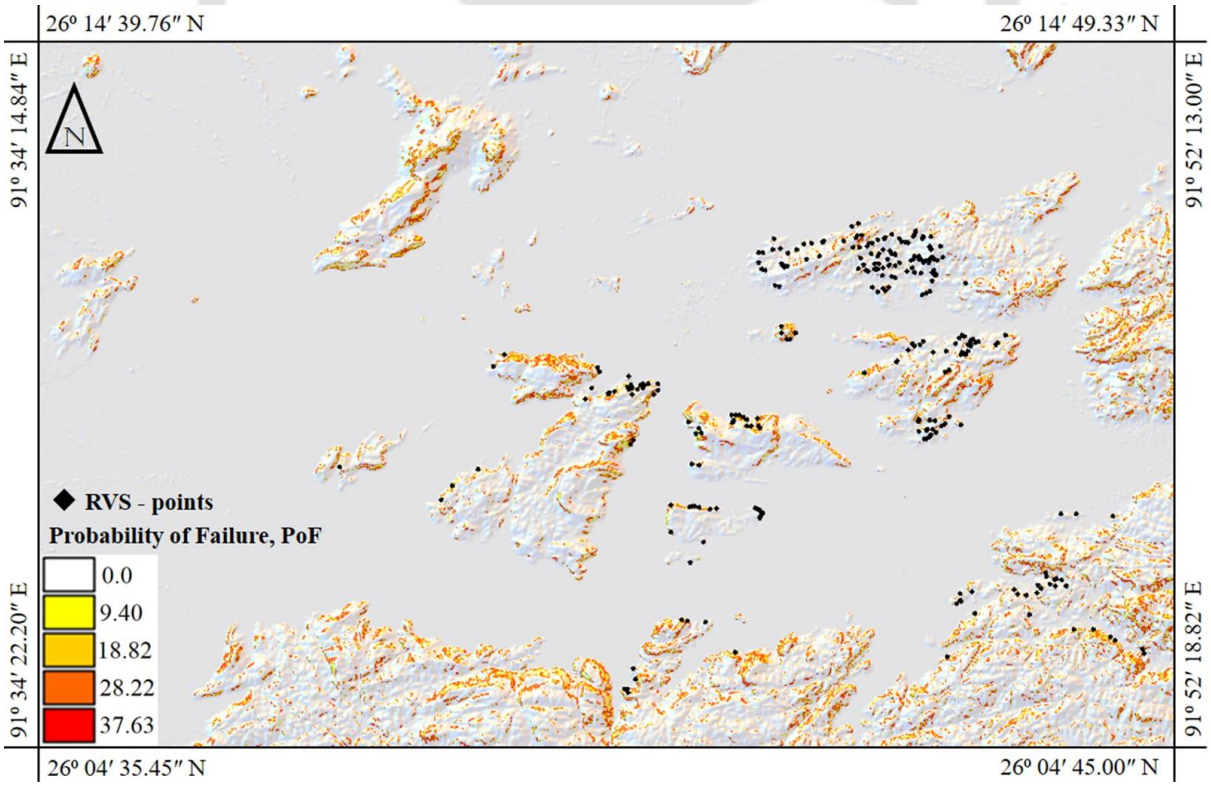

Figure 8.13 Probability of failure (PoF) map of the study area corresponding to rainfall event of 3 days duration and with return period of 20 years

The probability analysis output in the form of the probability of failure (PoF) map (Figure 8.12) showed that the maximum probability of failure of the hill slopes is around 37.63 %, i.e., out of the 10,000 simulation the FoS dropped below 1.0 from a total of 3763 times, which is significantly high number. The probability of failure ranged from 20.0–37.63 % in a major portion of the hill slope area.

It can be inferred from the PoF-map that hillslopes of the study area falls in the range of moderately stable state or marginally stable state and that minor to moderate destabilizing factors are required to cause instability. However, none of the area can be identified as unconditionally unstable i.e. no area is prone to landslides without any external causal factors. Thus, it can be concluded that the hill slopes of Guwahati region is in a very delicately balanced state of stability, and that the slightest disturbance to environment can cause catastrophic landsliding. This result can be considered a much closer approximation to reality considering the fact that anthropogenic activity has long been considered as the most potent causal factor with respect to occurrence of landslides in this region.

8.4. DISCUSSION

The probabilistic approach resulted in 10,000 number of model outputs, each representing the geographical distribution of the FoS values. Variability depends on mainly three factors vis., the natural variability in the geotechnical and hydrological properties of the soils, the inability of determining accurate values for the geotechnical and hydrological parameters, and that the models are simplified and are never capable for representing the natural (physical) conditions (Lee *et al.* 1983; Lacasse and Nadim, 1996).

The probabilistic approach allowed to take into account the combined effects of the natural variability inherent in the model parameters, and of the uncertainty associated with their definition over large areas. However, in the analysis, the other factors have been deliberately ignored, i.e., the inherent model assumption as considered in the TRIGRS model still holds.

During the analysis the probabilistic input parameters, vis., the geotechnical and hydrological properties were treated correlated variables, however the correlation were based on simplified assumption adopted from literature, only the trend of the correlation was observed from actual testing of the hill slope soils.

Results of the analysis were obtained adopting a lognormal distribution of the c and φ to describe the uncertainty. However, the methodology combining TRIGRS with MatLab can be extended to take into account any probability distribution, with any cross-correlation structure. Furthermore, in the analysis the soil depth is considered as a (non-linear) function of the local slope and constant for all probabilistic analysis. Rainfall history and geographical pattern also control the local stability/instability conditions, and their temporal and spatial variations. In the analysis, only one scenario of rainfall event is considered and applied uniformly over the entire study area.

8.5. SUMMARY

The analysis showed that TRIGRS can be run within MatLab, and that by doing so, the functionality of TRIGRS can be extended to perform probabilistic analysis. Combined effects of the natural variability inherent in the soil input parameters, and of the uncertainty associated with distribution over the study area were taken into account through the probabilistic approach. The outcome of the analysis in the form of the probability of failure map gave a better perception of the hillslope stability. The study showed that a slope with a given factor of safety could not describe the uncertainty depending on the variability of the soil input parameters. Depending on the in-situ condition, slopes that is considered to have a particular FoS may have different probability of failure and therefore will be associated with different risk levels. The methodology as presented above have significant scope of future development and the methodology itself provides a great deal of flexibility to incorporate such improvements.

Chapter 9. CONCLUDING REMARKS

9.1. INTRODUCTION

This chapter summarizes the contents of the research work including the data collected, the laboratory tests performed to obtain the soil parameters, the analyses conducted and their validation, sufficed by the obtained results and their interpretation. Based on the extensive work done, the concluding remarks are presented as obtained from the inferences from various analysis outcomes. The inherent assumptions and limitations of the methodology adopted in the present study is highlighted along with the listing of the future scope.

9.2. SUMMARY AND CONTRIBUTIONS

The objective of this study was to develop a comprehensive rainfall induced landslide hazard zonation map of the landslide prone areas of Guwahati. The effect of the geotechnical and geo-hydrological properties of prevalent soil and the rainfall characteristics (intensity-duration-frequency) in triggering of landslides is studied. Coupled transient seepage and stability analysis is simulated to assess the variation of safety factor of the slope with time, and capture the mechanism of rain-induced slope instability. The variability of soil properties is considered in the analysis incorporating a probabilistic analysis and generation of the probability of failure map. The results from the analysis is presented within a GIS framework to give the outcome as the Landslide Hazard Zonation map of Guwahati city. The summary of the research work conducted for this dissertation and the contributions from the study are listed as follows:

- A detailed investigation is conducted to study the influence of infiltration of rainfall leading to the progressive degradation of the hill-slope stability. In this regard, using Geostudio Seep/W module, seepage analysis is conducted for transient/steady state conditions considering saturated-unsaturated material model. The computed pore-water pressures are then imported in SLOPE/W module to conduct a limit equilibrium analysis to evaluate the temporal changes in stability considering unsaturated soil shear strength.
- Probabilistic slope stability analysis considering spatial variations for soil properties is conducted for local-scale landslide assessment. Covariance Matrix Decomposition

method is used for the generation of spatial variability and Monte Carlo Simulation (MCS) was used for evaluating the probability of failure. Finite difference numerical code FLAC2D, aided with MATLAB programming, were utilized for this purpose.

- Typical representative and undisturbed soil samples were collected from the slopes of different hill series in Guwahati city. Extensive in-situ investigations were conducted to determine the in-situ dry density, water content and infiltration characteristics. Exhaustive laboratory investigations were carried out on the collected soil specimens to estimate the specific gravity, grain size distribution, Atterberg's limits, shear strength parameters, hydraulic conductivity and the soil-water characteristic curve (SWCC).
- Physically based model TRIGRS was applied over grid-based approach to evaluate the stability conditions within a GIS framework. The same was coupled with a simplified hydrologic model to simulate the infiltration processes within the infinite slope model for the estimation of the safety of the slopes. The influence of rainfall pattern and its yearly variation is studied to develop a relation of rainfall events and landslide occurrences. Different realistic rainfall events that have occurred in the past in the Guwahati city were analyzed to study their influences in triggering landslides in the study area.
- The efficacy of landslide prediction by TRIGRS is quantitatively evaluated through Receiver Operating Characteristics (ROC) and LR_{class} evaluation method using confusion matrices. The GPS coordinates of the RVS locations were used in the ROC model to establish a comparison of the TRIGRS output to the in-situ scenarios.
- The influences of various types of DEMs (CartoDEM, ALOS-AW3D30-DEM, SRTM-DEM, and ASTER-GDEM) on the prediction capacity of rainfall-induced landslides in the hillslopes of the municipal precinct of Guwahati city were evaluated.
- The rainfall Intensity-Duration-Frequency (IDF) relationships were developed for the study area, which were used to determine the rainfall intensity corresponding to a particular return period and rainfall duration. By using the rainfall event as input to TRIGRS, the FoS maps corresponding to various such rainfall events were determined and further combined to form the landslide hazard map of the study area.
- The conventional methodology of deterministic landslide hazard assessment is extended to assess the probabilistic landslide hazard scenario of Guwahati city, India

by considering the uncertainty and variability of the parameters. Aided by Monte Carlo simulation techniques, the physically based model TRIGRS is executed in a MatLab environment to generate Probability of Failure maps for the study area.

9.3. PRACTICAL APPLICATIONS OF THE PRESENT STUDY

The primary outcomes of the present study are the development of the 'Landslide Hazard Maps' and 'Probability of Failure Maps' for the Guwahati city, India. The maps provide the extent of spatial and temporal susceptibility of the region to rainfall-induced landslides as subjected to various rainfall scenarios. The maps that are developed for the region have immense practical implication as follows:

- These maps will serve as a treatise to the Disaster Management Authorities of the state or the region, which can invariably aid the disaster management planners to develop practical and cost-effective methods to conduct landslide susceptibility zoning. The stated maps build up the interface between the scientific information and the development planning process.
- These maps can be used as a tool to help identify land areas that are best suited for development after duly examining the potential risk of landsliding with the change in the land use pattern.
- Furthermore, once landslide susceptibility is identified, investment projects can be developed which can attempt to avoid, prevent, or substantially mitigate the hazard.
- Comparing the location of an area of proposed development to the degree of existing landslide hazard, the planner can estimate the landslide risk. This can be used to define land use capability and appropriate low-cost mitigation measures.
- These maps can be used as a guide to control the land use pattern and growth of urbanization in the region so that the above-stated attempts may not jeopardize the currently predicted landslide hazard scenario.
- These maps efficiently demarcate the regions which are more susceptible to hazard. Hence, proper planning to develop and deploy early warning systems in these areas can be undertaken by the disaster management authorities, whether of the state (Assam State Disaster Management Authority, ASDMA) or of the center (National Disaster Management Authority, NDMA).

9.4. CONCLUSIONS

Based on the investigations and numerical simulations conducted for this study, the following are the conclusions drawn:

- The study showed that the hill-slopes within the city of Guwahati possess the potential to undergo rainfall-induced landslides. However, the potential of landsliding will depend on the type of soil and its response to rainwater infiltration, which in turn is governed by the soil water characteristics and hydraulic conductivity function of the soil.
- The probabilistic slope stability analysis showed that a slope with a given factor of safety can have different probability of failure depending upon the variability in soil parameters, and would therefore be associated with different risk levels. The probability of failure is adjudged as better representation of the slope stability condition than the deterministically estimated factor of safety.
- From a regional approach, the effectiveness of TRIGRS towards the predictability of spatiotemporal rainfall induced landslide occurrences in the hills of Guwahati city was utilized to address landslide hazard of the region.
- Actual rainfall event of June 2012 that triggered landslides within the Guwahati city was used as input in TRIGRS. The simulation results showed appreciable match with the actual landslides observed in-situ during the RVS field survey, thereby highlighting the applicability of TRIGRS in similar scenarios.
- The study conducted with different DEMs highlighted that the choice of DEM could make a significant impact on the TRIGRS simulation results. It is concluded that the resolution of the chosen DEM is secondary to the accuracy of the DEM in predicting the landslide scenarios in a region. ALOS-3D DEM was found to the best suited for the study of rainfall-induced landslides in the municipal precinct of Guwahati using TRIGRS simulation.
- As the soils of the hillslopes of Guwahati possess moderate-to-low permeability, longer duration rainfall events were observed to be more influential in triggering landslides.
- Antecedent rainfall condition plays a significant role in determining the severity of the rainfall-triggered landslide. Higher intensity rainfall leads to significant fraction of

rainwater to infiltrate into the hillslope soil, thereby enabling the rise in the water table and noticeable reduction in strength of soil. Thus, higher intensity rainfall leads to substantial destabilization of the slope.

- The FoS maps obtained through the analysis of different rainfall scenarios (generated based on IDF curves of the region) were combined to form the landslide hazard map of Guwahati city. The efficiency of the TRIGRS simulations were assessed through the ROC plots and more detailed LR_{class} evaluation method.
- The landslide hazard maps indicated minimal or negligible occurrences of landslide for rainfall events with return period of 4 years, while a 50-year return period highlighted a likely widespread occurrence of landslides across the region.
- The probability of failure (PoF) map showed that the maximum probability of failure of the hill slopes within a return period of twenty years is around 37.63 %, which is significantly high. The probability of failure ranged from 20.0–37.63 % in majority of the hill slope areas.
- Hillslopes of the study area falls in the range of moderate-to-marginal stability, and that a minor-to-moderate destabilizing factor is sufficient to cause instability. Based on the overall study, it can be understood that the hill slopes of Guwahati region are in a very delicately balanced state of stability, and that the slightest disturbance to environment can cause catastrophic landsliding. This result can be considered a much closer approximation to reality considering the fact that anthropogenic activity has long been considered as the most potent causal factor with respect to occurrence of landslides in this region.

Overall, the research conducted showed that physically based models, TRIGRS, could be successfully applied to assess the rainfall-induced landslide hazard scenarios of Guwahati city by taking into consideration the soil geotechnical characteristics, rainfall, slopes and topography of the concerned area. The methodology prescribed in this dissertation provides a detailed insight into the local and regional-scale landslide hazard assessment that can be successfully applied to any such rainfall-induced landslide prone regions of the world.

9.5. LIMITATIONS AND FUTURE SCOPE

Any research conducted will have its limitations of applicability due to the inherent assumptions involved in the analysis and numerical modeling of the same. Such limitations

are to be given due importance, and more realistic scenarios should be accommodated in further studies. Based on the limitation of the reported study, the following are adjudged as the future directions of research.

- The geotechnical input parameters, as well the applied rainfall, were considered uniform over the entire study area. Incorporation of spatial variability of geotechnical and hydrological features in a regional scale would bring essence that is more realistic to the study.
- Rainfall data for only 18 years were used in the analysis. The probability of exceedance of rainfall intensity within a particular return period was not considered in the analysis of landslide hazard involving rainfall recurrence. Such inclusion would help to address improved hazard scenarios.
- The soil depth was approximated with the help of exponential relation to the slope angle. The ground water table was considered to be at the same depth as the basal boundary and basal rock strata was assumed saturated at all times. The depth of basal boundary and the ground water table can be better approximated through in-situ borehole sub-soil investigation.
- The current methodology described in the study is unable to include the effect of other common causal factors such as anthropogenic activities and weathering. The future aspect of research in these domains should focus on including these phenomena in addition to the rainfall events.
- Only a single probabilistic analysis considering the rainfall event of 20 years return period was conducted. The same can be extended to other possible rainfall event scenarios as well.
- The probability distribution and the correlation between the various soil parameters were assumed as per existing literature. Further exhaustive in-situ and laboratory experimentations should be conducted to ascertain the actual probability distribution and the correlation of the various parameters for the study region.

REFERENCES

Abramson, L. W., Lee, T. S., Sharma, S. and Boyce, G. M. (1996), "*Slope Stability and Stabilization Methods*", A Wiley-Interscience publication, John Wiley & Sons

Alonso, E.E. (1976), "Risk analysis of slopes and its application to slopes in Canadian sensitive clays", *Geotechnique*, vol. 26, pp. 453–472.

Anbalagan, R. (1992), "Landslide hazard evaluation and zonation mapping in mountainous terrain", *Engineering Geology*, vol. 32, pp. 269-277

Anderson, M. G. and Richards, K. (1987), "Modelling slope stability: the complementary nature of geotechnical and geomorphological approaches," in: Anderson, M.G. (Ed.), *Slope Stability: Geotechnical Engineering and Geomorphology*. John Wiley & Sons Ltd, pp. 1-9.

Apel, H., Thieken, H. A., Merz, B., Blöschl, G. (2006), "A Probabilistic Modelling System for Assessing Flood Risks", *Natural Hazards*, vol. 38, pp. 79–100

Ardizzone, F., Cardinali, M., Carrara, A., Guzzetti, F. and Reichenbach, P. (2002), "Impact of mapping errors on the reliability of landslide hazard maps", *Natural Hazards and Earth System Sciences*, vol. 2, pp. 3–14

Armirza, S. (2004), "Problems of Sampling and Essential Test in Tropical Residual Soils", *e-USU Repository Universitas Sumatera Utara*.

ASDMA (2011), "*Assam State Disaster Management Plan*", Assam State Disaster Management Authority, http://sdmassam.nic.in/studies&projects. html

ASTM D7181 – 11 Method for Consolidated Drained Triaxial Compression Test for Soils

Aubertin, M., Mbonimpa, M., Bussière, B. and Chapuis, R.P. (2003), "A model to predict the water retention curve from basic geotechnical properties", *Canadian Geotechnical Journal*, vol. 40, pp. 6, pp. 1104-1122

Auvinet, G. and Gonzalez, J. L. (2000), "Three dimensional reliability analyses of earth slopes", *Computers and Geotechnics*, vol. 26, no. 3-4, pp. 247-261

Aydin A., (2006), "Stability of saprolitic slopes: nature and role of field scale heterogeneities", *Natural Hazards and Earth System Sciences*, vol. 6, pp. 89–96

Baecher, G. B. and Christian, J. T. (2003), "*Reliability and statistics in geotechnical engineering*", Wiley, Hoboken

Bai, S. B., Wang, J., Lu, G. N., Zhou, P. G., Hou, S. S. and Xu, S. N. (2009), "GIS-based and data-driven bivariate landslide-susceptibility mapping in the three gorges area, China", *Pedosphere*, vol. 19, no. 1, pp. 14–20

Bates, R. L. and Jackson, J. A. (1987), "*Glossary of Geology*", 3rd Edition, American Geological Institute, Alexandria

Baum, R. L., Savage, W. Z. and Godt, J. W. (2002), "TRIGRS - A FORTRAN program for transient rainfall infiltration and grid-based regional slope stability analysis", U.S. Geological Survey Open-File Report 2002-0424.

Baum, R. L., Savage, W. Z., and Godt, J. W. (2008), "TRIGRS - A FORTRAN program for transient rainfall infiltration and grid-based regional slope stability analysis, version 2.0", U.S. Geological Survey Open-File Report 2008-1159.

Baum, R. L., Godt, J. W. and Savage, W. Z. (2010), "Estimating the timing and location of shallow rainfall ‐ induced landslides using a model for transient, unsaturated infiltration", *Journal of Geophysical Research*, 115: F03013

Bear, J. (1979), "*Hydraulics of Groundwater*", McGraw-Hill, New York.

Beven, K. J. and Kirby, M. J. (1979), "A physically based variable contributing area model of basin hydrology", *Hydrological Science Bulletin*, vol. 24, pp. 43–69

Bhusan, K., Kundu, S. S., Goswami, K., and Sudhakar, S. (2014), "Susceptibility mapping and estimation of rainfall threshold using space based input for assessment of landslide hazard in Guwahati city in North East India", *The International Archives of the Photogrammetry, Remote Sensing and Spatial Information Sciences*, vol. XL-8, pp. 15–19.

Bishop, A. W. (1959), "The principle of effective stress", *Teknisk Ukeblad*, Norwegian Geotechnical Institute, vol. 106, no. 39, pp. 859—863.

Bothale, R. V. and Pandey, B. (2013), "Evaluation and comparison of multi resolution DEM derived through Cartosat-1 stereo pair – A case study of Damanganga Basin", *Journal of the Indian Society of Remote Sensing*, vol. 41, pp. 497–507

Bromhead, E. N. (1992), "*The Stability of Slopes*", 2nd ed., Taylor & Francis.

Budhu, M. (2007), "*Soil Mechanics and Foundations*", Wiley India Pvt. Ltd.

Carrara, A., Cardinali, M., Detti, R., Guzzetti, F., Pasqui, V. and Reichenbach, P. (1991), "GIS techniques and statistical models in evaluating landslide hazard", *Earth Surface Process and Landforms*, vol. 16, pp. 427–445.

Carrara, A., Cardinali, M. and Guzzetti, F. (1992), "Uncertainty in Accessing Landslide Hazard Risk." *ITC Journal*, vol. 2, pp. 172-183

Cascini, L., Cuomo, S. and Pastor, M. (2008), "The role played by mountain tracks on rainfall induced shallow landslides: a case study", *Fourth Biennial Meeting: International Congress on Environmental Modelling and Software (iEMSs 2008)*, Barcelona, Spain, pp. 1484–1491

Cascini, L. (2008), "Applicability of landslide susceptibility and hazard zoning at different scales", *Engineering Geology*, vol. 102, pp. 164–177

Cervi, F., Berti, M., Borgatti, L., Ronchetti, F., Manenti, F., and Corsini, A. (2010), "Comparing predictive capability of statistical and deterministic methods for landslides susceptibility mapping: a case study in the northern Apennines (Reggio Emilia Province, Italy)", *Landslides*, vol. 7, pp. 433–444.

Chawla, A., Chawla, S., Pasupuleti, S., Rao, A. C. S., Sarkar, K. and Dwivedi, R. (2018), "Landslide Susceptibility Mapping in Darjeeling Himalayas, India," *Advances in Civil Engineering*, vol. 2018, Article ID 6416492

Chen, W.F. (2007), "*Limit analysis and soil plasticity*", J. Ross Publishing

Cheng, Y. M., Lansivaara, T. and Wei, W. B. (2007), "Two-dimensional slope stability analysis by limit equilibrium and strength reduction methods", *Computers and Geotechnics*, vol. 34, no. 3, pp. 137-150

Cherubini, C. (2000), "Reliability evaluation of shallow foundation bearing capacity on *c'* and *φ'* soils", *Canadian Geotechnical Journal*, vol. 37, pp. 264-269.

Chetia, M. and Sreedeep, S. (2013), "A study on unsaturated hydraulic conductivity of hill soil of north-east India", *ISH Journal of Hydraulic Engineering*, vol. 19, no. 3, pp. 276–281

Childs, E. C. and Collis-George, N. (1950), "The Permeability of Porous Materials", *Proceedings of the Royal Society*, pp. 392-405

Cho, S. E. (2007), "Effects of spatial variability of soil properties on slope stability", *Engineering Geology*, vol. 92, pp. 97–109.

Cho, S. E. (2014), "Probabilistic stability analysis of rainfall-induced landslides considering spatial variability of permeability", *Engineering Geology*, vol. 171, no. 13, pp. 11-20

Christian, J. T., Ladd, C. C. and Baecher, G. B. (1994), "Reliability applied to slope stability analysis", *Journal of Geotechnical Engineering, ASCE*, vol. 120, no. 12, pp. 2180–2207

Cimmery, V. (2010), "*SAGA User Guide*"

Claessens L., Heuvelink G. B. M., Schoorl J. M. and Veldkamp A. (2005), "DEM resolution effects on shallow landslide hazard and soil redistribution modeling", *Earth Surface Process and Landforms*, vol. 30, pp. 461-477.

Conrad, O., Bechtel, B., Bock, M., Dietrich, H., Fischer, E., Gerlitz, L., Wehberg, J., Wichmann, V. and Böhner, J. (2015), "System for Automated Geoscientific Analyses (SAGA) v. 2.1.4", *Geoscientific Model Development*, vol. 8, pp. 1991–2007

Crosta, G. B. and Frattini, P. (2008), "Rainfall-induced landslides and debris flows", *Hydrological Processes*, vol. 22, pp. 473-477

Crozier, M. J. Glade, T. (2005), "Landslide hazard and risk: issues, concepts, and approach", in: Glade, T., Anderson, M. G. and Crozier, M. J. (Eds.), *Landslide Hazard and Risk*, pp. 1–38

Crozier, M. J. (1989), "*Landslides: Causes, consequences and environment*," Routledge.

Crozier, M. J., (1999), "Landslides", in: Alexander, D. E. and Fairbridge, R. W. (Eds.), *Encyclopedia of environmental science*, Dordrecht, Kluwer: 371-5

Cruden, D. M. and Varnes, D. J. (1996), "Landslide types and processes," in: Turner, A. K. and Schuster, R. L. (Eds.), *Landslides: Investigation and Mitigation*, National Research Council, Transportation and Research Board Special Report 247, Washington, D.C., USA, pp. 36-75

Cruden, D. M. (1991), "A simple definition of a landslide." *Bulletin of the International Association of Engineering Geology*, vol. 43, pp. 27-29

Dai, F. C., Lee C. F. and Ngai, Y. Y. (2002), "Landslide risk assessment and management: an overview", *Engineering Geology*, vol. 64, pp. 65-87

Das, U. K. and Saikia, B. D. (2010), "Shear Strength of Unsaturated Residual Soils of the Hills in Guwahati", *Proceedings of Indian Geotechnical Conference, GEOtrendz*, December 16–18, Bombay

Das, U. K. and Saikia, B. D. (2011), "Evaluation of a Prediction Model for Shear Strength of Unsaturated Soils", *Proceedings of Indian Geotechnical Conference*, December 15–17, Kochi.

Das, N. (1992), "*An investigation of Soil Characteristics of the Greater Guwahati landslide areas*", M.E. Thesis, Gauhati University

Das, H. K. (2003), "*A case study of recent landslides in Greater Guwahati*", M.E. Thesis, Gauhati University

Deka, G. (1991), "Landslides and its relation to geological features with particular reference to the area Guwahati", *Souvenir of IE(I)*, Assam Center

Delmonaco, G., Leoni, G., Margottini C., Puglisi, C. and Spizzichino, D. (2003), "Large scale debris flow hazard assessment: a geotechnical approach and GIS modelling", *Natural Hazards and Earth System Science*, vol. 3, no. 5, pp. 443-455.

Deo, R., Jain, M. and Rao, Y. S. (2016), "Comparison of TanDEM-X and Cartosat-1 stereo DEMs over different terrains of India", *International Geoscience and Remote Sensing Symposium*, Beijing, China, pp. 1-4

Devkota, S., Shakya, N. M., Sudmeier-Rieux, K., Jaboyedoff, M., vanWesten, C. J., Mcadoo, B. G. and Adhikari, A. (2018), "Development of Monsoonal Rainfall Intensity-Duration-Frequency (IDF) Relationship and Empirical Model for Data-Scarce Situations: The Case of the Central-Western Hills (Panchase Region) of Nepal", *Hydrology*, vol. 5, pp. 1-27

Dhakal, A. S., Amada, T. and Aniya, M. (2000), "Landslide hazard mapping and its evaluation using GIS: An investigation of sampling schemes for a grid-cell based quantitative method", *Photogrammetric Engineering and Remote Sensing*, vol. 66, no. 8, pp. 981-989

Dielectric water potential sensor, Operator's Manual Version 3 (2008), Decagon Devices, U.S.

Dikshit, A., Satyam, D. M. and Towhata, I. (2018), "Early warning system using tilt sensors in Chibo, Kalimpong, Darjeeling Himalayas, India", *Natural Hazards*, vol. 94, pp. 727–741

Duncan, J. M. (1996), "State of the art: Limit Equilibrium and Finite-Element Analysis of Slopes", *Journal of Geotechnical Engineering*, vol. 122, no.7, pp. 577-596

Durgin, P.B. (1977), "Landslides and the weathering of granitic rocks", *Reviews in Engineering Geology*, vol. 3, pp. 127–131.

EC-5 Soil Moisture Sensor, User's Manual Version 2 (2012), Decagon Devices, U.S.

Elkateb, T., Chalaturnyk, R. and Robertson, P. K. (2002), "An overview of soil heterogeneity: quantification and implications on geotechnical field problems", *Canadian Geotechnical Journal*, vol. 40, no. 1, pp. 1-15

Elrick, D. E., Reynolds, W. D. and Tan, K.A. (1989), "Hydraulic conductivity measurements in the unsaturated zone using improved well analyses", *Groundwater Monitoring Review*, vol. 9, pp. 184-193

EORC–JAXA-ALOS (2018) Global DSM AW3D30 Dataset Product Format Description for V 1.1, http://www.eorc.jaxa.jp/ALOS/en/aw3d30/aw3d30v11_format_e.pdf

Ering, P. and Sivakumar Babu, G. L. (2016), "Probabilistic back analysis of rainfall induced landslide - A case study of Malin landslide, India", *Engineering Geology*, vol. 208, pp. 154-164

Fell, R., Corominas J., Bonnard C., Cascini L., Leroi E. and Savage W. Z. (2008), on behalf of the JTC-1 Joint Technical Committee on Landslides and Engineered Slopes, "Guidelines for landslide susceptibility, hazard and risk zoning for land use planning", *Engineering Geology*, vol. 102, pp. 85–98

Fenton, G. A. and Griffiths, D. V. (2008), "*Risk Assessment in Geotechnical Engineering*", John Wiley & Sons, Inc., New Jersey

Fenton, G. A. and Vanmarcke, E. H., (1990), "Simulation of random fields via local average subdivision", *ASCE Journal of Engineering Mechanics*, vol. 116, no. 8, pp.1733-1749

Fredlund, D. G. and Krahn, J. (1977), "Comparison of slope stability methods of analysis", *Canadian Geotechnical Journal*, vol. 14, no. 3, pp. 429 439

Fredlund, D. G. and Morgenstern , N.R. (1976), "Constitutive Relations for Volume Change in Unsaturated Soils", *Canadian Geotechnical Journal*, vol. 13, pp. 261-276

Fredlund, D. G. and Morgenstern, N. R. (1977), "Stress State Variables for Unsaturated Soils", *Journal of Geotechnical and Geoenvironmental Engineering, ASCE*, vol. 103, pp. 447-464

Fredlund, D. G. and Rahardjo, H. (1993), "*Soil Mechanics for Unsaturated Soils*", John Wiley & Sons, Inc., New Jersey

Fredlund, D. G. and Xing, A. (1994), "Equations for the soil-water characteristic curve", *Canadian Geotechnical Journal*, vol. 31, pp. 521-532.

Fredlund, D. G., Morgenstern, N. R. and Widger, R. A. (1978), "Shear strength of unsaturated soils", *Canadian Geotechnical Journal*, vol. 15, pp. 313-321

Fredlund, D. G., Xing, A. Fredlund M. D. and Barbour, S. L. (1996), "The relationship of the unsaturated soil shear strength to the soil-water characteristic curve", *Canadian Geotechnical Journal*, vol. 33, pp. 440-448

Fredlund, D. G., Rahardjo, H. and Fredlund, M. D. (2012), "*Unsaturated Soil Mechanics in Engineering Practice*", John Wiley & Sons, Inc., Hobooken, New Jersey

Freeze, R. A. and Cherry, J. A. (1979), "*Groundwater*", Prentice-Hall

Froude, M. J. and Petley, D. N. (2018), "Global fatal landslide occurrence from 2004 to 2016", *Natural Hazards and Earth System Science*, vol. 18, pp. 2161-2181.

Gardner, W. R. (1958), "Some steady-state solutions of the unsaturated moisture flow equation with application to evaporation from a water table", *Soil Science*, vol. 85, pp. 228–232.

Gasmo, J. M., Rahardjo, H. and Leong, E. C. (2000), "Infiltration effects on stability of a residual soil slope", *Computers and Geotechnics*, vol. 26, pp. 145-165

GeoSlope (2007), Manuals of Geostudio 2007 software suite SEEP/W; SLOPE/W Manual, GEO-SLOPE International Ltd

Goddard Earth Sciences Data and Information Services Center maintained web portal Giovanni (http://disc.sci.gsfc.nasa.gov/giovanni)

Glade, T. and Crozier, M. J. (2005)a, "The nature of landslide hazard impact," in: Glade, T., Anderson, M. and Crozier, M. J. (Eds.), *Landslide hazard and risk*, John Wiley and Sons, 43-74

Glade, T. and Crozier, M. J. (2005)b, "A review of Scale Dependency in Landslide Hazard and Risk Analysis," in: Glade, T., Anderson, M. and Crozier, M. J. (Eds.), *Landslide hazard and risk*, John Wiley and Sons, 75-138

GMDA, (2009), "*Master Plan for Guwahati Metropolitan Area - 2025 (Part - 1)*", Guwahati Metropolitan Development Authority, Guwahati, Assam, India.

Godt, J. W., Baum, R. B., Savage, W. Z., Salciarini, D., Schulz, W. H. and Harp, E. L. (2008), "Transient deterministic shallow landslide modeling: Requirements for susceptibility and hazard assessments in a GIS framework", *Engineering Geology*, vol. 102, pp. 214–226

Goswami, R. K. and Singh, B. (2008), "An Analysis of Causes of Urban Landslides in Residual Lateritic Soil", *Sixth International Conference on Case Histories in Geotechnical Engineering*, Missouri University of Science and Technology, Aug 11-16

Goswami, D. (2013), "*Rapid Visual Screening for Potential Landslide Areas of Guwahati*", Assam State Disaster Management Authority, http://sdmassam.nic.in/studies&projects.html

Green, W. H. and Ampt, G. A. (1911), "Studies on soil physics", *Journal of Agricultural Science*, vol. 4, no. 1, pp. 1– 24

Green, R. E. and Corey, J. C. (1971), "Calculation of Hydraulic Conductivity: A Further Evaluation of Some Predictive Methods", *Soil Science Society of America Proceedings*, vol. 35, pp. 3-8

Griffiths, D. V., Fenton. G. A. and Denavit, M. D. (2007), "Traditional and advanced probabilistic slope stability analysis", *Probabilistic Applications in Geotechnical Engineering*, Geotechnical Special Publication No. 170, Proc. Geo-Denver 2007 Symposium, ASCE, Denver

Griffiths, D. V., Huang, J. and Fenton, G. A. (2009), "Influence of Spatial Variability on Slope Reliability Using 2-D Random Fields", *Journal of Geotechnical and Geoenvironmental Engineering*, vol. 135, no. 10, pp. 1367-1378

Griffiths, D. V., Huang, J. and Fenton, G. A. (2011), "Probabilistic infinite slope analysis", *Computers and Geotechnics*, vol. 38, no. 4, pp. 577-584

GSI (2013)a, Geological Survey of India, http://www.portal.gsi.gov.in, Landslide Home, accessed on 31 October 2013.

GSI (2013)b, Geological Survey of India, http://www.portal.gsi.gov.in, Post-disaster studies, accessed on 31 October 2013

Guzzetti, F., Carrara, A., Cardinali, M. and Reichenbach, P. (1999), "Landslide hazard evaluation: an aid to a sustainable development", *Geomorphology*, vol. 31, pp. 181-216.

Guzzetti, F. (2002), "Landslide Hazard Assessment and Risk Evaluation: Limits and Prospective." *Proceedings of the 4th EGS Plinius Conference*, Mallorca, Spain, October 2002.

Hillel, D. (1982), "*Introduction to soil physics*", Academic Press, San Diego, California

Huat, B. B. K., Ali, F. Hj. and Rajoo, R. S. K. (2006), "Stability Analysis and Stability Chart for Unsaturated Residual Soil Slope", *American Journal of Environmental Sciences*, vol. 2, no. 4, pp. 154-160

Hurley, D. G. and Pantelis, G. (1985), "Unsaturated and saturated flow through a thin porous layer on a hillslope", *Water Resource Research*, vol. 21, pp. 821–824

Hutchinson, J. N. (1988), "General report: morphological and geotechnical parameters of landslides in relation to geology and hydrogeology", *Proceedings of the 5th International Symposium on Landslides*, Lausanne, vol. 1, pp. 3–35

India Water Portal (2013), https://www.indiawaterportal.org/met_data/, accessed on 12 November 2013.

IS 14496, Part-2 (1998) "Preparation of landslide hazard zonation maps in mountainous terrain - Guidelines (Part 2 – Macrozonation)", Bureau of Indian Standards

IS 2720, Part-12 (1986) "Methods of Test for Soils Part 12 Determination of shear strength parameters of soil from consolidated undrained triaxial compression test with measurement of pore water pressure", Bureau of Indian Standards

IS 2720, Part-17 (1986) "Methods of Test for Soils Part 17 Laboratory Determination of Permeability", Bureau of Indian Standards

IS 2720, Part-4 (1985) "Methods of Test for Soils Part IV Grain Size Analysis", Bureau of Indian Standards

IS 2720, Part-5 (1985) "Methods of Test for Soils Part V Determination of Liquid and Plastic limit", Bureau of Indian Standards

Itasca, (2005), Fast Lagrangian Analysis of Continua, (FLAC Version 5.0), Itasca Consulting Group, Minneapolis

Iverson, R. M. (2000), "Landslide triggering by rain infiltration", *Water Resources Research*, vol. 36, no.7, pp. 1897–1910

Jain, S. K., Kumar, V. and Saharia, M. (2013), "Analysis of rainfall and temperature trends in northeast India", *International Journal of Climatology*, vol. 33, pp. 968-978

Jain, A. O., Thaker, T., Chaurasia, A., Patel, P. and Singh, A. K. (2018), "Vertical accuracy evaluation of SRTM-GL1, GDEM-V2, AW3D30 and CartoDEM-V3.1 of 30-m resolution with dual frequency GNSS for lower Tapi Basin India", *Geocarto International*, vol. 33, no. 11, pp. 1237-1256

Jaiswal, P., van Westen, C. J. and Jetten, V. (2010), "Quantitative landslide hazard assessment along a transportation corridor in southern India", *Engineering Geology*, vol. 116, pp. 236-250

Kalita, U. C. (2001), "A study of landslide hazards in North Eastern India." *Proceedings of the Fifteenth International Conference on Soil Mechanics and Geotechnical Engineering*, vol. 1-3, pp. 1167-1170, Istanbul, Turkey, August 27-31

Kim, J., Jeong, S., Park, S. and Sharma, J. (2004), "Influence of rainfall-induced wetting on the stability of slopes in weathered soils", *Engineering Geology*, vol. 75, pp. 251–262

Kim, D., Im, S., Lee, S. H., Hong, Y. and Cha, K. S. (2010), "Predicting the Rainfall-Triggered Landslides in a Forested Mountain Region Using TRIGRS Model", *Journal of Mountain Science*, vol., 7, no. 1, pp 83–91

Krahn, J. and Fredlund, D.G. (1972), "On total and osmotic suction", *Journal of Soil Science*, vol. 114, no. 5, pp. 339-348

Kumar, M., Rana, S., Pant, P. D. and Patel, R. C. (2017), "Slope stability analysis of Balia Nala landslide, Kumaun Lesser Himalaya, Nainital, Uttarakhand, India", *Journal of Rock Mechanics and Geotechnical Engineering*, vol. 9, pp. 150-158

Kuriakose, S. L., van Beek, L. P. H. and van Westen, C. J. (2009), "Parameterizing a physically based shallow landslide model in a data poor region", *Earth Surface Processes and Landforms*, vol. 34, pp. 867–881

Lacasse, S. and Nadim, F. (1996) "Uncertainties in characterizing soil properties", in: Shackleford, C. D., Nelson, P. P. and Roth, M. J. S. (Eds.), *Uncertainty in the Geologic*

Environment: From Theory to Practice, ASCE Geotechnical Special Publication, vol. 58, 49–75

Lakshmi, S. E. and Yarrakula, K. (2018), "Review and critical analysis on digital elevation models", *Geofizika*, vol. 35, no. 2, pp. 129–157

Lee, I. K., White, W. and Ingles, O. G. (1983), "*Geotechnical Engineering*", Pitman, Boston

Lee, S., Choi, J. and Woo, I. (2004), "The effect of spatial resolution on the accuracy of landslide susceptibility mapping: a case study in Boun, Korea", *Geosciences Journal*, vol. 8, no. 1, pp. 51–60

Leroueil, S. (2004), "Geotechnics of slopes before failure", in: Lacerda, W., Ehrlich, M., Fontoura, S. A. B. and Sayao, A. S. F. (Eds.), *Landslides: Evaluation and stabilization*, 9th International Symposium on Landslides, A. A. Balkema Publishers, Leiden, Rio de Janeiro, Brazil, pp. 863-884.

Li, K. S. and Lumb, P. (1987), "Probabilistic design of slopes", *Canadian Geotechnical Journal*, vol. 24, no. 4, pp. 520-535.

Li, J. and Zhou, C. H. (2003), "Appropriate grid size for terrain based landslide risk assessment in Lantau Island, Hong Kong", *Journal of Remote Sensing*, vol. 7, no. 2, pp. 86-92

Li, C., Ma, T., Sun, L., Li, W. and Zheng, A. (2012), "Application and verification of a fractal approach to landslide susceptibility mapping," *Natural Hazards*, vol. 61, pp. 169–185.

Liang, R. Y., Nusier, O. K. and Malkawi, A. H. (1999), "A reliability based approach for evaluating the slope stability of embankment dams", *Engineering Geology*, vol. 54, no. 3-4, pp. 271-285

Liu, C. N. and Wu, C. C. (2008), "Mapping susceptibility of rainfall triggered shallow landslides", *Environmental Geology*, vol. 55, no. 4, pp. 907–915.

Low, B. K., Gilbert, R. B. and Wright, S. G. (1998), "Slope reliability analysis using generalized method of slices", *Journal of Geotechnical and Geoenvironmental Engineering*, vol. 124, no. 4, pp. 350-362.

Lu, N. and Godt, J. (2013), "*Hillslope Hydrology and Stability*", Cambridge University Press.

Mahalingam, R. and Olsen, M. J. (2016), "Evaluation of the influence of source and spatial resolution of DEMs on derivative products used in landslide mapping", *Geomatics, Natural Hazards and Risk*, vol. 7, no. 6, pp. 1835–1855

Mani, S. and Saranaathan, S. E. (2017), "Landslide Hazard Zonation mapping on meso-scale in SH-37 Ghat section, Nadugani, Gudalur, The Nilgiris, India", *Arabian Journal of Geosciences*, 10:161

Mark, D. M. (1988), "Network models in geomorphology", in: Anderson, M. G., (Ed.) *Modelling in Geomorphological Systems*, John Wiley, pp. 73–79.

Maswood, Md. and Goswami, D. N. D. (1974), "Basic rocks from the Precambrian Terrain around Guwahati, Assam", *The Indian mineralogist: journal of the Mineralogical Society of India*, vol. 15, pp. 55–62.

Maswood, Md. (1981), "Granite Gneisses around Guwahati, Assam", *Journal of Geological & Mineralogical Society of India*, vol. 53, no.3-4, pp. 115–124.

Maswood, Md. (1982), "Structural history of the Precambrian rocks around Guwahati, Assam", *Quarterly Journal of Geological & Mineralogical Society of India*, vol. 54, no. 1-2, pp. 33–38.

Mathew, J., Jha, V. K. and Rawat, G. S. (2009), "Landslide susceptibility zonation mapping and its validation in part of Garhwal Lesser Himalaya, India, using binary logistic regression analysis and receiver operating characteristic curve method", *Landslides*, vol. 6, pp. 17–26

McCarthy, E. L., (1934), *Science*, vol. 80, Paper No. 2065.

Montgomery, D. R. and Dietrich, W. E. (1994), "A physically based model for the topographic control on shallow landsliding", *Water Resource Research*, vol. 30, pp. 1153–1170.

Montrasio, L. and Valentino, R. (2008), "A model for triggering mechanisms of shallow landslides", *Natural Hazards*, vol. 8, pp. 1149–1159.

Montrasio, L., Valentino, R. and Losi, G. L. (2012), "Shallow landslides triggered by rainfalls: modeling of some case histories in the Reggiano Apennine (Emilia Romagna Region, Northern Italy)", *Natural Hazards*, vol. 60, pp. 1231–1254.

Morgenstern, N. R. and Price, V. E. (1965), "The analysis of stability of general slip surfaces", *Geotechnique*, vol. 15, no. 1, pp. 79-93

Ng, C. W. W., Wang, B. and Tung Y. K. (2001), "Three-dimensional numerical investigations of groundwater responses in an unsaturated slope subjected to various rainfall patterns", *Canadian Geotechnical Journal*, vol. 38, pp. 1049–1062

O'Loughlin, E. M. (1986), "Prediction of surface saturation zones in natural catchments by topographic analysis", *Water Resource Research*, vol. 22, pp. 794–804

Pack, R. T., Tarboton, D. G. and Goodwin, C. N. (1998), "The SINMAP Approach to Terrain Stability Mapping", *Proceedings of International Congress of the International Association for Engineering Geology and the Environment*, Balkema, Rotterdam, Netherlands, pp. 1157-1165.

Pandey, A., Dabral, P. P., Chowdary, V. M. and Yadav, N. K. (2008), "Landslide Hazard Zonation using Remote Sensing and GIS: a case study of Dikrong river basin, Arunachal Pradesh, India", *Environmental Geology*, DOI 10.1007/s00254-007-0933-1

Pardeshi, S. D., Autade, S. E. and Pardeshi, S. S. (2013), "Landslide hazard assessment: recent trends and techniques", *SpringerPlus*, 2:523

Park, D. W., Nikhil, N. V. and Lee, S. R. (2013), "Landslide and debris flow susceptibility zonation using TRIGRS for the 2011 Seoul landslide event", *Natural Hazards Earth System Sciences*, vol. 13, pp. 2833–2849

Pawłuszeka, K., Borkowski, A. and Tarolli P. (2017), "Towards the optimal pixel size of dem for automatic mapping of landslide areas", *The International Archives of the Photogrammetry, Remote Sensing and Spatial Information Sciences*, Vol. XLII-1/W1, pp. 83-90

Petley, D. N. and Bulmer, M. H. K. (2004), "The application of earth observation technologies for landslide disaster mitigation" *Proceedings of the CEOS Workshop*, Beijing, China, pp. 1-8.

Phukon, P., Chetia, D. and Das, P. (2012), "Landslide Susceptibility Assessment in the Guwahati City, Assam using Analytic Hierarchy Process (AHP) and Geographic

Information System (GIS)", *International Journal of Computer Applications in Engineering Sciences*, vol. 2, no. 1, pp. 2231–4946.

Press, W. H., Flannery, B. P., Teukolsky, S. A. and Vetterling, W. T. (1986), "*Numerical recipes, the art of scientific computing*", Cambridge University Press, New York

Rahardjo, H., Ong, T. H., Rezaur, R. B. and Leong, E. C. (2007), "Factors Controlling Instability of Homogeneous Soil Slopes under Rainfall", *Journal of Geotechnical and Geoenvironmental Engineering*, ASCE, vol. 133, no. 12, pp. 1532-1543.

Rahimi, A., Rahardjo, H. and Leong, E. C. (2010), "Effect of hydraulic properties of soil on rainfall induced slope failure", *Engineering Geology*, vol. 114, pp. 135–143

Rahimi, A., Rahardjo, H. and Leong, E. C., (2011), "Effect of Antecedent Rainfall Patterns on Rainfall-Induced Slope Failure", *Journal of Geotechnical and Geoenvironmental Engineering*, vol. 137, no. 5, pp. 483-491

Raia, S., Alvioli, M., Rossi, M., Baum, R. L., Godt, J. W. and Guzzetti, F. (2014), "Improving predictive power of physically based rainfall-induced shallow landslide models: a probabilistic approach", *Geoscientific Model Development*, vol. 7, pp. 495–514

Ramesh, V., Mani., S., Baskar, M., Kavitha, G. and Anbazhagan, S. (2017), "Landslide Hazard Zonation Mapping and Cut Slope Stability Analyses along Yercaud Ghat Road (Kuppanur - Yercaud) Section, Tamil Nadu, India", *International Journal of Geo-Engineering*, 8:2

Reichenbach, P., Rossi, M., Malamud, B. D., Mihir, M. and Guzzetti, F. (2018), "A review of statistically-based landslide susceptibility models", *Earth-Science Reviews*, vol. 180, pp. 60–91

Richards, L. A. (1931), "Capillary conduction of liquids through porous mediums", *Physics*, vol. 1, no. 5, pp. 318–333.

Saadatkhah, N., Kassim A. and Lee, L.M. (2015), "Hulu Kelang, Malaysia regional mapping of rainfall-induced landslides using TRIGRS model", *Arabian Journal of Geoscience*, vol. 8, pp. 3183–3194.

Saaty, T. L. (1980), "*The Analytic Hierarchy Process*," McGraw Hill

Saha, A. K., Gupta, R. P., Sarkar, I., Arora M. K. and Csaplovics, E. (2005), "An approach for GIS-based statistical landslide susceptibility zonation—with a case study in the Himalayas", *Landslides*, vol. 2, pp. 61–69

Saikia, B. D., Sarma, A. K., Goswami, D. and Deka, G. (1996), "*Landslide Hazard Zonation of Guwahati Area*", Progress Report submitted to Directorate of Science and Technology, Govt. of India

Saikia, B. D. (2002), "Geotechnical Investigation of Probable Landslide Spots within Guwahati City Area", Progress Report submitted to Directorate of Science and Technology, Govt. of India

Salciarini, D., Godt, J. W., Savage, W. Z., Conversini, P., Baum, R. L. and Michael, J. A. (2006), "Modeling regional initiation of rainfall-induced shallow landslides in the eastern Umbria Region of central Italy", *Landslides*, vol. 3, pp.181–194.

Salciarini, D., Godt, J. W., Savage, W. Z., Baum, R. L. and Conversini, P. (2008), "Modeling landslide recurrence in Seattle, Washington, USA", *Engineering Geology*, vol. 102, pp. 227–237.

Sarkar, S. and Anbalagan, R. (2008), "Landslide Hazard Zonation Mapping and Comparative Analysis of Hazard Zonation Maps", *Journal of Mountain Science*, vol. 5, pp. 232–240

Sarma, A. K., and Bora, P. K. (1994), "Influence of Rainfall on Landslide", *International Conference on Landslides, Slope Stability and the Safety of Infra-Structures*, September 13–14, Malaysia.

Sarma, A. K. and Goswami, R. (1991), "A study of landslide in and around the city of Guwahati", *Proceedings of seminar of Building Regulation and Hydro meteorological condition*, November 19

Savage, W. Z., Godt, W. J. and Baum, R. L. (2004), "Modeling time–dependent slope stability", *Proceedings of IX International Symposium on Landslides*, Rio de Janeiro, Brazil, pp. 23–38.

Schilirò, L., Esposito, C. and Mugnozza, G. S., (2015), "Evaluation of shallow landslide-triggering scenarios through a physically based approach: an example of application in the southern Messina area (northeastern Sicily, Italy)", *Natural Hazards Earth System Sciences*, vol. 15, pp. 2091–2109.

Selby, M. J. (1993), "*Hillslope Materials and Processes*", Oxford University Press Inc., New York

Sengupta, A., Gupta, S. and Anbarasu, K. (2010), "Rainfall thresholds for the initiation of landslide at Lanta Khola in north Sikkim, India", *Natural Hazards*, vol. 52, pp. 31–42

Shen, H. (2012), "*Non-Deterministic Analysis of Slope Stability based on Numerical Simulation*", Ph.D. thesis, Faculty of Geosciences, Geoengineering and Mining of the Technische Universität Bergakademie Freiberg.

Shukla, R.C. (1989), "Study of Granite Rocks around Kamakhya hill and adjoining area", *Geological Survey of India*, Assam, Record–122 , Part. IV, pp. 72-73.

Soeters, R. and van Westen, C. J. (1996), "Slope instability recognition, analysis, and zonation", in: Turner, K. T. and Schuster, R. L. (Eds.), *Landslides: Investigation and Mitigation*, Special Report No. 247, Transportation Research Board National Research Council, Washington DC, pp. 129-177

Sorbino, G., Sica, C. and Cascini, L. (2010), "Susceptibility analysis of shallow landslides source areas using physically based models", *Natural Hazards*, vol. 53, pp. 313–332

Srivastava, R. and Yeh, T. C. J. (1991), "Analytical solutions for one-dimensional, transient infiltration toward the water table in homogeneous and layered soils", *Water Resources Research*, vol. 27, pp. 753–762

Srivastava, A., Sivakumar Babu, G. L. and Haldar, S. (2010), "Influence of spatial variability of permeability property on steady state seepage flow and slope stability analysis", *Engineering Geology*, vol. 110, pp. 93–101

Stark T. D., Choi, H. and McCone, S. (2005), "Drained Shear Strength Parameters for Analysis of Landslides", *Journal of Geotechnical and Geoenvironmental Engineering*, ASCE

Suchomel, R. and Masin, D. (2010), "Comparison of different probabilistic methods for predicting stability of a slope in spatially variable c-phi soil", *Computers and Geotechnics*, vol. 37, no. 1-2, pp. 132-140

Tadono, T., Ishida, H., Oda, F., Naito, S., Minakawa, K. and Iwamoto, H. (2014), "Precise global DEM generation by ALOS-PRISM", *ISPRS Annals of the Photogrammetry, Remote Sensing and Spatial Information Sciences*, vol. II-4, pp. 71-76.

Tadono, T., Nagai, H., Ishida, H., Oda, F., Naito, S., Minakawa, K. and Iwamoto, H. (2016), "Initial Validation of the 30 m-mesh Global Digital Surface Model Generated by ALOS PRISM", *The International Archives of the Photogrammetry, Remote Sensing and Spatial Information Sciences*, ISPRS, vol. XLI-B4, pp.157-162

Takaku, J. and Tadono, T. (2017), "Quality updates of 'AW3D' global DSM generated from ALOS PRISM," *Proc. IGARSS2017*, IEEE, Fort Worth, TX, USA, pp. 5666-5669

Takaku, J., Tadono, T. and Tsutsui, K. (2014), "Generation of High Resolution Global DSM from ALOS PRISM", *The International Archives of the Photogrammetry, Remote Sensing and Spatial Information Sciences*, ISPRS, vol. XL-4, pp.243-248

Takaku, J., Tadono, T., Tsutsui, K. and Ichikawa, M. (2016), "Validation of 'AW3D' Global DSM Generated from ALOS PRISM", *ISPRS Annals of the Photogrammetry, Remote Sensing and Spatial Information Sciences*, vol.III-4, pp.25-31

Tan, C. H., Ku, C. Y., Chi, S. Y., Chen, Y. H., Fei, L. Y., Lee, J. F. and Su, T. W. (2008), "Assessment of regional rainfall-induced landslides using 3S-based hydro-geological model", in: Chen et al., (eds), *Landslides and Engineered Slopes*, Taylor & Francis Group, London, pp. 1639-1645

Tarboton, D. G. (1997), "A new method for the determination of flow directions and contributing areas in grid digital elevation models", *Water Resources Research*, vol. 33, no. 2, pp. 309–319

Terzaghi, K. (1926), "Principles of soil mechanics", McGrawHill, New York

Tofani, V., Dapporto, S., Vannocci, P. and Casagli N. (2006), "Infiltration, seepage and slope instability mechanisms during the 20–21 November 2000 rainstorm in Tuscany, central Italy", *Natural Hazards and Earth System Sciences*, vol. 6, pp. 1025–1033

Tsaparas, I., Rahardjo, H., Toll, D. G. and Leong, E. C. (2002), "Controlling parameters for rainfall-induced landslides", *Computers and Geotechnics*, vol. 29, pp. 1–27

Van Beek, L. P. and Van Asch, T. J. (2004), "Regional assessment of the effects of land-use Change on landslide hazard by means of physically based modeling", *Natural Hazards*, vol. 31, pp. 289–304

van Genuchten, M. Th. (1980), "A closed-form equation for predicting the hydraulic conductivity of unsaturated soils", *Soil Science Society of America Journal*, vol. 44, pp. 892–898

van Westen, C. J., Castellanos, E. and Kuriakose, S. L. (2008), "Spatial data for landslide susceptibility, hazard, and vulnerability assessment: An overview", *Engineering Geology*, vol. 102, pp. 112–131

van Westen, C. J., Ghosh, S., Jaiswal, P., Martha, T. R. and Kuriakose, S. L. (2011), "From Landslide Inventories to Landslide Risk Assessment; An Attempt to Support Methodological Development in India", in: Margottini, C. (Ed.), *Landslide Science and Practice*, Second World Landslide Forum, vol. 1

Vanapalli, S. K. and Fredlund, D. G. (2000), "Comparison of different procedures to predict unsaturated soil shear strength", in: Shackelford, C. D., Houston, S. L. and Chang, N. Y. (Eds.), *Advances in unsaturated geotechnics*, Proceedings of Geo-Denver 2000, Denver,

Colorado, August 5–8, American Society of Civil Engineers, Geotechnical Special Publication vol. 99, pp. 195–209.

Vanmarcke, E. H. (1977)a, "Probabilistic modeling of soil profiles", *Journal of the Geotechnical Engineering Division*, ASCE, vol. 103, pp. 1227–1246.

Vanmarcke, E. H. (1977)b, "Reliability of earth slopes", *Journal of the Geotechnical Engineering Division*, ASCE, vol. 103, pp. 1247–1265.

Vanmarcke, E. H. (1983), "*Random Fields: Analysis and Synthesis*", The MIT Press, Cambridge

Varnes, D. J. (1978), "Slope Movement. Types and Processes", in: Schuster, R. L. and Krizek, R. J. (Eds.), *Landslides: Analysis and control*, Washington, DC, Transportation Research Board, National Academy Press. Special Report, vol. 176, pp. 11-33

Varnes, D. J. (1984), "*Landslide Hazard Zonation: a review of principles and practice*", United Nations International, Paris

Vaze, J., Teng, J. and Spencer, G. (2010), "Impact of DEM accuracy and resolution on topographic indices", *Environmental Modelling and Software*, vol. 25, pp. 1086–1098

Vieira, B. C., Fernandes, N. F. and Filho, O. A. (2010), "Shallow landslide prediction in the Serra do Mar, São Paulo, Brazil", *Natural Hazards Earth System Science*, vol. 10, pp. 1829–1837

Viet, T. Th, Lee, G., Thu, T. M. and An, H. U. (2016), "Effect of Digital Elevation Model Resolution on Shallow Landslide Modeling using TRIGRS", *Natural Hazards Review*, (ASCE) NH.1527-6996.0000233, 04016011, 1-14

Viet, T. Th, Alvioli, M., Lee, G., and An, H. U. (2018), "Three-dimensional, time-dependent modeling of rainfall-induced landslides over a digital landscape: a case study", *Landslides*, vol. 15, pp. 1071–1084

Wang, T., Liu, J., Shi, J. and Wu, S. (2017), "The influence of DEM resolution on seismic landslide hazard assessment based upon the Newmark displacement method: a case study in the loess area of Tianshui, China", *Environmental Earth Sciences*, vol. 76, paper no. 604, pp. 1-10

Wesley, L. D. (2010), "*Geotechnical Engineering in Residual Soils*", John Wiley & Sons, Inc.

Wolff, T. H. (1985), "Analysis and design of embankment dam slopes: a probabilistic approach", Ph.D. Thesis, Purdue University, Lafayette, Indiana.

Wu, W. S. and Sidle, R. (1995), "A distributed slope stability model for steep forested basins", *Water Resources Research*, vol. 31, no. 8, 2097–2110

Yamsani, S. K., Sreedeep, S. and Rakesh, R. R. (2016), "Frictional and Interface Frictional Characteristics of Multi-layer Cover System Materials and Its Impact on Overall Stability", *International Journal of Geosynthetic and Ground Engineering*, 2:23

Yubonchit, S., Chinkulkijniwat, A., Horpibulsuk, S., Jothityangkoon, C., Arulrajah, A. and Suddeepong, A. (2016), "Influence Factors Involving Rainfall-Induced Shallow Slope Failure: Numerical Study", *International Journal of Geomechanics*, vol. 17, no. 7, 04016158

Zevenbergen, L. W. and Thorne C. R. (1987), "Quantitative analysis of land surface topography", *Earth Surface Processes and Landforms*, vol. 12, no. 1, pp. 47-56

Zhan, T. L. T., Ng, C. W. W. and Fredlund, D. G. (2007), "Field study of rainfall infiltration into grassed unsaturated expansive soil slope", *Canadian Geotechnical Journal*, vol. 44, pp. 392-408

Zhang, Z.F., Groenevelt, P.H., and Parkin, G.W. (1998), "The well shape factor for the measurement of soil hydraulic properties using the Guelph Permeameter", *Soil Tillage*, vol. 49, pp. 219-221

Zhang L. L., Zhang J., Zhang L. M. and Tang W. H. (2015), "Stability analysis of rainfall-induced slope failure: a review", *Geotechnical Engineering*, Proceedings of the Institution of Civil Engineers, vol. 164, pp. 299–316

Zhang, R. (1997), "Determination of Soil Sorptivity and Hydraulic Conductivity from the Disk Infiltrometer", *Soil Science Society of America Journal*, vol. 61, pp. 1024-1030

LIST OF PUBLICATIONS

- **Journals:**
  - **Sarma, C. P.**, Dey, A. and Murali Krishna, A. (2020), "Influence of digital elevation models on the simulation of rainfall-induced landslides in the hillslopes of Guwahati, India" ***Engineering Geology***. (DoI: 10.1016/j.enggeo.2020.105523)
  - **Sarma, C. P.**, Dey, A. and Murali Krishna, A. "Influence of rainfall patterns on landslide triggering: A study of Guwahati city using TRIGRS analysis" ***Journal of Mountain Science***. (**Under Review**)
  - **Sarma, C. P.**, Dey, A. and Murali Krishna, A. Rainfall induced landslide hazard study of Guwahati region using TRIGRS model" ***Geomatics, Natural Hazards and Risk***. (**Under Review**)
- **Book Chapters:**
  - **Sarma, C. P.**, Dey, A. and Murali Krishna, A. (2019), "Investigation of rainfall induced landslides at hillslopes of Guwahati region, Assam" In: Katsumi T., Murali Krishna, A. (Eds.) *Developments in Geotechnical Engineering, Geotechnics for Natural Disaster Mitigation and Management*, Springer.
  - **Sarma C.P.**, Murali Krishna A., Dey A. (2019) "Geotechnical characterization of hillslope soils of Guwahati region" In: Stalin V., Muttharam M. (eds) *Geotechnical Characterisation and Geoenvironmental Engineering. Lecture Notes in Civil Engineering*, vol 16. Springer, Singapore
  - **Sarma, C. P.**, Dey, A. and Murali Krishna, A. (2014), "Probabilistic slope stability analysis considering spatial variability of soil properties: Influence of correlation length" in Oka, Murakami, Uzuoka & Kimoto (Eds.), *Computer Methods and Recent Advances in Geomechanics*, Taylor & Francis Group, pp. 1125 – 1130
- **Conferences:**
  - **Sarma, C. P.**, Murali Krishna, A. and Dey, A. (2017), "Landslide evolution through catastrophe theory based on planar–slip slope model" *52nd Indian Geotechnical Conference (GeoNEst-IGC-2017)*, Guwahati, India, pp. 1-4.
  - **Sarma, C. P.**, Dey, A. and Murali Krishna, A. (2015), "Landslide early warning based on geotechnical slope stability model for the Guwahati region" *50th Indian Geotechnical Conference*, Pune, India, pp. 1-4.
  - **Sarma, C. P.**, Murali Krishna, A. and Dey, A. (2015), "Landslide hazard assessment of Guwahati region using physically based models," *6th Annual Conference of the International Society for Integrated Disaster Risk Management – Disaster Risk Reduction: Challenges and Opportunities for Sustainable Growth* (IDRIM-TIFAC), New Delhi, India, pp. 1-13.